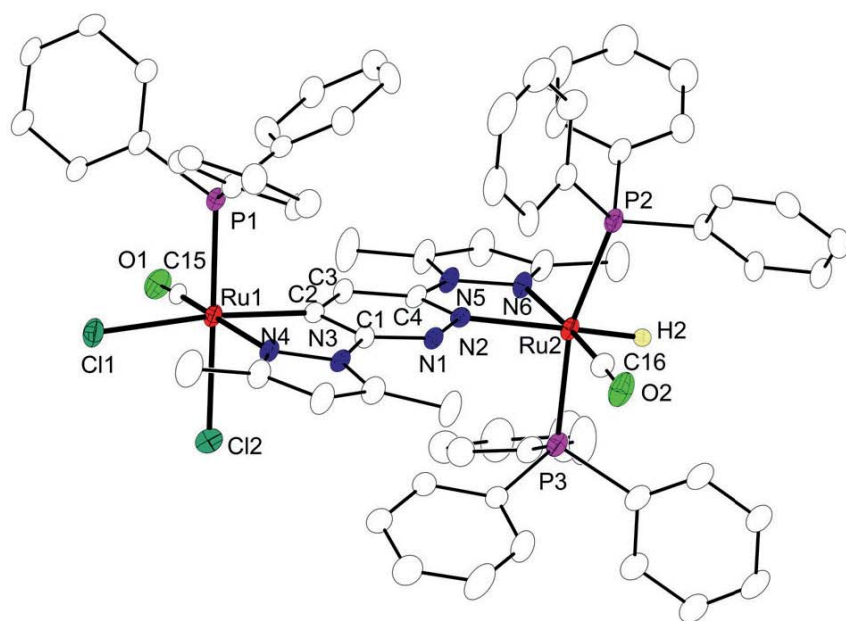


Novel *N*-Heterocyclic Carbene Ligands and their Metal Complexes

Tongxun Guo



Cuvillier Verlag Göttingen
Internationaler wissenschaftlicher Fachverlag



Novel *N*-Heterocyclic Carbene Ligands and their Metal Complexes

Dissertation

zur Erlangung des mathematisch-naturwissenschaftlichen Doktorgrades

“Doctor rerum naturalium”

der Georg-August-Universität Göttingen



im Promotionsprogramm

“Catalysis for Sustainable Synthesis”



der Georg-August-University School of Science (GAUSS)

vorgelegt von

Tongxun Guo

aus Handan, Hebei, VR China

Göttingen, 2014



Bibliografische Information der Deutschen Nationalbibliothek

Die Deutsche Nationalbibliothek verzeichnet diese Publikation in der Deutschen Nationalbibliografie; detaillierte bibliografische Daten sind im Internet über <http://dnb.d-nb.de> abrufbar.

1. Aufl. - Göttingen : Cuvillier, 2015
Zugl.: Göttingen, Univ., Diss., 2014

© CUVILLIER VERLAG, Göttingen 2015

Nonnenstieg 8, 37075 Göttingen

Telefon: 0551-54724-0

Telefax: 0551-54724-21

www.cuvillier.de

Alle Rechte vorbehalten. Ohne ausdrückliche Genehmigung des Verlages ist es nicht gestattet, das Buch oder Teile daraus auf fotomechanischem Weg (Fotokopie, Mikrokopie) zu vervielfältigen.

1. Auflage, 2015

Gedruckt auf umweltfreundlichem, säurefreiem Papier aus nachhaltiger Forstwirtschaft.

ISBN 978-3-95404-999-8

eISBN 978-3-7369-4999-7



Novel *N*-Heterocyclic Carbene Ligands and their Metal Complexes

Dissertation

- zur Erlangung des mathematisch-naturwissenschaftlichen Doktorgrades
 - "Doctor rerum naturalium"
 - der Georg-August-Universität Göttingen
-
- im Promotionsprogramm CaSuS "Catalysis for Sustainable Synthesis"
 - der Georg-August University School of Science (GAUSS)
-
-

vorgelegt von

Tongxun Guo

- aus Handan, Hebei, VR China
 - Göttingen, 2014



Betreuungsausschuss

Prof. Dr. Franc Meyer, Institut für Anorganische Chemie

Prof. Dr. Guido Clever, Institut für Anorganische Chemie

Prof. Dr. Lutz Ackermann, Institut für Organische und Biomolekulare Chemie

Mitglieder der Prüfungskommission

Referent: Prof. Dr. Franc Meyer, Institut für Anorganische Chemie

Korreferent: Prof. Dr. Dietmar Stalke, Institut für Anorganische Chemie

Weitere Mitglieder der Prüfungskommission:

Prof. Dr. Guido Clever, Institut für Anorganische Chemie

Prof. Dr. Lutz Ackermann, Institut für Organische und Biomolekulare Chemie

Dr. Inke Siewert, Institut für Anorganische Chemie

Dr. Alexander Breder, Institut für Organische und Biomolekulare Chemie

Tag der mündlichen Prüfung: 11.07.2014



Acknowledgement

I would like to express my greatest gratitude towards my thesis supervisor, Prof. Dr. Franc Meyer, for his patience, encouragement and understanding on me and giving me high degree of freedom throughout the entire study. Without his generous guidance and suggestion, this thesis would not be possible.

I would like to offer my special thanks to my secondary supervisors Prof. Dr. Lutz Ackermann and Prof. Dr. Guido Clever for their valuable advice during my research.

I am thankful to Prof. Dr. Dietmar Stalke (as the coreferee), Dr. Inke Siewert and Dr. Alexander Breder for serving on my thesis examination committee, reading my thesis detail and giving me valuable suggestions.

I would like to express my heartiest thanks to Dr. Sebastian Dechert for his assistance in collecting X-ray diffraction data, solving the structures and also in performing DFT calculations and analyzing the results.

I wish to acknowledge the following people for their assistance:

Mr. Jörg Teichgräber and Mr. Andreas Schwarz for their technical assistance.

Dr. Michael John and other staffs for helping me with the NMR measurements.

Dr. Holm Frauendorf and other colleagues for their assistance in MS experiments.

Ms. Angelika Wraage and her colleagues for their help in elemental analysis.

Ms. Unger Petra, Dr. Hanna Steininger and Dr. A. Claudia Stückl and other supporting staffs in Institute of Inorganic Chemistry for helping me in various ways.

I would like to say thanks to all the past and present members in Prof. Meyer's working group, especially to my laboratory mates Mr. Dennis Manz, Mr. Sebastian Menge and Miss Anastasia Herter for their daily help, and to Mr. Torben Böhnisch and Mr. Sven Neudeck for their support, assistance and cooperation in CaSuS program.

I am particularly grateful for the financial support from the doctoral program 'Catalysis for Sustainable Synthesis' funded by the Ministry for Science and Culture of the State of Lower Saxony.

Finally, I would like to record my sincere indebtedness to my family, my friends and my brothers and sisters in Church for their love, encouragement and sacrifice.





TABLE OF CONTENT

CHAPTER 1.INTRODUCTION.....	1
1.1 History of <i>N</i> -Heterocyclic Carbene Chemistry.....	1
1.2 Imidazole Derived Carbenes.....	3
1.2.1 Imidazol-2-ylidene carbenes	3
1.2.2 Imidazol-4/5-ylidene carbenes.....	4
1.3 Carbenes Based on Other <i>N</i> -Heterocycles	11
1.3.1 Triazole derived carbenes	13
1.3.2 Pyrazole derived carbenes	18
1.3.3 Pyridine and diazines derived carbenes	19
1.4 Novel <i>N</i> -Heterocyclic Carbene Chemistry	24
1.4.1 <i>N</i> -substituted-imidazolylidene metal complexes	24
1.4.2 Carbodicarbene	26
1.5 Pyrazole Bridged Ligands and their Complexes	29
1.6 Conclusion	32
CHAPTER 2.PYRIDAZINE DERIVED <i>N</i>-HETEROCYCLIC CARBENE PALLADIUM COMPLEXES	33
2.1 Introduction and Motivation.....	33
2.2 Result and Discussion.....	36
2.2.1 Synthesis of ligand precursors.....	36
2.2.2 Synthesis of novel NHC complexes	38
2.2.3 Functionalization of the second nitrogen atom	49
2.3 Conclusion	51
CHAPTER3.PYRAZOLE BRIDGED BIS(NHC) LIGANDS AND THEIR DINUCLEAR PALLADIUM COMPLEXES	53
3.1 Introduction and Motivation.....	53
3.2 Result and Discussion.....	55
3.2.1 Material and methodology.....	55
3.2.2 Synthesis of $[\text{}^n\text{L}^{\text{R}}_2\text{Pd}_2](\text{PF}_6)_2$ and $[\text{}^a\text{L}^{\text{R}}_2\text{Pd}_2](\text{PF}_6)_2$	57
3.2.3 Mechanistic consideration	65
3.2.4 Synthesis of $\text{}^n\text{L}^{\text{R}}\text{Pd}_2\text{Cl}_3$ and $\text{}^a\text{L}^{\text{R}}\text{Pd}_2\text{Cl}_3$	69
3.3 Conclusion	74



CHAPTER 4. *N*-METALLATED *N*-HETEROCYCLIC CARBENE RUTHENIUM COMPLEXES 75

4.1	Introduction and Motivation.....	75
4.1.1	Chemical shifts of metallated carbenes	75
4.1.2	Motivation	79
4.1.3	Material and methodology.....	80
4.2	Result and Discussion.....	82
4.2.1	Synthesis of complex 16.....	82
4.2.2	Computational study	88
4.2.3	Mechanistic consideration	91
4.2.4	Synthesis of complex 18.....	93
4.3	Conclusion	102

CHAPTER 5. SYNTHESIS OF NOVEL INDENE DERIVED CARBENE LIGANDS 103

5.1	Introduction and Motivation.....	103
5.1.1	Cyclopentadiene derived carbenes	103
5.1.2	NHC substituted carbon compounds	105
5.2	Ligand Synthesis.....	109
5.3	Conclusion	116

CHAPTER 6. EXPERIMENTAL SECTION 117

6.1	General Remarks.....	117
6.2	Synthesis of Ligand Precursors	119
6.3	Synthesis of Metal Complexes	124

REFERENCES 141

APPENDIX 147



List of Abbreviation

Abbreviation	Full Name or Description
ABSA	4-acetamidobenzenesulfonyl azide
Ad	adamantyl
aNHC	abnormal N-heterocyclic carbene
Ar	aryl
bipy	2,2'-bipyridine
cat.	catalyst
cod	1,5-cyclooctadiene
Cp	cyclopentadienyl
Cp*	pentamethylcyclopentadienyl
Cy	cyclohexyl
cym	cymene
dba	dibenzylideneacetone
DCM	dichloromethane
Dipp	2,6-diisopropylphenyl
ditz	1,2,4-triazolyl-3,5-diylidene
dme	dimethoxyethane
DMF	dimethylformamide
DMSO	dimethyl sulfoxide
e	electron
E	energy
Eq	equation
Et	ethyl
HMDS	hexamethyldisilazide
HOMO	Highest Occupied Molecular Orbital
ⁱ Pr	<i>iso</i> -propyl
IPr	1,3-bis(2,6-diisopropylphenyl)imidazol-2-ylidene
L	two-electron donating neutral ligand
L _n M	metal fragment with n L ligands
LUMO	Lowest Unoccupied Molecular Orbital
M	metal, metal ion, metal center



Abbreviation	Full Name or Description
Me	methyl
Mes	mesityl, 1,3,5-trimethylphenyl
MIC	mesoionic carbene
MS	Mass Spectroscopy
NBO	Natural Bond Orbital
ⁿ Bu	<i>n</i> -butyl
NHC	N-heterocyclic carbene
NMR	Nuclear Magnetic Resonance
nNHC	normal N-heterocyclic carbene
OAc	acetate
OTf	triflate, trifluoromethanesulfonate
Ph	phenyl
py	pyridine
pz	pyrazole
R	organic group
^t Bu	<i>tert</i> -butyl
THF	tetrahydrofuran
TMS	trimethylsilyl
Tol	tolyl
Tp	hydrotris(pyrazoyl)borate
TS	Transition State
Ts (Tos)	tosyl
X or Y	one-electron anion ligand
δ	chemical shift (NMR)
η	descriptor for hapticity
κ	shows hapticity in σ -bonding ligands
μ	descriptor for bridging
$\tilde{\nu}$	spectroscopic wavenumber



CHAPTER 1. Introduction

1.1 History of *N*-Heterocyclic Carbene Chemistry

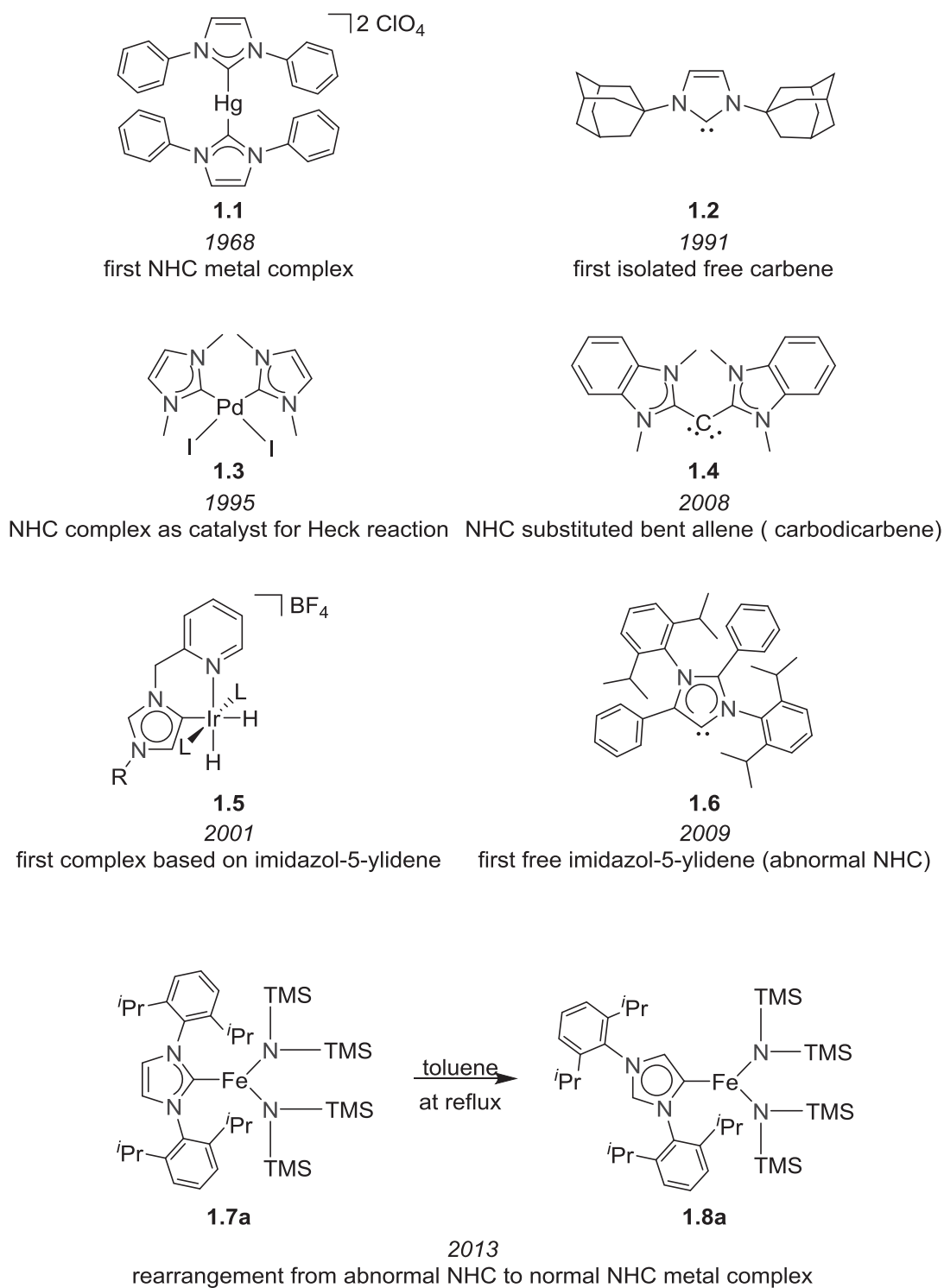
N-heterocyclic carbenes have found robust development in the past two decades,¹ and were widely used as ubiquitous ligands in organometallic catalysis² and organocatalysis.³ Selected milestones in the history of *N*-heterocyclic carbene chemistry are shown in **Scheme 1.1**.

The first well-defined metal complex **1.1** based on an *N*-heterocyclic carbene ligand was reported by Wanzlick in 1968.⁴ Yet, the importance of this new carbene type as ligands for metal complexes was not widely recognized in the following years until in 1991, Arduengo isolated the first stable crystalline imidazol-2-ylidene compound **1.2** from its imidazolium precursor, in which the bulky wingtip was thought to have provided crucial kinetic stabilization effect.⁵ In 1995, the first class of *N*-heterocyclic carbene palladium complexes, such as complex **1.3** as homogeneous catalyst for Heck reaction, were synthesized and showed higher stability in the presence of oxygen and moisture, compared to the widely-used phosphine/phosphite ligands.⁶ This discovery pulled a trigger to the robust development of *N*-heterocyclic carbene chemistry, especially for NHC metal complexes catalyzed organic reactions.^{2a}

N-heterocyclic carbenes served as ligands not only for metal atoms, but also for non-metal atoms, such as carbon. For instance, bis(NHC) assisted bent allene **1.4**, also known as carbodicarbene, was synthesized and showed peculiar chemistry properties, which challenged the prevailing comprehension of carbon chemistry.⁷

In 2001, an unusual *N*-heterocyclic carbene iridium complex **1.5** was reported.⁸ Different from imidazol-2-ylidenes, in the *N*-heterocyclic carbene ligand of **1.5**, the carbenic carbon located at the C4/5 position. Thereafter, more complexes with this type of ligands were reported and these ligands were referred to as ‘abnormal *N*-heterocyclic carbenes’. After the studies on abnormal *N*-heterocyclic carbene chemistry for almost one decade, the first free abnormal carbene species, *i. e.* imidazol-5-ylidene **1.6** was isolated.⁹

The transfer reaction from normal NHC iron complex **1.6a** to its abnormal NHC congener **1.7a** by heating suggested that encumbering substituents on the wingtip of the NHC could drive the rearrangement between these two isomers (**Scheme 1.1**).¹⁰



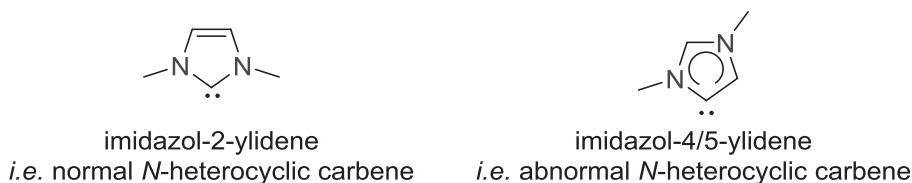
Scheme 1.1. Milestones of chemistry on *N*-heterocyclic carbenes.



1.2 Imidazole Derived Carbenes

1.2.1 Imidazol-2-ylidene carbenes

Among all N-heterocyclic carbenes, imidazol-2-ylidenes, also referred to as Arduengo carbenes in early times, are certainly the most important. Synthesis of the imidazolium precursors, synthetic strategy of imidazole based carbene metal complexes (specially silver,¹¹ palladium,¹² ruthenium,¹³ gold¹⁴ and copper^{14b} complexes) and their application in catalysis were well studied and summarized.^{2, 15}



An early DFT calculation study on zirconium imidazol-2-ylidene complexes claimed that ‘the Arduengo carbene ligand acts as a pure σ -donor ligand at these very electrophilic group 4 metallocene complexes’.¹⁶ The Arduengo carbene ligand acted as a pure donor in this special situation was probably because there were no d-electrons in the metal center to donate to the ligand *via* back-bonding. Later studies showed that, for complexes with d-orbital electrons at the metal center, Arduengo carbenes no longer served as ‘pure σ -donor ligand’ and they also had π acceptor character, just like other σ -donor ligands such as phosphine ligands (**Figure 1.1**).¹⁷

The π^* orbitals of the ligands could accept electrons from the electron-rich metal centers and the back-donation was not negligible. As for the electron-poor metal center, like that in d^0 complexes, the electron could also be donated from the π orbital of the ligand into the metal center, although the π orbital was normally not considered as a major donating party. Therefore, the electronic properties of imidazol-2-ylidene ligands were more complicated than ‘pure donors’. Yet, both theoretical and experimental studies still suggested that imidazol-2-ylidenes were stronger donor ligands than phosphines and phosphites in general.

For example, the donating capacity of an NHC ligand was evaluated by the CO vibrational frequency of the related NHC metal carbonyl complexes.¹⁸ With other variables fixed in a metal complex, a stronger donating NHC ligand made the metal center to become more electron-rich. Therefore, the CO ligand obtained more back-donation from

the metal into its anti-bonding π^* orbital, resulting in a weaker CO bond and thus a smaller value of its vibrational frequency.¹⁸ Meanwhile, by comparison of the energies of HOMOs of different ligands, an early study confirmed the conclusion that imidazol-2-ylidenes were better donating ligands than phosphine ligands.¹⁸

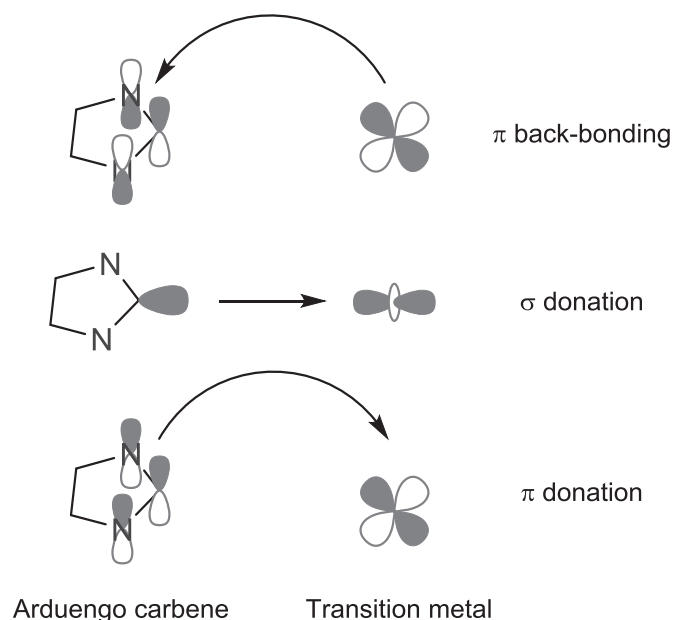
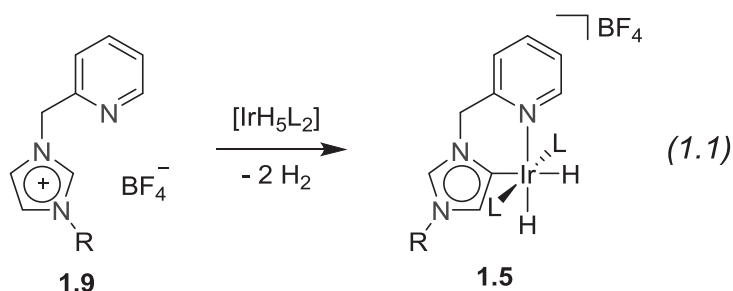


Figure 1.1. Selected molecular orbitals of *N*-heterocyclic carbene and their relationship to metal fragment.

1.2.2 Imidazol-4/5-ylidene carbenes

From the beginning of the new millennium, imidazol-4/5-ylidenes, constitutional isomers of the imidazol-2-ylidene counterparts, have attracted lots of attention. Several reviews were published to discuss various types of unconventional NHCs¹, the precursors¹⁹, complexes^{15b} and the application of their complexes in catalysis.²⁰

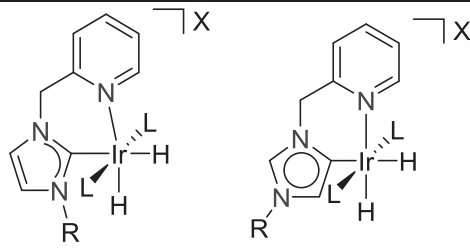
In 2001, Crabtree and his co-workers serendipitously isolated an unusual NHC iridium complex **1.5** with the metal atom bound to the C5 of the imidazole ring (Eq 1.1), evidenced by the ¹H NMR spectroscopic data that the C2-H and C4-H signals remained.⁸ This new type of NHC was then termed as ‘abnormal’ NHC, in order to be differentiated from normal NHC with the carbenic carbon atom at 2-position of the imidazole ring. Complex **1.5** was quite stable and showed no tendency to rearrange to the normal carbene isomer.



Considering that the C2 proton was more acidic than the C5 proton, the cleavage of C2-H was easier. Thus, the cause of the unexpected formation of complex **1.5** was generally not related to electronic reason.

The mechanism of the formation of the abnormal NHC iridium complex was then studied. A series of similar reactions (like that in Eq 1.1) with different variables (various R groups and counterions) indicated that both steric congestion of the wingtips on the azolium ring, and the counterions of the precursor influenced the selective formation of normal or abnormal NHC metal complexes (**Table 1.1**).²¹

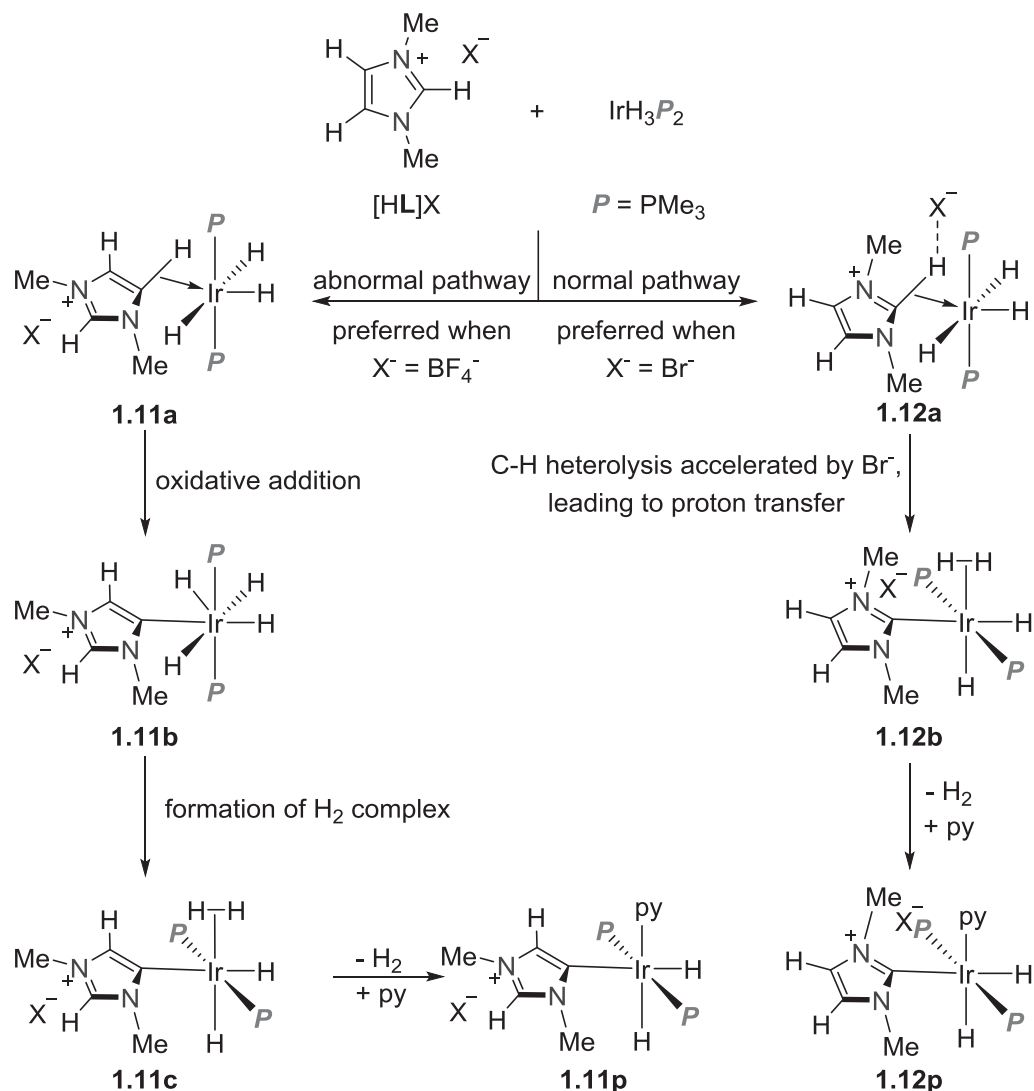
Table 1.1. Formation of normal/abnormal carbene complexes affected by counterions.

Entry	R	X		
			1.10a	1.10b
a	Me	Br	91	9
b	Me	OAc	80	20
c	Me	BF ₄	45	55
d	Me	PF ₆	50	50
e	Me	SbF ₆	11	89
f	<i>i</i> Pr	BF ₄	0	100

Comparison of **Entry c** and **Entry f** implied that a ligand precursor with bulkier wingtips preferred to form abnormal NHC complex (**Entry f**). The steric repulsion between the wingtip and co-ligands of the product was significantly reduced in **Entry f**; while for the ligand precursor with less bulkier wingtip in **Entry c**, the normal NHC complex became more stable from thermodynamic point of view.

The counterions of the ligand precursor also had strong influence on the ratio of the normal and abnormal carbene complexes formed. With non-coordinating counterion

$[\text{SbF}_6]^-$ (**Entry e**), abnormal NHC metal complexes were preferred, while with Br^- , which could easily form H-bondings with protons of the imidazolium ring of the ligand precursors, normal NHC complexes were more likely to be generated. Note that, both of the products were reasonably stable and no transformation reaction between them was observed under various reaction conditions, even in highly acidic environment.



Scheme 1.2. Proposed mechanism of the selective formation of normal *versus* abnormal NHC metal complexes.

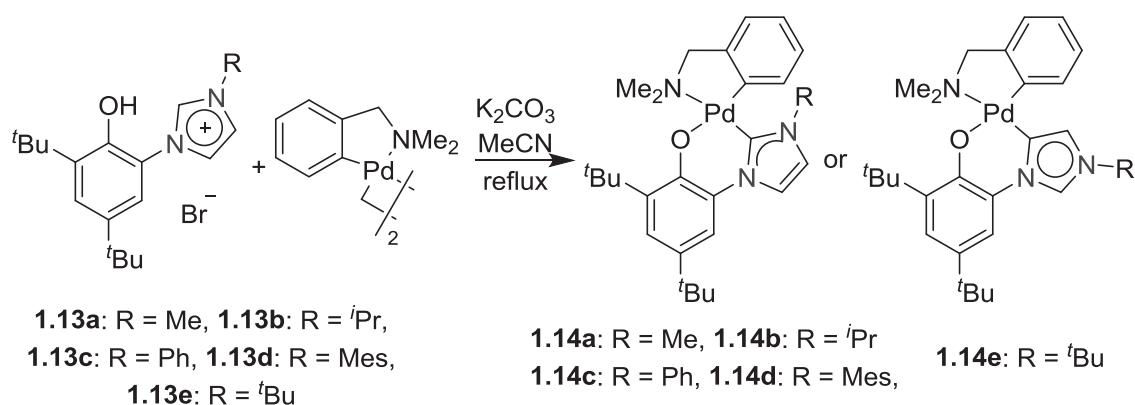
Based on the experimental observations and the subsequent computational studies with simplified models, a plausible mechanism for the selective formation of abnormal or normal NHC complexes **1.11p** and **1.12p** was proposed (**Scheme 1.2**).

In the proposed mechanism, $[\text{BF}_4]^-$ induced the oxidative addition of the C5-H onto $[\text{Ir}^{\text{III}}\text{H}_3(\text{PMe}_3)_2]$, forming an Ir^{V} intermediate **1.11b**, which then rearranged to the H_2 -adduct complex **1.11c** and finally the abnormal NHC complex **1.11p**; while Br^- acceler-

ated the heterolysis of the weaker C2–H bond (compared to the C5–H bond) in **1.12a** to form the H₂-adduct complex **1.12b** directly, eventually yielding the normal NHC complex **1.12p**.²¹

As a conclusion, ligand precursors with bulkier wingtip on the azolium rings and with non-coordinating counterion tended to form abnormal NHC complexes and ligand precursors with less hindered wingtips and with counterions that could easily form H-bonding preferred to form normal NHC complexes. The conclusion was consistent with other reports.

For example, in the reactions of ligand precursors **1.13a-1.13e** with palladium(II) species in the presence of potassium carbonate, when R was methyl, *iso*-propyl, phenyl or mesityl group, normal NHC palladium complexes **1.13a-1.13d** was formed; while when R group was the highly bulky *tert*-butyl group, abnormal NHC complex **1.13e** was formed (Scheme 1.3).²²



Scheme 1.3. Selective formation of normal/abnormal carbene complexes determined by bulkiness of R group.

Table 1.2. Vibration frequencies of CO in complex **1.15a-1.15d**.

1.15a	1.15b	1.15c	1.15d
$\nu_{\text{avg}}(\text{CO})/\text{cm}^{-1}$	2003	2017	2017
			2019

By means of comparing the vibrational frequency of CO of their metal carbonyl complexes, the new abnormal NHCs proved to be better donating ligands. For instance, the average CO vibrational frequency of the abnormal NHC iridium complex **1.15a** was



considerably lower than those in the similar normal NHC complexes **1.15b-1.15d** (Table 1.2),²³ indicating that abnormal NHCs were stronger donors than normal NHCs.

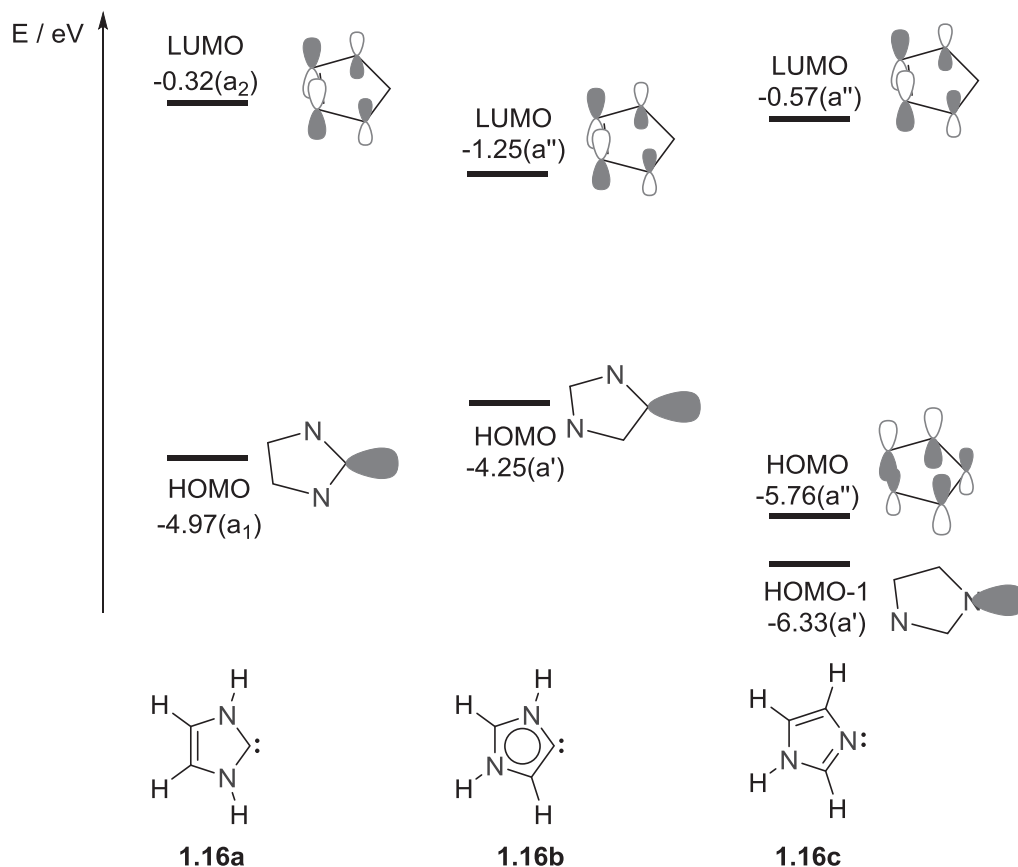
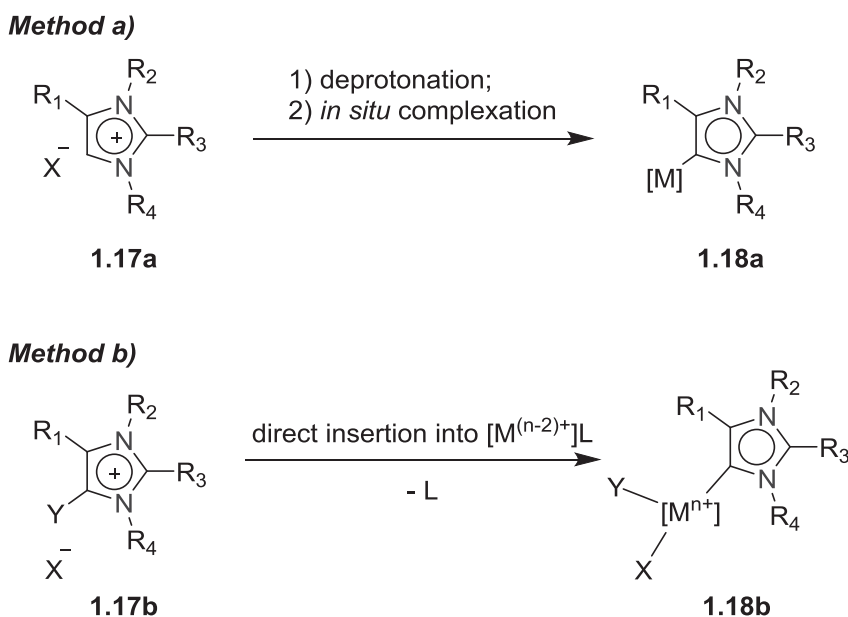


Figure 1.2. LUMO and HOMO of imidazol-2-ylidene, imidazoly-4/5-ylidene and imidazolyl.

The conclusion was consistent with a DFT computational study (Figure 1.2).²⁴ The energies of HOMOs of the calculated normal and abnormal NHC models (**1.16a** and **1.16b**, respectively) were -4.97 eV and -4.25 eV, respectively, indicating that the abnormal NHC had a stronger tendency to act as an electron donor; the energy gaps between LUMO and HOMO for normal and abnormal NHC were 4.65 eV and 4.00 eV, respectively, suggesting that the normal NHC was more stable than the abnormal NHC. It was noteworthy that the σ -donating orbital of **1.16c**, which would coordinate to metal fragments, was HOMO-1 instead of HOMO. The HOMO-1 energy (-6.33 eV) was much smaller than those of HOMOs of **1.16a** and **1.16b**, implying that imidazole as a nitrogen-coordinating ligand was a reasonably poor σ -donor compared to the isomeric carbene donors.²⁴

Synthesis of abnormal NHC metal complexes became more attractive after their stronger donating capacity had been revealed. Besides several fortuitous isolations of abnormal

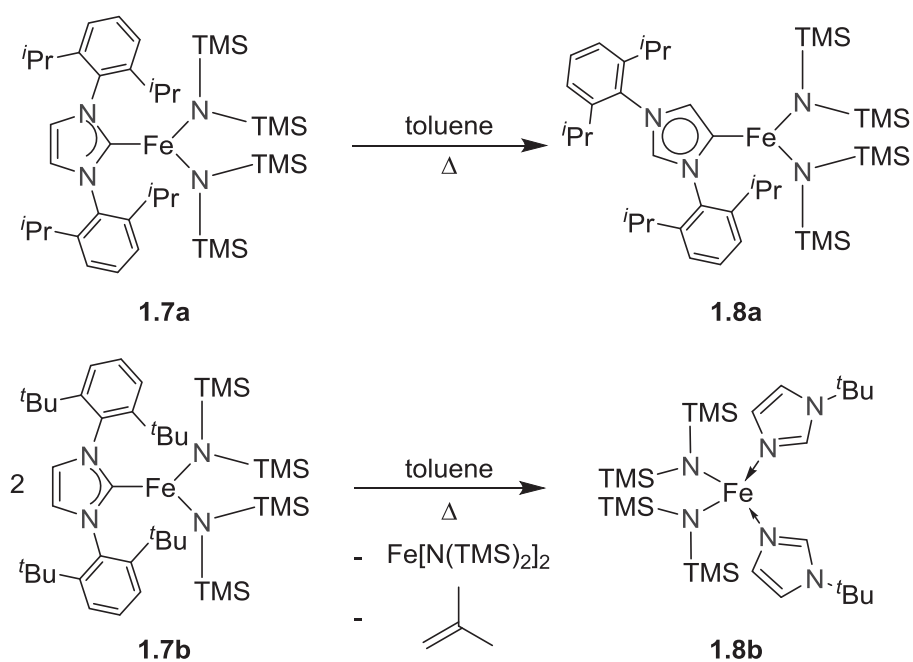
carbene species,²⁵ general strategies were also developed to synthesize abnormal NHC metal complexes. Basically, abnormal NHC complexes could be prepared either a) from the imidazolium precursors **1.17a** with their C2 positions blocked with inert functional groups^{23, 26} to form complex **1.18a**, or b) by oxidative addition of C4/5–X (X = hydrogen²⁷ or halogen atoms²⁸) bonds of the imidazolium precursors **1.17b** onto low-valence metal fragments (**Scheme 1.4**) to generate **1.18b**, in which the value of oxidation state of the central metal ion was increased by two units.



Scheme 1.4. Two synthetic methods to abnormal NHC metal complexes **1.18a-1.18b**.

The transformation between normal and abnormal NHC complexes was quite rare.²⁹ Recent research found that an iron normal NHC complex **1.7a** was easily transferred to its abnormal NHC isomer **1.8a** by heating at reflux in toluene.¹⁰ A plausible driving force was the release of the steric congestion caused by the bulky wingtip group, 2,6-di(isopropyl)phenyl, in **1.7a**. Meanwhile, the rearrangement pathways were also strongly influenced by the wingtip; when the wingtip was *tert*-butyl group, the normal NHC complex **1.7b** was transformed to a tetrahedral bis(*N-tert*-butylimidazole) iron complex **1.8b** under the same reaction condition (**Scheme 1.5**).

The transformation between normal and abnormal NHC metal complexes was a relatively new topic and the reaction mechanism was still unclear.

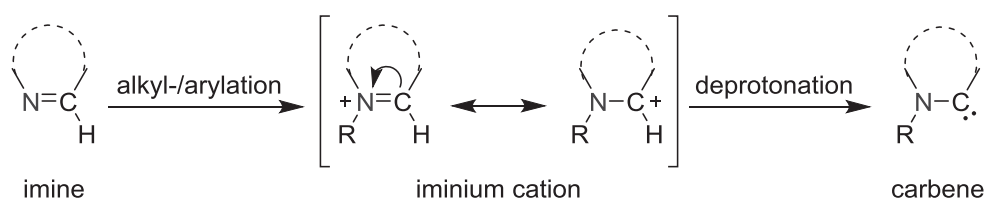


Scheme 1.5. Reactions of normal NHC complex to the abnormal NHC metal complex or imidazole metal isomer.

1.3 Carbenes Based on Other *N*-Heterocycles

Despite the robust development of imidazolylidene chemistry, imidazole is not the only *N*-heterocycle that can be functionalized to become a carbene. In principle, all other *N*-heterocyclic compounds containing C=N bonds have the potential to be transformed into carbene species (**Scheme 1.6**).

As shown in the scheme, imine derivative can be alkylated or arylated to iminium salt. In one of the isomeric structure of the iminium cation, the positive charge is located on the carbon atom. Removal of the proton leads to the formation of a carbene compound. Singlet carbene has six valence electrons and one empty p orbital, the presence of an empty p orbital is one of the crucial reasons why singlet carbenes are highly reactive. In the carbene species in **Scheme 1.6**, the empty p orbital of the carbenic carbon is stabilized by the electron pair in the p orbital of the adjacent nitrogen, which makes *N*-heterocyclic carbenes comparatively stable.



Scheme 1.6. From imine to imidium, then to *N*-substituted carbene.

In the case of imidazolylidenes, not only the empty p orbital of the carbenic carbon atom is stabilized by the electron pair(s) in the adjacent nitrogen atom(s), but also the formation of the aromaticity (*i. e.*, six-electron-five-center) of the imidazolylidene ring further enhances the stability of the carbene (**Figure 1.3**).

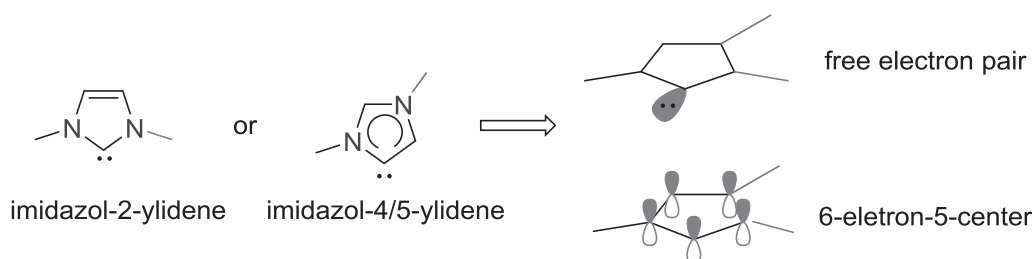


Figure 1.3. Orbital of imidazol-2-ylidene (left) and imidazol-4/5-ylidene (right).

In the same manner, it is not compulsory to have a nitrogen atom directly bound to the carbenic carbon, and as long as the empty p orbital is stabilized in an aromatic system, the stability of the carbene will be increased. As a matter of fact, recently, novel NHCs

based on aromatic *N*-heterocycles other than imidazole were also widely studied (**Chart 1.1**).

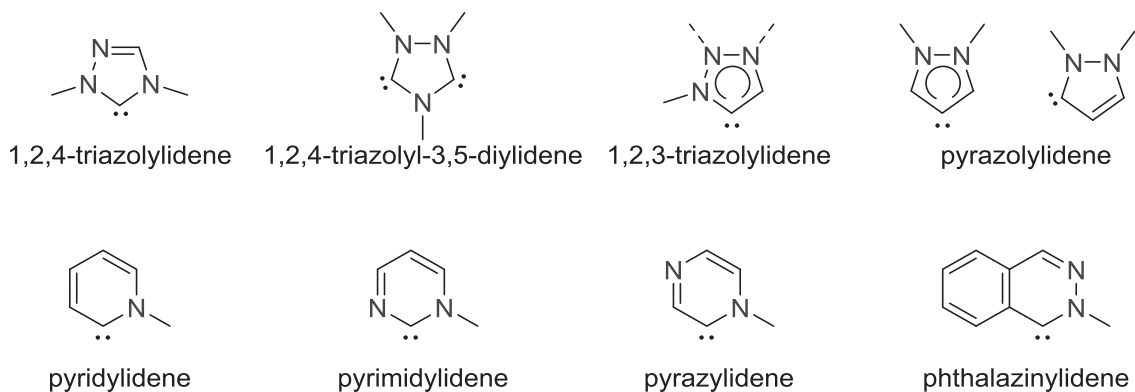


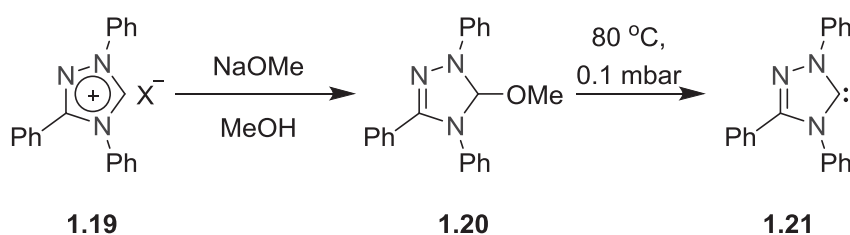
Chart 1.1. Structures and names of novel *N*-heterocyclic carbenes.

Synthesis, characterization and properties of selected examples of novel NHCs are discussed as follows.

1.3.1 Triazole derived carbenes

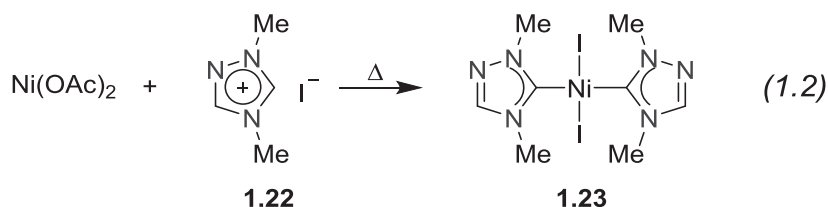
1.3.1.1 1,2,4-Triazole derived carbenes

Before the isolation of the first abnormal imidazolylidene compound **1.6**, triazole derived free carbene, 1,3,4-triphenyl-1,2,4-triazol-5-ylidene **1.21**, had already been isolated in 1995 (**Scheme 1.7**),³⁰ which pulled a trigger to the fast development of novel carbenes based on *N*-heterocycles other than imidazole.



Scheme 1.7. First example of 1,2,4-triazolylidene **1.21**.

Subsequently, the first metal complex **1.23** based on 1,2,4-triazolylidene ligand was synthesized from the reaction of the 1,2,4-triazolium salt **1.22** with nickel acetate (Eq 1.2).³¹

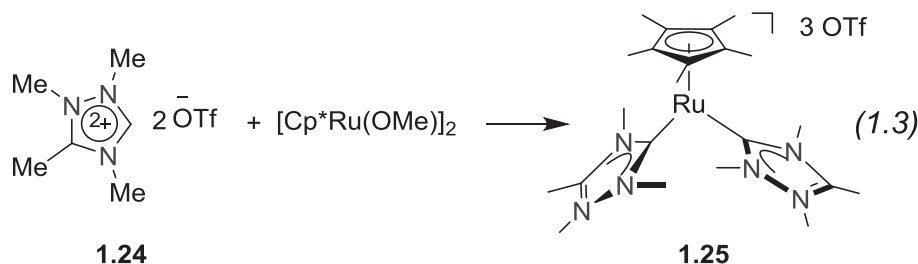


A CO vibrational frequency study of the 1,2,4-triazolylidene iridium complex indicated that 1,2,4-triazolylidene was not such a strong σ -donor as imidazol-2-ylidene species, yet, it was still stronger than any phosphine ligands.¹⁸

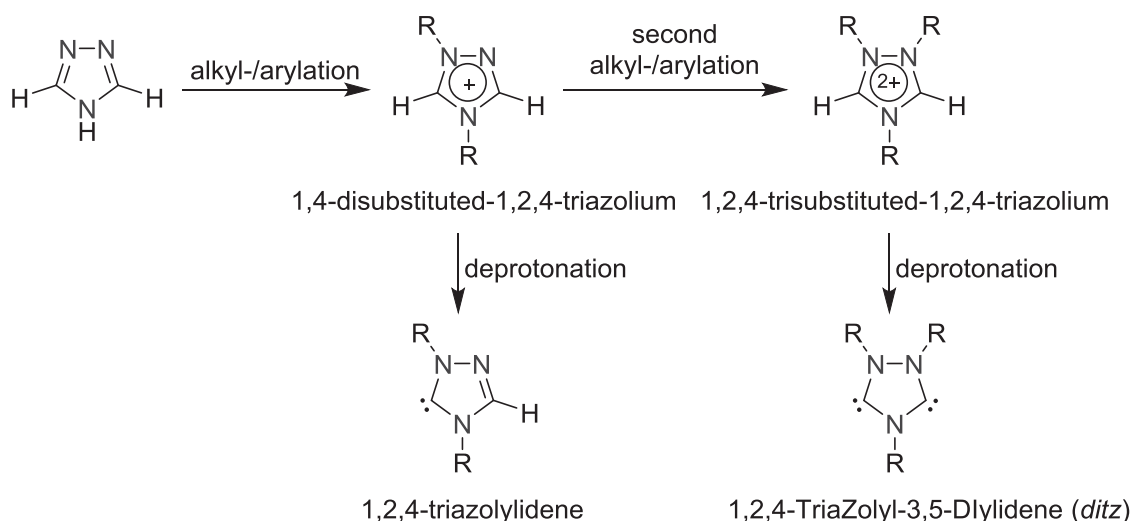
The 1,2,4-triazolylidene ligand is a weaker donor than the imidazol-2-ylidene ligand, because from imidazol-2-ylidene to 1,2,4-triazolylidene, one C–H bond is replaced by nitrogen atom, and according to the orbital perturbation theory, nitrogen is more electronegative carbon and the replacement of the C–H bond by a nitrogen atom will increase the stability of the HOMO orbital containing the donating electron pair, thus leading to the poorer donating capacity of 1,2,4-triazolylidene.

After full methylation of all the nitrogen atoms of the triazole ring, a 1,2,4-triazolium salt **1.24** was formed. The reaction of **1.24** with $[Cp^*Ru(OMe)]_2$ led to the formation of complex **1.25** (Eq 1.3). In complex **1.25**, the two triazole derived ligands were still posi-

tively charged and the carbene signals of the NHC ligands resonated in $\delta = 188.6$ -203.42 ppm region in the ^{13}C NMR spectra.³²

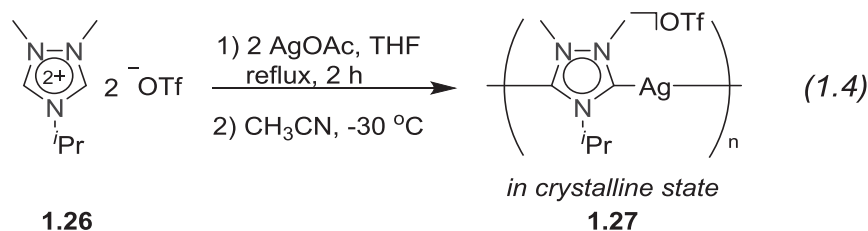


The above 1,2,4-triazolylidene derived ‘cationic’ NHC was a potential κ^2 -ligand, which was named *ditz* ligand.³³ The *N,N,N*-trisubstituted-1,2,4-triazolium precursor can be deprotonated twice to form 1,2,4-triazolyl-3,5-diylidene ligand (**Scheme 1.8**).

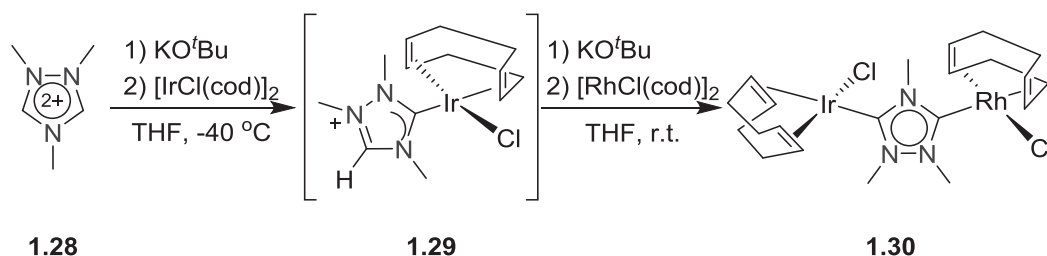


Scheme 1.8. From 1,2,4-triazolylidene to 1,2,4-triazolyl-3,5-diylidene.

Treatment of triazolium salt **1.26** with silver acetate led to the formation of silver dicarbene complex, which was crystallized in solid state as a polymer **1.27** with the dicarbene ligand serving as a linker of silver atoms (Eq 1.4). *Ab initio* calculation showed that a free 1,2,4-triazol-3,5-diylidene had two lone pairs on two carbenic carbon atoms in the plane of the aromatic ring.³⁴



Despite of the robust development of 1,2,4-triazolylidene metal complexes in the late 1990s, the applications of the *ditz* ligand were surprisingly rare until 2007, the second example of a 1,2,4-triazol-3,5-diylidene-based heteronuclear complex **1.30** was synthesized (**Scheme 1.9**). The two protons in the 1,2,4-trialkyltriazolium precursor were removed by KO^tBu one by one and two metal fragments were then coordinated.³⁵



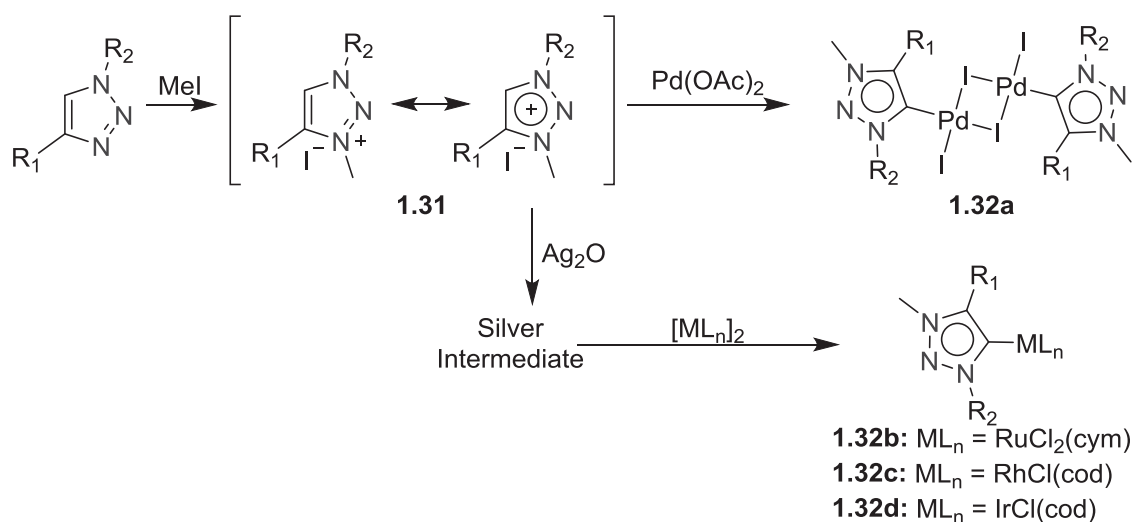
Scheme 1.9. First example of hetero-dinuclear complex **1.15** based on *ditz* ligand.

So far, only a few examples based on this ligand, as well as their applications, were reported, for example, dinuclear ruthenium(II) complexes and their application in β -alkylation of secondary alcohol to primary alcohol,³⁶ homo- and hetero-dinuclear iridium(III)/rhodium(III) complexes and their application in tandem reactions,³⁷ heteronuclear palladium(II)/iridium(III) complexes and their application in tandem reactions,^{33, 38} dipalladium(II) complexes and their application in Sonogashira/cyclic hydroalkoxylation reactions³⁹, direct acylation of aryl halides with aldehydes⁴⁰ and Mizoroki-Heck coupling reactions,⁴¹ iridium(III)/platinum(II) dinuclear complexes and their application in the addition of alkynyl alcohols to indoles,⁴² and iridium(III)/gold(I) complexes and their application in reaction of nitrobenzene and benzyl alcohol⁴³.



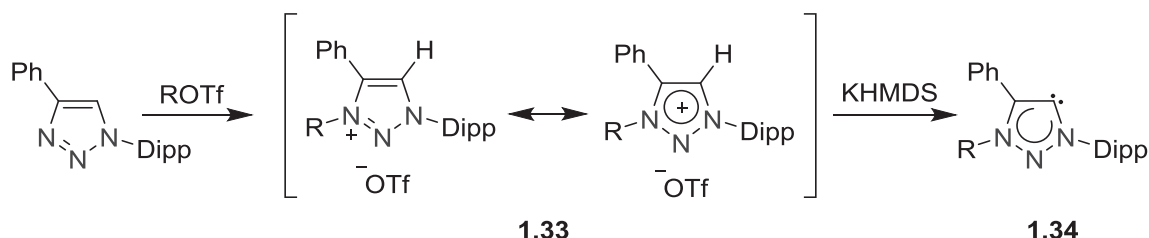
1.3.1.2 1,2,3-Triazole derived carbenes

Versatile 1,2,3-triazoles are easily accessible *via* [3+2] ‘click’ cycloaddition reactions of acetylenes and azides.⁴⁴ It was reported that, direct alkylation of 1,2,3-triazole selectively occurred at the 3-position, generating 1,3-disubstituted-1,2,3-triazolium **1.31**, which was the ligand precursor for the formations of 1,3-disubstituted-1,2,3-triazolylidene metal complexes **1.32a-1.32d**. It was noteworthy that, similar to imidazole-4/5-ylidene, no free-carbene mesomeric structure could be drawn for this new carbene species, which was thus referred to as ‘abnormal’ 1,2,3-triazolylidene (**Scheme 1.10**).⁴⁵



Scheme 1.10. First examples of 1,2,3-triazole based abnormal NHCs metal complexes.

$Pd(II)$,⁴⁵⁻⁴⁶ $Ru(II)$,^{45, 47} $Rh(I)$,⁴⁵⁻⁴⁶ $Ir(I)$,⁴⁵ $Ir(III)$,^{47f} $Os(II)$,^{47g} $Cu(I)$ ⁴⁸ and $Au(I)$ ⁴⁹ complexes based on 1,2,3-triazol-5-ylidene were synthesized and some of them were examined for catalytic activity.⁵⁰

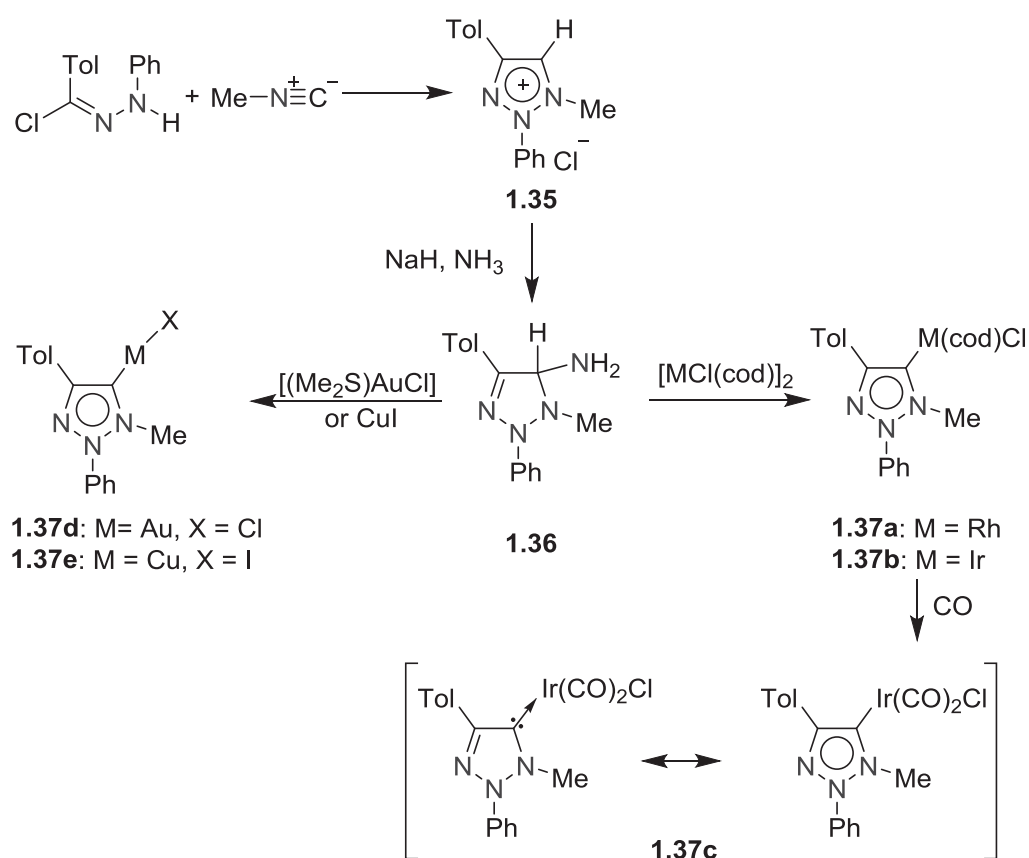


Scheme 1.11. Synthesis of stable free 1,2,3-triazol-5-ylidene compound **1.34**.

One year later, after the successful isolation of imidazol-5-ylidene,⁹ a free 1,2,3-triazolylidene **1.34** was isolated (**Scheme 1.11**). The CO vibrational frequency of its iridium carbonyl complex indicated that the donating capacity of 1,3-disubstituted-1,2,3-

triazolylidene was slightly stronger than imidazol-2-ylidene but much weaker than imidazol-4/5-ylidene.⁵¹

Very recently, 1,2-disubstituted-1,2,3-triazolium salt **1.35** was synthesized. The reaction of **1.35** with sodium hydride and ammonia formed an ammonia adduct **1.36**, which was stable at low temperature. Compound **1.36** reacted with other metal fragments, like Ir(I), Au(I) or Cu(I), resulting in the corresponding metal complexes **1.37a-1.37c** (Scheme 1.12). Mesomeric structure of free carbene could be drawn for this type (as depicted for complex **1.37c** for instance), and it was therefore referred to as the first example of ‘normal’ 1,2,3-triazolylidene species afterward.



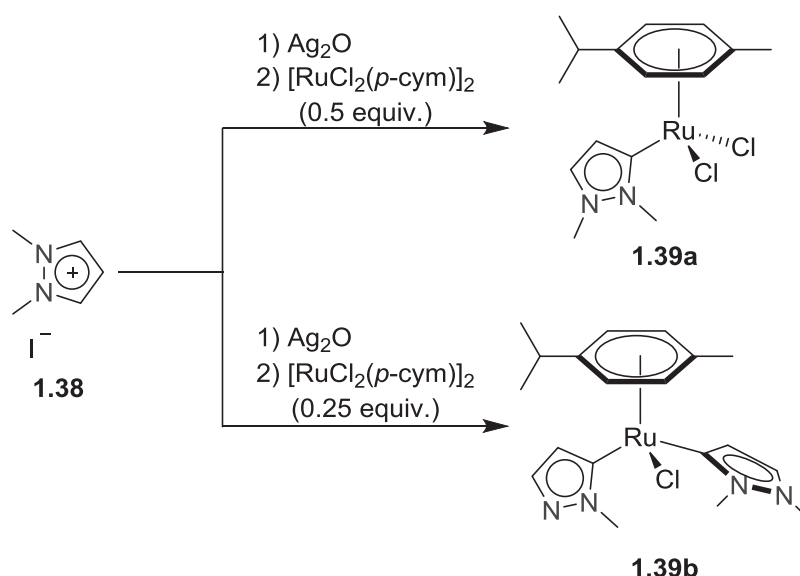
Scheme 1.12. Synthesis of normal 1,2,3-triazolylidene metal complexes.

According to the CO vibrational frequency of the iridium complex, the ‘normal’ 1,2,3-triazolylidenes were only slightly stronger σ -donating than the ‘abnormal’ congeners.⁵²



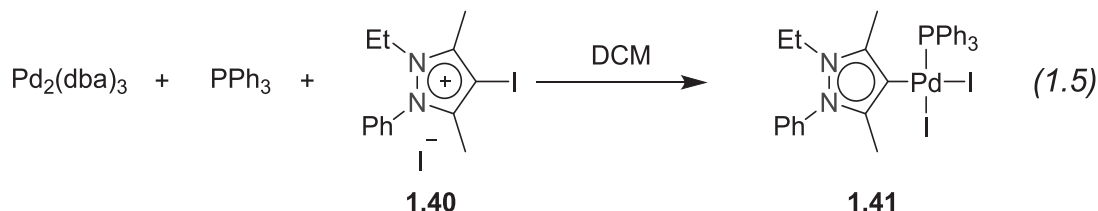
1.3.2 Pyrazole derived carbenes

So far, no free pyrazolylienes have been successfully isolated. The first metal complexes based on pyrazolylidenes were pyrazol-3-ylidene metal complexes. For instance, ruthenium pyrazol-3-ylidene carbene complexes **1.39a** and **1.39b** were synthesized from the ligand precursor **1.38** by transmetallation *via* silver intermediates (**Scheme 1.13**) and the complexes showed fine catalytic activity for dimerization and cyclotrimerization reaction of phenylacetylene.⁵³ Similar method was applied for the synthesis of several gold(I)/gold(III)⁵⁴ and rhodium(I)^{54b} complexes.



Scheme 1.13. Synthesis of pyrazol-3-ylidene ruthenium complexes by transmetallation.

Computational study demonstrated that pyrazol-3-ylidene ligands were better σ -donors than imidazol-2-ylidenes but weaker than imidazol-4/5-ylidenes.⁵⁵



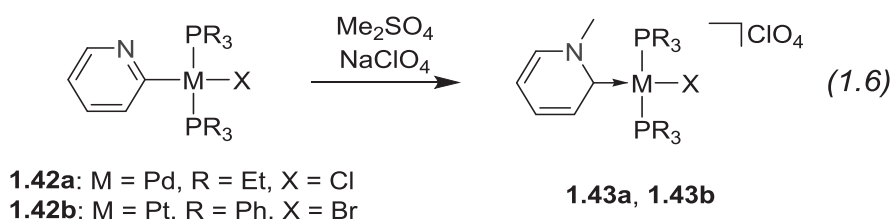
The removal of the proton on the 4-position of the pyrazolium cation is not as easy as that on the 3-position of the cation. Thus, the direct synthesis of pyrazol-4-ylidenes or their metal complexes by means of *in situ* deprotonation of a pyrazolium salt has never been reported. The first example of pyrazol-4-ylidene metal complex **1.41** was only synthesized recently by oxidative addition of C–I bond of the 4-iodo-1,2,3,5-substituted

pyrazolium salt **1.40** onto $\text{Pd}_2(\text{dba})_3$ with the presence of co-ligand PPh_3 (Eq 1.5)⁵⁶. This complex and its derivatives showed satisfactory catalytic activity in Suzuki reaction.⁵⁷ Shortly after that, the same group reported a bridged bis(pyrazolyldiene) ligand and its palladium(II) complexes.⁵⁸

1.3.3 Pyridine and diazines derived carbenes

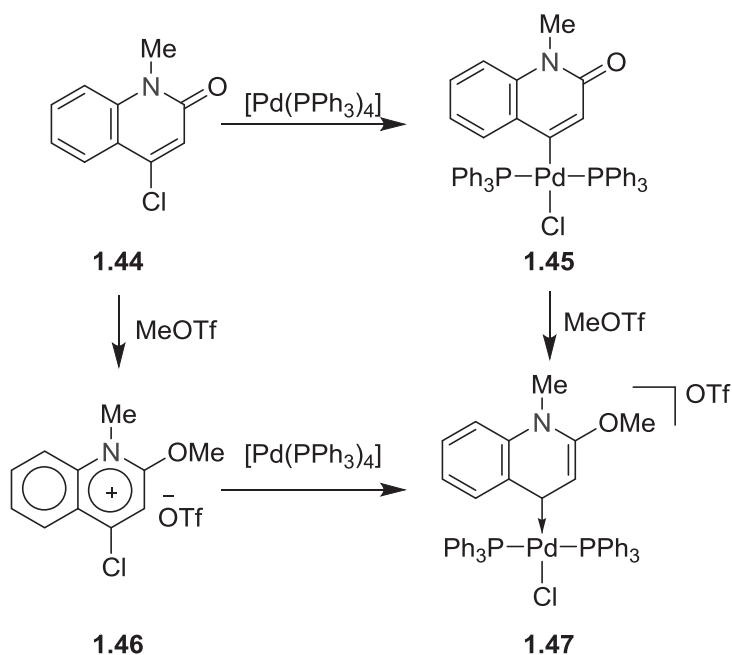
A large number of metal ($\text{M} = \text{Pd}$,⁵⁹ Pt ,^{59a, 59b, 60} Ru ,⁶¹ Os ,^{61d, 62} or Ir ⁶³) carbene complexes based on pyridylidene ligands have been synthesized and reviews on this topic were also published.⁶⁴ Interesting examples of these complexes are shown below.

The first well-defined pyridine derived metal carbene complexes were reported in 1983. Methylation of 2-pyridyl palladium (**1.42a**) or platinum complexes (**1.42b**) resulted in the corresponding *N*-methyl-pyrid-2-ylidene species **1.43a** and **1.43b** (Eq 1.6).



An *in situ* NMR study showed that, the metal-carbon bonds in **1.43a** and **1.43b** were not able to rotate freely under ambient conditions, and they were depicted as metal-carbene complexes.^{59a} CO stretching frequencies of pyridyl-2-ylidene iridium carbonyl complexes indicated that pyridyl-2-ylidenes had similar donating capacity to 1,2,3-triazolyldienes, *i. e.*, between the donating abilities of imidazol-2-ylidenes and imidazol-4/5-ylidenes.⁶⁵

Besides metal pyridyl-2-ylidene complexes **1.43a** and **1.43b**, metal pyridyl-4-ylidene derivatives **1.47** have also been synthesized *via* quinolinone (**1.44**) or quinolinium precursors (**1.46**) (Scheme 1.14).^{59b} The related computational study showed that the energy of HOMO orbital of the 4-quinolyldiene, which served as the σ -donating orbital for metal complexes, was much higher than that of the imidazolyldiene (both normal and abnormal) species, making 4-quinolyldiene an even better donating ligand.^{64a}



Scheme 1.14. Synthesis of pyrid-2-ylidene metal complexes *via* quinolinone/quinolinium precursors.

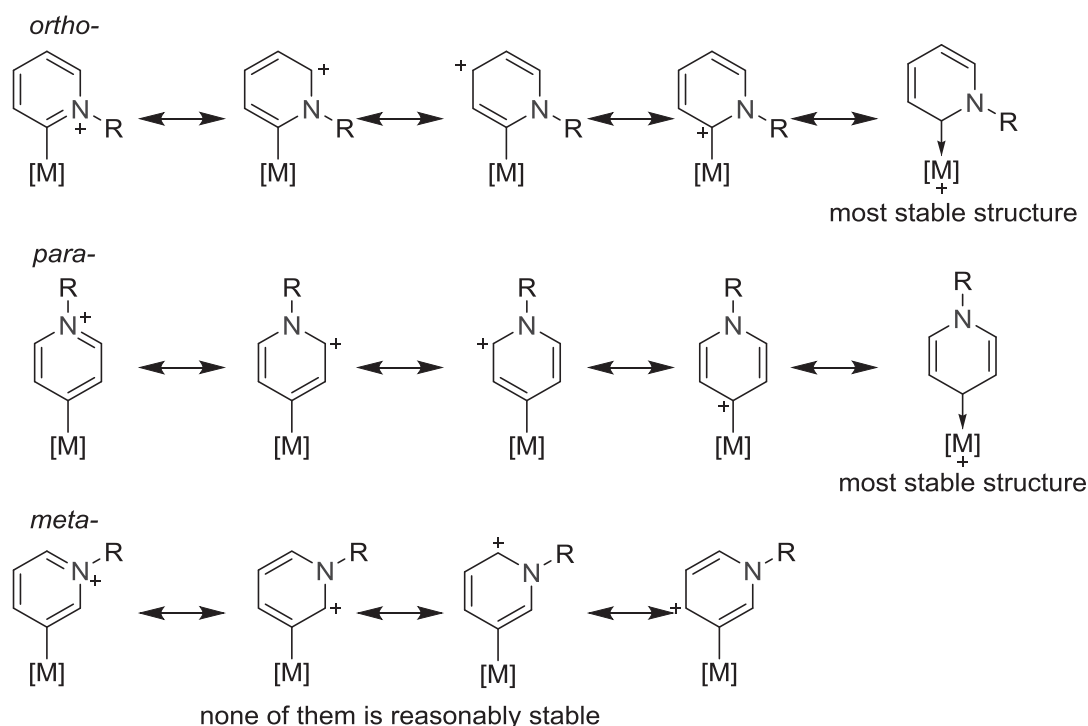
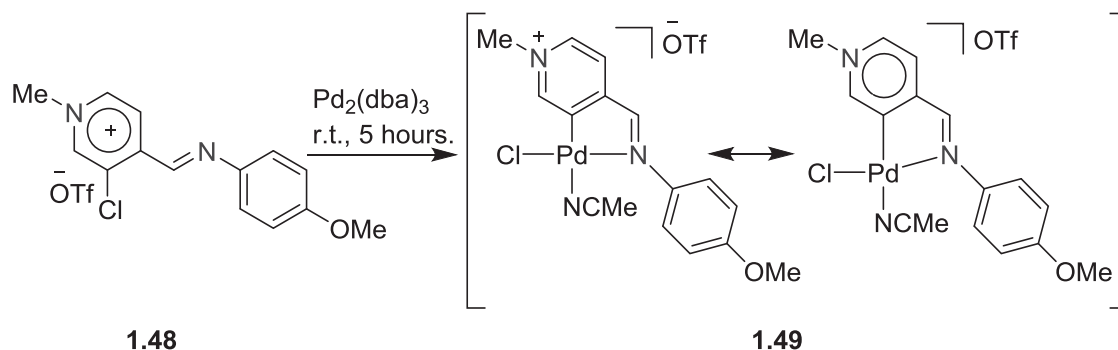


Chart 1.2. Resonance structures of different types of pyridylidene metal complexes.

Examples for *ortho*-, *para*- and *meta*- pyridylidene metal complexes are **1.43(a/b)**, **1.47** and **1.49**, respectively.

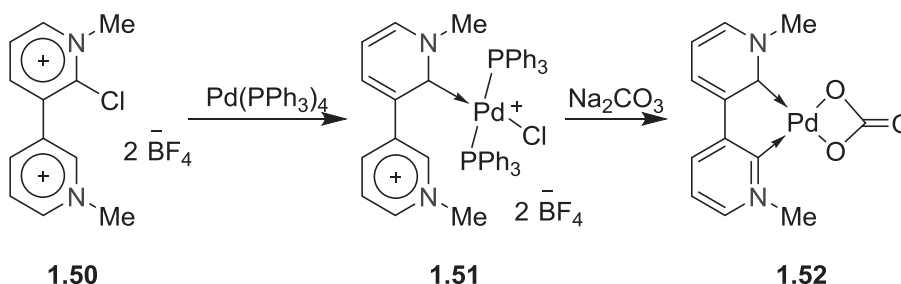
The pyridyl-3-ylidene metal complex **1.49**, although it does not have a stable resonance structure like its siblings (**Chart 1.2**), was also successfully synthesized from the

pyridinium precursors **1.48** (Scheme 1.15).^{59d} No data for the donating ability of pyridyl-3-ylidene is so far available.



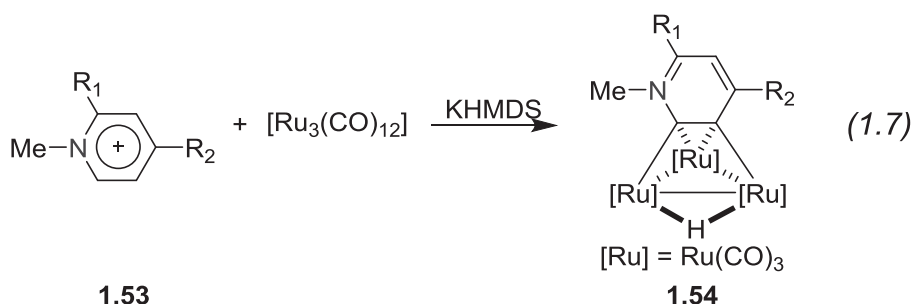
Scheme 1.15. Synthesis of pyridyl-3-ylidene metal complex *via* C–Cl bond activation.

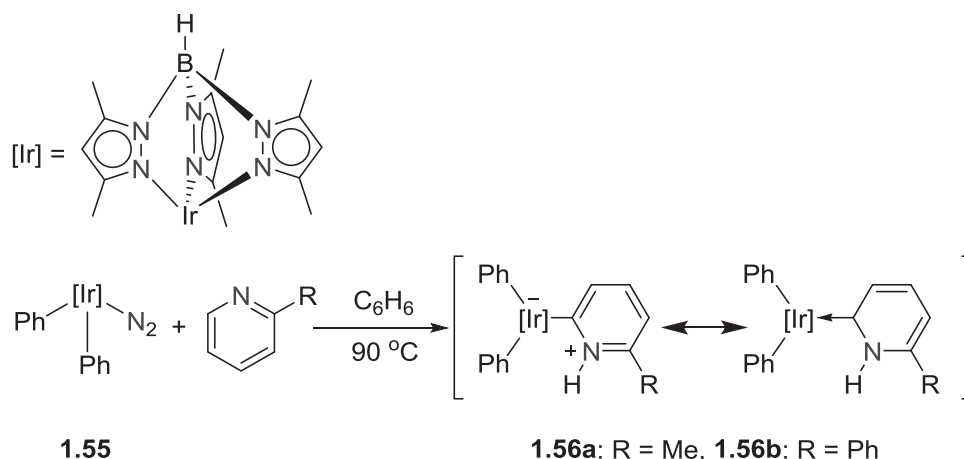
Most recently, the first bidentate bis(pyridyl-2-ylidene) palladium complex **1.52** was synthesized *via* C–Cl oxidative addition and C–H metallation (Scheme 1.16).^{59e}



Scheme 1.16. Synthesis of the first bis(pyridyl-2-ylidene) palladium complex **1.52**.

Some unconventional pyridylidene metal complexes have also been reported. For example, ruthenium pyridylidene metal cluster **1.54** was synthesized from the reaction of pyridinium precursor **1.53** and $[\text{Ru}_3(\text{CO})_{12}]$ in the presence of base (Eq 1.7).^{61a} Osmium⁶² and iridium pyridylidene complexes^{63a} were synthesized by means of direct C–H metallation reaction of pyridine with metal precursors (example complexes **1.27a** and **1.27b** in Scheme 1.17). Instead of an organic substituent, the nitrogen atom of the pyridine ring was bound to the proton which stemmed from the C–H bond activation.





Scheme 1.17. Synthesis of complexes **1.27a** and **1.27b** via direct C–H metallation of iridium reagent to 2-substituted pyridine.

Although a great number of metal carbene complexes have been synthesized based on 2-nitrogen-5-membered and 1-nitrogen-6-membered ring heterocycles, the related species derived from 2-nitrogen-6-membered ring heterocycles, *i. e.* diazine, were still quite rare.⁶⁶ Some of the examples are as shown in **Chart 1.3**.

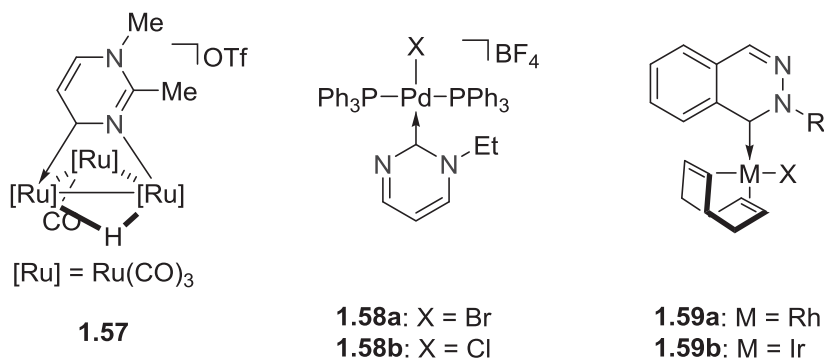


Chart 1.3. Metal carbene complexes based on diazine derivatives.

As a summary for Section **1.2** and **1.3**, the combination of computational studies by comparing the energies of HOMOs of the models of free NHCs^{55, 67} and experimental studies by comparing the CO vibration frequencies of the NHC metal complexes suggested the relative donating abilities of the above NHCs, as shown in **Chart 1.4**.

Generally, NHC with less nitrogen atoms in the ring has stronger donating ability, and in the series of NHC with the same ring, a carbene farther away from nitrogen atoms has better donating ability.

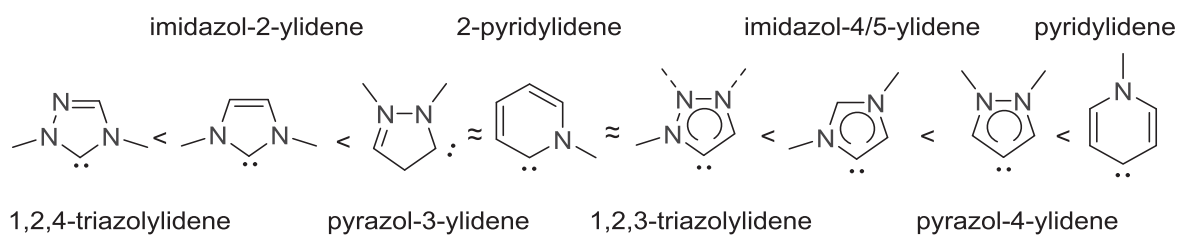
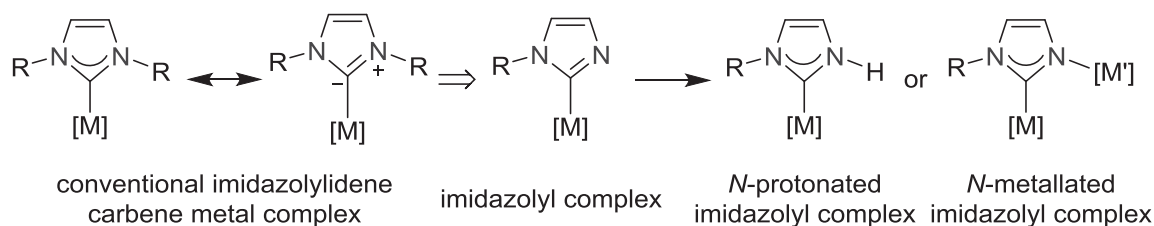


Chart 1.4. Related σ -donating abilities of different NHCs. The relative donating abilities of the NHCs increase from left to right.

1.4 Novel *N*-Heterocyclic Carbene Chemistry

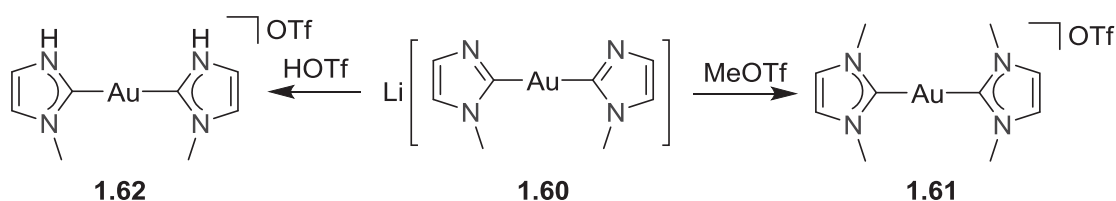
1.4.1 *N*-substituted-imidazolylidene metal complexes

A conventional imidazolylidene carbene metal complex (**Scheme 1.8**) is based on the structure of an *N,N*-disubstituted imidazolylidene ring with one carbon atom coordinated to a metal fragment. Practically, organic substituents on the nitrogen atoms are adjusted to tune the steric parameter of the ligand, yet, they have limited influence on the electronic properties of the ligand.^{15d} If only one nitrogen atom is furnished with an organic substituent, the imidazolylidene metal complex becomes an imidazolyl complex. Protonation or metallation of the other nitrogen atom in the imidazolyl ring leads to the formation of *N*-protonated or *N*-metallated imidazolyl complex (**Scheme 1.18**). The *N*-protonated or *N*-metallated imidazolyl complexes have similar mesomeric structures to imidazolylidene metal complexes, thus, they may also be *N*-heterocyclic carbene complexes.



Scheme 1.18. Imidazol-2-ylidene metal complexes in which one nitrogen is substituted by other groups.

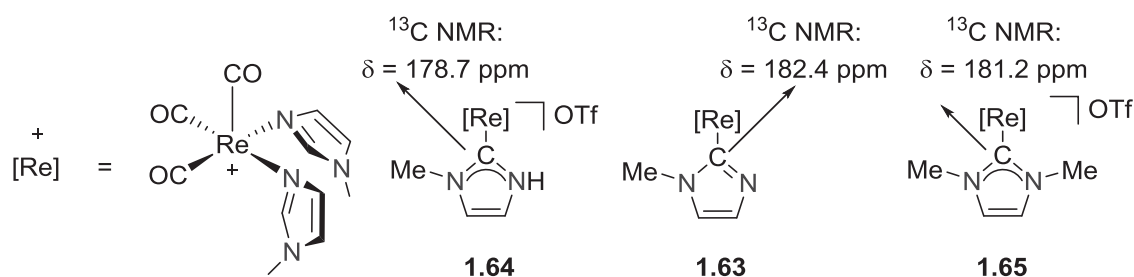
Early in 1996, Cronje reported the first example of a well-characterized gold(I) bis(imidazol-2-yl) complex **1.60**, which was protonated or methylated to complex **1.61** or **1.62** (Scheme 1.19).⁶⁸



Scheme 1.19. Early reports of gold-imidazolyl complexes.

Other metal imidazol-2-yl complexes (M = Ru,⁶⁹ Mo,⁷⁰ Mn,⁷⁰ Ni⁷¹ and Pt⁷¹) were also synthesized in the following years.

Very recently, special attention was drawn to the suspiciously low-field chemical shifts of the metallated carbon atoms of metal imidazol-2-yl complexes in the ^{13}C NMR spectra. For example, *N*-methyl imidazolidine (1-methyl-1*H*-imidazol-2-ide) coordinated to a rhenium fragment *via* C2 carbon to form an imidazolyl metal complex **1.63**, which was then protonated or methylated to complex **1.64** and **1.65**. Apparently, complex **1.65** was a typical metal carbene complex, and its analogue **1.64** was also considered as a carbene metal complex. However, it was noticed that the chemical shift of the metal-bound carbon atom in complex **1.63** was observed at $\delta = 182.4$ ppm in the ^{13}C NMR spectrum, very close to those of **1.64** and **1.65** ($\delta = 178.7$ and 181.2 ppm, respectively). Thus, the author mentioned that complex **1.63** ‘features an unprecedented NHC ligand containing a nonsubstituted nitrogen’ (Scheme 1.20).⁷²



Scheme 1.20. Chemical shifts of metal-bound carbon signals of imidazole derived rhenium complexes.

The ‘naked’ nitrogen atoms in the imidazolyl metal complexes are more nucleophilic, compared to the free nitrogen atom in an *N*-substituted-imidazole compound. Therefore, their coordinating capacities are also stronger.

Dimers or oligomers of the complexes were formed *via* the naked nitrogen atoms. Examples were these with Au(I),⁷³ Rh(I),⁷⁴ Ir(I),⁷⁴ Fe(II),⁷⁵ Pd(II)⁷⁶ and Pt(II).⁷¹ Examples are shown in **Chart 1.5**.

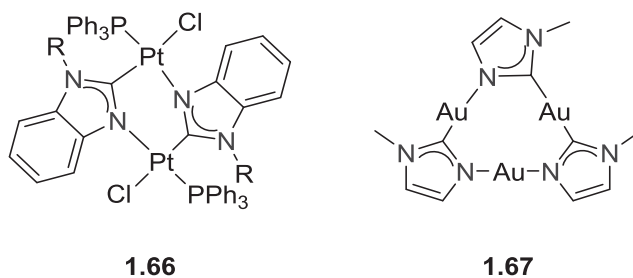
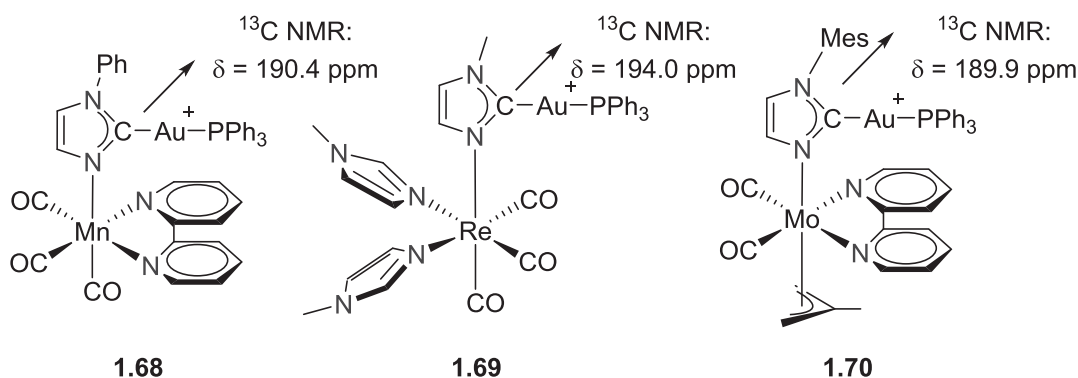


Chart 1.5. Examples of dimerized or oligomerized imidazolyl metal complexes.

The highly nucleophilic free nitrogen atom on the imidazolyl ring could also be stabilized by other metal fragments. This topic was still relatively new and only a few complexes were reported (**Scheme 1.21**).^{72, 77} Because of relatively low field signals of the metallated carbon atoms of these complexes in the ^{13}C NMR spectra, some of them were regarded as metal carbene complexes. The term ‘*N*-metallated *N*-heterocyclic carbene metal complex’ seems proper for this new type of complexes, like **1.68-1.70**.



Scheme 1.21. Examples of novel *N*-metallated *N*-heterocyclic complexes and chemical shifts of their metallated carbon atoms in the ^{13}C NMR spectra.

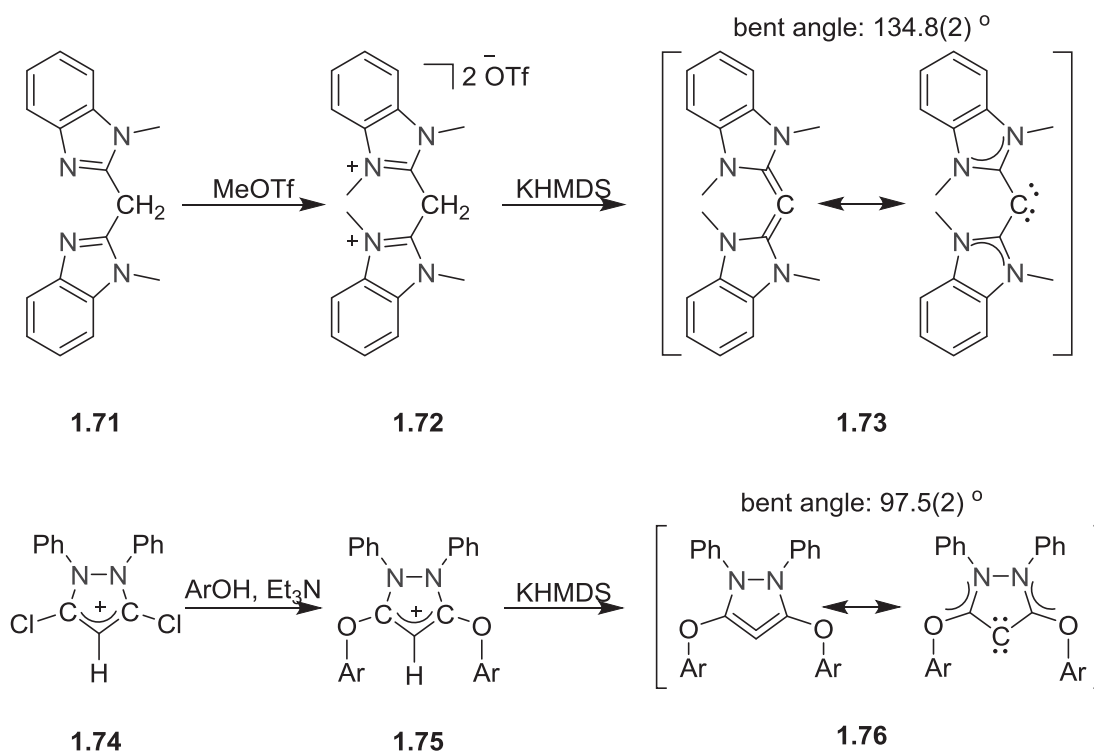
1.4.2 Carbodicarbene

A conventional allene prefers a linear geometry with the central carbon atom sp hybridized and the terminal carbon atoms sp^2 hybridized. Any effort to bend the $\text{C}-\text{C}-\text{C}$ angle from 180° , even to a small extent, will significantly decrease the stability of the compound.

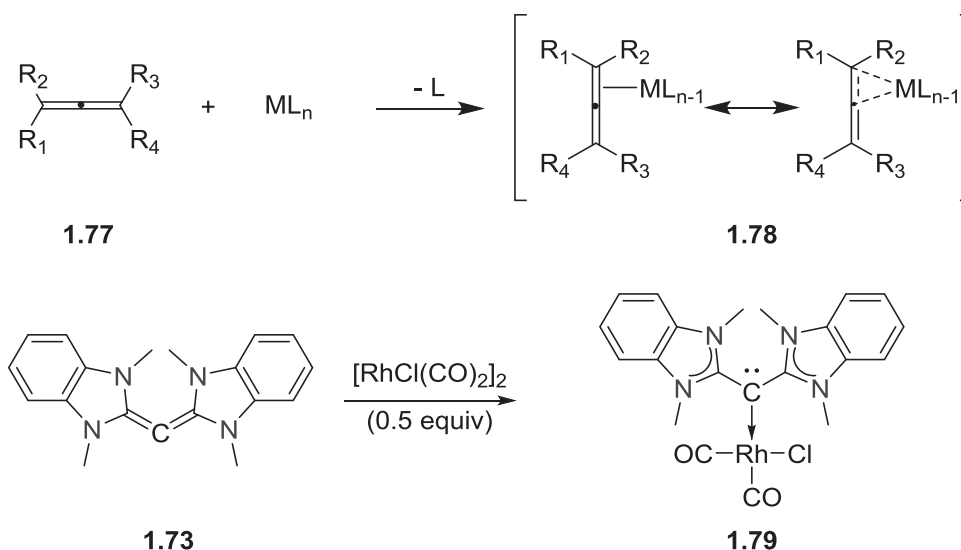
The synthesis of bent allenes, as a small topic in organic chemistry, has attracted lots of attention.⁷⁸ However, there was no significant development in this area until recently, DFT calculations signified that, strongly nucleophilic substituents on the terminal carbon atoms were able to stabilize bent allenes.⁷⁹

One year later, Bertrand and his co-workers synthesized the first example of stable bent allene, compound **1.73**, in which the central carbon was coordinated with two NHC ligands and the angle of the allenic $\text{C}-\text{C}-\text{C}$ is $134.8(2)^\circ$. Although named as ‘bent allene’, this new compound showed no similar properties to conventional allenes.⁷ At the same time, another stable bent allene **1.76** was synthesized, in which the central carbon was stabilized by aryloxy groups (**Scheme 1.22**) and the bent angle was reduced significantly to 97.5° . Both **1.73** and **1.76** showed stronger donor capacity than phosphines, five-membered ring NHCs and even strongly basic bis(diisopropylamino)carbene, according

to comparison of CO stretching vibration frequencies of their rhodium carbonyl complexes.⁸⁰



Scheme 1.22. Recent reports on extremely bent allenes.



Scheme 1.23. Different coordinative capacities of conventional allene and carbodicyclopentadiene.

The NHC-substituted bent allenes, *i. e.* carbodicyclopentadiene, were certainly a very appealing class of compounds. Normally, a conventional allene **1.77** preferred to coordinate to a metal fragment through one of its double bonds to form a π -coordination complex **1.78**;

while the carbodicarbene **1.73** coordinated to a metal fragments *via* the central carbon to generate a σ -coordination complex **1.79** (Scheme 1.23).

The central carbon in the bent allene **1.73** was sp^3 hybridized; two orbitals were occupied by two electron pairs from its own valence electrons, and the remaining two orbitals were substituted by two σ -donating NHCs, respectively. The term ‘carbodicarbene’ was chosen for this new species.

1.5 Pyrazole Bridged Ligands and their Complexes

Compartmental ligands have played an important role in controlling the cooperation of metal ions involved in the ligand system.⁸¹ As a bridging moiety, there are two adjacent nitrogen atoms available for coordination in pyrazole, which can bring metal ions in very close proximity. Therefore, pyrazole is frequently used in the designs of promising compartmental ligands.

A great number of complexes based on pyrazole-bridged compartmental ligands were reported and showed appealing results. Selected examples, such as the $[2 \times 2]$ grid complex **1.80**,⁸² the ruthenium catalyst **1.81** for water oxidation *via* the mechanism of water nucleophilic attack⁸³ and pyrazole bridged expanded porphyrin complex **1.82**,⁸⁴ are shown in **Chart 1.6**.

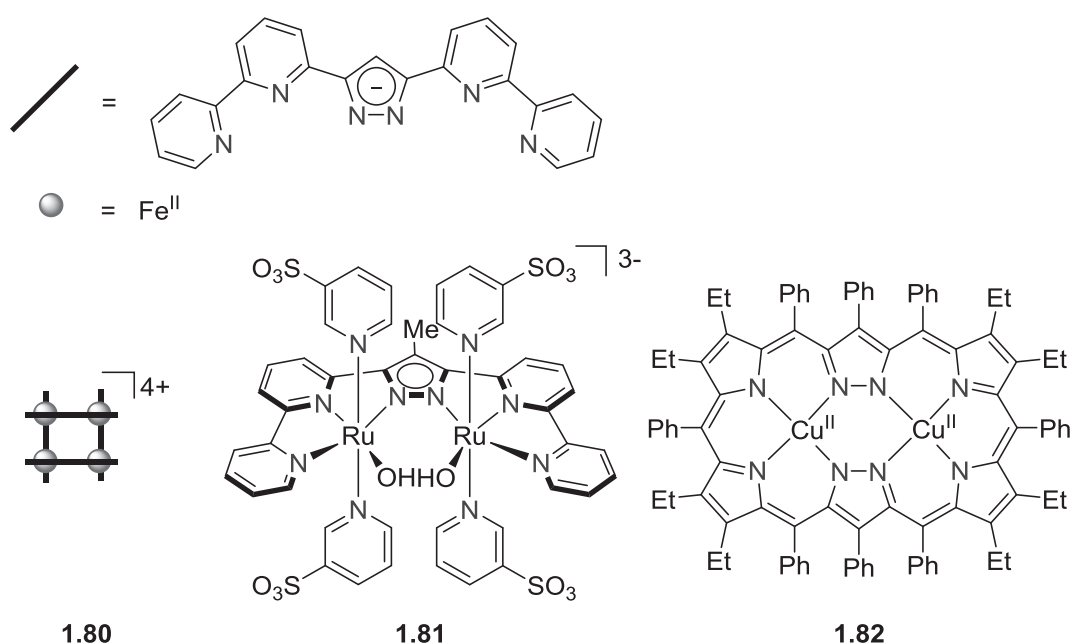
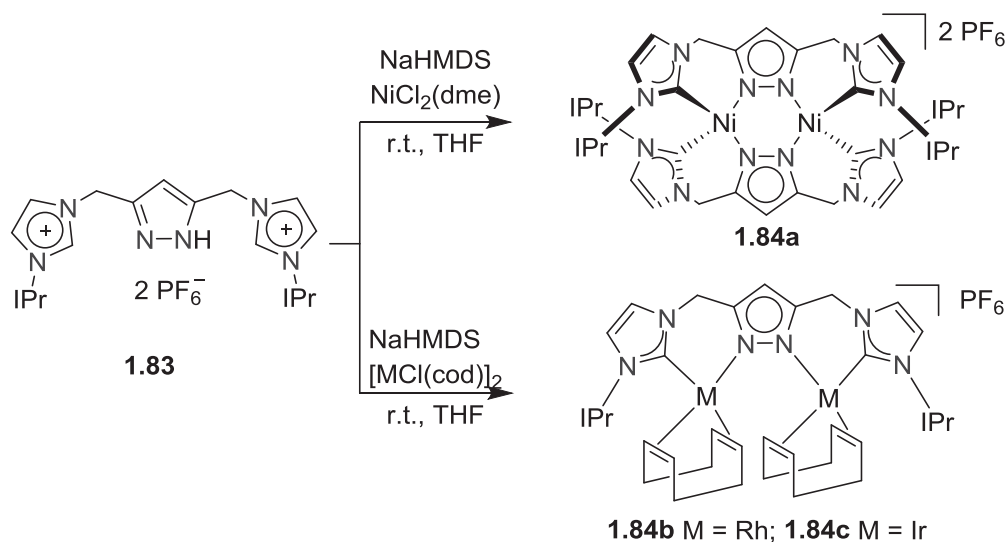


Chart 1.6. Selected recent research based on pyrazole bridged ligands.

Recently, pyrazole bridged bis(NHC) ligands (for example, **1.83** in **Scheme 1.24**) attracted some attention. The first metal complexes based on these ligands were reported in 2007. Treatment of the ligand precursors with Ag₂O formed a four-core cluster with two ligands coordinating peripherally and after transmetalation with [(Me₂S)AuCl], a similar gold cluster was formed.⁸⁵ Subsequent study on related silver complexes found that there were two possible products from the reaction of [H₃L](PF₆)₂ and Ag₂O, depending on the solvents used. If the reaction was carried out in acetone, a [(H₂L)₄Ag₄](PF₆)₂ species was formed; while if the reaction was carried out in acetonitrile,

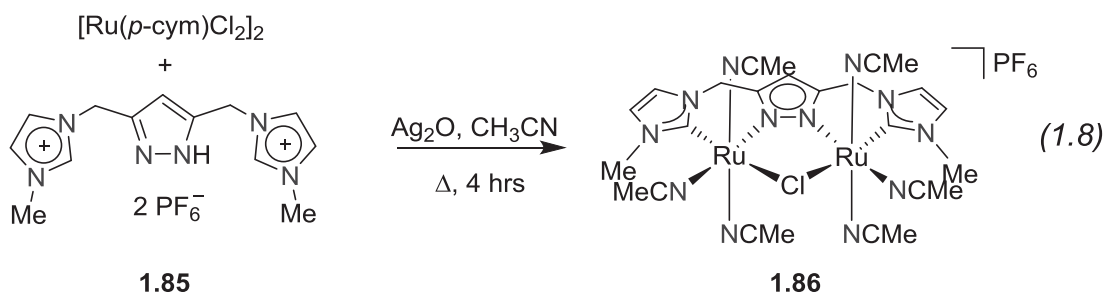
trile, the product became $[L_2Ag_2](PF_6)_2$.⁸⁶ Silver complexes based on the ligands were important intermediates for the formation of other metal complexes *via* transmetallation, for example, the formation of palladium allyl complexes based on pyrazole bridged bis(NHC) ligands.⁸⁷

Besides transmetallation *via* silver intermediates, pyrazole-bridged bis(NHC) metal complexes were also synthesized by other means. In 2008, synthesis of a class of complexes **1.84a-1.84c** was reported from the reaction of ligand precursors **1.83** and metal reagents in the presence NaHMDS.⁸⁸ Note that, the reaction of the ligand precursor with $Ni(dme)Cl_2$ in presence of NaHMDS did not give the neutral species LNi_2Cl_3 (L = ligand), but a $[L_2Ni_2]^{2+}$ cationic species **1.38a**, in which both nickel coordination cores were severely distorted from square planar, probably due to the repulsion between the two neighbored wingtips (**Scheme 1.24**).



Scheme 1.24. Dinuclear metal complexes based on pyrazole bridged bis(NHC) ligand.

In 2013, the first ruthenium complex **1.86** based on pyrazole-bridged bis(NHC) ligand **1.85** was reported and the complex showed interesting electrochemical properties (Eq 1.8).⁸⁹ It was noteworthy that Ag_2O was added as exterior base for the deprotonation of the ligand precursors; however, the actual mechanism might still contain transmetallation *via* silver intermediates.





1.6 Conclusion

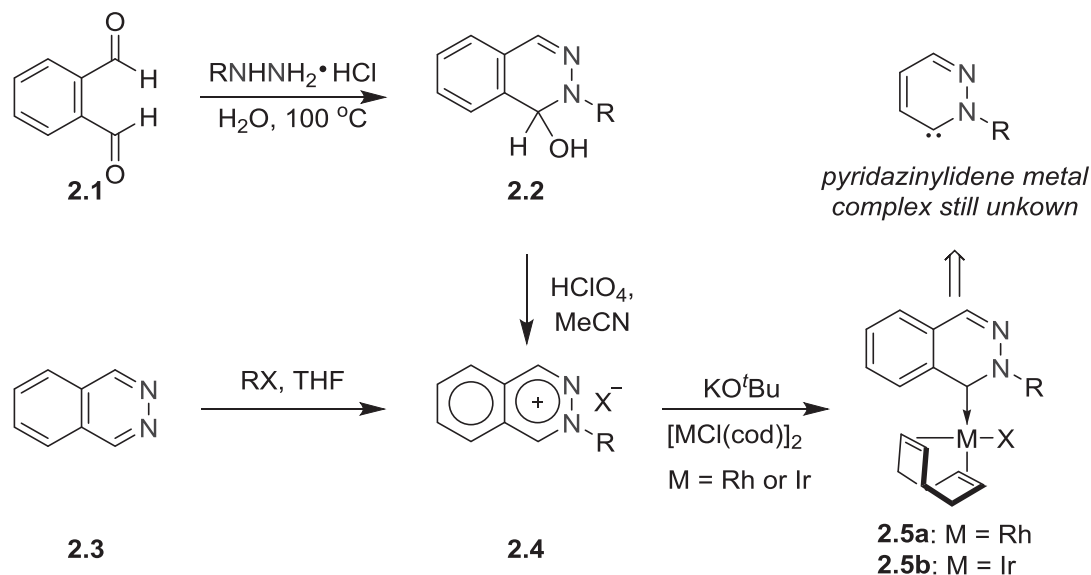
As one of the most important ligand systems for metal complexes, NHCs have been widely studied and applied in various areas. The discovery of unconventional NHCs opened a new era for the development of NHC chemistry. More attention has been focused on their applications in catalysis and functionalization in larger ligand systems. Meanwhile, the prevailing concept ingrained in chemists that carbon is a nonmetallic element is challenged by the recent synthesis of carbodicarbene compound.⁹⁰

CHAPTER 2. Pyridazine Derived *N*-Heterocyclic Carbene Palladium Complexes

2.1 Introduction and Motivation

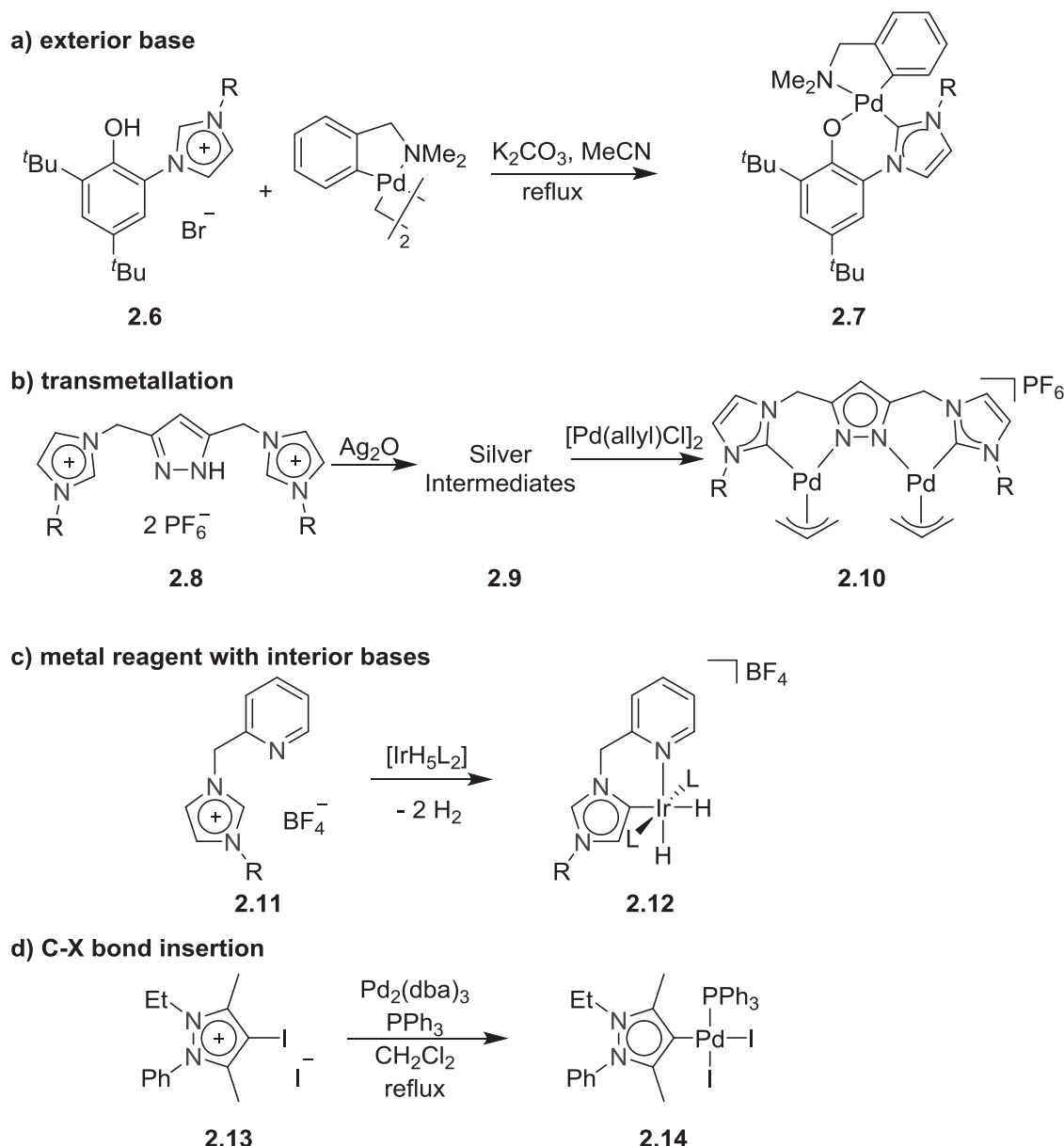
Despite the fact that lots of metal pyridylidene complexes have been synthesized (§1.3.3, Chapter 1), complexes based on diazine derived carbenes, especially pyridazine derivatives, were still rare (**Chart 1.3**, Chapter 1). So far only one class of metal carbene complexes based on phthalazine have been reported (**Scheme 2.1**).^{66c} Alkylation of phthalazine **2.3** or dehydration of compound **2.2** led to the formation of phthalazinium salt **2.4**, which was treated with metal species ($M = \text{Rh}$ or Ir) in the presence of potassium *tert*-butoxide to give phthalazinylidene carbene metal complexes **2.5a** and **2.5b**.

However, metal carbene complexes based on pyridazinylidene are still unknown. The target of this work is to synthesize the first examples of pyridazinylidene palladium complexes.



Scheme 2.1. Report on synthesis of phthalazine derived metal carbene complexes.

Previously, *N*-heterocyclic carbene metal complexes were synthesized by various methods. Examples of most common synthetic strategies are shown in **Scheme 2.2**:



Scheme 2.2. Synthetic strategy for the formation of metal NHC complexes.

a) the ligand precursor **2.6** was deprotonated by the exterior base, generating a free carbene species, which would coordinate to metal fragments *in situ* to form the related complex **2.7**;^{22b}

b) pro-ligand **2.8** reacted with silver oxide to give a silver complex **2.9**, which was then treated with palladium species, resulting in palladium carbene complex **2.10**;⁹¹

c) the direct reaction of ligand precursor **2.11** with metal hydride complex $[\text{IrH}_5(\text{PPh}_3)_2]$ (or other metal complex involving an interior base, such as acetate or acetylacetonate) to form metal complex **2.12**;²³ and



d) the oxidative addition of C–I bond onto low valent metal complex $[\text{Pd}_2(\text{dba})_3]$, generating the corresponding complex **2.14**, in which the oxidation state of the palladium atom was increased to +II⁵⁶.

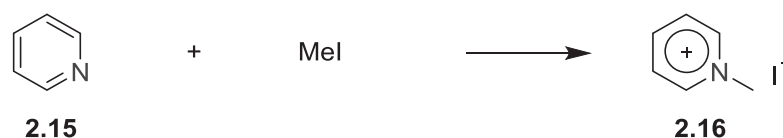
The last method had an obvious disadvantage that only limited types of metal complexes were able to be synthesized; however, the advantages of the method included mild reaction condition and comparatively higher yield. Particularly, recent reports on remote *N*-heterocyclic carbene complexes frequently adopted this methodology,^{28b, 56} which was also applied in this work for the formation of the first examples of pyridazine derived palladium(II) carbene complexes.⁹²

2.2 Result and Discussion

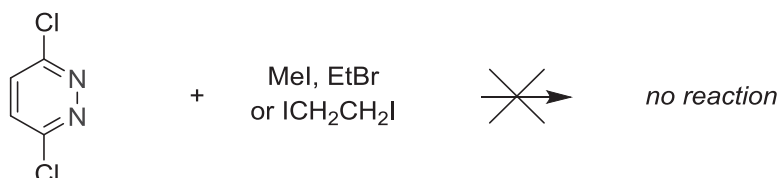
2.2.1 Synthesis of ligand precursors

The reaction of pyridine **2.15** with methyl iodide could easily form the *N*-methyl pyridinium salt **2.16**.⁹³ However, a primary trial to synthesize pyridazinium from the treatment of 3,6-dichloropyridazine with alkyl halide failed. Under varied reaction conditions, including longer reaction time, higher reaction temperature and pressure, the starting material 3,6-dichloropyridazine still remained intact (**Scheme 2.3**). Considering the fact that phthalazine **2.3** could be alkylated by regular alkyl halide to form phthalazinium salt **2.4** (**Scheme 2.1**),^{66c} it was assumed that the chloride atoms on the 3-/6- position of pyridazine reduced the nucleophilicity of the nitrogen atoms of 3,6-dichloropyridazine.

Literature:

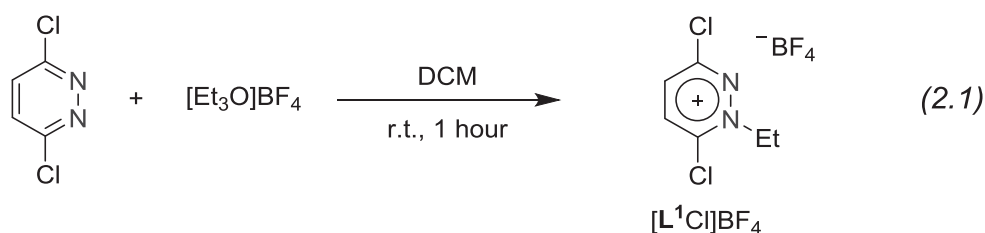


This work:

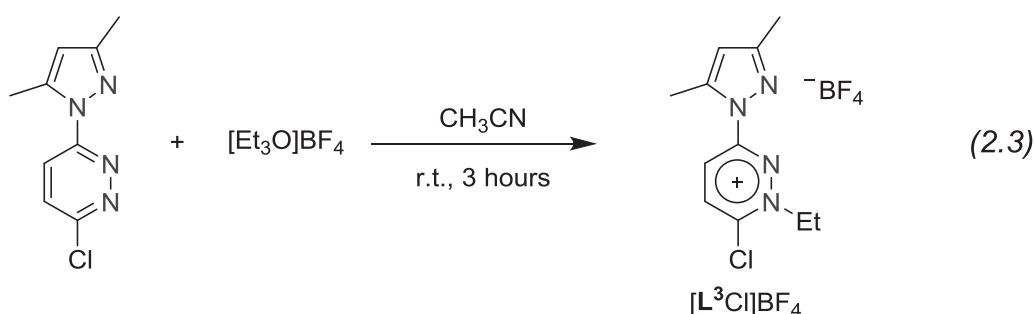
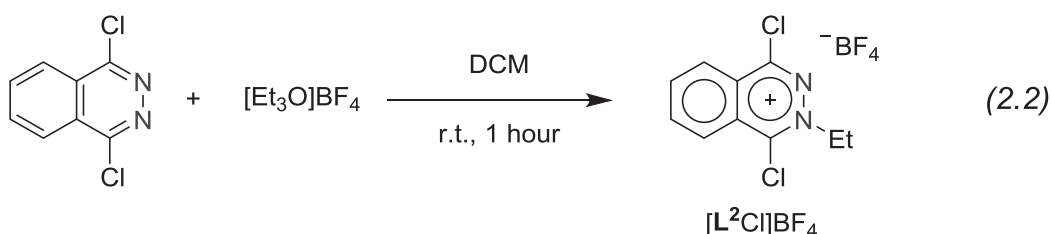


Scheme 2.3. Alkylation of the nitrogen atom of 3,6-dichloropyridazine by regular alkylation reagents failed.

Meerwein's salt, [Et₃O]BF₄, is a strong alkylation reagent and treatment of 3,6-dichloropyridazine with [Et₃O]BF₄ in dichloromethane gave a white precipitate after stirring at room temperature for one hour, which was confirmed to be 1-ethyl-3,6-dichloropyridazinium tetrafluoroborate, [L¹Cl]BF₄ (Eq 2.1), by multinuclear NMR spectroscopic data.



In the ^1H NMR spectrum, the signals of the aromatic protons shift from $\delta = 7.71$ ppm for 3,6-pyridazine to 8.46 ppm and 8.54 ppm for $[\text{L}^1\text{Cl}]\text{BF}_4$; in the ^{13}C NMR spectrum, the signal of C3 and C6 shift from $\delta = 155.8$ ppm for 3,6-dichloropyridazine to 154.3 ppm of C6 and 156.7 ppm of C3 for $[\text{L}^1\text{Cl}]\text{BF}_4$. High resolution ESI mass spectrum showed a major peak at $m/z = 176.9980$, consistent with the calculated data (176.9981) and with the characteristic isotope pattern of $[\text{L}^1\text{Cl}]^+$.



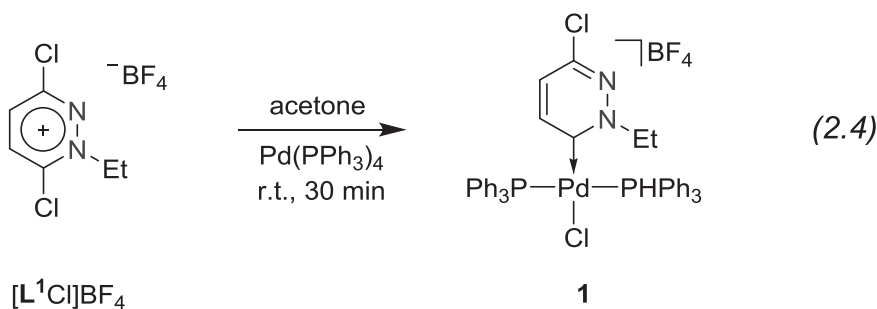
Similar reactions of 1,4-phthalazine or 3-chloro-6-(3,5-dimethylpyrazol-1-yl)pyridazine with $[\text{Et}_3\text{O}]\text{BF}_4$ resulted in the required diazinium salts, 2-ethyl-1,4-phthalazinium tetrafluoroborate ($[\text{L}^2\text{Cl}]\text{BF}_4$) and 1-ethyl-3-chloro-6-(3,5-dimethylpyrazol-1-yl)pyridazinium tetrafluoroborate ($[\text{L}^3\text{Cl}]\text{BF}_4$), respectively (Eq 2.2 and Eq 2.3). The formation of $[\text{L}^3\text{Cl}]\text{BF}_4$ took longer reaction time and gave comparatively low yield. Both of the two ligand precursors were confirmed by the data from the multinuclear NMR spectroscopy and high resolution mass spectrometry. Comparison of the data for these three ligands is shown in **Table 2.1**. It is noteworthy that the carbon atom at α position of the ethylated nitrogen atom has a higher-field chemical shift than that of the carbon atom at δ position of the ethylated nitrogen atom in each precursor.

Table 2.1. Selected ^1H , ^{13}C and ^{31}P NMR data for the three ligand precursors.

		$[\text{L}^1\text{Cl}]\text{BF}_4$	$[\text{L}^2\text{Cl}]\text{BF}_4$	$[\text{L}^3\text{Cl}]\text{BF}_4$
^1H NMR	CH^{Pyri}	8.54 (d), 8.46 (d)	<i>n./a.</i>	8.85 (d), 8.45 (d)
	CH_2	4.93 (q)	5.05 (q)	4.91 (q)
	CH_3	1.65 (t)	1.71 (t)	1.67 (t)
^{13}C NMR	Cl–C(α to N–Et)	154.3 (s)	156.4 (s)	155.2 (s)
	Cl/Pz–C	156.7 (s)	155.6 (s)	154.7 (s)
	CH^{Pyri}	139.6 (s),	128.8 (s),	138.7 (s),
		139.5 (s)	128.0 (s)	130.3 (s)

2.2.2 Synthesis of novel NHC complexes

Under inert gas atmosphere was the mixture of $[\text{L}^1\text{Cl}]\text{BF}_4$ and $\text{Pd}(\text{PPh}_3)_4$ stirred in acetone at room temperature for 30 minutes. A white solid could be isolated after purification, which was confirmed to be a novel pyridazinylidene metal carbene complex **1** by multinuclear NMR spectroscopic data (Eq 2.4).



The product is soluble in dichloromethane, slightly soluble in acetone, acetonitrile or THF and insoluble in diethyl ether, toluene or hexanes. The product is reasonably stable in aerobic and moisture condition. In the ^{13}C NMR spectrum, the triplet ($J_{\text{PC}} = 6.9$ Hz) at $\delta = 192.6$ ppm was assigned to the Pd–C carbon, which was also consistent with the reported chemical shifts of the carbenes of palladium pyrimidinylidene complexes (197.1–199.5 ppm).^{66b} The multinuclear NMR data of complexes **1–4** in this chapter are collected in **Table 2.2**.

The high resolution ESI mass spectrum of complex **1** in acetonitrile showed a base peak at $m/z = 809.0837$, consistent with the calculated data 809.0837 of the isotope pattern of $[\text{M} - \text{BF}_4]^+$ cation (**Figure 2.1**).

Table 2.2. Selected NMR data for the comparison of complex **1** to complex **4**.

		1	2	3	4
¹ H NMR	CH ^{Pyri}	7.72 (d), 6.70 (d)	<i>n./a.</i>	7.95 (dd), 6.89 (d)	<i>merged in</i> 7.62-7.28
	CH ₂	4.59 (q)	4.84 (q)	5.38 (dq), 4.55 (m)	4.50 (q)
	CH ₃	1.14 (t)	1.15 (t)	1.53 (t)	1.06 (s)
¹³ C NMR	PdC	192.6 (t)	199.4 (t)	191.5 (s)	187.5 (t)
	Cl/Pz-C	154.4 (s)	154.9 (s)	153.6 (s)	154.2 (s)
	CH ₂	64.3 (s)	63.4 (s)	64.7 (s)	63.9 (s)
	CH ₃	13.9 (s)	13.4 (s)	14.6 (s)	13.8 (s)
³¹ P NMR	PPh ₃	20.9 (s)	21.1	26.1	21.5

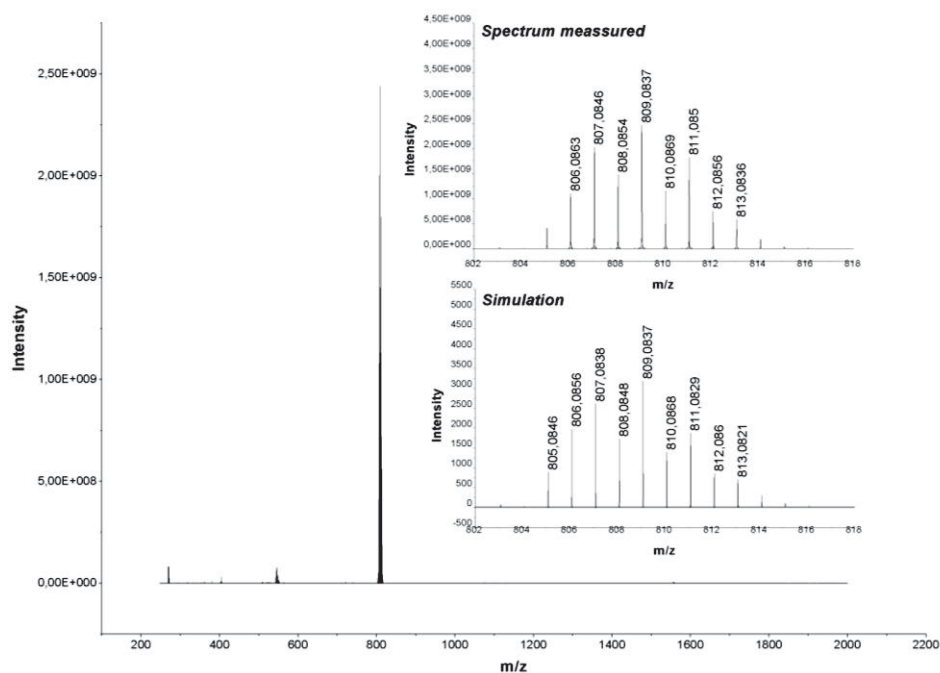


Figure 2.1. High resolution ESI mass spectrum of complex **1** in acetonitrile. The inset shows the experimental and simulated isotopic distribution patterns for $[\text{C}_{42}\text{H}_{37}\text{N}_2\text{Cl}_2\text{P}_2\text{Pd}]^+$.

Crystalline materials of complex **1** could be obtained by slow diffusion of diethyl ether into the solution of raw material in dichloromethane. Its structure was confirmed by X-ray diffraction (**Figure 2.2**). The metal center adopts a square-planar geometry with two

phosphines *trans* to one another; while the pyridazinylidene and chloride ligands are *trans* to each other.

The bond length of Pd1–C1 is 1.996(2) Å, very close to that of a related pyrid-2-ylidene palladium complex (1.98–2.00 Å).^{59d} The bond length of C1–N1 (1.337(3) Å) is larger than N2–C4 (1.301(3) Å), indicating the C1–N1 bond is elongated due to the back-bonding from palladium to the carbene and the delocalization of the conjugated π system is partially influenced. The pyridazinylidene ligands are found almost orthogonal to the square-plane core with a dihedral angle of 87°. Note that, obvious π – π interaction between the pyridazine ring and two phenyl groups of the phosphine ligands is observed, forming a ‘sandwich’ pattern. In order to do so, the phenyl groups deviate from the P–C bond by 10.5° and 11.2°, compared to the cases of other phenyl groups with the bending angles of only 1.3–2.8°. The distance of the ring centroids is 3.4 Å, though both phenyl rings are not perfectly overlapped with the pyridazine ring. A possible explanation for the phenomenon is that the *N*-alkylated pyridazine ring is electron-deficient and the phenyl groups serve as π -donors to stabilize the pyridazine ring.

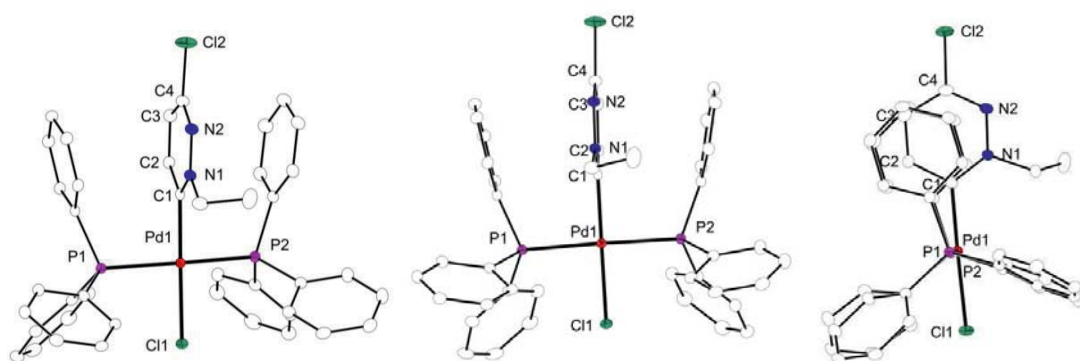
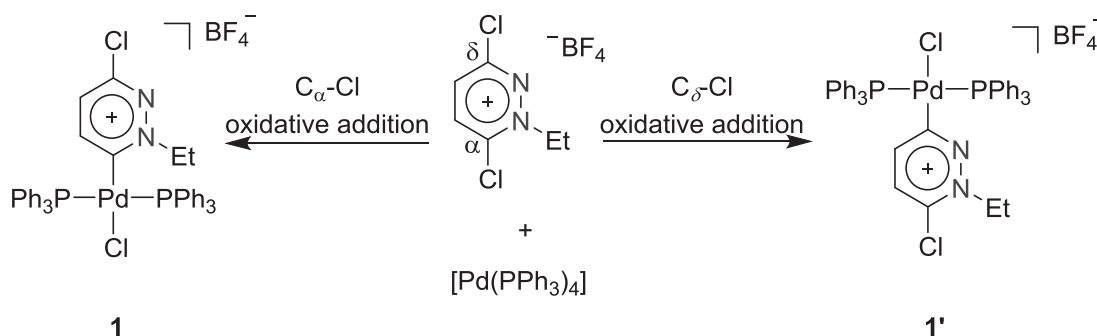


Figure 2.2. Different views of the molecular structure of the cation of **1** (middle and right views for emphasizing the π – π interaction). Anisotropic displacement ellipsoids drawn at 30% probability level. BF_4^- and hydrogen atoms have been omitted for clarity. Selected bond lengths [Å] angles [°]: Pd1–C1 1.996(2), Pd1–P1 2.3331(5), Pd1–P2 2.3343(5), Pd1–Cl1 2.3422(5), C1–Pd1–P1 91.50(6), C1–Pd1–P2 89.72(6), P1–Pd1–Cl1 88.962(19), P2–Pd1–Cl1 90.10(2)..

During the formation of complex **1**, it was noticed that, there were two C–Cl bonds (labeled as C_α –Cl and C_δ –Cl) in the ligand precursor $[\text{L}^1\text{Cl}]\text{BF}_4$. Recall the formation of pyrid-3-ylidene metal complex **1.49** (Scheme 1.15, Chapter 1) after the oxidative addition of the C–Cl bond at the *meta* position of the alkylated nitrogen atom onto the Pd(0) species, in the same manner, it was assumed that the oxidative addition of C_δ –Cl bond of

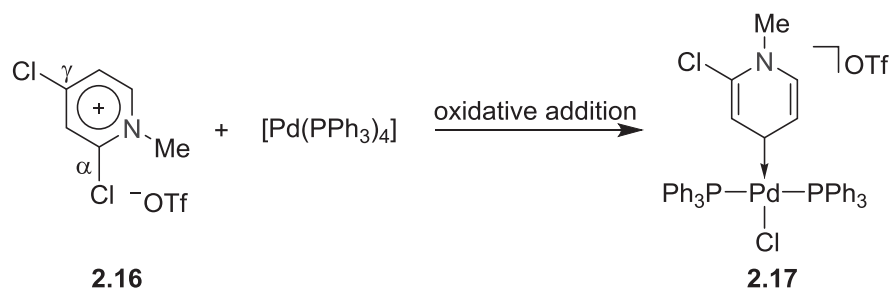
$[\text{L}^1\text{Cl}]\text{BF}_4$ onto $[\text{Pd}(\text{PPh}_3)_4]$ was also possible, thus forming complex **1'**, an isomer of complex **1** (Scheme 2.4).



Scheme 2.4. Hypothetical formation of two isomers from the reaction.

Clearly, during the formation of complex **1'**, the steric congestion between the co-ligands and the ethyl group on the NHC ligand would be better avoided. Thus, from the kinetic point of view, the formation of complex **1'** might be favored. However, an *in situ* ^1H NMR monitoring showed that, during the reaction, there was no signal indicating the formation of a second complex, thus, complex **1** was the sole product from the reaction.

It was reported that the reaction of *N*-methyl-2,4-dichloropyridinium salt **2.16** with $[\text{Pd}(\text{PPh}_3)_4]$ selectively formed the remote carbene, pyridyl-4-ylidene, metal complex **2.17** (Scheme 2.5), when there was another C–Cl bond available for oxidative addition. In the paper, the selective formation of complex **2.17** was rationalized that $\text{Pd}(0)$ complexes, with d^{10} configurations, were strong nucleophiles and preferred to insert onto more electrophilic bond, which was the $\text{C}_\gamma\text{--Cl}$ instead of $\text{C}_\alpha\text{--Cl}$ bond in **2.16**, according to their chemical shifts in the ^{13}C NMR spectra. Thus, the oxidative addition occurred at the $\text{C}_\gamma\text{--Cl}$ bond, generating the remote NHC metal complex **2.17**.⁹⁴



Scheme 2.5. Reported example of selective formation of complex **2.17** when there were two C–Cl bonds in ligand precursor **2.16**.

In this work, the 2D $^{13}\text{C}\text{--}^1\text{H}$ HMBC NMR spectroscopy (Figure 2.3) of $[\text{L}^1\text{Cl}]\text{BF}_4$ shows the carbon chemical shift of C_α at slightly higher field (154.3 ppm) than that of C_δ (156.7

ppm), suggesting the C_α is more shielded and thus more nucleophilic. Since the insertion of Pd(0) species selectively occurs at the less electrophilic C_α -Cl bond, the electrophilicity of the C-Cl bond is not the reason for the selective formation of complex **1**.

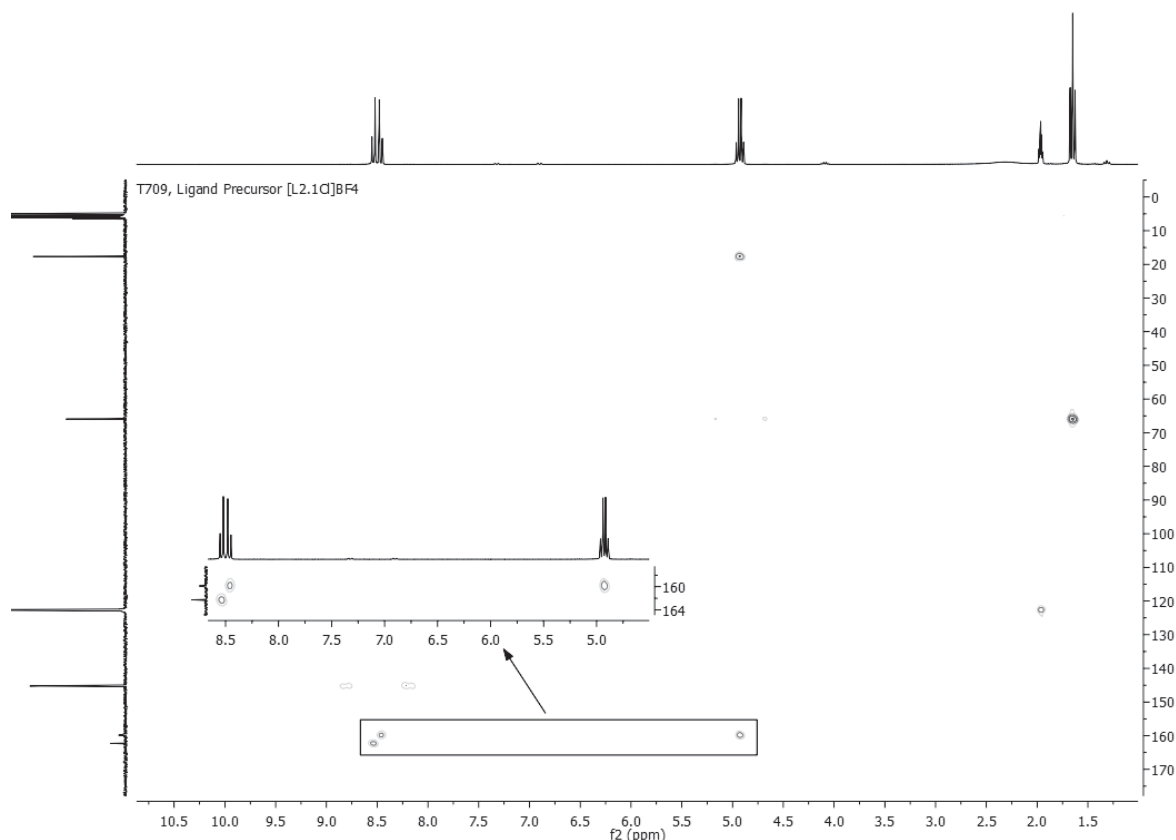
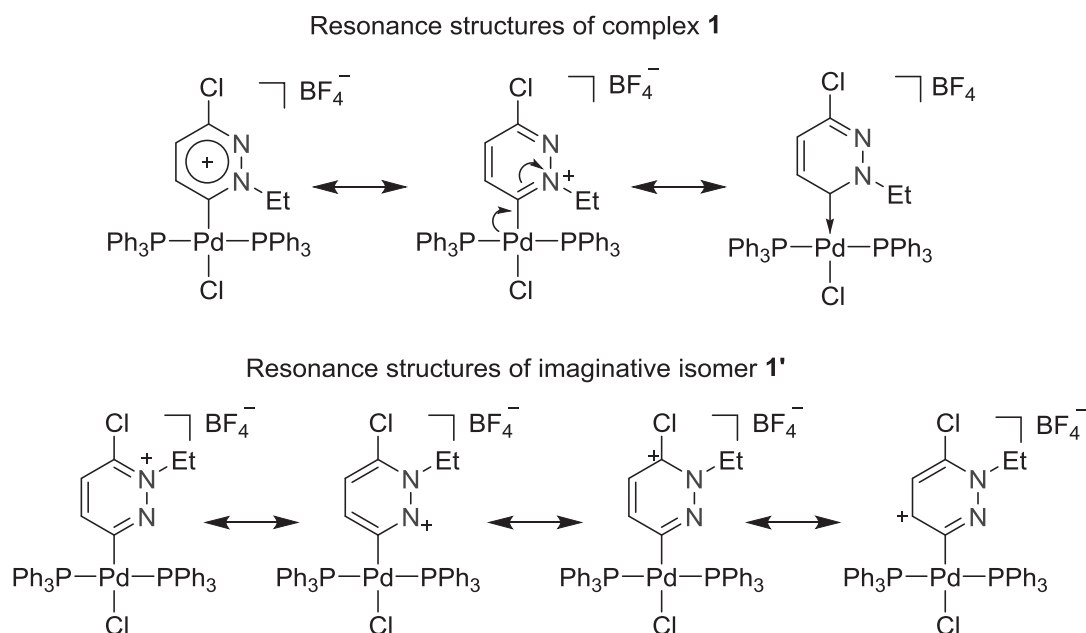


Figure 2.3. The 2D ^{13}C - ^1H HMBC NMR of $[\text{L}^1\text{Cl}]\text{BF}_4$, indicating a more shielded C_α -Cl carbon.

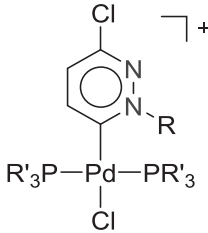
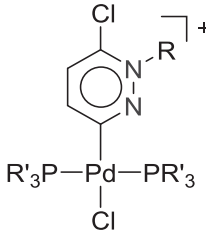
Another instinctive explanation is that complex **1** has stable mesomeric structures to hold the positive charge generated from the ethylation on the nitrogen atom; while no similar resonance structures of its congener **1'** can be drawn (**Scheme 2.6**). Thus, it is assumed that **1** is thermodynamically favored.

To confirm the above hypothesis, DFT calculations were carried out. Relative energies (E_{rel}) have been computed at the BP86/TZVPP level of theory. To avoid any possible π - π stacking effect between the pyridazine ring and the adjacent phenyl groups, calculations on models in which PPh_3 was replaced by PMe_3 were also performed. Moreover, to see the steric effect of the *N*-alkyl group, models with $\text{R} = \text{Me}$ were also processed (results in **Table 2.3**). **A1-A4** series are the models for pyridazin-6-ylidene palladium complexes and **B1-B4** series are the models for pyridazin-3-ylidene palladium complexes.



Scheme 2.6. Resonance structures of complex **1** and its imaginative isomer **1'**.

Table 2.3. Computation on the relative energies between model **A**, where Pd(0) inserts to C_α-Cl, and model **B**, where Pd(0) inserts to C_δ-Cl.

Entry				$E_{\text{rel}}(\mathbf{B}-\mathbf{A})$ (kcal/mol)
1	R = Et, R' = Ph	A1	B1	+8.4
2	R = Me, R' = Ph	A2	B2	+9.7
3	R = Et, R' = Me	A3	B3	+7.5
4	R = Me, R' = Me	A4	B4	+7.1

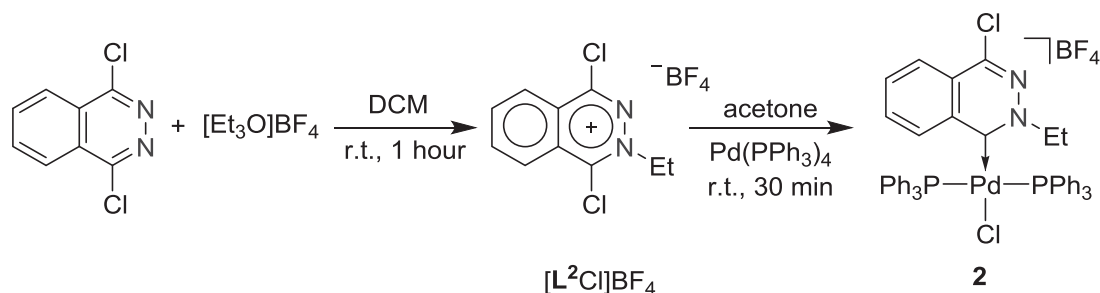
The calculated molecular structure **A1** is in good agreement with the molecular structure of **1** in solid state as determined by X-ray diffraction, except for some difference in the Pd-P bond lengths (**Table A24**). A likely reason for this discrepancy might be the attractive π - π interaction of the phenyl of the PPh₃ and the pyridazine ring, which is not con-

sidered appropriately at the applied level of theory. Since the effect of the attractive π - π interaction is not profound, the calculated result can be regarded as reliable.

The result shows that, in all cases, model **A** is more stable than its congener **B** by about 7.1 to 9.7 kcal/mol. The energy difference between **A1** and **B1** is 8.4 kcal/mol, which is large enough to allow only one isomer **A1** to form, from the thermodynamic stability point of view; while the energy difference between **A2** and **B2** is even larger (9.7 kcal/mol), indicating that the bulkiness of the R group on the pyridazine ring does influence the stability of **A** series. Comparison of **Entry 1** and **Entry 3** suggests that the bulkiness of the phosphine ligands has some influence to the relative stability of two isomers, yet, the impact is not profound.

Reaction of 1,4-dichlorophthalazine with $[\text{Et}_3\text{O}]\text{BF}_4$ resulted in a white powder of 2-ethyl-1,4-dichlorophthalazinium tetrafluoroborate, $[\text{L}^2\text{Cl}]\text{BF}_4$. Different from $[\text{L}^1\text{Cl}]\text{BF}_4$, $[\text{L}^2\text{Cl}]\text{BF}_4$ is slightly hygroscopic, and in aerobic conditions, the white solid became a colorless gel and gave a strong acidic smell, indicating the possible decomposition of the ligand precursor. Thus, the ligand precursor should be kept under inert gas atmosphere.

Ligand precursor $[\text{L}^2\text{Cl}]\text{BF}_4$ reacted with $\text{Pd}(\text{PPh}_3)_4$ in acetone at room temperature gave the expected palladium carbene complex **2** (**Scheme 2.7**). The formation of complex **2** was confirmed by multinuclear NMR spectroscopic data and the structure was confirmed by X-ray diffraction (**Figure 2.4**).



Scheme 2.7. Synthesis of ligand precursor $[\text{L}^2\text{Cl}]\text{BF}_4$ and complex **2**.

The product is a white powder, stable in aerobic and moist atmosphere and soluble in dichloromethane, slightly soluble in acetonitrile, THF or acetone and insoluble in diethyl ether, toluene and hexanes. Similar to complex **1**, the signal of the metallated carbon of complex **2** was observed as a triplet ($J_{\text{PC}} = 6.3$ Hz) at $\delta = 199.4$ ppm in the ^{13}C NMR spectrum. The $\text{Pd}-\text{C}_{\text{carbene}}$ bond length of **2** is 1.989(5) Å, slightly shorter than that of complex **1**. Because of the presence of the fused benzene ring, the L^2 -NHC ligand is more electron-rich than L^1 -NHC, which means L^2 -NHC is a better electron donor, thus leading to a stronger NHC-metal bond.

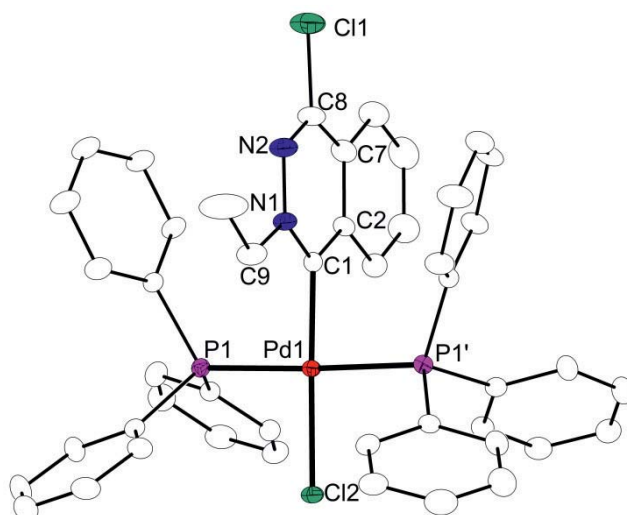
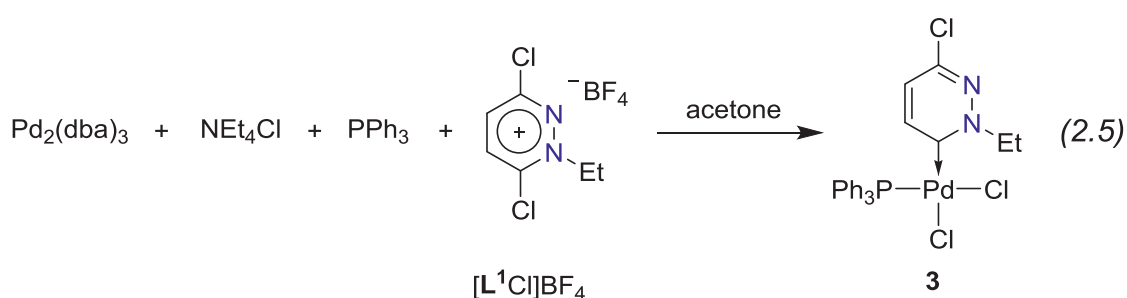


Figure 2.4. Molecular structure of **2**. Anisotropic displacement ellipsoids drawn at 30% probability level. The solvent molecule, BF_4^- and hydrogen atoms have been omitted for clarity. Selected bond lengths[Å] angles [°]: Pd1–C1 1.989(5), Pd1–P1 2.3439(8), Pd1–P2 2.3438(8), Pd1–Cl2 2.3513(12), C1–Pd1–P1 88.89(2), C1–Pd1–P2 88.89(2), P1–Pd1–Cl2 91.08(2), P2–Pd1–Cl2 91.08(2).

In order to get the information of the rotational dynamics of the novel pyridazinylidene ligand, the synthesis of the complex with only one phosphine ligand was also sought. After several trials, it was found that a mixture of $[\text{L}^1\text{Cl}]\text{BF}_4$, $\text{Pd}_2(\text{dba})_3$ (0.5 equiv), NEt_4Cl (1.0 equiv) and PPh_3 (1.0 equiv) in acetone gave a grey precipitate, which could be purified by re-crystallization as a white powder of complex **3** (Eq 2.5).



Crystalline material of **3** could be obtained by slow diffusion of diethyl ether into the solution of raw material in dichloromethane. Complex **3** is soluble in dichloromethane, slightly soluble in acetonitrile, acetone or THF and insoluble in toluene, diethyl ether or hexanes. It is not as stable as its analogue **1** and its solution in dichloromethane gradually gave some palladium black in air. It becomes slightly green in solid state under light after several days.

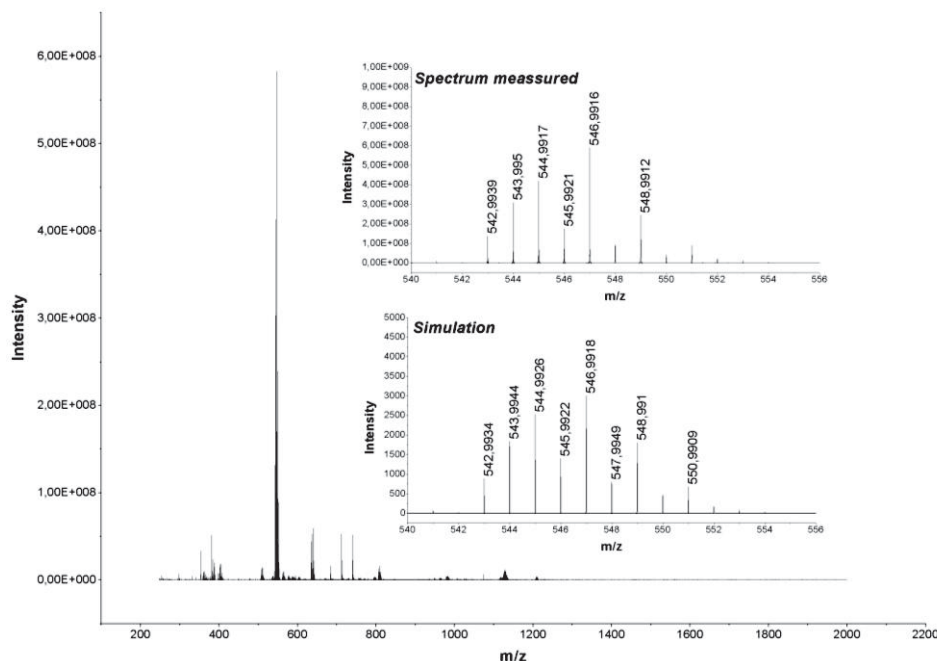


Figure 2.5. High resolution ESI mass spectrum of complex **3** in acetonitrile. The inset shows the experimental and simulated isotopic distribution patterns for $[\text{C}_{24}\text{H}_{22}\text{N}_2\text{Cl}_2\text{PPd}]^+$.

The formation of **3** was confirmed by the data from high resolution ESI mass spectrometry (**Figure 2.5**) and the structure of **3** was confirmed by X-ray diffraction (**Figure 2.6**).

As expected, the complex adopts a square-planar geometry with a chloride ligand *trans* to the NHC ligand and the other chloride ligand *trans* to the phosphine ligand. The NHC and phosphine ligands, both with medium to strong *trans* influence,⁹⁵ prefer to be *cis* to one another; though the steric congestion is larger than that in the congener where these two are *trans* to each other. The NHC ring is almost perpendicular to the square-plane core, with a dihedral angle of about 76° , very close to that in complex **1**. In the ^1H NMR spectrum, the signal of one proton of the pyridazinyldene ligand is found at $\delta = 7.95$ ppm as a doublet of doublet ($^3J_{\text{HH}} = 8.8$ Hz, $^4J_{\text{HP}} = 1.1$ Hz), while the signal of the other one is found at $\delta = 6.89$ ppm as a doublet ($^3J_{\text{HH}} = 8.8$ Hz). Methylene protons of the *N*-ethyl group are diastereotopic that one of them resonates at $\delta = 5.38$ ppm as doublet-quartet ($J_1 = 12.4$ Hz, $J_2 = 7.2$ Hz) and the other at $\delta = 4.62$ – 4.48 ppm as multiplet. The data shows that rotation around the $\text{Pd}-\text{C}_{\text{carbene}}$ bond is hindered on the NMR time scale, probably due to the π - π stacking effect between the pyridazinyldene ring and the phenyl group of the phosphine ligand and the fact that the $\text{Pd}-\text{C}_{\text{carbene}}$ bond has double bond character and the rotation of the bond normally involves braking the back-bonding from the metal center to the NHC ligand.

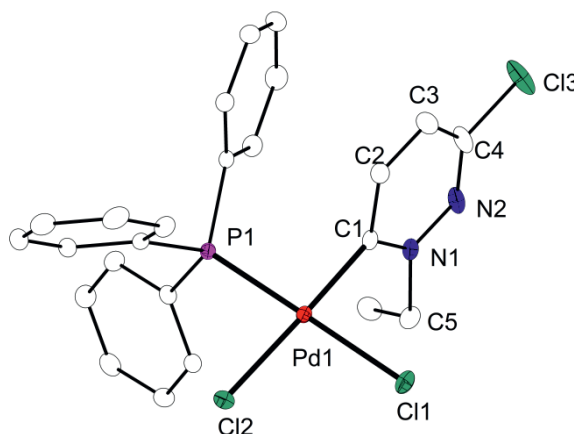
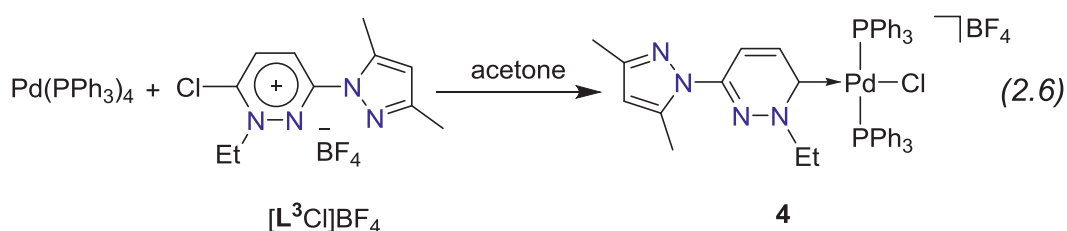


Figure 2.6. Molecular structure of **3**. Anisotropic displacement ellipsoids drawn at 30% probability level. The solvent molecule and all hydrogen atoms have been omitted for clarity. Selected bond lengths [Å] angles [°]: Pd1–C1 1.9772(18), Pd1–P1 2.2618(5), Pd1–Cl1 2.3693(5), Pd1–Cl2 2.3540(5), C1–Pd1–P1 90.86(5), C1–Pd1–Cl1 89.15(5), P1–Pd1–Cl2 88.342(17), Cl1–Pd1–Cl2 91.700(18).

The Pd–C_{carbene} bond length is 1.977(2) Å, smaller than those for complexes **1** and **2**. The Pd–Cl bond *trans* to the NHC ligand (2.3540(5) Å) is slightly shorter than the Pd–Cl bond *trans* to the phosphine ligand (2.3693(5) Å), suggesting a subtly stronger *trans* influence of PPh₃ compared to the novel NHC ligand.

In pyridazinyliene ring, there is another nitrogen atom that can be used to chelate metal fragments, thus ligand precursor [L³Cl]BF₄ was designed. Fortunately, treatment of 3-chloro-6-(3,5-dimethylpyrazol-1-yl)pyridazine with [Et₃O]BF₄ gave [L³Cl]BF₄ as the major product (Eq 2.3), although an *in situ* ¹H NMR monitoring showed that there were some by-products. Reaction of [L³Cl]BF₄ with Pd(PPh₃)₄ resulted in complex **4** (Eq 2.6).



Complex **4** is soluble in dichloromethane, slightly soluble in acetone, acetonitrile or THF and insoluble in diethyl ether, toluene or hexanes. The product is reasonably stable in aerobic and moisture condition. The formation of **4** was confirmed by the data from the multinuclear NMR spectroscopy and high resolution ESI mass spectroscopy (**Figure 2.7**) and the structure of complex **4** was confirmed by X-ray diffraction (**Figure 2.8**).

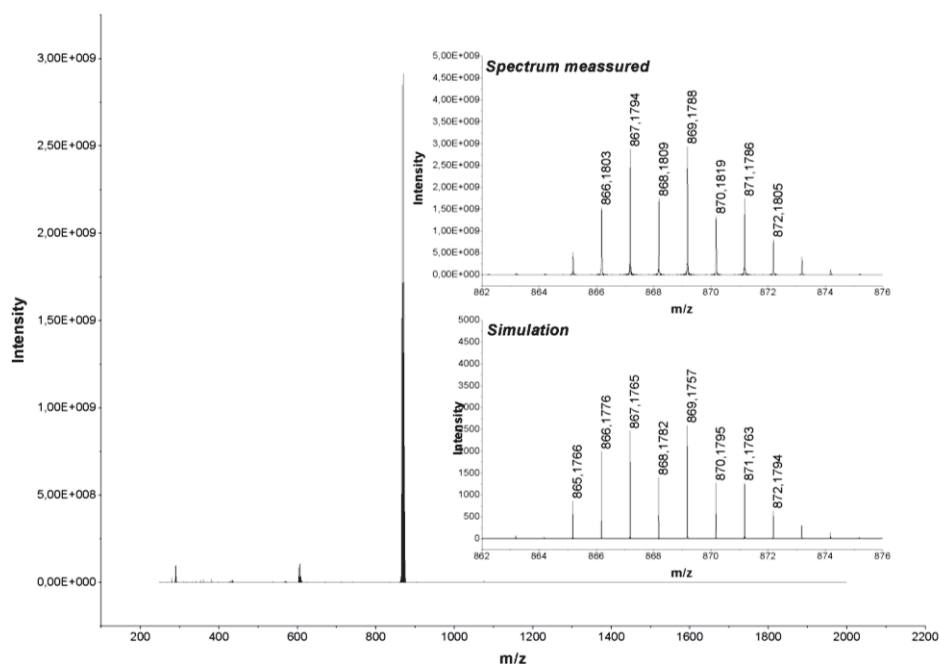


Figure 2.7. High resolution ESI mass spectrum of complex **4** in acetonitrile. The inset shows the experimental and simulated isotopic distribution patterns for $[\text{C}_{47}\text{H}_{44}\text{N}_4\text{ClP}_2\text{Pd}]^+$.

The basic geometry of **4** is similar to that of **1**. The Pd–C_{carbene} bond length is 1.982(4) Å, which is slightly smaller than that in **1**. The torsion angle between the NHC and the pyrazole ring is 21°. The N3–N4 bond is found pointing away from N2 in the pyridazinylidene ring, suggesting that the *N,N*-chelating pocket in the ligand is not pre-organized and the coordination of the second metal complex is probably not favored.

We then tried the reaction of **4** with other metal complexes, including $\text{RuCl}_2(\text{PPh}_3)_n$ ($n = 3$ or 4), $\text{RuCl}_2(\text{DMSO})_4$, $\text{PdCl}_2(\text{CH}_3\text{CN})_2$ and $[\text{Cu}(\text{CH}_3\text{CN})_4]\text{BF}_4$, however, the *in situ* ^1H NMR monitoring showed that the complex **4** remained intact. Possible reasons why the coordination of another metal fragment in the *N,N*-chelating pocket failed might include two possibilities: a) steric congestion caused by the neighbored phosphine ligands, and b) the fact that the NHC is more electron-deficient than a free pyridazine ring and N2 of the pyridazinylidene ring is no longer feasible to coordinate metal fragment.

The comparison of the bond lengths and angles of the four complexes are depicted in **Table A21** in Appendix.

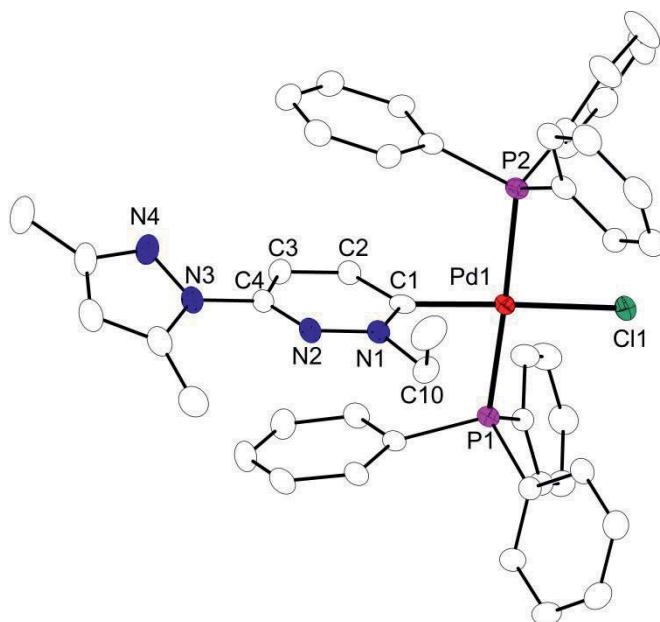
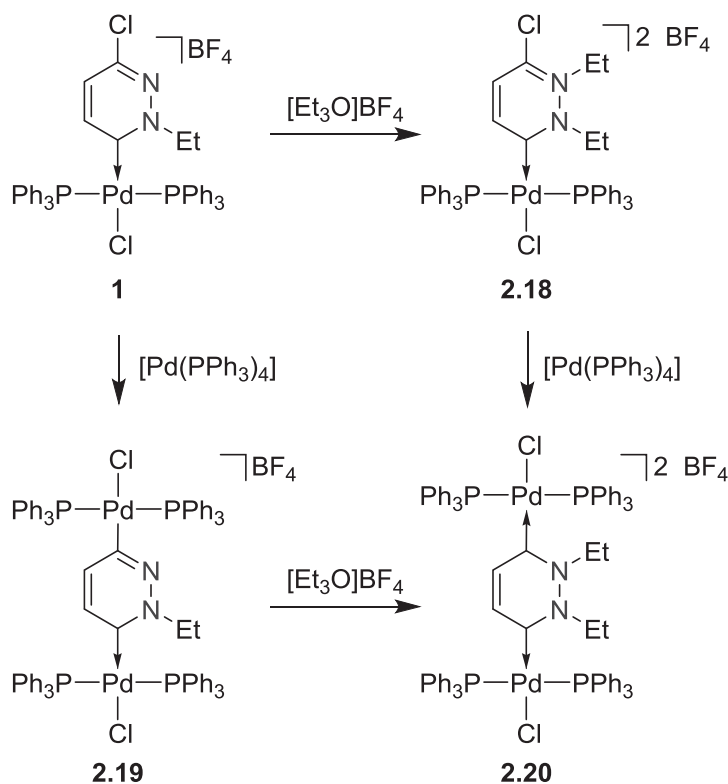
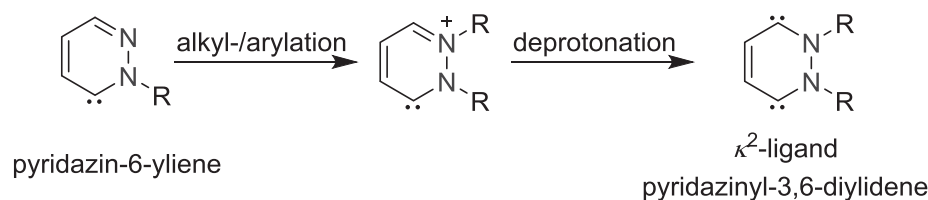


Figure 2.8. Molecular structure of **4**. Anisotropic displacement ellipsoids drawn at 30% probability level. The solvent molecule, BF_4^- and hydrogen atoms have been omitted for clarity. Selected bond lengths [\AA] angles [$^\circ$]: Pd1–C1 1.982(4), Pd1–P1 2.3208(9), Pd1–P2 2.3431(10), Pd1–Cl1 2.3463(10), C1–Pd1–P1 89.40(10), C1–Pd1–P2 89.39(10), P1–Pd1–Cl1 88.99(3), P2–Pd1–Cl1 92.24(4).

2.2.3 Functionalization of the second nitrogen atom

As mentioned in Chapter 1, 1,2,4-triazolylidene can be further functionalized to become a 1,2,4-triazolyl-3,5-diylidene as a κ^2 -ligand (**Scheme 1.11**). Because of the second nitrogen atom in the ring, the pyridazinylidene ligand might also be functionalized to become a novel NHC κ^2 -ligand. Starting from complex **1**, two reaction routes to synthesize the dinuclear complex were designed (**Scheme 2.8**). Both routes are combinations of alkylation by $[\text{Et}_3\text{O}]\text{BF}_4$ and oxidative addition of C–Cl bond onto $[\text{Pd}(\text{PPh}_3)_4]$. Initial trial showed that, complex **1** was inert to $[\text{Et}_3\text{O}]\text{BF}_4$ since no obvious change was observed in the *in situ* ^1H NMR monitoring reaction of **1** with $[\text{Et}_3\text{O}]\text{BF}_4$.

Meanwhile, treatment of complex **1** with $[\text{Pd}(\text{PPh}_3)_4]$ in dichloromethane at room temperature for prolonged time led to a dark solution with a yellow crystalline material, which was suggested by the structure determined by X-ray diffraction to be $\text{PdCl}_2(\text{PPh}_3)_2$.



Scheme 2.8. Schematic structure of a κ^2 -ligand based on pyridazine, and designed synthetic routes from complex **1** to the dinuclear complex **2.20** based on a pyridazinyl-3,6-diylidene ligand.

According to the molecular structure of **1** determined by X-ray diffraction, the pyridazinylidene ligand is stacked between two phenyl groups from the phosphine ligands, forming a highly crowded ‘pseudo’ sandwich structure. Since $[\text{Et}_3\text{O}]\text{BF}_4$ is a strong ethylation reagent, the only reason why the alkylation of complex **1** failed is that the second nitrogen is sterically blocked.



2.3 Conclusion

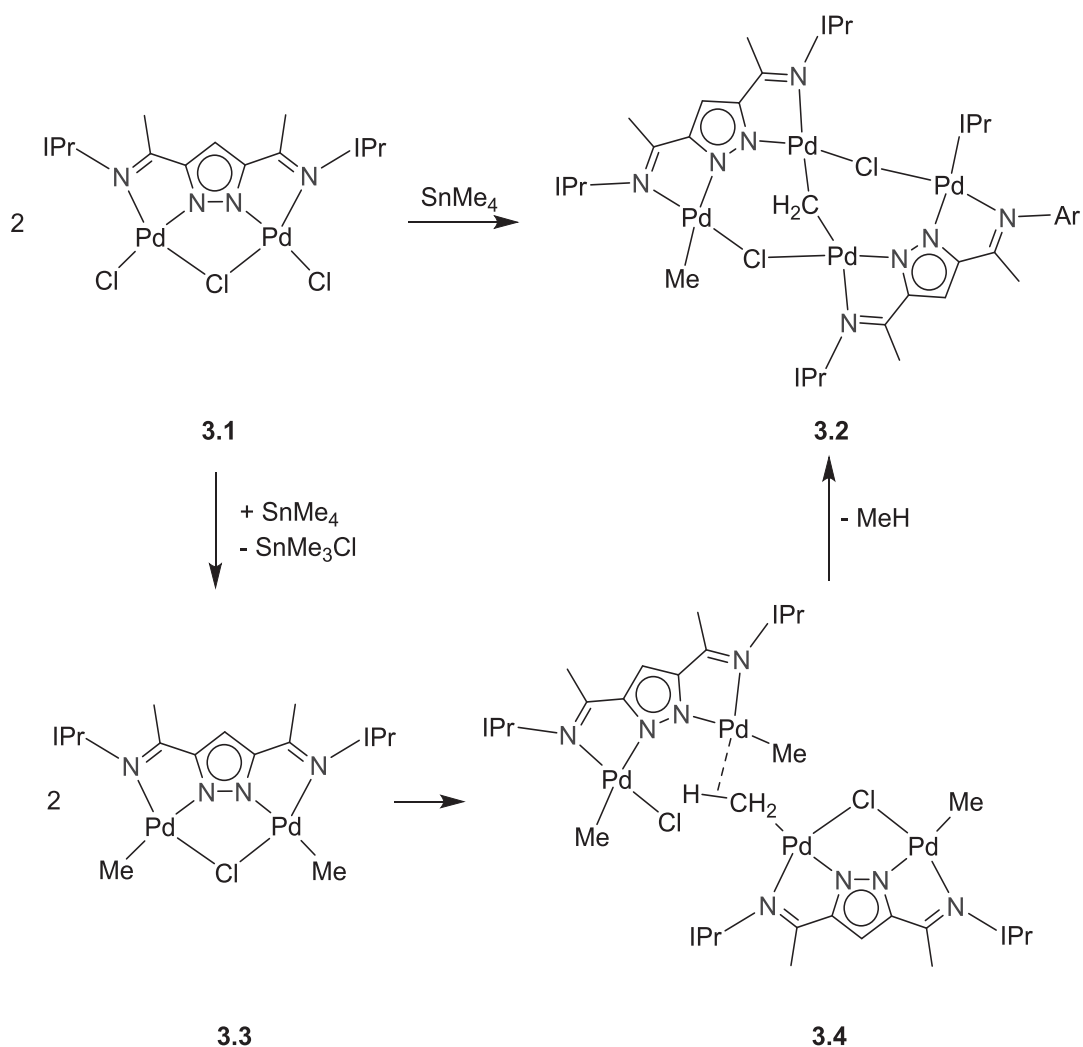
In this work, a convenient synthetic route to new pyridazinylidene palladium complexes by means of oxidative addition of C–Cl bonds onto Pd(0) species has been developed. The strategy selectively forms only pyridazin-6-ylidene metal complexes, although the C3–Cl bonds are also available for oxidative addition reactions. The pyridazin-6-ylidene palladium complexes are much more stable than the pyridazin-3-ylidene counterparts, suggested by the corresponding DFT calculations. The functionalization of the second nitrogen atom of the pyridazinylidene ligand to generate κ^2 -NHC ligands out of complex **4** failed, probably because of the strong steric repulsion caused by the ancillary phosphine ligands. Further studies aiming at elucidating the donating ability of pyridazinylidene ligand, the synthesis of κ^2 -pyridazine ligands and the catalytic activity of pyridazinylidene palladium complexes are still on-going.



CHAPTER 3. Pyrazole Bridged bis(NHC) Ligands and their Dinuclear Palladium Complexes

3.1 Introduction and Motivation

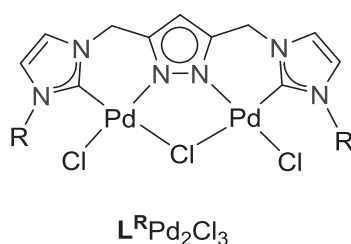
Neutral dinuclear palladium complexes based on the pyrazole bridged ligand system are important intermediates to study the cooperative behaviors of the two metal centers chelated in the ligand.



Scheme 3.1. Cooperative C–H activation of central metal atoms from two molecules of complex 3.3.

For example, reaction of pyrazolate-based dinuclear palladium complex **3.1** with SnMe_4 resulted in methylene-bridged tetranuclear palladium complex **3.2**.⁹⁶ The proposed mechanism showed that, the terminal chlorides of complex **3.1** were replaced by methyl groups, forming complex **3.3**. The attachment of the central chloride atom to the metal ions was labile and its dissociation from one palladium ion gave a vacant site for the C–H bond of a methyl group in another molecule of **3.3** to coordinate *via* agostic interaction, as shown in the structure **3.4**. After C–H bond activation and reductive elimination, methane was released and complex **3.2** was formed after the adjustment of ancillary ligands (**Scheme 3.1**).

Pyrazole bridged bis(NHC) species are also promising ligands for metal complexes, such as those depicted in §1.3, Chapter 1. Although complexes based on pyrazole-bridged bis(NHC) ligands have been synthesized in the past decade, seldom did people report the formation of their neutral metal complexes. In this work, efforts to synthesize the neutral complexes $\text{L}^{\text{R}}\text{Pd}_2\text{Cl}_3$ (L^{R} = pyrazolate bridged bis(NHC) ligands) were sought.

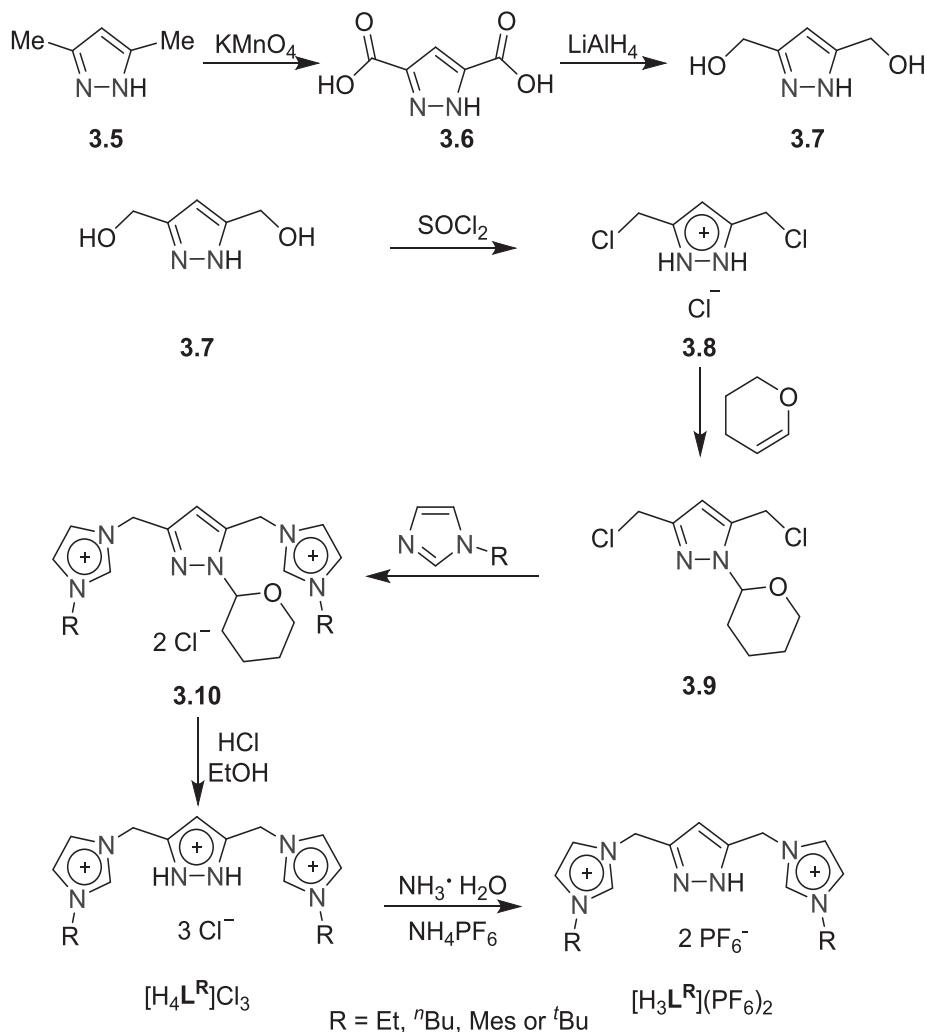




3.2 Result and Discussion

3.2.1 Material and methodology

In this work, two types of ligand precursors $[\text{H}_4\text{L}^{\text{R}}]\text{Cl}_3$ and $[\text{H}_3\text{L}^{\text{R}}](\text{PF}_6)_2$ were used. The synthetic route has been reported previously⁹¹ and is briefly summarized in **Scheme 3.2**.

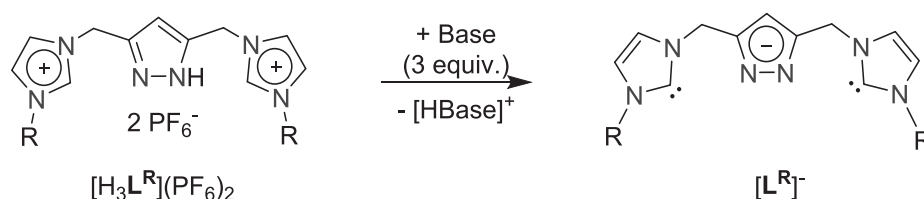


Scheme 3.2. Synthesis of the ligand precursors.

As mentioned in Chapter 2, four strategies to form metal NHC complexes are frequently used. Obviously, oxidative addition of C–X bond (X = halogen atoms) onto Pd(0) species to form palladium(II) NHC complex is not optional because there are no C–X bonds (X = halogen atoms) in the ligand precursors in this case. Transmetalation *via* silver intermediates was previously pursued for the formation of dinuclear palladium allyl complexes

$[\mathbf{L}^{\mathbf{R}}\text{Pd}_2(\text{allyl})_2]\text{PF}_6^{91}$ and attempts of synthesizing neutral complex $\mathbf{L}^{\mathbf{R}}\text{Pd}_2\text{Cl}_3$ by this method failed.

Ligand precursors $[\text{H}_3\mathbf{L}^{\mathbf{R}}](\text{PF}_6)_2$ are much easier to handle because ligand precursors $[\text{H}_4\mathbf{L}^{\mathbf{R}}]\text{Cl}_3$ are highly hygroscopic. Therefore, initial attempts started with ligand precursors $[\text{H}_3\mathbf{L}^{\mathbf{R}}](\text{PF}_6)_2$. Stoichiometrically, three equivalents of base are needed for the full deprotonation of $[\text{H}_3\mathbf{L}^{\mathbf{R}}](\text{PF}_6)_2$ to give the free pyrazolate bridged bis(NHC) ligand $[\mathbf{L}^{\mathbf{R}}]^-$ (**Scheme 3.3**), which can then react with palladium reagents, such as PdCl_2L_2 ($\text{L}_2 = \text{cod}$, $(\text{CH}_3\text{CN})_2$ or $(\text{PPh}_3)_2$), to give the neutral species directly.



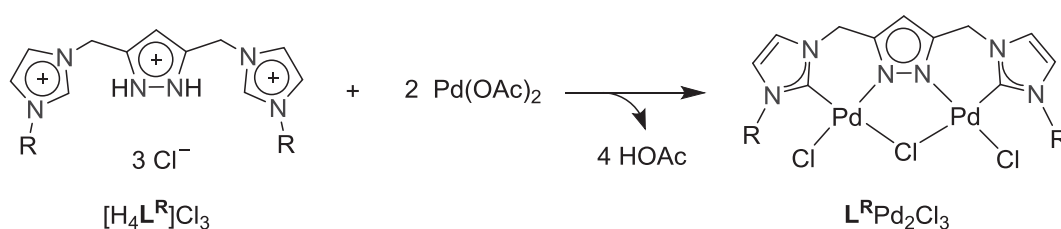
Scheme 3.3. Three equivalents of base are needed to form the free carbene ligand $[\mathbf{L}^{\mathbf{R}}]^-$ after full deprotonation.

Under inert gas, a suspension of $[\text{H}_3\mathbf{L}^{\mathbf{R}}](\text{PF}_6)_2$ in THF was treated with a solution of KO^tBu in THF (or other reagents, such as KHMDs , $^n\text{BuLi}$ or MeLi in ether) and the mixture was stirred for half an hour. A suspension of PdCl_2L_2 ($\text{L}_2 = \text{cod}$, $(\text{CH}_3\text{CN})_2$ or $(\text{PPh}_3)_2$) in THF was added to the reaction mixture. The color of the reaction mixture turned to dark brown immediately and a black precipitate formed in the solution. The precipitate was collected by filtration and the solvent of the filtrate was removed under vacuum to give a brown solid. The ^1H NMR spectra of both the black precipitate and the brown solid suspended in CD_3CN showed no signals of the CH groups of the imidazole rings or the CH group of the pyrazole ring, suggesting a possible decomposition of the ligand precursors under strongly basic conditions. Therefore, it was not optional to synthesize the targeted complexes by means of the *in situ* generation of free carbene by strong exterior bases.

So far, the only remaining method for the synthesis of metal NHC complexes is the reactions of ligand precursors and metal reagents containing weak interior bases (method c, **Scheme 2.2**).

3.2.2 Synthesis of $[^n\text{L}^{\text{R}}_2\text{Pd}_2](\text{PF}_6)_2$ and $[^a\text{L}^{\text{R}}_2\text{Pd}_2](\text{PF}_6)_2$

$\text{Pd}(\text{OAc})_2$ is an important palladium(II) source containing a mild interior base (acetate) and is widely used to synthesize palladium complexes.⁴⁵ Meanwhile, non-coordinating counter anions like PF_6^- should be excluded so as to get the expected neutral dinuclear complex. Therefore, ligand precursors $[\text{H}_4\text{L}^{\text{R}}]\text{Cl}_3$ and palladium(II) acetate are combined for the following reaction (**Scheme 3.4**).



Scheme 3.4. Designed synthetic route to neutral dinuclear palladium complex.

Reaction of $[\text{H}_4\text{L}^{\text{tBu}}]\text{Cl}_3$ with $\text{Pd}(\text{OAc})_2$ (2.0 equiv.) in d^6 -DMSO at 105 °C overnight in an NMR tube resulted in the formation of a yellow solution and a bright yellow crystalline solid with trace amount of palladium black. The ^1H NMR spectra of both the solution and the solid dissolved in d^6 -DMSO were basically the same, but the spectrum of the crystalline material was cleaner. The ^1H NMR spectrum of the solid showed two signals at $\delta = 8.97$ ppm and 7.07 ppm, typical for one C2 proton and one C4/5 proton of the imidazolyliene ring, respectively.

The precipitated solid contained single crystals, which were suitable for X-ray diffraction. The obtained structure (**Figure 3.1**) was consistent with the ^1H NMR data that, instead of the anticipated complex **5'**, its isomeric abnormal carbene complex **5** was formed (**Scheme 3.5**).

The complex adopts a 'saddle-shaped' geometry with C_2 symmetry. Both $\{\text{CNPdCl}_2\}$ fragments are approximately square-planar with the dihedral angle between the C6/N1/Cl12/Pd1 plane and the C11–Pd1 bond of 89.7°. The $\{\text{CNPdCl}_2\}$ fragment and the NHC ligand bound to the same palladium atom are not perfectly parallel to each other with the dihedral angle between the C6/N3/C5/N4 plane and the Pd1/N1/C6/Cl11/Cl12 plane of 26.2°. Both Pd-involved six-membered rings are roughly boat-shaped instead of chair-shaped. The $\text{Pd}-\text{C}_{\text{carbene}}$ bond lengths are 1.96–1.97 Å, shorter than the reported $\text{Pd}-\text{C}_{\text{carbene}}$ bond lengths (2.03–2.19 Å) of palladium allyl complexes based on similar ligands,⁹¹ signifying a stronger $\text{Pd}-\text{C}_{\text{carbene}}$ bond in the new complex. The bond lengths of $\text{Pd}-\text{Cl}_{\text{bridging}}$ (2.39–2.41 Å) are

significantly longer than those of Pd–Cl_{terminal} (2.31–2.32 Å). The Pd···Pd distance is 3.55 Å, significantly smaller than those (3.97–4.05 Å) in the related palladium allyl complexes;⁹¹ Probably, the bridging chloride brings the two metal centers closer in the new complex.

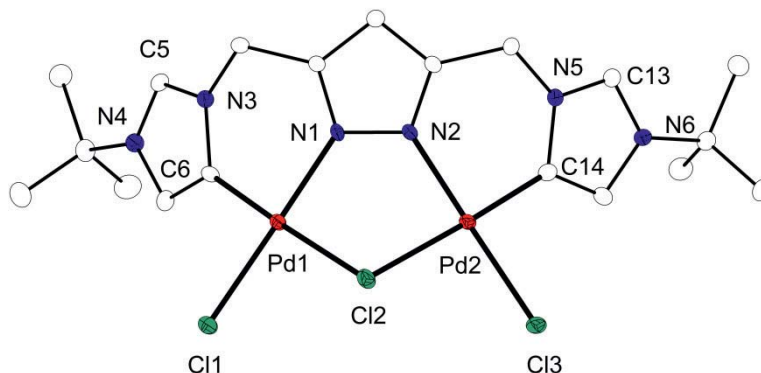
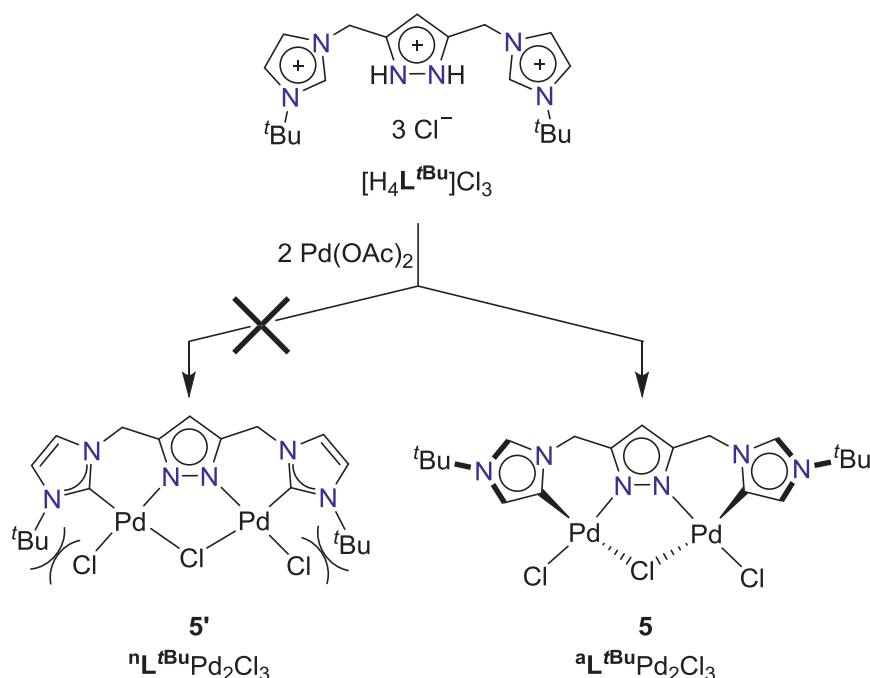


Figure 3.1. Molecular structure of **5**. All proton atoms are omitted for clarity. Anisotropic displacement ellipsoids drawn at 30% probability level. Selected bond lengths [Å] angles [°]: Pd1···Pd2 3.5525(5), Pd1–C6 1.965(5), Pd1–N1 2.007(4), Pd1–Cl1 2.3219(13), Pd1–Cl2 2.4096(12), Pd2–Cl2 2.3929(13), Pd2–Cl3 2.3131(12), C6–Pd1–N1 88.00(18), C6–Pd1–Cl1 91.24(14), N1–Pd1–Cl2 89.83(11), Cl1–Pd1–Cl2 90.93(4), Pd1–Cl2–Pd2 95.41(5), C6–N1–Pd1–Cl2 177.812(150).

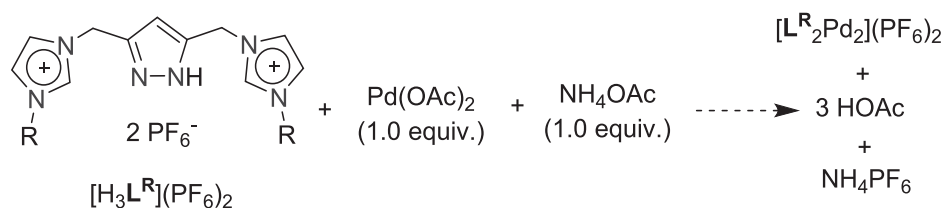


Scheme 3.5. Selective formation of ^aL^{tBu}Pd₂Cl₃ instead of ⁿL^{tBu}Pd₂Cl₃.

In order to differentiate the two binding modes (**Scheme 3.5**), the symbol of $^n\mathbf{L}^R$ for normal carbene type and $^a\mathbf{L}^R$ for abnormal carbene type are used. Therefore, the new complex **5** will be noted as $^a\mathbf{L}^{tBu}Pd_2Cl_3$. The unexpected formation of the abnormal NHC metal complex **5** can be explained from the thermodynamic point of view; in complex **5**, the two bulky *tert*-butyl groups point away from the terminal chlorides; while in the imaginative normal NHC metal complex **5'**, assumed that its fundamental skeleton is similar to that of **5**, there will be a strong steric congestion between the bulky *tert*-butyl group and the adjacent terminal chloride, which causes a decreased stability of the normal NHC complex (**Scheme 3.5**). Previously, an NHC palladium complex, in which the wingtip *tert*-butyl group was *cis* to chloride and palladium was involved in a six-membered ring, has been reported, however, in the complex, the six-membered ring was severely distorted so that the space between the *tert*-butyl group and the chloride was large enough to avoid the steric repulsion.⁹⁷

Based on the above assumption that the formation of abnormal NHC metal complex **5** was caused by the bulkiness of the wingtips, reaction of $Pd(OAc)_2$ and $[H_4\mathbf{L}^{Mes}]Cl_3$, which carried less bulky wingtips, might result in the related normal carbene complex $^n\mathbf{L}^{Mes}Pd_2Cl_3$. Reaction of $[H_4\mathbf{L}^{Mes}]Cl_3$ with $Pd(OAc)_2$ (2.0 equiv.) in DMSO under the same condition gave a brown solution without precipitates. The *in situ* 1H NMR spectrum of the reaction solution showed the characteristic signals of two C4/5 protons ($\delta = 7.77$ and 7.39 ppm, respectively), indicating the formation of a normal carbene complex. Grey powder was separated by the addition of acetonitrile and its ESI mass spectrum showed a base peak at $m/z = 569.8$, which was consistent with the signal of a $[\mathbf{L}^{Mes}_2Pd_2]^{2+}$ fragment. After several trials, no suitable crystalline material for X-ray diffraction could be obtained from the raw product and the precise structure of the complex was not confirmed. Yet, the above evidence suggested that either the $[\mathbf{L}^{Mes}_2Pd_2]^{2+}$ cation was formed in the product, or a product of normal carbene complex transferred to the $[\mathbf{L}^{Mes}_2Pd_2]^{2+}$ cation in the ionization process during the measurement of ESI mass spectrometry. Either way, the $[\mathbf{L}^{Mes}_2Pd_2]^{2+}$ cation seemed to be a relatively stable species.

It was noticed that in the $[\mathbf{L}^{Mes}_2Pd_2]^{2+}$ cation, the ratio of ligand to palladium is 1:1, indicating one equivalent of $Pd(OAc)_2$ would be sufficient for the formation of the $[\mathbf{L}^{Mes}_2Pd_2]^{2+}$ cation. Moreover, to assist the removal of all three protons bound to nitrogen atoms in the ligand precursor $[H_3\mathbf{L}^R](PF_6)_2$, one equivalent of an additional exterior base was necessary. In addition, non-coordinating counterions like PF_6^- were better options to grow single crystals out of the product. Therefore, the following reaction of $[H_4\mathbf{L}^{Mes}]Cl_3$, $Pd(OAc)_2$ (1.0 equiv.) and NH_4OAc (1.0 equiv.) was designed for the synthesis of a palladium complex containing the $[\mathbf{L}^{Mes}_2Pd_2]^{2+}$ cation.



Several trials of the above reaction only resulted in yellow mixtures of unidentified products. Alternative reaction conditions, such as different solvents, concentration of the reagents, reaction temperatures or various R groups, did not give better results. However, an *in situ* NMR tube monitoring for the reaction of $[\text{H}_4\text{L}^{\text{Et}}](\text{PF}_6)_2$ with $\text{Pd}(\text{OAc})_2$ in DMSO, where two equivalents of NH_4OAc were added, surprisingly gave a reasonably clean ^1H NMR spectrum with two characteristic C4/5 proton signals at $\delta = 7.70$ and 7.59 ppm, respectively, indicating the formation of a normal carbene complex (**Figure 3.2**).

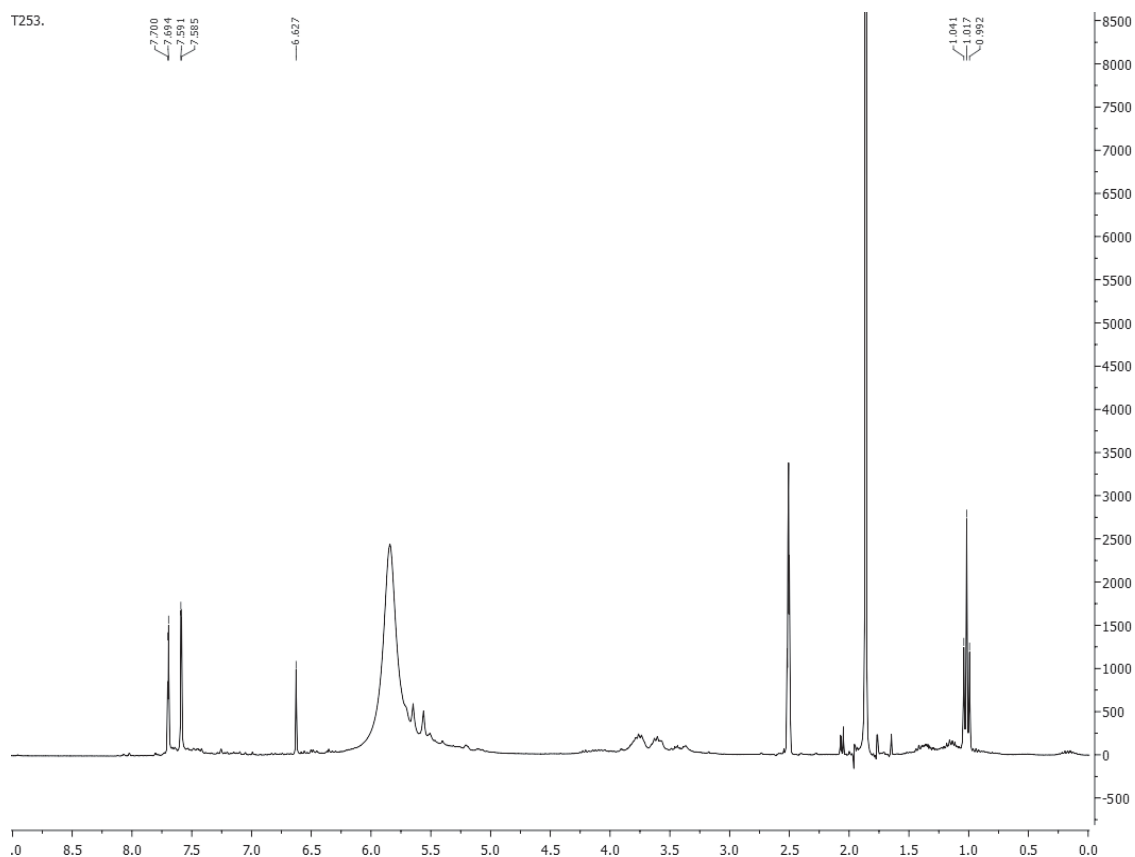
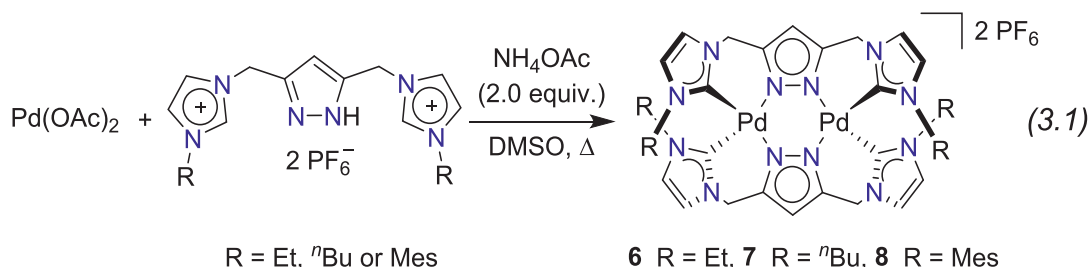


Figure 3.2. ^1H NMR spectroscopy of the *in situ* reaction of $[\text{H}_3\text{L}^{\text{Et}}](\text{PF}_6)_2$, $\text{Pd}(\text{OAc})_2$ and NH_4OAc (2.0 equiv.), at 105 °C for overnight.

The reaction was then carried out on a larger scale and a bis(ligand) dinuclear palladium complex **6**, $[\text{L}^{\text{Et}}_2\text{Pd}_2](\text{PF}_6)_2$, was isolated. The same strategy was also used for the formation of other normal carbene complexes **7**, $[\text{L}^{\text{nBu}}_2\text{Pd}_2](\text{PF}_6)_2$, and **8**, $[\text{L}^{\text{Mes}}_2\text{Pd}_2](\text{PF}_6)_2$

(Eq 3.1); however, the reaction of $[\text{H}_3\text{L}^{\text{tBu}}](\text{PF}_6)_2$, $\text{Pd}(\text{OAc})_2$ and two equivalents of NH_4OAc did not give any clean product (**Figure A12** in Appendix). Probably the strong steric repulsion between two adjacent *tert*-butyl groups from each ligand prevented the formation of the normal NHC bis(ligand) complex.



Crystalline material of these complexes could be obtained by slow diffusion of diethyl ether to the solutions of the raw materials in acetonitrile. The formation of **6**, **7** and **8** was confirmed by the data from high resolution ESI mass spectroscopy (**Figure A1-Figure A3**) and multinuclear NMR spectroscopy. Molecular structures of the cations of complexes **7** and **8** were determined by X-ray diffraction (shown in **Figure 3.3** and **Figure 3.4**, respectively).

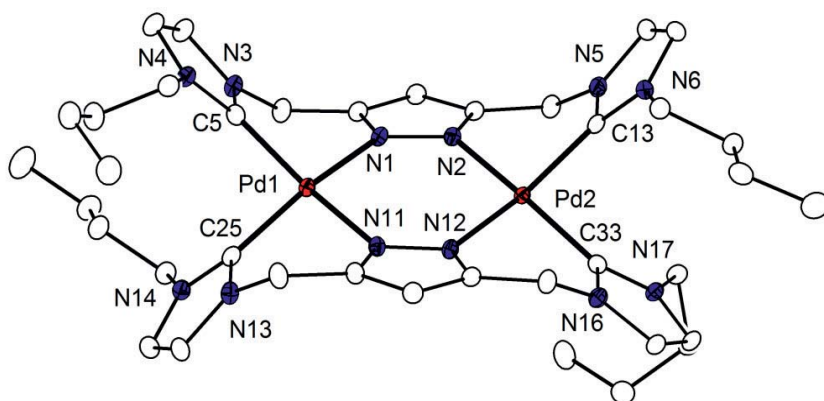


Figure 3.3. Molecular structure of the cation of **7** $[\text{L}^{\text{nBu}}_2\text{Pd}_2](\text{PF}_6)_2$; all H atoms are omitted for clarity. Anisotropic displacement ellipsoids drawn at 30% probability level. Selected bond lengths [Å] angles [°]: Pd1...Pd2 4.0376(2), Pd1–C5 1.973(2), Pd1–N1 2.0767(17), Pd1–C25 1.979(2), Pd1–N11 2.0873(17), C5–Pd1–C25 91.57(9), C5–Pd1–N1 87.13(8), C25–Pd1–N11 87.18(8), N1–Pd1–N11 100.34(6), C5–N1–Pd1–C25 -87.009(216), C5–Pd1–N1–N11 163.814(80).

In complex **7**, the cation $[\text{L}^{\text{nBu}}_2\text{Pd}_2]^{2+}$ has a C_{2h} symmetry. Both $\{\text{PdC}_2\text{N}_2\}$ cores adopt distorted square-planar geometry so as to avoid the steric congestion between two adjacent *n*Bu groups from each ligand. For example, the dihedral angle between the C5/Pd1/N1/N11

plane and the Pd1–C25 bond is 68.5°. Both palladium-involved six-membered rings are boat-shaped, similar to those in complex **5**. The Pd–C_{carbene} bond lengths are 1.97–1.98 Å, which is also close to those in **5**, and the distance of the two metal centers is 4.04 Å, significantly larger than that in **5**, in which two metal ions are bridged by the same chloride anion.

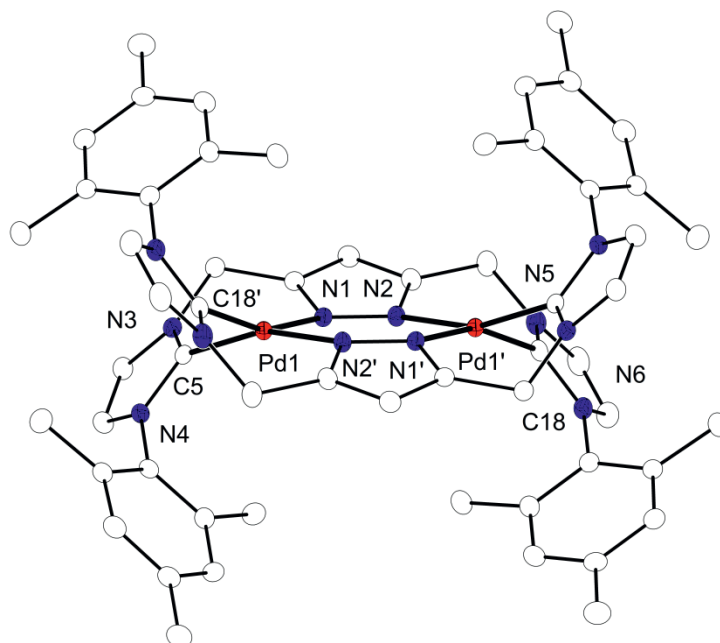


Figure 3.4. Molecular structure of the cation of **8** [$n\text{L}^{\text{Mes}}_2\text{Pd}_2$](PF₆)₂; all H atoms are omitted for clarity. Anisotropic displacement ellipsoids drawn at 30% probability level. Selected bond lengths [Å] angles [°]: Pd1...Pd2 3.9606(3), Pd1–C5 1.965(2), Pd1–N1 2.0738(18), Pd1–C18' 1.967(2), Pd1–N2' 2.0721(18), C5–Pd1–C18' 93.36(9), C18'–Pd1–N2' 85.18(8), C5–Pd1–N1 85.55(8), N2'–Pd1–N1 102.62(7), C5–N1–Pd1–C18' -87.680(245), C5–Pd1–N1–N2' -161.554(86).

The ¹H NMR spectra of **6–8** show the signals of two characteristic C4/5 protons at δ = 7.33–7.37 and 7.15–7.24 ppm, respectively. The 2D ¹³C–¹H HMBC NMR technique was used to identify the chemical shift of the carbene carbon. For example, the HMBC NMR spectrum of complex **8** (**Figure 3.5**) indicates that the carbenic carbon of the NHC ligand resonates at 161.8 ppm. Carbene signals of complexes **6–8** are in the range δ = 154.8–161.8 ppm in the ¹³C NMR spectra.

It is noteworthy that the carbenic carbon ¹³C NMR signals of these complexes are not in the typical metal-carbene signal region, which is normally around 200 ppm.⁹⁸ This observation shed some light on the assumption that metal carbenes do not necessarily have low field chemical shifts in the ¹³C NMR spectra, which will be discussed in details in Chapter 4.

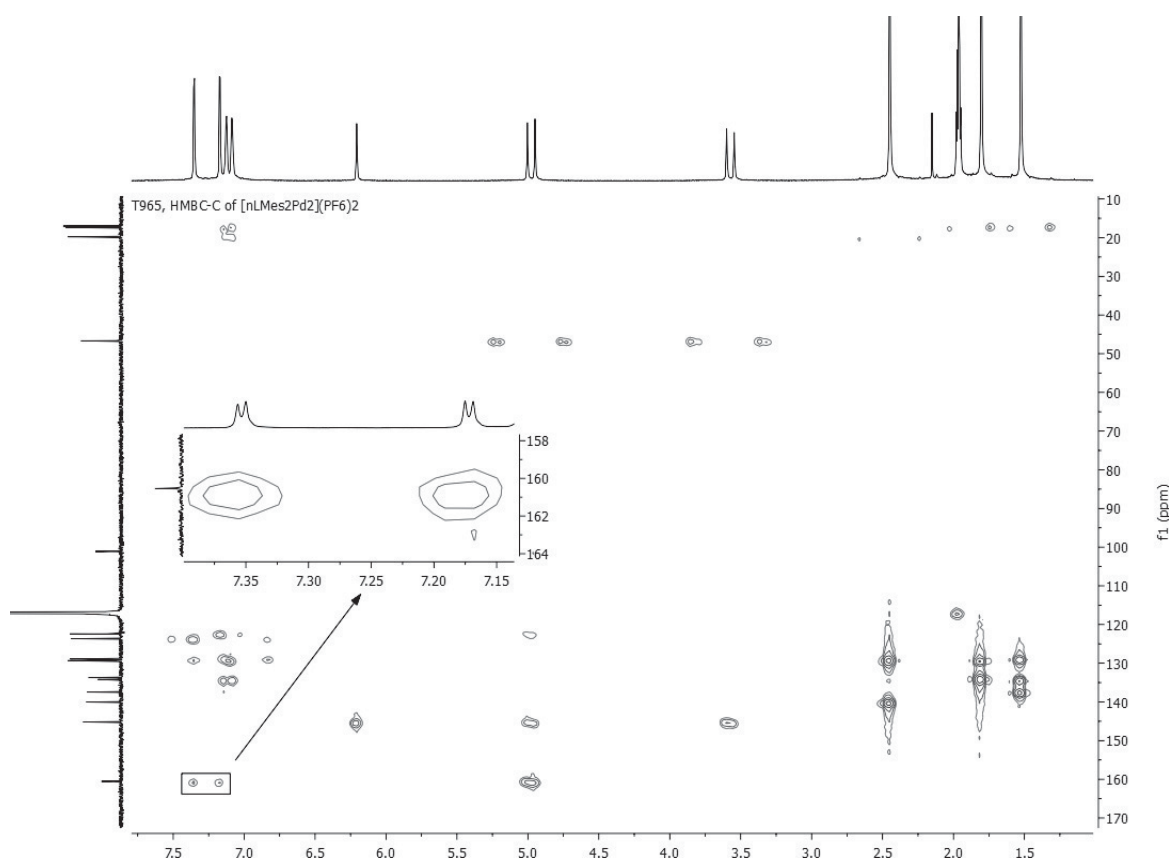
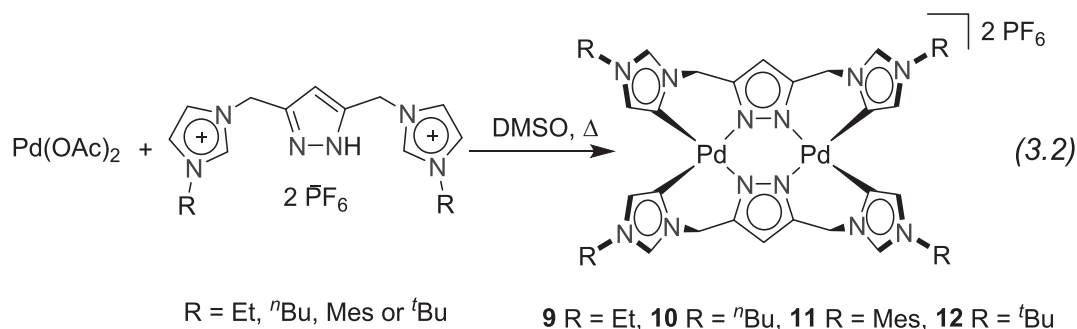


Figure 3.5. The 2D ^{13}C - ^1H HMBC NMR spectrum of complex **3.4** $[\text{nL}^{\text{Mes}}_2\text{Pd}_2](\text{PF}_6)_2$.

As a short summary, two or more equivalents of NH_4OAc induced the formation of bis(ligand) dinuclear normal carbene complexes; while one equivalent of NH_4OAc led to mixtures of unidentified complexes (**Figure A8** in Appendix). Apparently, the reaction route was strongly influenced by the amount of NH_4OAc used and it was intriguing how the reaction might proceed without extra base.

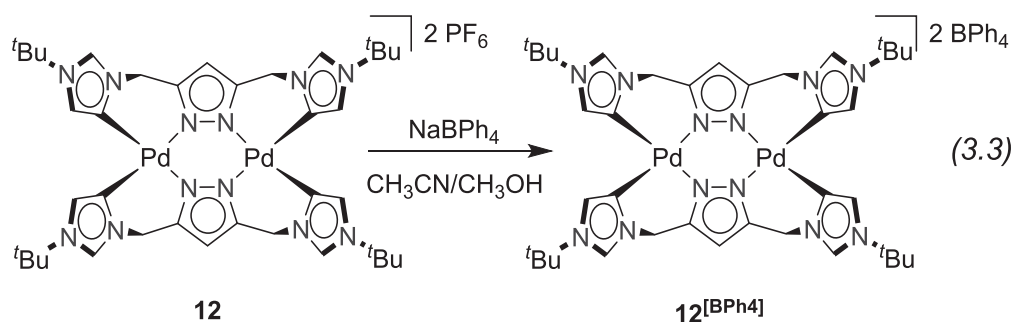
The mixture of $[\text{H}_4\text{L}^{\text{R}}](\text{PF}_6)_2$ and $\text{Pd}(\text{OAc})_2$ (1.0 equiv.) in DMSO was kept at $95\text{ }^\circ\text{C}$ for 1.5 hours and then NH_4OAc (1.0 equiv.) was added for work-up. Then water was added to the solution to precipitate an off-white solid, which was dried under reduced pressure and purified by column chromatography to give a fine white powder.

The data from multinuclear NMR spectra and ESI mass spectra indicated the formation of bis(ligand) dinuclear abnormal carbene complexes **9-12**, $[\text{aL}^{\text{R}}_2\text{Pd}_2](\text{PF}_6)_2$ (Eq 3.2). It is noteworthy that both $[\text{aL}^{\text{R}}_2\text{Pd}_2](\text{PF}_6)_2$ and $[\text{nL}^{\text{R}}_2\text{Pd}_2](\text{PF}_6)_2$ are reasonably stable and no interconversion reaction between them was observed, even when their solutions in DMSO were heated to over $150\text{ }^\circ\text{C}$.



Their ^1H NMR spectra show signals of characteristic C4/5 and C2 protons at $\delta = 7.04$ – 7.21 ppm and 8.29 – 8.46 ppm, respectively. The ^{13}C NMR spectra show the signals of carbenes at $\delta = 139.0$ – 139.4 ppm, which are in even higher field than those of normal carbene complexes $[\text{L}^{\text{R}}_2\text{Pd}_2](\text{PF}_6)_2$ and also not ‘typical’ for palladium(II) carbene complexes.

Unfortunately, slow diffusion of diethyl ether into solutions of the products in acetonitrile did not give any suitable single crystals for X-ray diffraction. Yet, by means of anion exchange with NaBPh_4 , single crystals of $[\text{L}^{{}^t\text{Bu}}_2\text{Pd}_2](\text{BPh}_4)_2$ out of $[\text{L}^{{}^t\text{Bu}}_2\text{Pd}_2](\text{PF}_6)_2$ were obtained (Eq 3.3).



The structure of complex $\mathbf{12}^{[\text{BPh}_4]}$ determined by X-ray diffraction (**Figure 3.6**) shows that, $[\text{L}^{{}^t\text{Bu}}_2\text{Pd}_2]^{2+}$ adopts a saddle-shaped geometry with C_2 symmetry, with the *tert*-butyl groups *cis* to each other with respect of the $\{(\text{C}_2\text{PdN}_2)_2\}$ core (schematic models of the different types of $[\text{L}^{\text{R}}_2\text{Pd}_2]^{2+}$ and $[\text{L}^{\text{R}}_2\text{Pd}_2]^{2+}$ are shown in **Figure 3.7**). Both Pd atoms are found with almost perfect square-planar geometry and the dihedral angle between the Pd1–C6 bond and the C44/N12/N1/Pd1 plane is 84.7° . All the four Pd-involved six-membered rings are boat-shaped, like those in the cation $[\text{L}^{\text{R}}_2\text{Pd}_2]^{2+}$. The Pd–C_{carbene} bond lengths are 1.98–1.99 Å, almost the same to those of the related normal NHC complexes (1.97–1.98 Å). The distance between the metal centers is 3.82 Å, slightly shorter than that in $[\text{L}^{\text{R}}_2\text{Pd}_2]^{2+}$.

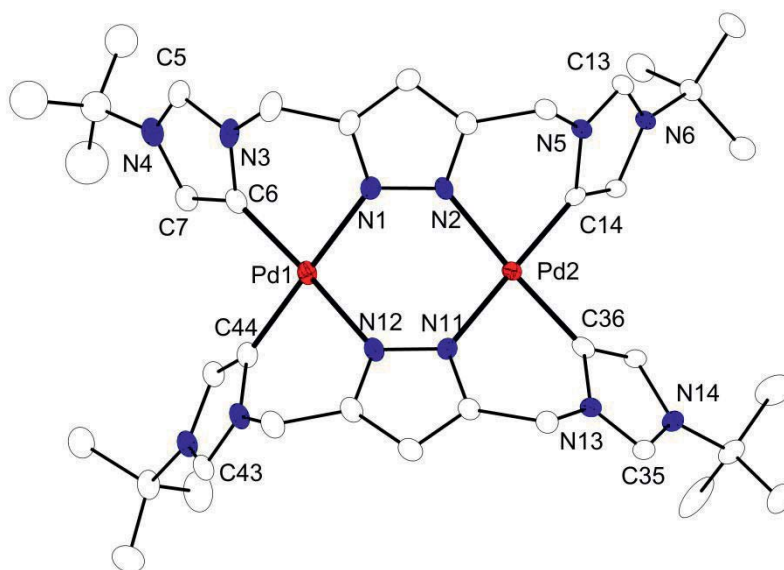


Figure 3.6. Molecular structure of the cation of **12**^[BPh₄]. All H atoms are omitted for clarity. Anisotropic displacement ellipsoids drawn at 30% probability level. Selected bond lengths [Å] angles [°]: Pd1···Pd2 3.8157(5), Pd1–C6 1.980(4), Pd1–N1 2.061(3), Pd1–C44 1.990(4), Pd1–N12 2.063(3), C6–Pd1–N1 87.54(14), C6–Pd1–C44 92.61(16), C44–Pd1–N12 86.07(14), N12–Pd1–N1 93.93(12), C6–N1–Pd1–C44 95.230(4846), C6–N1–Pd1–N12 - 174.668(146).

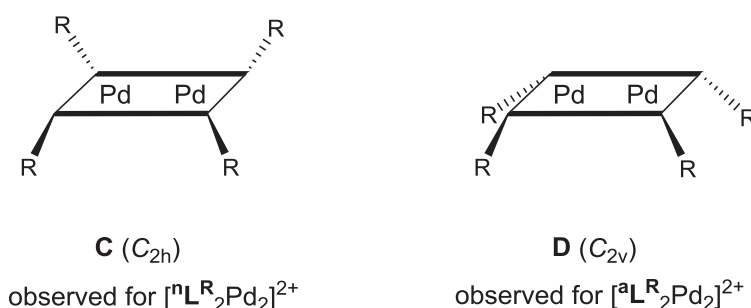


Figure 3.7. Different stereoisomers of approximate (non-crystallographic) C_{2h} and C_{2v} symmetry observed for the $[^n\text{L}_2\text{Pd}_2]^{2+}$ and $[^a\text{L}_2\text{Pd}_2]^{2+}$ platforms, respectively.

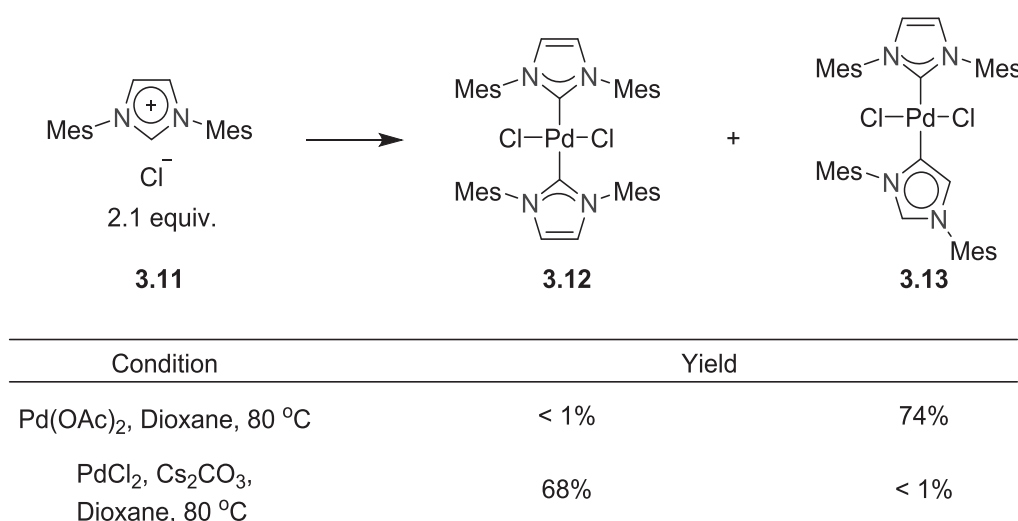
3.2.3 Mechanistic consideration

The base-dependent selective formation of normal or abnormal complexes was interesting. As mentioned in Chapter 1, ligand precursors with bulky wingtips and non-coordinating counterions preferred to form abnormal NHC complexes *via* the oxidative addition of C4/5–H bonds onto the metal fragments; while ligand precursors with less-bulky wingtips and counterions, which could form strong H-bonding, preferred to generate normal NHC

complexes *via* the C2–H bond heterolysis.²¹ In this work, except for $[\text{H}_3\text{L}^{\text{tBu}}](\text{PF}_6)_2$, all other ligand precursors were able to be transformed to both normal and abnormal carbene complexes, if proper conditions were provided. This result revealed that, different from the reported scenarios, neither of the bulkiness of the wingtip (except for the case of $[\text{H}_3\text{L}^{\text{tBu}}](\text{PF}_6)_2$) nor the counterion was the determining factor for the selective formation of normal or abnormal NHC complexes in this work.

Considering the possible reaction pathways in this work; on one hand, for the activation of C4/5–H, oxidative addition of C4/5–H onto Pd^{II} species to form a Pd^{IV} hydride complex has never been reported before and it is probably quite unstable, thus, a mechanism involving the formation of Pd^{IV} hydride intermediate is unlikely; on the other hand, the heterolysis of the C2–H bond with the assistance of base is reported before.

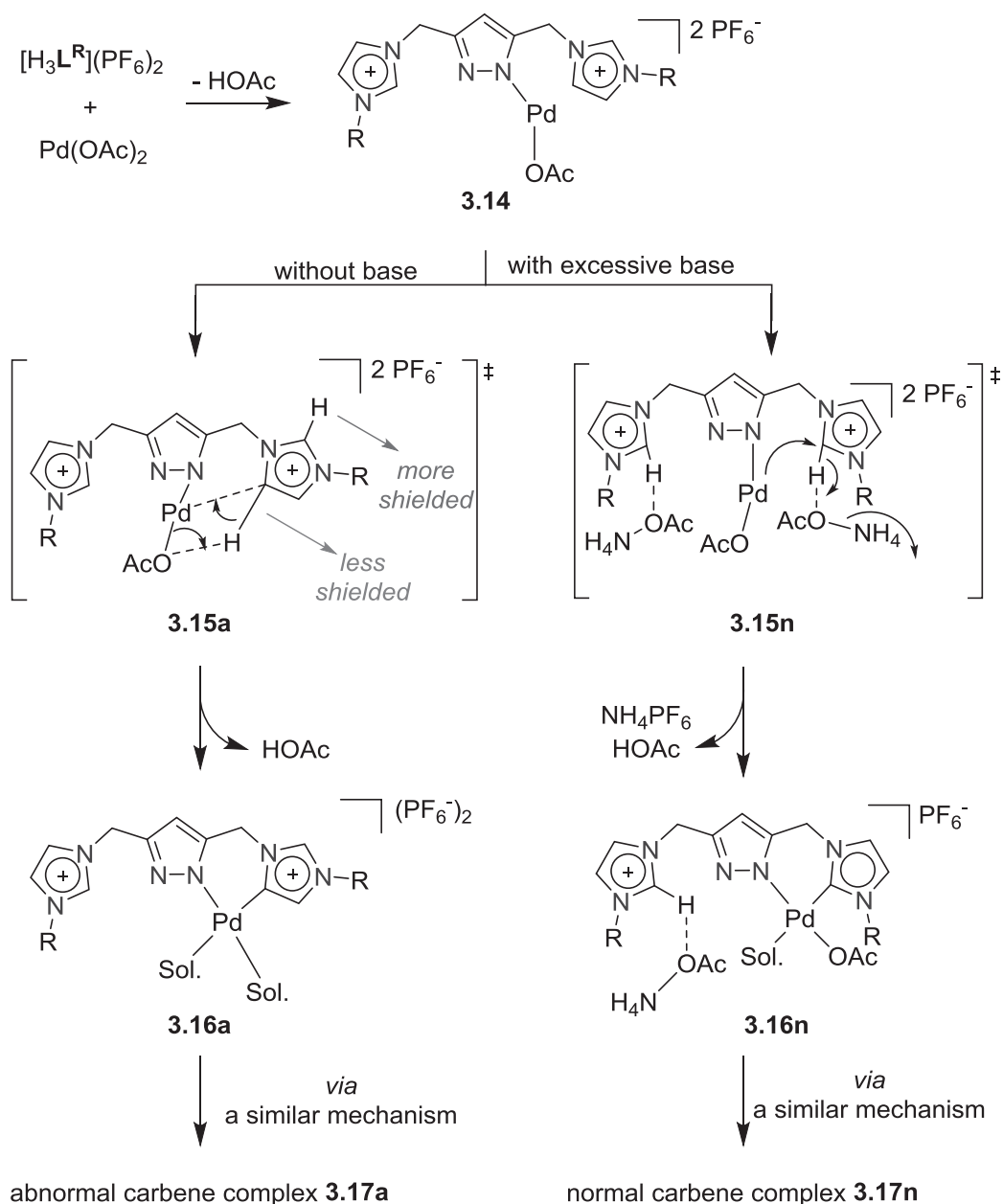
For example, previous research showed that, the reaction of the pro-ligand **3.11** and $\text{Pd}(\text{OAc})_2$ mainly gave the normal-abnormal NHC complex **3.13** and the reaction of pro-ligand, PdCl_2 and Cs_2CO_3 (9.95 equiv.) gave normal-normal NHC complex **3.12** as the major product (**Scheme 3.6**).⁹⁹ The result suggested that exterior base could accelerate the cleavage of C2–H bond and therefore induce the formation of normal carbene complexes.



Scheme 3.6. Formation of normal-normal complex **3.12** and normal-abnormal complex **3.13** in literature.

The analysis outlined above suggests an important knot to the selective formation of abnormal or normal NHC complexes, which is the H-bonding formed between the more acidic C2 proton and the exterior base. Due to the interaction with the exterior base, the C2–H bond is significantly weakened and the attack of the palladium atom to C2 position becomes easier

than that to C4/5 position. Plausible mechanisms for both reaction pathways are proposed, as shown in **Scheme 3.7**.



Scheme 3.7. Plausible mechanism of the formation of normal/abnormal carbene complexes. Sol. = solvent molecule.

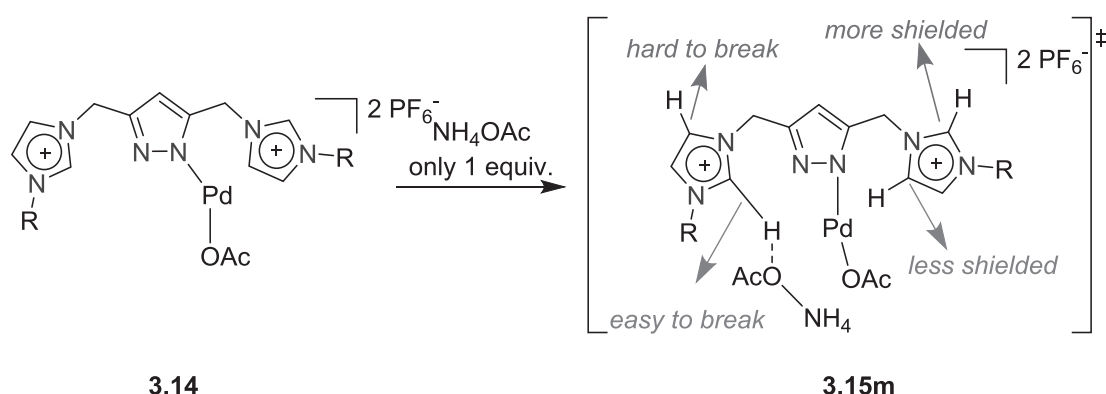
Both reactions start with the coordination of the palladium fragment $[\text{Pd}(\text{OAc})_2]^+$ to a nitrogen atom of the pyrazole ring after the detachment of acetic acid to form complex **3.14**, regardless of the amounts of exterior base used.

For the reaction without extra base, from kinetic point of view, the palladium atom prefers to coordinate to the C4/5–H bond because C4/5 region is less shielded compared to the C2

region; after a 4-membered ring transition state with the structure **3.15a**, a mononuclear abnormal carbene intermediate **3.16a** is formed after the dissociation of one molecule of acetic acid. Probably, the intermediate **3.16a** is stabilized by two solvent molecules, since there are no additional other ligands available. Subsequent reaction of two molecules of **3.16a** via a similar mechanism leads to the formation of the abnormal carbene complex **3.17a** and HPF_6 .

For the reaction with extra base, the more acidic C2-proton tends to form H-bonding with the base, thus making the C2–H bond easily breakable. Noticeably, there are two C2-protons on one ligand precursor; therefore, at least two equivalents of base are required so both C2 protons can form H-bonding (as depicted in **3.15n**). After the cleavage of the C2–H bond, the coordination of the palladium ion to C2 and the dissociation of acetic acid and ammonium hexafluorophosphate, a mononuclear palladium intermediate **3.16n** is formed. Similar to **3.16a**, one solvent molecule is coordinated to the metal ion for stabilization. Afterward, the reaction of two molecules of **3.16n** results in the product, normal carbene complex **3.17n**.

This hypothesis also explains why the reaction with one equivalent of NH_4OAc resulted in a mixture of unidentified products (**Scheme 3.8**).



Scheme 3.8. Possible pathway of reaction with only one equivalent of base.

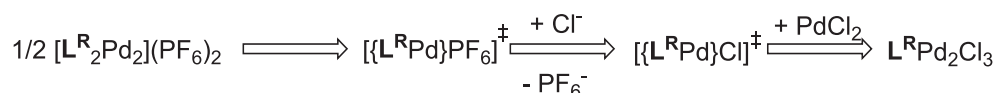
If there is only one equivalent of NH_4OAc in the reaction, the C2 proton on only one side forms H-bonding with one equivalent of base; while the other side remains intact, forming the transition state with the structure **3.15m**, in which both the coordination of C4/5–H bond to palladium fragment and the heterolysis of C2–H bond are likely to occur. Thus, the palladium ion has two attacking possibilities, either to form a normal carbene on the left part or an abnormal carbene on the right part. Considering the subsequent interaction between two molecules of any possible mononuclear palladium intermediates, the products are more complicated, as observed in the experiment.

More experimental and computational efforts are needed to testify the proposed mechanism.

3.2.4 Synthesis of $^n\text{L}^{\text{R}}\text{Pd}_2\text{Cl}_3$ and $^a\text{L}^{\text{R}}\text{Pd}_2\text{Cl}_3$

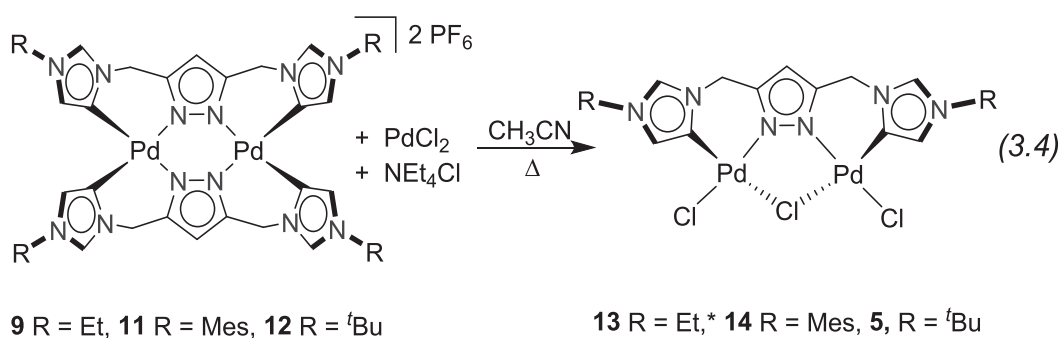
Although several palladium normal/abnormal NHC complexes $[\text{L}^{\text{R}}_2\text{Pd}_2](\text{PF}_6)_2$ and $[\text{L}^{\text{R}}_2\text{Pd}_2](\text{PF}_6)_2$ were synthesized, complex **5** was still the only neutral palladium complex with the formula of $\text{L}^{\text{R}}\text{Pd}_2\text{Cl}_3$.

The formulary relationship between $[\text{L}^{\text{R}}_2\text{Pd}_2](\text{PF}_6)_2$ and $\text{L}^{\text{R}}\text{Pd}_2\text{Cl}_3$ is shown as below (**Scheme 3.9**). $[\text{L}^{\text{R}}_2\text{Pd}_2](\text{PF}_6)_2$ can be regarded as two molecules of an imaginative species with the formula of $[\{\text{L}^{\text{R}}\text{Pd}\}\text{PF}_6]$, which transfers to $[\{\text{L}^{\text{R}}\text{Pd}\}\text{Cl}]$ after anion exchange. The simple addition of $[\text{PdCl}_2]$ to the $[\{\text{L}^{\text{R}}\text{Pd}\}\text{Cl}]$ formula leads to the formula of the expected complex $\text{L}^{\text{R}}\text{Pd}_2\text{Cl}_3$ (Eq 3.4).



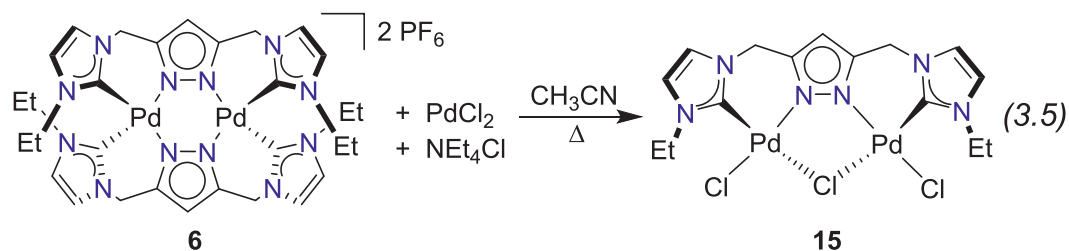
Scheme 3.9. Formulary relationship between $[\text{L}^{\text{R}}_2\text{Pd}_2](\text{PF}_6)_2$ and $\text{L}^{\text{R}}\text{Pd}_2\text{Cl}_3$.

The theoretical thought was put into test in experiment. Fortunately, reaction of $[\text{L}^{\text{tBu}}_2\text{Pd}_2](\text{PF}_6)_2$, NEt_4Cl (1.1 equiv.) and PdCl_2 (1.0 equiv.) in acetonitrile gave a bright-yellow precipitate, which was confirmed to be the known complex $^a\text{L}^{\text{tBu}}\text{Pd}_2\text{Cl}_3$.



* when R = Et, another conformer of 13 is also observed, see Table A14 in Appendix.

Compared to the old method (**Scheme 3.5**), this method involved neither the fragile reagent $\text{Pd}(\text{OAc})_2$ nor the hard-to-remove solvent DMSO, hence, the work-up was easier and cleaner product was obtained. The method could also be applied to synthesize other neutral abnormal carbene complexes **13** and **14** $^a\text{L}^{\text{R}}\text{Pd}_2\text{Cl}_3$ (Eq 3.4). Their formation was confirmed by the data of multinuclear NMR spectroscopy.



The same method was tried for normal NHC complexes $^n\text{L}^{\text{R}}\text{Pd}_2\text{Cl}_3$ (Eq 3.5); however, only one complex **15** $^n\text{L}^{\text{Et}}\text{Pd}_2\text{Cl}_3$ was successfully synthesized. Complex **15** was confirmed by multinuclear NMR spectroscopic data. The molecular structure of **15** was verified by X-ray diffraction (**Figure 3.8**).

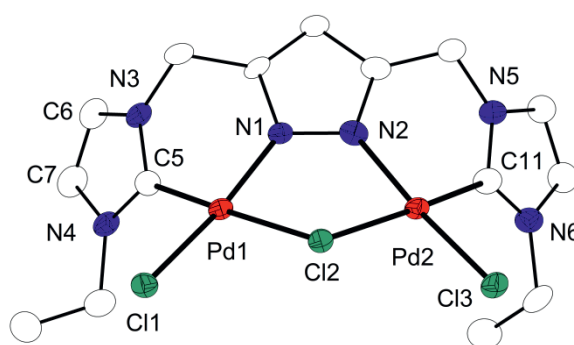


Figure 3.8. Molecular structure of the cation of $^n\text{L}^{\text{Et}}\text{Pd}_2\text{Cl}_3$; all H atoms are omitted for clarity. Anisotropic displacement ellipsoids drawn at 30% probability level. Selected bond lengths [Å] angles [°]: Pd1...Pd2 3.6517(9), Pd1–C5 1.971(8), Pd1–N1 1.966(6), Pd1–Cl1 2.3052(18), Pd1–Cl2 2.3729(17), Pd2–Cl2 2.3834(18), Pd2–Cl3 2.3089(19), C5–Pd1–N1 86.2(3), C5–Pd1–Cl1 93.7(2), Cl1–Pd1–Cl2 92.79(6), N1–Pd1–Cl2 88.16(17), Pd1–Cl2–Pd2 100.30(6), C5–N1–Pd1–Cl2 173.681(249), C5–N1–Pd1–Cl1 89.585(1263).

Reaction of **7** or **8** with PdCl_2 and NEt_4Cl gave dark-brown solid. According to the base peaks in their ESI mass spectrum, fragments of $[\text{L}^{\text{R}}_2\text{Pd}_2]^{2+}$ are still the major components. The result suggested that $[\text{L}^{\text{R}}_2\text{Pd}_2]^{2+}$ cations were not able to be transformed into $^n\text{L}^{\text{R}}\text{Pd}_2\text{Cl}_3$ species in the given reaction conditions, if the R groups were too bulky.

During the reactions of the formations of complexes $^n\text{L}^{\text{Et}}\text{Pd}_2\text{Cl}_3$ and $^n\text{L}^{\text{tBu}}\text{Pd}_2\text{Cl}_3$, the binding modes of NHC to palladium, either *via* C2 or C4/5 position, were fully retained, despite the fact that the cleavage of some $\text{Pd}-\text{C}_{\text{carbene}}$ bonds and formation of new $\text{Pd}-\text{C}_{\text{carbene}}$ bonds definitely had to occur.

Complexes ${}^n\mathbf{L}^{\text{Et}}\text{Pd}_2\text{Cl}_3$ and ${}^n\mathbf{L}^{\text{tBu}}\text{Pd}_2\text{Cl}_3$ adopt conformation **F** with approximate (non-crystallographic) C_s symmetry. Interestingly, two crystallographic structures were obtained in the crystal lattice of ${}^a\mathbf{L}^{\text{Et}}\text{Pd}_2\text{Cl}_3$, one with conformation **E** (C_2 symmetry) and the other with **F** (C_s symmetry, **Figure 3.9**), suggesting that for complex ${}^a\mathbf{L}^{\text{Et}}\text{Pd}_2\text{Cl}_3$, **E** and **F** should be close in energy, which was also confirmed by DFT calculations (discussed later).

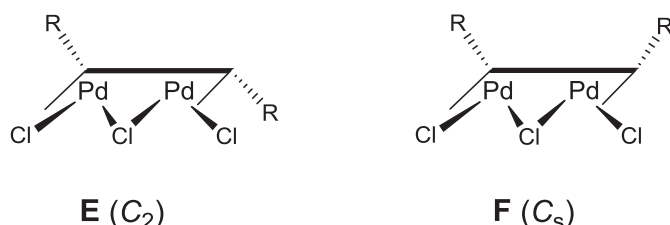
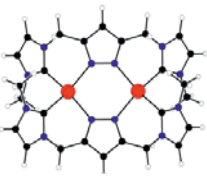
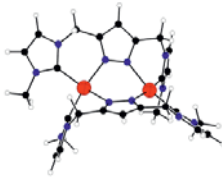
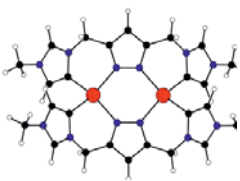
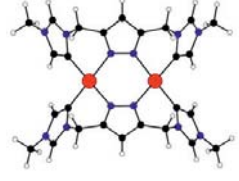
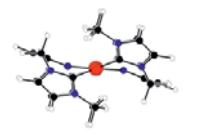
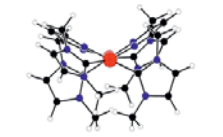
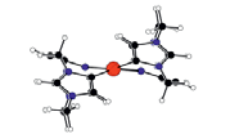
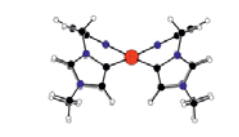


Figure 3.9. Different stereoisomers of approximate (non-crystallographic) C_2 and C_s symmetry observed for the $\mathbf{L}^{\text{R}}\text{Pd}_2\text{Cl}_3$ complexes.

The difference between the Pd...Pd distances of the two structures of ${}^a\mathbf{L}^{\text{Et}}\text{Pd}_2\text{Cl}_3$ (complex **13**) is 0.26 Å, which is reasonably large (3.75 Å in conformer **E** and 3.49 Å in conformer **F**). Comparison of bond lengths and angles of two conformers of complex **13** is collected in **Table A14** in Appendix.

Table 3.1. Different perspectives from both top and bottom for models of $[\mathbf{L}^{\text{Me}}_2\text{Pd}_2]^{2+}$ and $[\mathbf{L}^{\text{Me}}_2\text{Pd}_2]^{2+}$. Color code: Pd = red, N = blue, C = black.

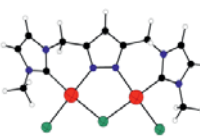
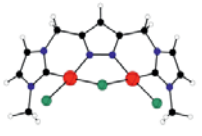
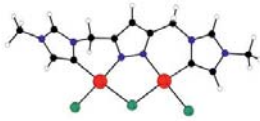
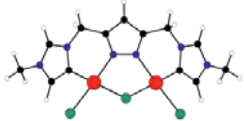
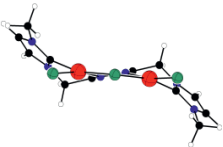
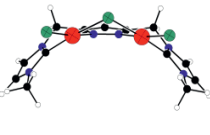
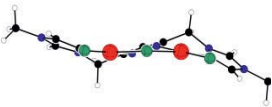
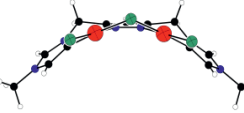
Model	$[\mathbf{L}^{\text{Me}}_2\text{Pd}_2]^{2+}$		$[\mathbf{L}^{\text{Me}}_2\text{Pd}_2]^{2+}$	
	C	D	C	D
Axial View				
Side View				
Calc. Energy	0.0 kcal/mol	+3.9 kcal/mol	+12.7 kcal/mol	+2.9 kcal/mol

DFT calculations were carried out to investigate the thermodynamic stabilities of these four types of dinuclear palladium complexes mentioned above. To best avoid the influence of the steric repulsion, ligands with methyl group on the wingtips were applied in all models. Both conformer C_{2h} (**C**) and C_{2v} (**D**) for $[\text{aL}^{\text{Me}}_2\text{Pd}_2]^{2+}$ and $[\text{nL}^{\text{Me}}_2\text{Pd}_2]^{2+}$, as well as conformer C_2 (**E**) and C_s (**F**) for $\text{nL}^{\text{Me}}\text{Pd}_2\text{Cl}_3$ and $\text{aL}^{\text{Me}}\text{Pd}_2\text{Cl}_3$ were calculated. Calculated energies of these models are shown in **Table 3.1** and **Table 3.2**. Selected bond lengths and angles of the models are collected in **Table A25** and **Table A26** in Appendix.

Calculated parameters are in good agreement with experimental data of the molecular structures determined by X-ray diffraction. In all cases, the bond lengths of $\text{Pd}-\text{C}_{\text{carbene}}$ of the calculated results are slightly longer; while the angles in the NHC rings are approximately the same.

Table 3.2. Different perspectives from both top and bottom

for models of $\text{aL}^{\text{Me}}\text{Pd}_2\text{Cl}_3$ and $\text{nL}^{\text{Me}}\text{Pd}_2\text{Cl}_3$. Color code: Pd = red, N = blue, C = black.

Model	$\text{nL}^{\text{Me}}\text{Pd}_2\text{Cl}_3$		$\text{aL}^{\text{Me}}\text{Pd}_2\text{Cl}_3$	
	E	F	E	F
Axial View				
Side View				
Calc. Energy	+5.0 kcal/mol	0.0 kcal/mol	+22.0 kcal/mol	+20.4 kcal/mol

The $\text{Pd}\cdots\text{Pd}$ distance strongly depends on the conformation, as well as the distance between the palladium atom from the plane of its coordination atoms: for $[\text{nL}^{\text{Me}}_2\text{Pd}_2]^{2+}$ and $[\text{aL}^{\text{Me}}_2\text{Pd}_2]^{2+}$, the palladium atoms are almost in the coordination-plane with a long $\text{Pd}\cdots\text{Pd}$ distance in all **C** conformers; while in **D** conformers, the $\text{Pd}\cdots\text{Pd}$ distances are shorter and



the palladium atoms are located outside the plane. In line with this shortest Pd···Pd distance is found experimentally in **D** conformer of $[\text{aL}^{\text{Me}}_2\text{Pd}_2](\text{BPh}_4)_2$ (3.82 Å). In case of neutral complexes, all calculated Pd···Pd distances are slightly longer than those found by X-ray crystallography, but the trends are well-reproduced that, Pd···Pd distances of conformers **F** are significantly shorter than for conformers **E**.

The calculated energies indicate that, for the model of normal carbene cation $[\text{nL}^{\text{Me}}_2\text{Pd}_2]^{2+}$, **C** conformer is more stable than **D** conformer by about 3.9 kcal/mol; while for the model of abnormal carbene cation $[\text{nL}^{\text{Me}}_2\text{Pd}_2]^{2+}$, the **D** conformer is much more stable than **C** conformer by about 9.8 kcal/mol.

Generally, the normal carbene palladium cation is more stable than the abnormal carbene counterpart, although the conformer **C**- $[\text{nL}^{\text{Me}}_2\text{Pd}_2]^{2+}$ is only slightly more stable than **D**- $[\text{aL}^{\text{Me}}_2\text{Pd}_2]^{2+}$ by 2.9 kcal/mol. Yet, considering the increased steric repulsion caused by larger R groups on the wingtips in normal carbene cation, it is safe to draw the conclusion that the abnormal NHC isomer with bulkier wingtips can be thermodynamically more stable.

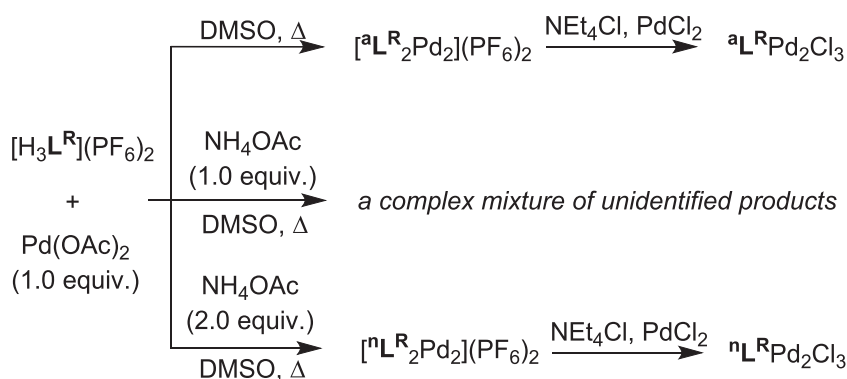
It is noticeable that the energy difference between two conformers of $\text{aL}^{\text{Me}}\text{Pd}_2\text{Cl}_3$ is reasonably small (only 1.6 kcal/mol), which is also consistent with the observation that both crystallographically independent **E** and **F** of $\text{aL}^{\text{Et}}\text{Pd}_2\text{Cl}_3$ were observed in the crystals, assuming that the steric effect of methyl and ethyl groups are similar. For $\text{nL}^{\text{Me}}\text{Pd}_2\text{Cl}_3$, **F** is much more stable than **E** by 5.0 kcal/mol and that is also the reason why only **F** were found experimentally.

Normal NHC complex $\text{nL}^{\text{Me}}\text{Pd}_2\text{Cl}_3$ is more stable than the abnormal NHC isomer $\text{aL}^{\text{Me}}\text{Pd}_2\text{Cl}_3$. Yet, based on the fact that the synthesis of $\text{nL}^{\text{R}}\text{Pd}_2\text{Cl}_3$ with bulky R groups normally failed, it is possible that the steric congestion between the R group and the terminal chloride dramatically decreases the stability of $\text{nL}^{\text{R}}\text{Pd}_2\text{Cl}_3$, thus leading to a greater stability of $\text{aL}^{\text{R}}\text{Pd}_2\text{Cl}_3$.

The expected neutral species of pyrazole-NHC based dinuclear palladium complexes ($\text{nL}^{\text{R}}\text{Pd}_2\text{Cl}_3$ and $\text{aL}^{\text{R}}\text{Pd}_2\text{Cl}_3$) have been successfully synthesized and characterized. Attempt showed that these complexes were inert to SnMe_4 , even when the reaction was carried out at high reaction temperatures; while reaction of $\text{nL}^{\text{R}}\text{Pd}_2\text{Cl}_3/\text{nL}^{\text{R}}\text{Pd}_2\text{Cl}_3$ with strong alkylation reagents, such as LiMe , simply gave lots of palladium black precipitates.

3.3 Conclusion

In summary, four types of dinuclear palladium complexes based on the pyrazole-bridged bis(NHC) ligand systems, $[\text{}^n\text{L}^{\text{R}}_2\text{Pd}_2](\text{PF}_6)_2$, $[\text{}^a\text{L}^{\text{R}}_2\text{Pd}_2](\text{PF}_6)_2$, $\text{}^n\text{L}^{\text{R}}\text{Pd}_2\text{Cl}_3$ and $\text{}^a\text{L}^{\text{R}}\text{Pd}_2\text{Cl}_3$ are successfully synthesized and some of the complexes are fully characterized. The selective formation of $[\text{}^n\text{L}^{\text{R}}_2\text{Pd}_2](\text{PF}_6)_2$ or $[\text{}^a\text{L}^{\text{R}}_2\text{Pd}_2](\text{PF}_6)_2$ is mainly determined by the amount of base used in the reaction. Consistent with the reported literature, an excess amount of base assists the formation of normal NHC complexes. The synthesis is also influenced by the bulkiness of the wingtip on the imidazole ring; when the wingtip is *tert*-butyl, no normal NHC complexes are synthesized. The neutral species $\text{}^n\text{L}^{\text{R}}\text{Pd}_2\text{Cl}_3$ and $\text{}^a\text{L}^{\text{R}}\text{Pd}_2\text{Cl}_3$ are generated from their related $[\text{}^n\text{L}^{\text{R}}_2\text{Pd}_2](\text{PF}_6)_2$ or $[\text{}^a\text{L}^{\text{R}}_2\text{Pd}_2](\text{PF}_6)_2$ precursors. It is noteworthy that, only normal NHC complexes $\text{}^n\text{L}^{\text{R}}\text{Pd}_2\text{Cl}_3$ with small wingtip, like ethyl, on the imidazole ring is able to be synthesized.





CHAPTER 4. *N*-Metallated *N*-Heterocyclic Carbene Ruthenium Complexes

4.1 Introduction and Motivation

4.1.1 Chemical shifts of metallated carbenes

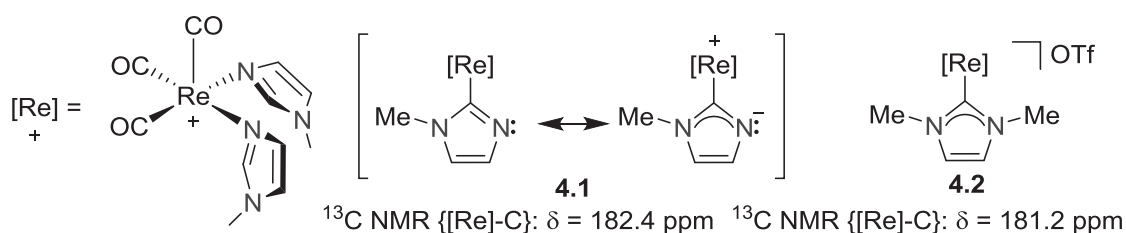
The standard *N*-heterocyclic carbene is a singlet carbene and the carbenic carbon atom has six valence electrons and an empty p orbital orthogonal to the free electron pair. The empty p orbital is stabilized either by adjacent nitrogen atoms or by a delocalized aromatic π system.

One reliable method for the characterization of the carbenic carbon atoms of *N*-heterocyclic carbenes is their chemical shifts in ^{13}C NMR spectra.⁹⁸ Normally, chemical shifts of the carbenes lie in the $\delta = 200\text{--}300$ ppm region. The factors influencing the chemical shifts of the carbenes, take ‘Arduengo-type’ carbenes for instance, include the anisotropy at the carbene center, variation of the ring size and annulation and replacement of one or both nitrogen atoms by other element atoms.⁹⁸ Yet, the substituents on the nitrogen atoms have little impact on the chemical shifts.^{15d}

Upon complexation, the free electron pair of a carbene is donated to the Lewis acidic metal fragments, and the chemical shift of the carbene changes to higher field. The change strongly depends on the Lewis acidity of the metal fragment attached. Factors that influence the acidities of the metal fragments include the types of the metal centers, the oxidation states of the metal centers and ancillary ligands. When a free carbene coordinates to a metal center with higher oxidation states and more electron-deficient co-ligands, the change of the chemical shift of the carbene to higher field is larger. Usually, the metal-carbene chemical shifts are observed in the region of $\delta = 170\text{--}220$ ppm in the ^{13}C NMR spectra. However, unlike the case for carbenic carbon chemical shifts of free carbenes, chemical shifts of metal-bound carbene signals do not necessarily appear in low-field, thus, it is not vigorous to verify or deny the formation of a metallated carbene simply by its chemical shift in the ^{13}C NMR spectrum.

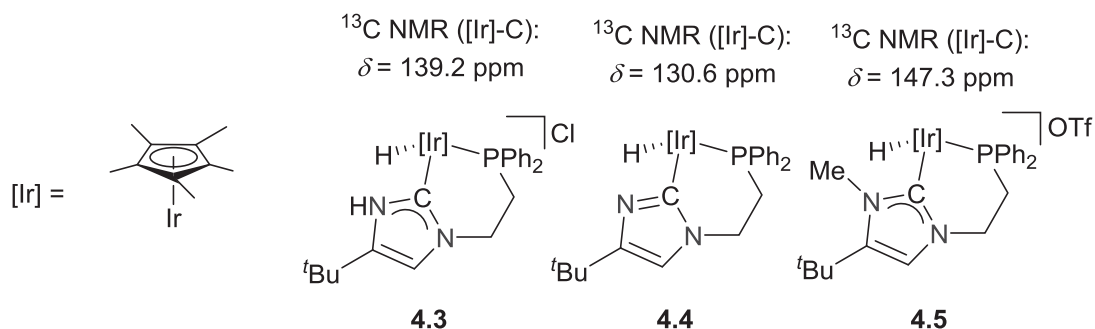
For instance, a number of imidazol-2-yl metal complexes were reported, as depicted in Chapter 1. Only recently, the suspiciously low-field chemical shifts of their metallated

carbon atoms in ^{13}C NMR spectra were accentuated (**Scheme 1.21**). For example, it was mentioned that complex **4.1** ‘features an unprecedented NHC ligand containing a non-substituted nitrogen’.⁷² The claim was probably based on the observation that the ^{13}C NMR chemical shift of the metallated carbon atom of the imidazolyl ring in **4.1** resonated at 182.4 ppm, which was quite close to that of the well-defined NHC metal complex **4.2**. However, this provocative assumption needed more scrutiny for the reason that, if complex **4.1** was a carbene complex similar to complex **4.2**, its isomeric structure involved a negative charge on the naked nitrogen atom and a positive charge on the rhenium atom, which was highly unlikely (**Scheme 4.1**).



Scheme 4.1. Reported imidazolyl complex **4.1** and the related imidazolylidene metal complex **4.2**.

Meanwhile, the chemical shifts of typical metallated carbenes do not necessarily appear in low-field in the ^{13}C NMR spectra. For example, a series of iridium complexes based on imidazole derived ligands were reported in 2004.¹⁰⁰ The ^{13}C NMR chemical shifts of the metallated carbon atoms in selected complexes are shown below (**Scheme 4.2**).



Scheme 4.2. Chemical shifts of metal carbon signals in related iridium complexes.

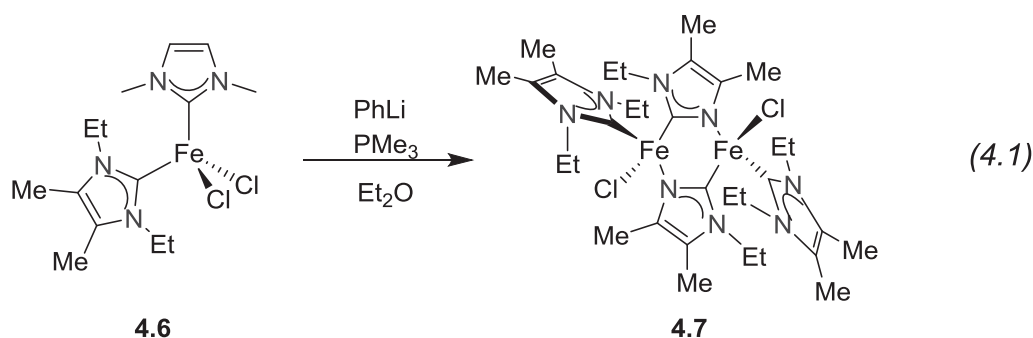
Complex **4.5** was a typical iridium NHC complex; yet, its carbene signal resonated only at $\delta = 147.3$ ppm. The reason for the observation of the carbene signal in such high-field was that the oxidation state of the metal atom in complex **4.5** was +III and the metal fragment was a relatively strong Lewis acid, which led the signal of the metallated carbene to much higher field. In the paper, an imidazolyl iridium complex **4.4** was also

synthesized. Note that, the chemical shift of the metallated carbon atom in the imidazolyl ring was at $\delta = 130.6$ ppm. The chemical shift difference of the two metallated carbon atoms of complex **4.5** and **4.4** was less than 20 ppm.

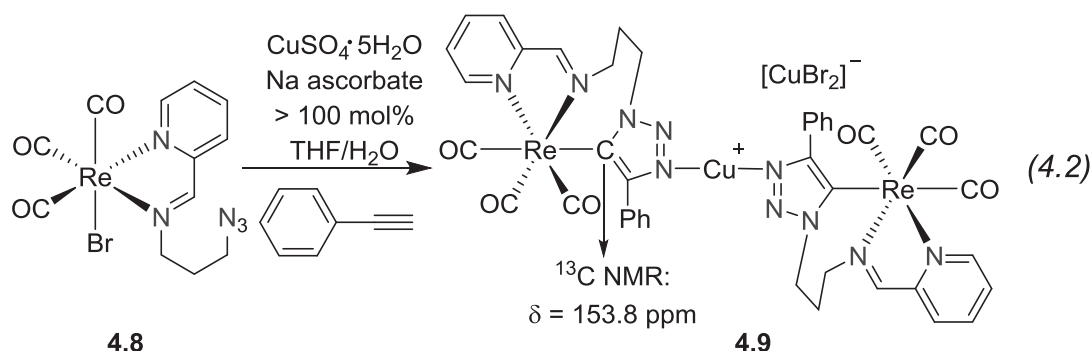
Therefore, the observation of a metallated carbon signal in low-field (near $\delta = 200$ ppm) does not indicate the formation of a metallated carbene species, and *vice versa*.

Recently, several metal complexes, in which both nitrogen atoms and carbon atoms of the *N*-heterocyclic rings were coordinated to metal fragments, were reported.^{72, 77} Most of the efforts were focused on their structural particularities, yet a clear comprehension of the bonding modes in these complexes was still lacking.

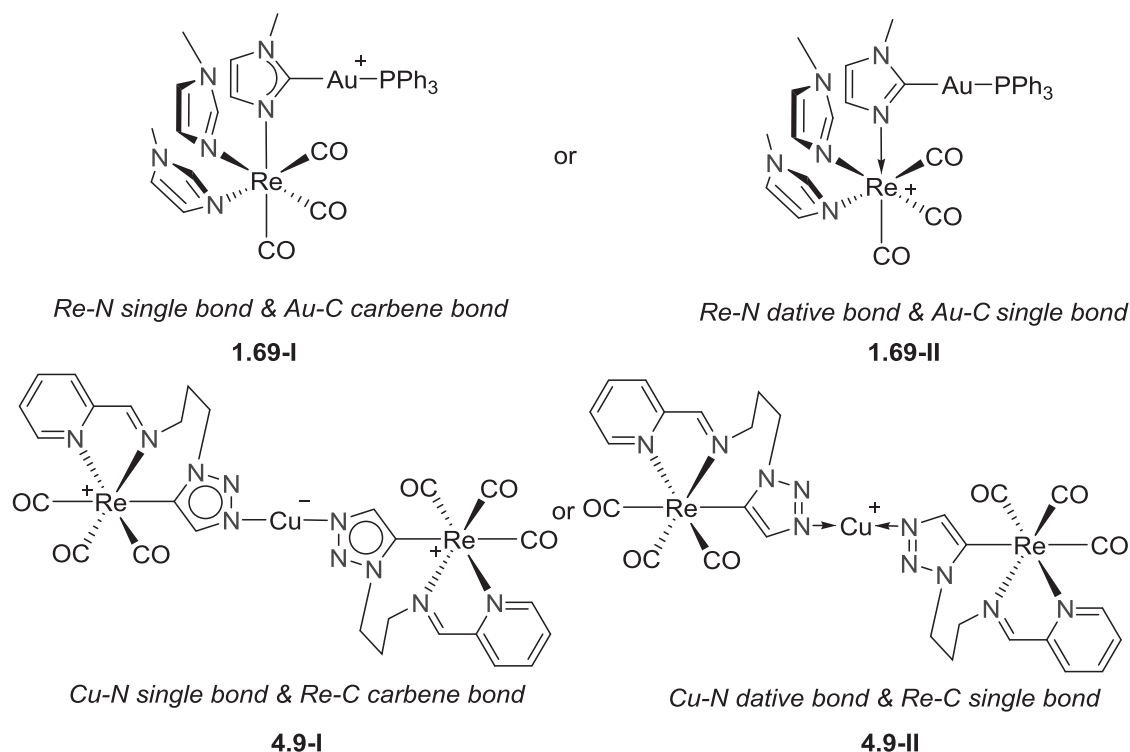
For instance, Deng reported an unusual dinuclear iron complex **4.7** from the reaction of bis(*n*NHC) iron complex **4.6** with phenyl lithium (Eq 4.1). Although it was not specially described in the paper, according to the drawings of its structure, complex **4.7** was regarded as a carbene complex, probably because its precursor **4.6** was a carbene species. However, no solid evidence was presented to prove it in the paper, not even a ¹³C NMR spectrum (complex **4.7** was paramagnetic).⁷⁵



A trinuclear rhenium-copper complex **4.9** based on triazole derived ligand was synthesized by Miguel and co-workers from the [3+2] click reaction of acetylene and rhenium complex **4.8** in the presence of copper salt (Eq 4.2). In **4.9**, two rhenium fragments were bridged by a copper atom *via* nitrogen atoms of the triazole rings. It was assumed in the paper^{50d} that the Re–C_{triazole} bonds remained single bond, and the Cu–N bonds were dative bonds, according to the drawings. The chemical shifts of the metallated carbon atoms in the triazole ring were found at $\delta = 153.5$ ppm in the ¹³C NMR spectrum. No further bond analysis was provided in the paper.



The bonding modes of the metal–carbon and metal–nitrogen bonds in the above trinuclear complex **4.9** are essentially the same to the dinuclear complex **1.69** mentioned in Scheme **1.21**. The schematic structures (Scheme **4.3**) suggest that, in both complexes, either the metal–carbon bonds are single bonds when the metal–nitrogen bonds are dative bonds (in **1.69-II** and **4.9-II**); or the metal–carbon bonds are carbene bonds when the metal–nitrogen bonds are single bonds (in **1.69-I** and **4.9-I**), depending on the location of the charges. Hence, a persuasive criterion is demanded to verify the real bonding types in these novel *N*-metallated *N*-heterocycle complexes.



Scheme 4.3. Two possible drawings for *N*-metallated *N*-heterocycle derived complexes.

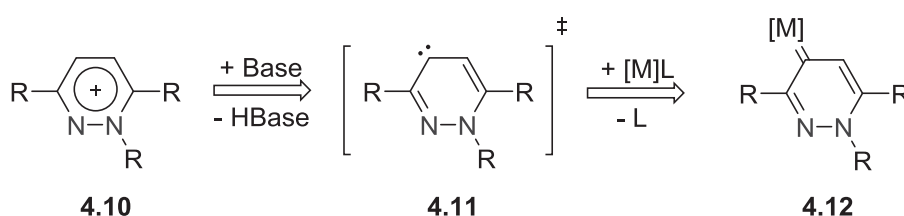


4.1.2 Motivation

Previously, the first class of pyridazine derived NHC palladium complexes **1-4** were synthesized by oxidative addition of a C–Cl bond onto Pd(0) species. In these complexes, the insertion of Pd(0) species selectively occurred in C–Cl bonds at the *ortho* positions of the alkylated nitrogen atoms, generating metal pyridazin-6-ylidene complexes (see Chapter 2).⁹² Pyridazin-6-ylidenes or their derivatives were so far the only examples of NHCs based on pyridazine derivatives.

In a pyridazin-6-ylidene carbene, the carbenic carbon atom is at the *ortho*-position of the alkylated nitrogen atom. *N*-heterocyclic carbenes with the carbenic carbon atoms more remote from nitrogen atoms in the *N*-heterocyclic rings are normally stronger donating ligands, according to the empirical conclusion depicted in **Chart 1.4**. Thus, it would be interesting to synthesize other pyridazinylidene ligands, such as pyridazin-4-ylidene, in which the carbenic carbon atom is at the *para*-position of the substituted nitrogen atom.

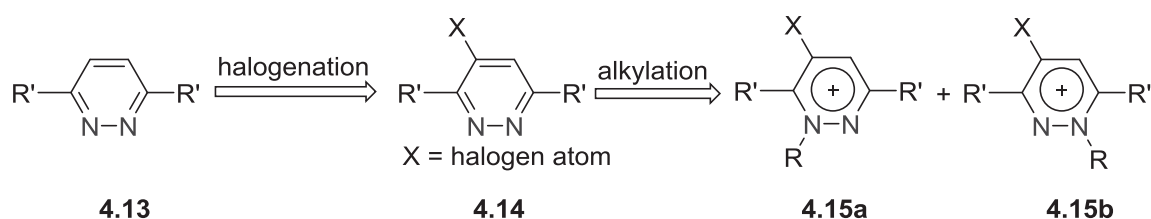
The initial target of pyridazin-4-ylidene metal complexes was designed as below (**Scheme 4.4**). Similarly to the formation of pyridazin-6-ylidene metal complexes,^{66c} the ligand precursor **4.10** can be deprotonated to give a free carbene species **4.11**. The carbene of **4.11** coordinates to a vacant site of a metal fragment, forming a pyridazin-4-ylidene metal complex **4.12**.



Scheme 4.4. Hypothetic formation of pyridazin-4-ylidene metal complex.

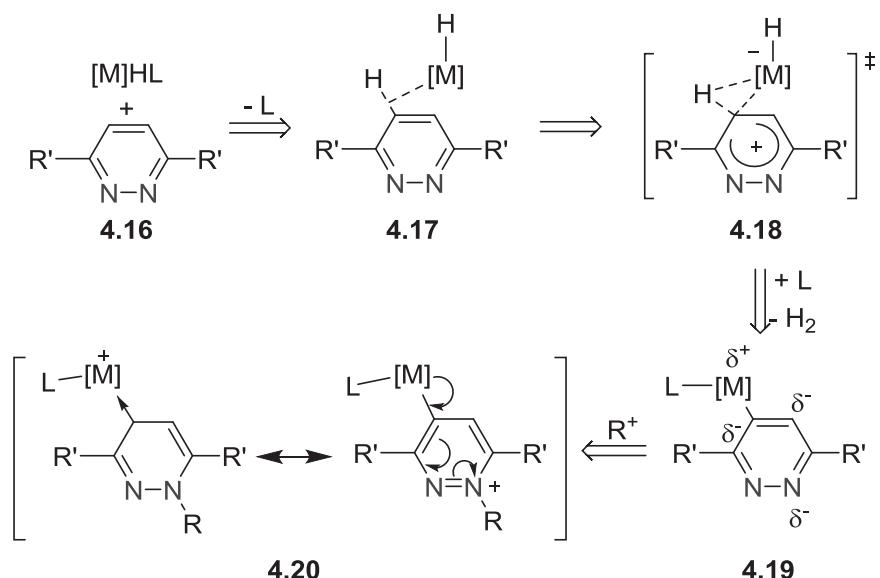
4.1.3 Material and methodology

By means of oxidative addition of C–X (X = halogen atom) bonds of C-halogenated-*N*-heterocyclic cations onto low valent metal complexes, such as Pd(0) and Ir(I) reagents, corresponding metal carbene complexes can be readily obtained, in which the oxidation states of the metal centers are increased by two units in the new complexes (method **d**, **Scheme 2.2**). However, this strategy is not a good option for the proposed reaction in **Scheme 4.4** because the syntheses of ligand precursors 4-halogenated-pyridazinium salts are not easy (**Scheme 4.5**).



Scheme 4.5. Possible problems for the synthesis of *para*-halogenated pyridazinium.

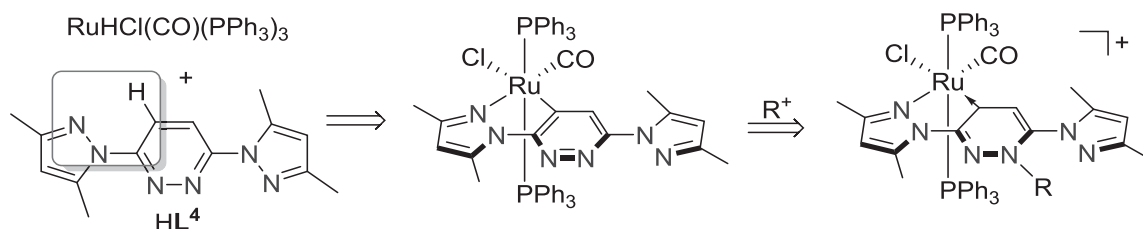
The first step of the halogenations of a 3,6-disubstituted-pyridazine **4.13** to form **4.14** is not known so far. The second step of the alkylation of the 4-halogenated-pyridazine **4.14** may take place on both nitrogen atoms, leading to a mixture of two constitutional isomers **4.15a** and **4.15b**, which probably have close physical properties and are hard to be separated.



Scheme 4.6. Alternative synthetic route to *para*-carbene complexes derived from pyridazine.

To avoid these possible troubles, a different synthetic route was designed (**Scheme 4.6**). One C–H bond in pro-ligand **4.16** is agostically coordinated to a metal hydrido fragment to form a labile intermediate **4.17**, which transforms into intermediate **4.19** after a three-membered ring species **4.18** and detachment of dihydrogen. Alkylation is likely to occur at the *para*-nitrogen atom to the metallated carbon in **4.19**, because this nitrogen atom is more electron-rich due to the mesomeric effect, thus leading to the targeted pyridazin-4-ylidene complex **4.20**.

Ligand precursor **HL**⁴, 3,6-bis(3,5-dimethyl-1*H*-pyrazol-1-yl)pyridazine, and a ruthenium hydride complex, RuHCl(CO)(PPh₃)₃ were chosen for the designed reaction. It was expected that the pyrazole sidearm were able to coordinate to the hydride complex, brought it closer to the pyridazine ring, and thus accelerated the C–H bond activation (**Scheme 4.7**).



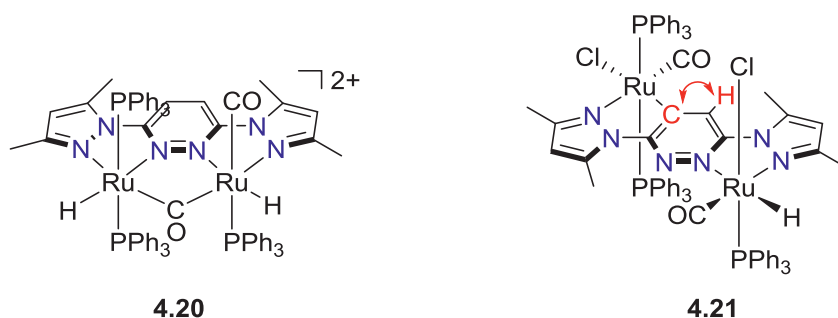
Scheme 4.7. Proposed reaction to synthesize the anticipated pyridazin-4-ylidene metal complex.

4.2 Result and Discussion

4.2.1 Synthesis of complex 16

Treatment of **HL**⁴ with one equivalent of RuHCl(CO)(PPh₃)₃ in toluene at reflux for one day gave a dark-brown solution with some yellow crystalline material. The crystalline material was soluble in dichloromethane, slightly soluble in acetone and acetonitrile and insoluble in diethyl ether, toluene or hexane. It was stable in air and moisture in solid state. Its solution in dichloromethane gradually turned greenish after several days, but the ¹H NMR spectroscopy of the product in *d*²-dichloromethane showed no obvious change.

In the ¹H NMR spectrum of the product, a *dd* peak is found at $\delta = -11.42$ ppm ($J_1 = 13.2$ Hz, $J_2 = 11.7$ Hz), indicating the presence of metal hydride(s) in the complex. The ³¹P NMR spectrum shows a singlet at $\delta = 51.8$ ppm and two doublets $\delta = 46.1$ ppm ($J = 273.1$ Hz) and 41.4 ppm ($J = 272.9$ Hz), respectively, implying that there are two metal centers respectively tethered with one and two phosphine ligands. Two possible structures (**4.20** and **4.21**, **Scheme 4.8**) for the product were proposed, in **4.20**, both ruthenium atoms are chelated in *N,N*-pockets and they are on the same side with respect to the pyridazine ring; while in **4.21**, one ruthenium atom chelated in an *N,N*-pocket is pointing away from the other chelated in a *C,N*-pocket.



Scheme 4.8. Possible structures of the product from the reaction of **HL**⁴ and RuHCl(CO)(PPh₃)₃.

A singlet peak at reasonably low field $\delta = 187.0$ ppm in the ¹³C NMR spectrum is observed, signifying that there may be a carbon atom attached to a metal ion (the signals of carbonyls groups were also spotted, but they were usually observed in $\delta > 200.0$ ppm region in the ¹³C NMR spectra). Meanwhile, the high resolution ESI mass spectrum (**Figure 4.1**) shows a major peak consistent with the simulated isotope pattern of

$[\text{L}^4\text{HRu}_2(\text{CO})_2(\text{PPh}_3)_3\text{Cl}]^+$, which is consistent with the molecular formula of $[\text{M} - \text{Cl}]^+$ of **4.21**.

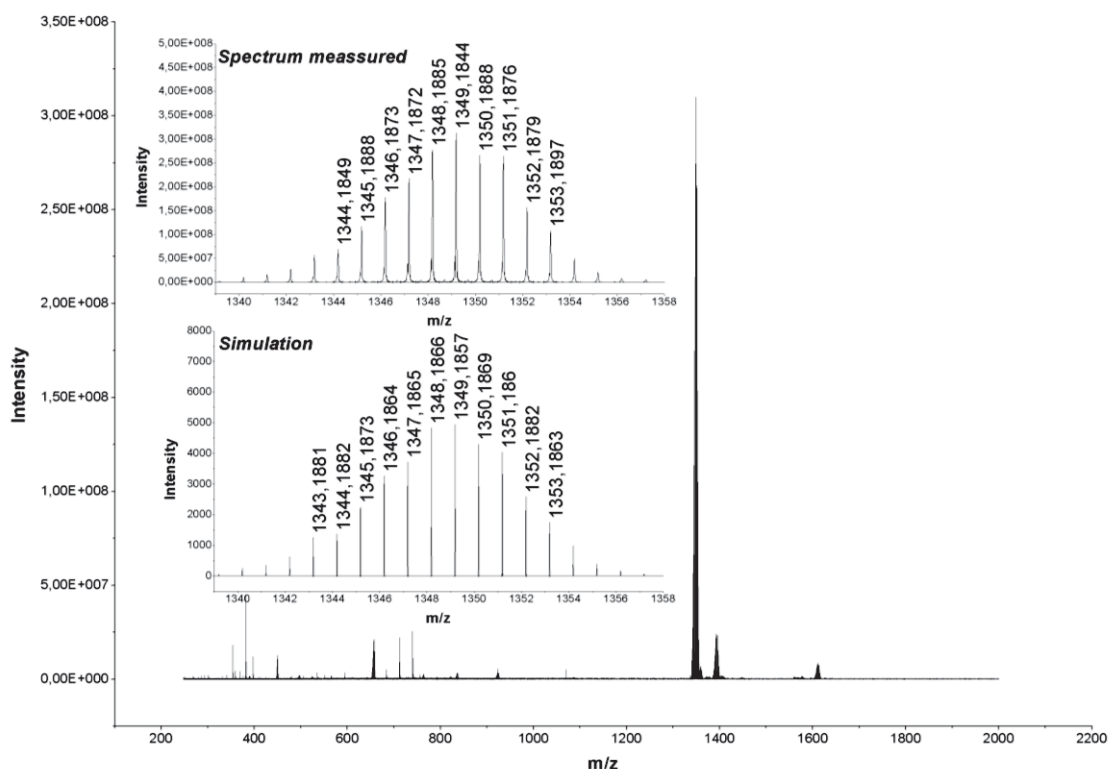


Figure 4.1. High resolution ESI mass spectrum of the product. The inset shows the experimental and simulated isotopic distribution patterns for $[\text{C}_{70}\text{H}_{62}\text{N}_6\text{Cl}_2\text{O}_2\text{P}_3\text{Ru}_2]^+$, *i. e.*, $[\text{L}^4\text{HRu}_2(\text{CO})_2(\text{PPh}_3)_3]^+$

Moreover, the 2D ^{13}C - ^1H HMBC NMR spectrum (**Figure 4.2**) suggests that one aromatic proton is correlated to the carbon atom with the signal resonating at $\delta = 187.0$ ppm. Since all other aromatic protons are from phosphine ligands, this proton can only be assigned to the one of the pyridazine ring (as labeled in red in **4.21**). All the evidence pointed to the formation of complex **4.21**.

However, the subsequent X-ray crystallographic result revealed a new structure, complex **16**. Albeit the structure determined by X-ray diffraction was quite close to **4.21**, the arrangements of the ancillary ligands in these two structures were different.

In the molecular structure of complex **16** determined by X-ray diffraction (**Figure 4.3**), N3–N4 and N5–N6 bonds are on the opposite sides of the pyridazine ring, in line with the expectation. Two coordination pockets, namely the *C,N*-pocket and the *N,N*-pocket, are formed to chelate Ru1 and Ru2, respectively. In the *C,N*-pocket, Ru1 is bound to two chlorides, one carbonyl and one phosphine; while in the *N,N*-pocket, Ru2 is bound to

two phosphines, one carbonyl and one hydride. The three *N*-heterocyclic rings are almost in the same plane; the dihedral angle between the pyrazole_(N3–N4) plane and the pyridazine plane and the dihedral angle between the pyrazole_(N5–N6) plane and the pyridazine plane are 6.3° and 2.3°, respectively.

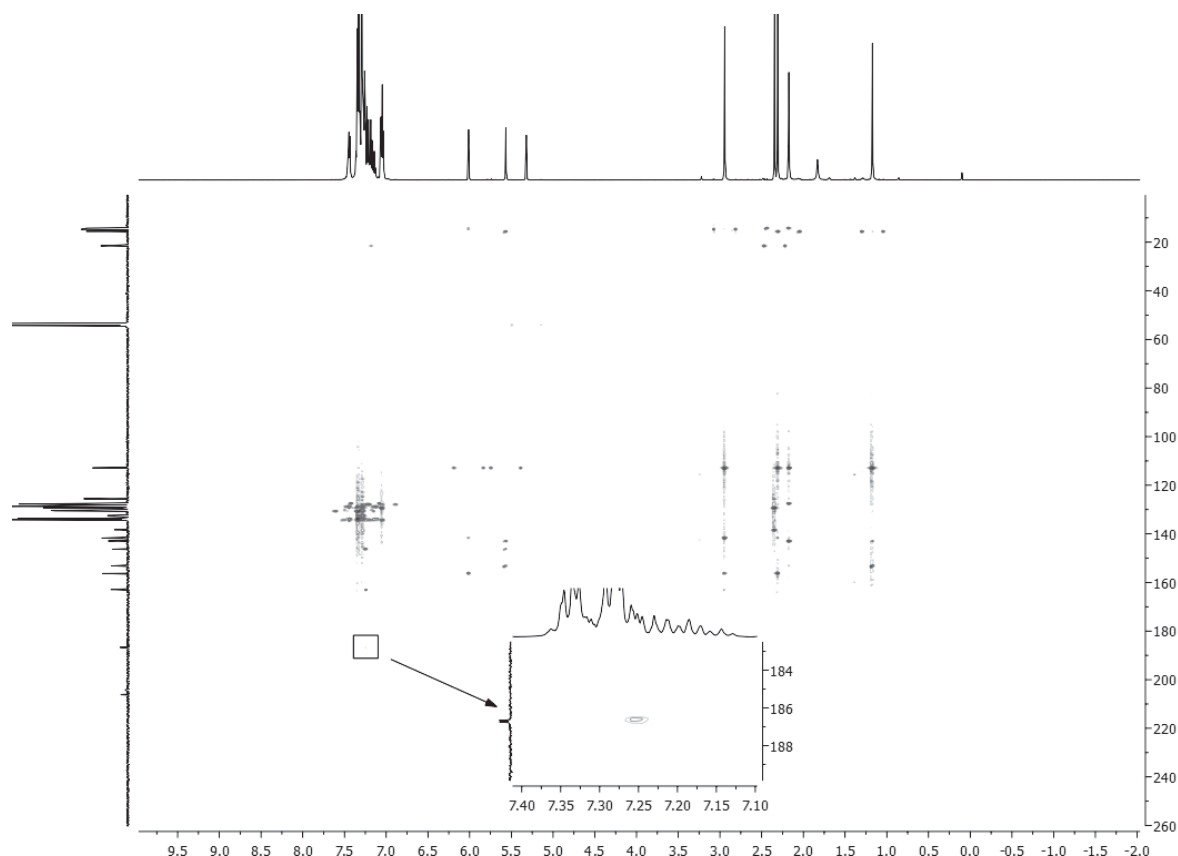


Figure 4.2. The 2D ^{13}C -HMBC/ ^1H NMR spectrum of the product.

Ru1 adopts an almost perfectly octahedral geometry with the carbonyl group *trans* to N4 and one chloride *trans* to the metallated carbon atom; while the octahedral configuration of the Ru2 fragment is distorted in a way that the angle between the N2–Ru2–N6 plane and the Ru2–P2 bond is 12.2°. Presumably, the steric congestion between the phenyl groups on the two phosphine ligands causes the distortion of the Ru2 geometry away from octahedral. However, it is unclear why it does not occur to the Ru1–P1 bond. In Ru2 fragment, the hydride is *cis* to both phosphine ligands and the two phosphine ligands are *trans* to each other, which is consistent with the data from the multinuclear NMR spectra; in the ^1H NMR spectroscopy of **16**, the hydride is *dd* splitted with two close coupling constants ($J_1 = 13.2$ Hz, $J_2 = 11.7$ Hz) and in the ^{31}P NMR spectroscopy, two phosphorous signals appear to be doublets at $\delta = 46.1$ ppm and 41.4 ppm, respectively. The large coupling constants $J = 272.9$ –273.1 ppm indicate that the two phosphorus atoms are *trans* to each other.

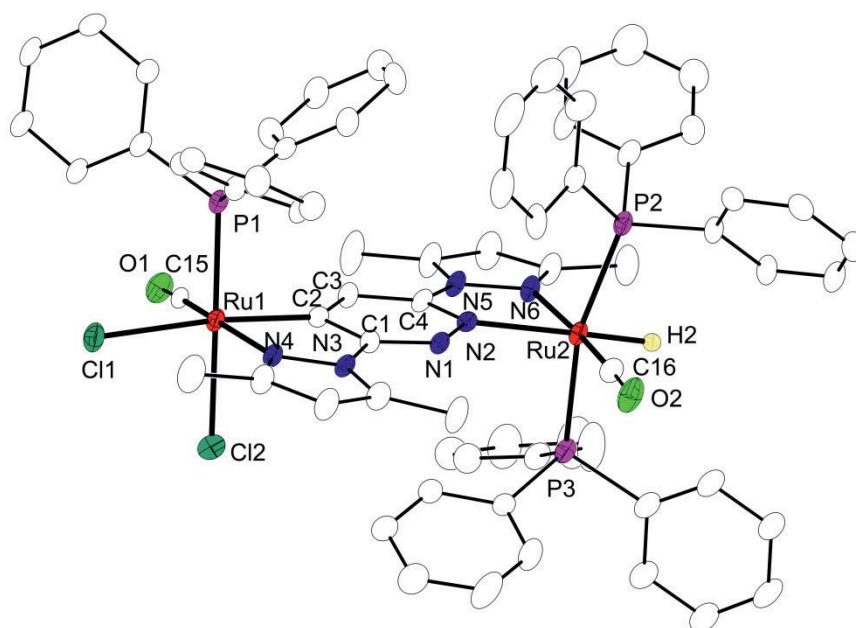
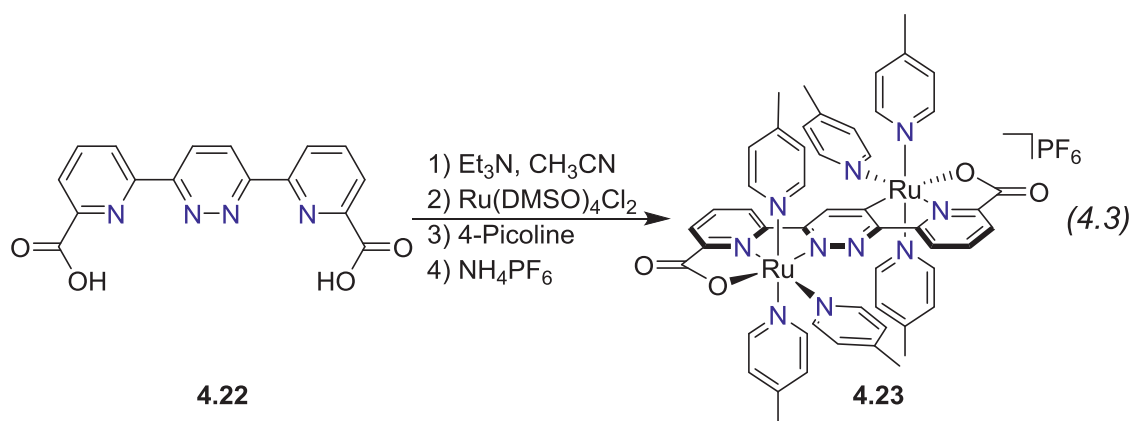


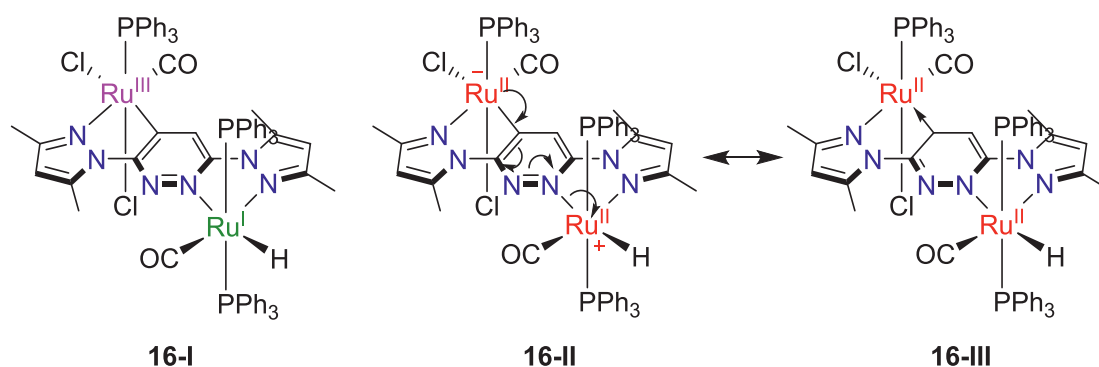
Figure 4.3. Molecular structure of **16**. Anisotropic displacement ellipsoids drawn at 30% probability level (except for the metal hydride, which drawn at 5% probability for clarity). The solvent molecule, hydrogen atoms have been omitted for clarity (except ruthenium hydride). Selected bond lengths [Å] angles [°]: Ru1–C2 2.020(5), Ru1–N4 2.163(4), Ru1–Cl1 2.5005(12), Ru1–C15 1.823(5), Ru1–P1 2.2856(13), Ru1–Cl2 2.4430(16), Ru2–N2 2.141(4), Ru2–N6 2.114(4), Ru2–C16 1.847(6), Ru2–P2 2.3437(15), Ru2–P3 2.3416(15), N4–Ru1–C2 78.21(18), P1–Ru1–Cl2 178.96(6), N2–Ru2–N6 74.42(14), P2–Ru2–P3 165.08(4).

Similar dinuclear ruthenium complexes based on pyridazine bridged ligands with two metal centers on the opposite sides of the ligands were reported earlier.¹⁰¹ In 2005, a series of dinuclear ruthenium complexes based on 3,6-bis(ligand)-pyridazine were synthesized. According to the paper, two ruthenium fragments were coordinated to the *N,N*- and *C,N*-pockets, respectively,¹⁰² forming Janus-type metal complexes. In 2009, another group reported a well-defined 3,6-bis(2'-pyridyl)-pyridazine **4.22** derived dinuclear complex **4.23**, and its structure was confirmed by X-ray diffraction (Eq. 4.3).^{101a}

According to the structure drawn in the paper, it was assumed that a dative N→Ru bond and a single C–Ru bond were formed (Eq. 4.3). A subsequent study revealed that complex **4.23** had high catalytic activity for water oxidation.^{101b} As far as is concerned, complex **4.23** has been the only well-defined *C,N*-dimetallated ruthenium complex based on a pyridazine derived ligand.



Comparison of structural data of complex **16** and **4.23** shows that, the Ru–C_{pyridazine} bond (2.020(5) Å) in complex **16** is close to that of complex **4.23** (2.005(3) Å); while the Ru–N_{pyridazine} bond (2.141(4) Å) in **16** is significantly longer than that of complex **4.23** (1.955(3) Å) by 0.186 Å,^{101a} probably due to the strong *trans* influence of the hydrido ligand, which increases the Ru–N_{pyridazine} bond length in complex **16**.



Scheme 4.9. Consideration of the oxidation states of the two ruthenium atoms in complex **16**.

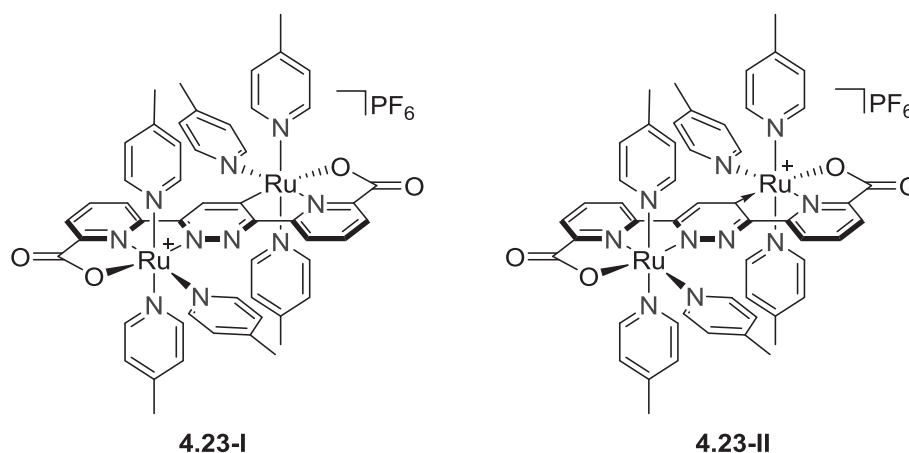
Meanwhile, the arrangement of the ancillary ligands of complex **16** is intriguing. In complex **16**, Ru^I is coordinated with two chlorides; since the reaction was carried out in toluene, the only chloride source should be RuHCl(CO)(PPh₃)₃. Apparently, there is only one chloride in RuHCl(CO)(PPh₃)₃ and the formation of **16** must have involved the rearrangement of the ancillary ligands. It is unlikely that two Ru^{II} ions of two molecules of RuHCl(CO)(PPh₃)₃ disproportionate into one Ru^I ion and one Ru^{III} ion in complex **16** (**16-I**, **Scheme 4.9**), thus, the oxidation states of the two Ru atoms in complex **16** should remain +II. The eighteen-electron rule, which works perfectly for close-shell octahedral complexes of group VIII transition metals, implies that the two Ru^{II} atoms are negatively and positively charged, respectively (**16-II**). Structure **16-II** resonates to a more stable mesomeric structure **16-III** after the transfer of the charge. Thus, the pyridazine ring be-

comes a two electron donor to the Ru atom in the *C,N*-pocket; *i. e.*, the pyridazine ring turns to a carbene species.

Here, the bond types in complex **16** come to the fore that, instead of a single bond as expected, a metal-carbene bond between the Ru atom in the *C,N*-pocket and the carbon atom of the pyridazine ring is formed.

In other words, an unusual pyridazinyl-4-ylidene metal complex is synthesized, considering the metallated carbon atom is at the *para* position of the metallated nitrogen atom in the pyridazine ring. Moreover, complex **16** is the first example of a well-defined *N*-metallated *N*-heterocyclic carbene complex.

Recently, several metal complexes containing *N*-heterocyclic rings, of which both carbon atoms and nitrogen atoms were bound to metal fragments, were reported. Some of them were also claimed to be *N*-metallated carbene species, based on the observation of the low-field metallated carbon signals in the ^{13}C NMR spectra. However, as discussed before, low-field ^{13}C chemical shifts do not necessarily indicate the formation of metallated carbene bonds. Therefore, whether the complexes of this type contain metal carbenes is still undetermined.



Scheme 4.10. Different locations of the positive charge in complex **4.23** lead to two different structures.

Take complex **4.23**,¹⁰¹ which has a similar structure to complex **16**, for instance (**Scheme 4.10**), because of the presence of a positive charge, there are two possible structures for the complex. If the positive charge locates on the Ru atom in the *N,N*-pocket, the Ru–C_{pyridazine} bond is a single bond (**4.23-I**); if the positive charge locates on the Ru atom in the *C,N*-pocket, the Ru–C_{pyridazine} bond becomes a two-electron dative bond (**4.23-II**). In all likelihood to complex **16**, structure **4.23-II** seems to be more possible; however no solid conclusion can be drawn without further evidence.

To the best of our knowledge, all other reported metal complexes containing *N*-metallated *N*-heterocyclic fragments were positively charged, which means their bonding modes are also unclear, like the scenario for complex **4.23**.

4.2.2 Computational study

In order to understand the relative stability of pyridazinylidene ligands (in which the carbenic carbon atoms are at 4-, 5- or 6-position of the substituted nitrogen) to pyridazine and also to investigate the donating capacities of pyridazinylidenes and pyridazine, DFT calculations were carried out.²⁴

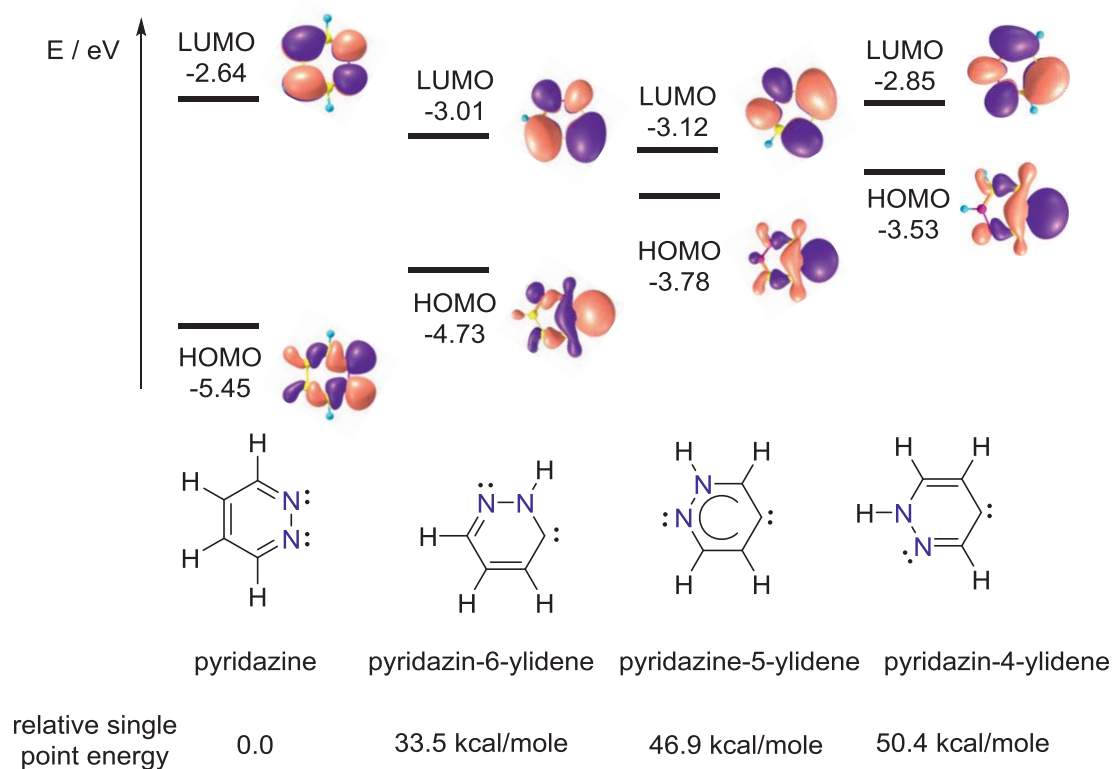
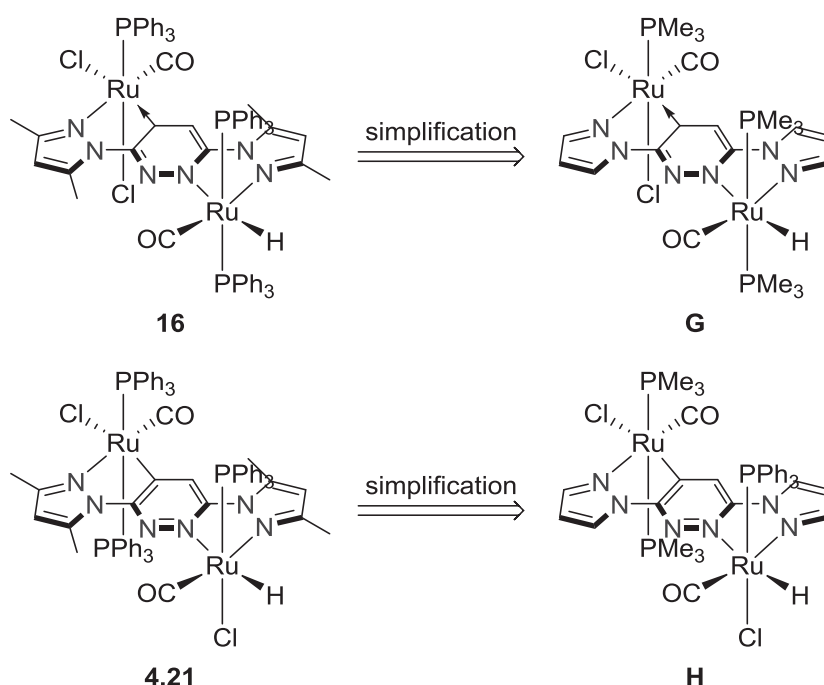


Figure 4.4. LUMOs, HOMOs and relative single point energies of pyridazine and pyridazinylidenes

The HOMOs, LUMOs and relative single point energies of these species are depicted in **Figure 4.4**. According to the relative energies, pyridazinylidenes are highly unstable species compared to pyridazine and the stability order of the three pyridazinylidenes decreases as pyridazin-6-ylidene > pyridazin-5-ylidene > pyridazin-4-ylidene.

The HOMOs describe the donating groups of each ligand. In pyridazine, the HOMO is in the plane of the six-membered ring and mainly located in the two nitrogen atoms; while in pyridazinylidenes, HOMOs are also in the plane of the six-membered rings but

mainly located in the carbenic carbon atoms. Higher HOMO energies represent stronger donating capacities of the corresponding ligands and apparently, pyridazine is the weakest donating ligand with the HOMO energy of -5.45 eV. Both pyridazin-4-ylidene (with HOMO energy of -3.53 eV) and pyridazin-5-ylidene (with HOMO energy of -3.78 eV) are stronger donating ligands than most reported NHC ligands, except for pyridyl-4-ylidene (with HOMO energy of -3.31 eV).⁵⁵ The donating capacity of pyridazin-6-ylidene is mediocre, which is slightly larger than that of imidazol-2-ylidene (with HOMO energy of -4.97 eV).²⁴ The order of donating capacity of three pyridazinylienes is consistent with the empirical conclusion that in the same *N*-heterocyclic carbene ring, the farther the carbenic carbon is remote from the nitrogen atoms, the stronger its donating capacity will be.



Scheme 4.11. Calculational models **G** and **H** from complex **16** and the theoretical isomer **4.21**.

In order to understand the stability of complex **16** and also to shed some light on the reaction mechanism of the formation of **16**, DFT calculations on the models **G** and **H** based on complex **16** and its imaginative isomer **4.21**, respectively, were carried out. To reduce the calculation expense, PPh₃ in **16** and **4.21** were replaced by PMe₃ and the (3,5-dimethyl-1*H*-pyrazol-1-yl) rings were replaced by (1*H*-pyrazol-1-yl) rings in the calculated models (**Scheme 4.11**).

In the calculated result, all the ruthenium fragments adopt slightly distorted geometry away from octahedral. In model **G**, the dihedral angles between the pyridazine ring and

the pyrazole rings are 11.3/11.4°. The dihedral angles between the pyridazine ring and the five-membered rings containing ruthenium atoms are 10.3/12.5°. In model **H**, the dihedral angles between the pyridazine ring and the pyrazole rings are 6.8/10.8°. The dihedral angles between the pyridazine ring and the five-membered rings containing ruthenium atoms are 5.6/12.8°.

Comparison of selected bond lengths and angles of complex **16** and models **G** and **H** are collected in **Table A27**. The important bond lengths in **G** are close to those found experimentally in the structure of **16** in solid state determined by X-ray diffraction and the absolute values of bond length differences between **16** and model **G** are mostly smaller than 0.015 Å.

The bond lengths of model **G** and **H** are generally close to each other, except for those in the five-membered ring involving the *C,N*-pocket and the ruthenium ion (**Table A28**). The Ru–C bond length in the ring in **G** (1.987 Å) is significantly smaller than that in **H** (2.028 Å) by 0.041 Å. The C–C bond length in the ring in **G** (1.435 Å) is reasonably larger than that in **H** (1.422 Å) by 0.013 Å. The drastic differences that occur in this specific area indicate that the pyridazine ring in **G** serves as a strong donating species and the Ru–C bond length is significantly influenced.

The calculated LUMOs and HOMOs of models **G** and **H** are shown in **Figure A11** and **Figure A12**. These orbitals are depicted by schematic drawings in **Figure 4.5**. Both of the HOMOs of the models are non-bonding orbitals from the interactions of d orbitals of the metal atoms and the p orbitals of the chloride ligands, however, in model **G**, the HOMO is on the metal fragment [Ru₁] in the *C,N*-pocket, while in model **H**, the HOMO is on the metal fragment [Ru₄] in the *N,N*-pocket. Both of the LUMOs of the models are π^* anti-bonding orbitals; in the LUMO of model **G**, p orbitals of the atoms of the pyridazine ring and the [Ru₂]-bound pyrazole ring are conjugated to form the anti-bonding orbital; while in the LUMO of model **H**, p orbitals of all atoms in the three heterocyclic rings are conjugated. The energy difference of HOMOs in **G** and **H** is almost negligible; as well as for the case of LUMOs.

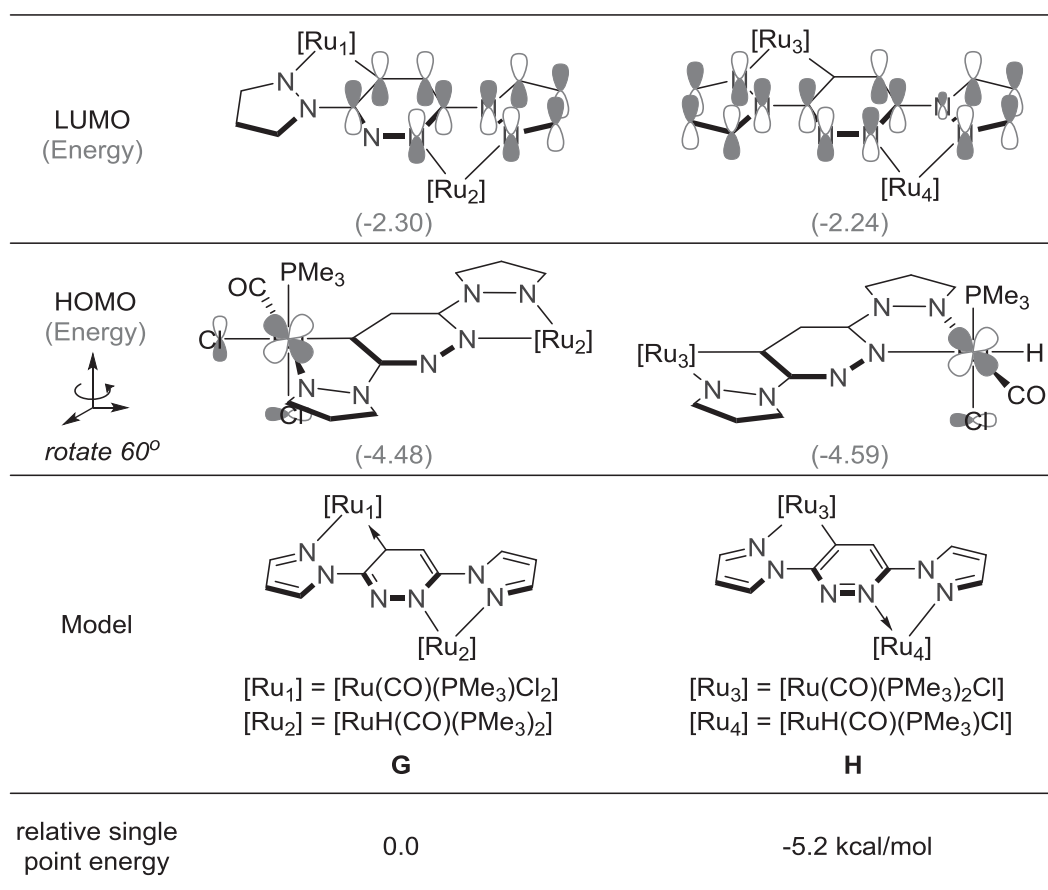


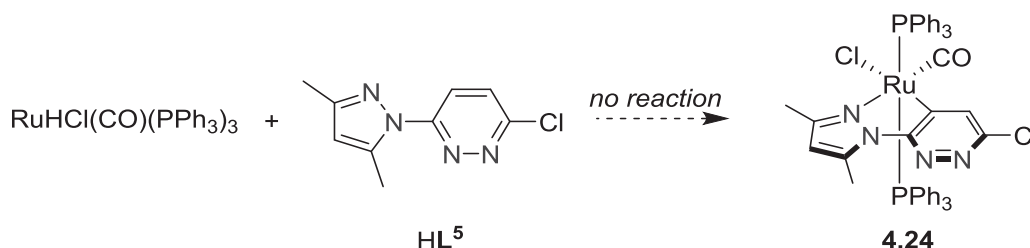
Figure 4.5. Relative single point energies and LUMOs/HOMOs of the calculated models **G** and **H**.

The single point energy difference between **G** and **H** is -5.2 kcal/mol, which means that model **G** is thermodynamically less stable than model **H**. Therefore, the formation of complex **16** instead of **4.21** should be kinetically controlled, which will be discussed later.

4.2.3 Mechanistic consideration

The formation of complex **16** under the given condition was highly preferred, and even when extra amount of the ligand precursor was used in the reaction, complex **16** was still the sole isolable product. In order to prevent the formation of a dinuclear complex and to obtain a putative 4-pyridazinyl ruthenium complex **4.24**, the reaction of $RuHCl(CO)(PPh_3)_3$ with ligand precursor that provided only one binding pocket, 3-chloro-6-(3,5-dimethyl-1*H*-pyrazol-1-yl)pyridazine (**HL**⁵) was carried out. Unfortunately, after heating at reflux in toluene for more than one day, there was no change to the signals of ligand in the ¹H NMR spectrum, implying that no reaction occurred

(**Scheme 4.12**). Therefore, the activation of a C–H bond of the pyridazine ring of **HL**⁵ was reluctant under the given condition.



Scheme 4.12. Reaction of **HL**⁵ with $\text{RuHCl(CO)(PPh}_3)_3$.

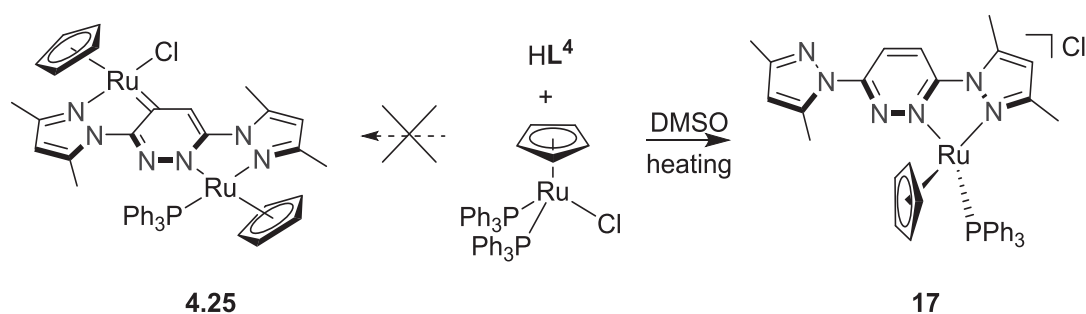
The above observation was consistent with previous reports. For example, it was reported that pre-functionalized six-membered aromatic species, such as aryl mercury(II) complexes,¹⁰³ could react with ruthenium hydride complexes, resulting in Ru–C bond. However, straight reactions of ruthenium hydride complexes and aromatic compounds without pre-functionalization¹⁰³ or any directing groups¹⁰⁴ to form Ru–C bonds *via* C–H bond activation have never been reported, as far as is concerned.

Hence, the substitution of pyrazole rings on both side arms of **HL**⁴ provided a crucial enhancement for the C–H bond activation. It was assumed that, the first step of the formation of **16** was not the C–H bond activation, but the coordination of the $\text{RuH(CO)(PPh}_3)_3$ to the *N,N*-pocket after the detachment of some of the ancillary ligands. In other words, the coordination of the ruthenium fragment in the *N,N*-pocket changed the properties of the C–H bond and made it easier to be activated by another molecule of $\text{RuHCl(CO)(PPh}_3)_3$.

During the reaction of **HL**⁴ with $\text{RuHCl(CO)(PPh}_3)_3$, an *in situ* ESI mass spectrum showed a major peak consistent with simulated isotope pattern of $[\text{L}^4\text{RuH(CO)(PPh}_3)_2]^+$. Other than that, although some changes in the solution were observed by an *in situ* ³¹P NMR monitoring (in a mixture of $\text{C}_6\text{H}_5\text{Cl}$ and *d*⁸-toluene), unfortunately, no pure intermediate could be isolated. Probably, the hydride complex $\text{RuHCl(CO)(PPh}_3)_3$ and its derived other hydride complexes were active enough to immediately capture the key intermediates and transform them into complex **16**.

4.2.4 Synthesis of complex 18

To see whether the synthesis of the new type of dinuclear ruthenium carbene complex was general and also to shed some light on the possible intermediate, the reaction of a hydride-free ruthenium complex, $\text{RuCpCl(PPh}_3)_2$, with HL^4 was carried out. The reaction of $\text{RuCpCl(PPh}_3)_2$ with HL^4 (1.1 equiv.) at high temperature in DMSO overnight gave a dark red product, mononuclear ruthenium complex **4.2** (Scheme 4.13).



Scheme 4.13. Formation of mononuclear ruthenium complex **17**.

The product is soluble in dichloromethane and hot DMSO, slightly soluble in acetone and acetonitrile and insoluble in toluene, diethyl ether and hexane. Longer reaction time did not give the anticipated dinuclear ruthenium complex **4.25**. Probably because of the strong attachment of the phosphine ligands to the metal center in $\text{RuCpCl(PPh}_3)_2$, there is no vacant site to activate the C–H bond of the pyridazine ring.

In the ^1H NMR spectra, the proton signal of the pyridazine ring for HL^4 splits into two peaks at $\delta = 8.18$ (dd, $J_1 = 9.8$ Hz, $J_2 = 0.9$ Hz, 1H) and 8.03 (d, $J = 9.8$ Hz, 1H) ppm, respectively for complex **17**. In the ^1H NMR spectrum of **17**, the signals at $\delta = 4.77$ ppm (5 protons) and in the aromatic region (15 protons) are assigned to a cyclopentadienyl ligand and a PPh_3 ligand, respectively. In the ^{31}P NMR spectrum, the signal of the PPh_3 ligand is found at $\delta = 46.6$ ppm as a singlet. In ^{13}C NMR spectrum, the signals of the CH on the pyridazine are two singlets at $\delta = 122.0$ and 120.3 ppm, respectively.

The integrity of the product in solution indicated by the high resolution ESI mass spectrometry shows a base peak at $m/z = 697.1791$ for the $[\text{LRuCp(PPh}_3)]^+$ cation, as shown in Figure 4.6. The structure of complex **17** was eventually confirmed by X-ray diffraction (Figure 4.7).

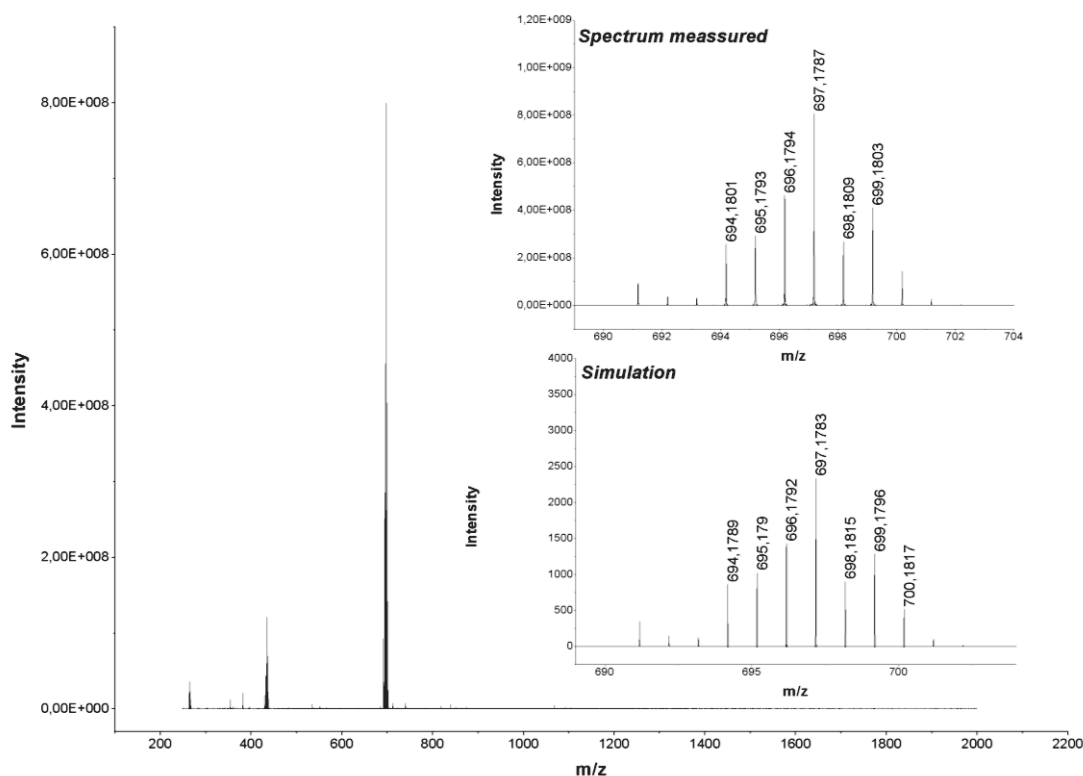


Figure 4.6. High resolution ESI mass spectrum of **17**. The inset shows the experimental and simulated isotopic distribution patterns for $[\text{C}_{37}\text{H}_{36}\text{N}_6\text{PRu}]^+$.

In the molecular structure determined by X-ray diffraction (**Figure 4.7**), Cl^- is the counterion. In the cation, Ru1 is coordinated in the *N,N*-pocket and with phosphine and η^5 -cyclopentadienyl co-ligands, and the fragment adopts a distorted pyramidal geometry. The geometric center of the cyclopentadienyl ligand is defined as C_{ctr} and the Ru1– C_{ctr} distance is 1.8345(2) Å. The angles of C_{ctr} –Ru1–N1, C_{ctr} –Ru1–P1 and C_{ctr} –Ru1–N3 are 129.221(44)°, 123.852(12)° and 131.801(44)°, respectively. The Ru1–N1 bond length is 2.0591(15) Å, slightly shorter than that of Ru1–N3 (2.0830(16) Å), suggesting a slightly stronger bonding between Ru1 and the pyridazine ring than that between Ru1 and the pyrazole ring.

The non-coordinated pyrazole ring is slightly rotated around the N6–C4 bond with the dihedral angle of the pyridazine plane and the pyrazole plane of 9.3°. The N5–N6 bond in the pyrazole ring already points away from the metal fragment, probably due to the interaction between the C3 proton and the lone pair of N5.

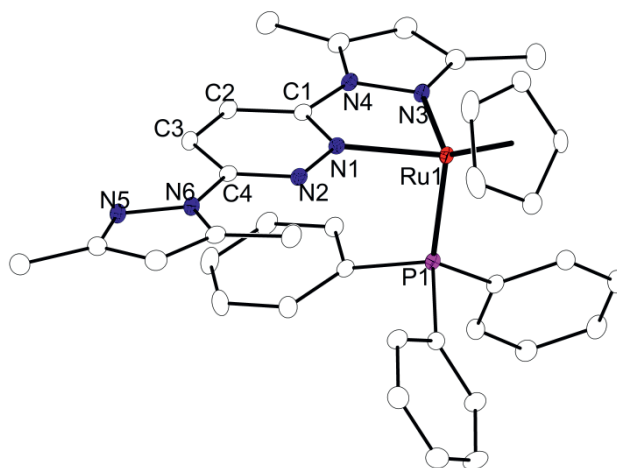
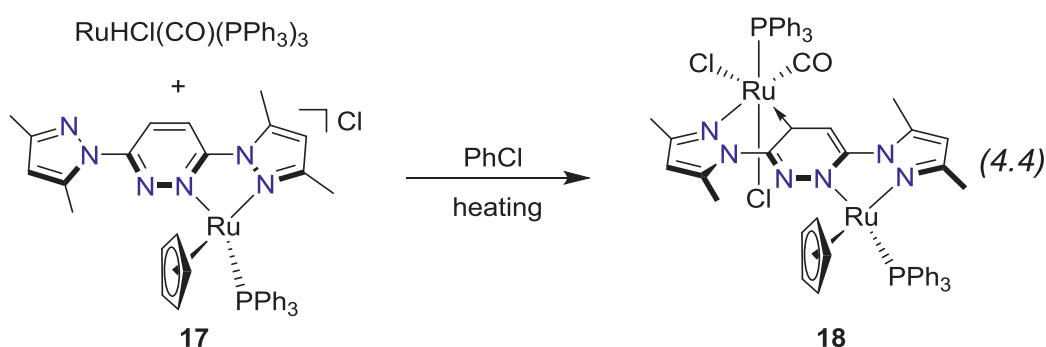


Figure 4.7. Molecular structure of the cation of **17**. Anisotropic displacement ellipsoids drawn at 30% probability level. The solvent molecule and all hydrogen atoms have been omitted for clarity. Selected bond lengths [Å] angles [°]: Ru1–N1 2.0591(15), Ru1–N3 2.0830(16), Ru1–P1 2.3238(5), N1–Ru1–N3 75.74(6), N1–Ru1–P1 88.68(4), N3–Ru1–P1 92.27(4).

The C–H bond activation of **17** by a second molecule of $\text{RuCpCl}(\text{PPh}_3)_2$ was not favored, therefore, the more active species $\text{RuHCl}(\text{CO})(\text{PPh}_3)_3$ was used again. Treatment of complex **17** with $\text{RuHCl}(\text{CO})(\text{PPh}_3)_3$ at 120 °C in chlorobenzene for 3 hours gave a bright-yellow precipitate, later identified as complex **18** (Eq 4.4).



Complex **18** is soluble in dichloromethane, slightly soluble in acetone, acetonitrile or chlorobenzene and insoluble in toluene, diethyl ether or hexane. It is reasonably stable in both solid state and solution in air and moisture.

The ^1H NMR spectrum of **18** shows only one proton of the pyridazine ring, at $\delta = 7.02$ ppm as a singlet, indicating the successful activation of the C–H bond. The ^{31}P NMR spectrum displays two singlets at $\delta = 48.6$ and 48.5 ppm, respectively, implying that the two phosphine ligands are on different metal ions. In the ^{13}C NMR spectrum, a doublet at $\delta = 77.1$ ppm is assigned to cyclopentadienyl group while a singlet at $\delta =$

185.6 ppm is assigned to the carbenic carbon atom in the pyridazine ring. The high resolution ESI mass spectrum shows a major peak at $m/z = 1123.1305$, which is consistent with the isotopic pattern of $[\text{L}^4\text{Ru}_2(\text{PPh}_3)_2(\text{CO})\text{Cl}]^+$ (**Figure 4.8**).

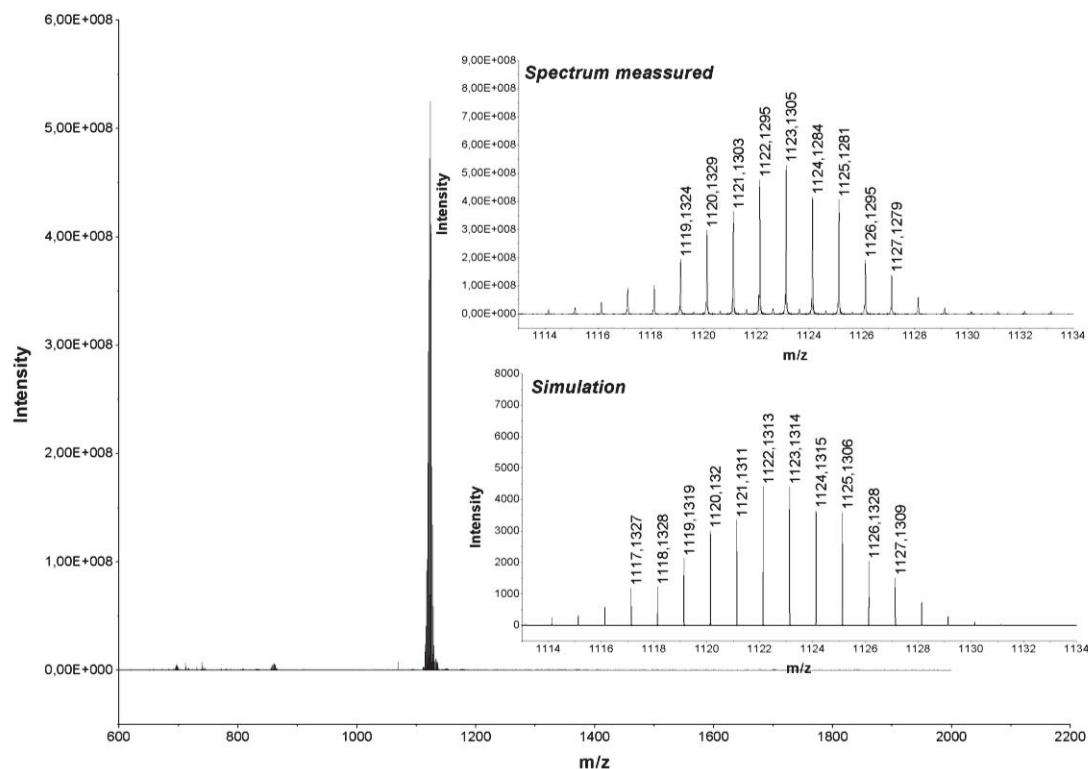


Figure 4.8. High resolution ESI mass spectrum of complex **18** in CH_3CN . The inset shows the experimental and simulated isotopic distribution patterns for $[\text{C}_{56}\text{H}_{50}\text{N}_6\text{ClOP}_2\text{Ru}_2]^+$.

All these observations supported the formation of the expected complex **18**, and its structure was confirmed by X-ray diffraction (**Figure 4.9**).

The structural skeleton of complex **18** is very similar to that of **16**. In complex **18**, the core ligand $[\text{L}^4]$ is more distorted, with the dihedral angle between the pyridazine ring and the pyrazole_{N3–N4} ring, and the dihedral angle between the pyridazine ring and the pyrazole_{N5–N6} ring of 7.4° and 10.8° , respectively. The Cp–Ru1 fragment in the *N,N*-pocket is almost unchanged compared to that in complex **17**, the angles of $\text{C}_{\text{ctr}}\text{–Ru1–N1}$, $\text{C}_{\text{ctr}}\text{–Ru1–P1}$ and $\text{C}_{\text{ctr}}\text{–Ru1–N3}$ are 128.3° , 128.5° and 129.5° , respectively; Ru1–N1 is enlarged from $2.0591(15) \text{ \AA}$ to $2.076(3) \text{ \AA}$ by 0.0172 \AA , indicating the shift from a dative $\text{N} \rightarrow \text{Ru}$ bond to a N–Ru single bond.

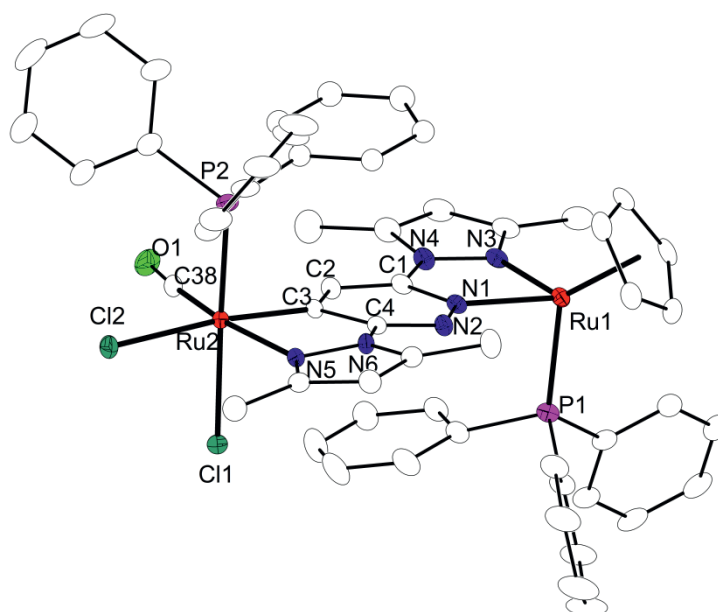


Figure 4.9. Molecular structure of **18**. Anisotropic displacement ellipsoids drawn at 30% probability level. The solvent molecule and all hydrogen atoms have been omitted for clarity. Selected bond lengths[Å] angles [°]: Ru1–N1 2.076(3), Ru1–N3 2.072(3), Ru1–P1 2.3252(9), Ru2–C3 2.003(3), Ru2–N5 2.181(3), Ru2–Cl2 2.5050(9), Ru2–C38 1.823(4), Ru2–P2 2.3076(9), Ru2–Cl1 2.4492(8), N1–Ru1–N3 75.19(10), N3–Ru1–P1 89.80(8), N1–Ru1–P1 88.73(8), N5–Ru1–C3 78.31(11), P2–Ru2–Cl1 178.25(3).

The Ru–C_{pyridazine} bond length is 2.003(3) Å, very close to that (2.005(3) Å) in complex **4.23**, but shorter than that (2.020(5) Å) in complex **16**. The Ru–N_{pyridazine} bond length is 2.076(3) Å, shorter than that (2.141(4) Å) in complex **16**, but still longer than that (1.955(3) Å) in complex **4.23**.

Two phenyl groups on two phosphine ligands form π - π interactions with the pyridazine ring, generating a ‘sandwich-like’ structure, although the pyridazine ring is only partially involved in the pattern (**Figure 4.10**). The phenyl groups have to bend along the P–C axial so as to become more parallel to the pyridazine ring, the bending angles are 6.2–8.1°, compared to the cases of other phenyl groups with the bending angles of only 0.4–4.0°. Similar structures are observed in pyridazin-6-ylidene metal complexes **1** to **4** described in Chapter 1. Note that, in complex **16**, there is no such π - π interaction observed, probably because of the severe steric congestion in the complex.

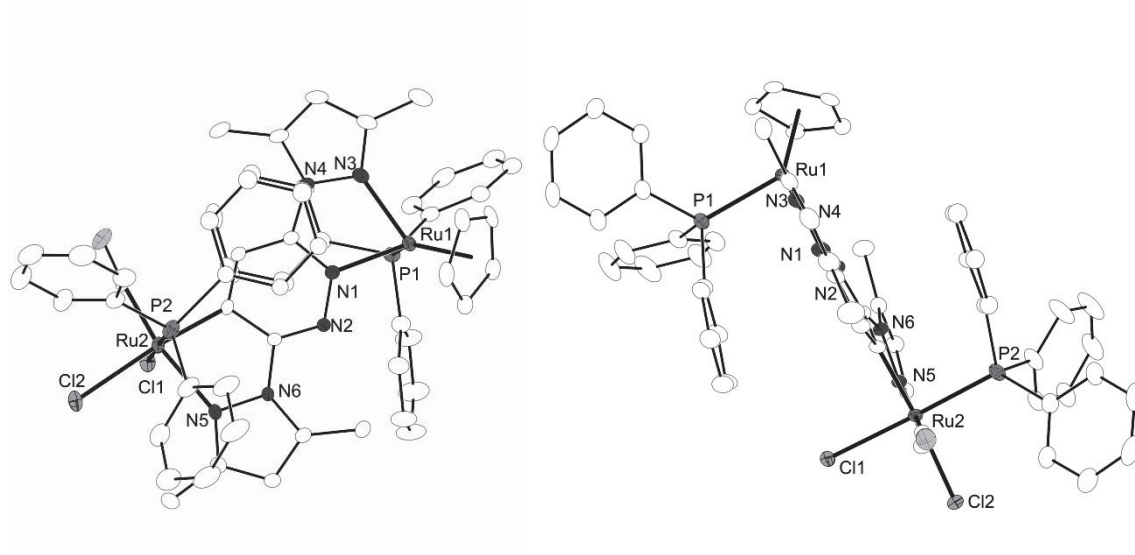


Figure 4.10. Topview (left) and sideview (right) of complex **18**.

Selected ^1H , ^{13}C and ^{31}P NMR spectral data of complexes **16**, **17** and **18** are collected in **Table 4.1**. The comparison of the selected bond lengths and angles of complex **16**, **17** and **18** are collected in **Table A23**.

Table 4.1. Comparison of NMR data of complex **16**, **17** and **18**.

		16	17	18
^1H NMR	CH^{Pyri}	7.80-6.80 merged in multiplet	8.18 (dd), 8.03 (d)	7.02 (s)
	CH^{Pyra}	5.99 (s), 5.53 (s)	6.29 (s), 6.20 (s)	6.00 (s, 2 H)
^{31}P NMR	PPh_3	51.8 (s), 46.1 (d), 41.1 (d)	46.6 (s)	48.6 (s), 48.5 (s)
	CH^{Pyri}	136.0-127.0 merged in multiplet	122.0 (s), 120.3 (s)	127.3 (s)
^{13}C NMR	$\text{CH}_3\text{C}^{\text{Pyra}}$	156.6 (s), 153.4 (s)	156.5 (s), 152.9 (s)	156.4 (s), 154.3 (d)
	$\text{Ru}-\text{C}$	187.0 (d, $J = 10.2$ Hz)	<i>n./a.</i>	185.6 (d, $J = 10.8$ Hz)
	CO	206.4 (d), 204.4 (t)	<i>n./a.</i>	206.2 (d)

According to the literature, the C4/5-proton resonances in ^1H NMR spectra are particularly sensitive indicators of the positive charge and delocalization of the imidazole ring in the formation of imidazolylidene metal complexes.⁹⁸ Similarly, from complex **17** to



18, the resonances of the protons in the pyridazine ring are also sensitive indicators. The ^1H NMR signal of the pyridazine CH proton shifts from at $\delta = 8.03\text{--}8.18$ ppm to higher field at $\delta = 7.02$ ppm, suggesting that the remaining CH bond is strongly shielded by the attachment of the ruthenium fragment in the *C,N*-pocket. The ^{13}C NMR signal of the pyridazine C(H) group shifts from at $\delta = 120.3\text{--}122.0$ ppm to much lower field at $\delta = 185.6$ ppm

From complex **17** to **18**, the Ru–N^{pyridazine} bond length is slightly largened, signifying that this bond is weakened in **18**. Bond lengths C1–C2 and N2–C4 are smaller in complex **18**, indicating larger bond orders and more double bond character; while bond lengths C2–C3 and C3–C4 are larger in complex **18**, suggesting smaller bond orders and more single bond character. The above observation points out that, compared to complex **17**, the aromaticity of the pyridazine ring in complex **18** is slightly sabotaged. The change of aromaticity of the *N*-heterocyclic ring might be a possible reason why the calculated model **G** is less stable than model **H**.

To sum it up, during the generation of complex **17**, a chloride anion is removed from RuCpCl(PPh₃)₃ and plays the role of counterion for the entire complex. The counterion Cl[−] finally attaches to the ruthenium atom in the *C,N*-pocket in complex **18**.

Based on the above analysis and the result suggested by the DFT calculations that the formation of complex **16** should be kinetically controlled, a plausible reaction mechanism is proposed for the formation of complex **16** (**Scheme 4.14**).

One molecule of RuHCl(CO)(PPh₃)₃ coordinates to the *N,N*-pocket of HL⁴ after the dissociation of PPh₃ and Cl[−] ion, forming a mononuclear ruthenium salt **4.26** in which the previously dissociated Cl[−] ion acts as the counterion. The C–H bond at the *para* position of the metallated nitrogen atom in **4.26** is activated by a second molecule of RuHCl(CO)(PPh₃)₃, resulting in complex **4.27-I**. The positive charge on the ruthenium ion in the *N,N*-pocket can transfer to the other ruthenium ion to give intermediate **4.27-II**. The counterion Cl[−] tends to attack the cation of **4.27** due to the electrostatic attraction. There are two possible reaction pathways depending on the attacking spots of Cl[−] ion in the cation.

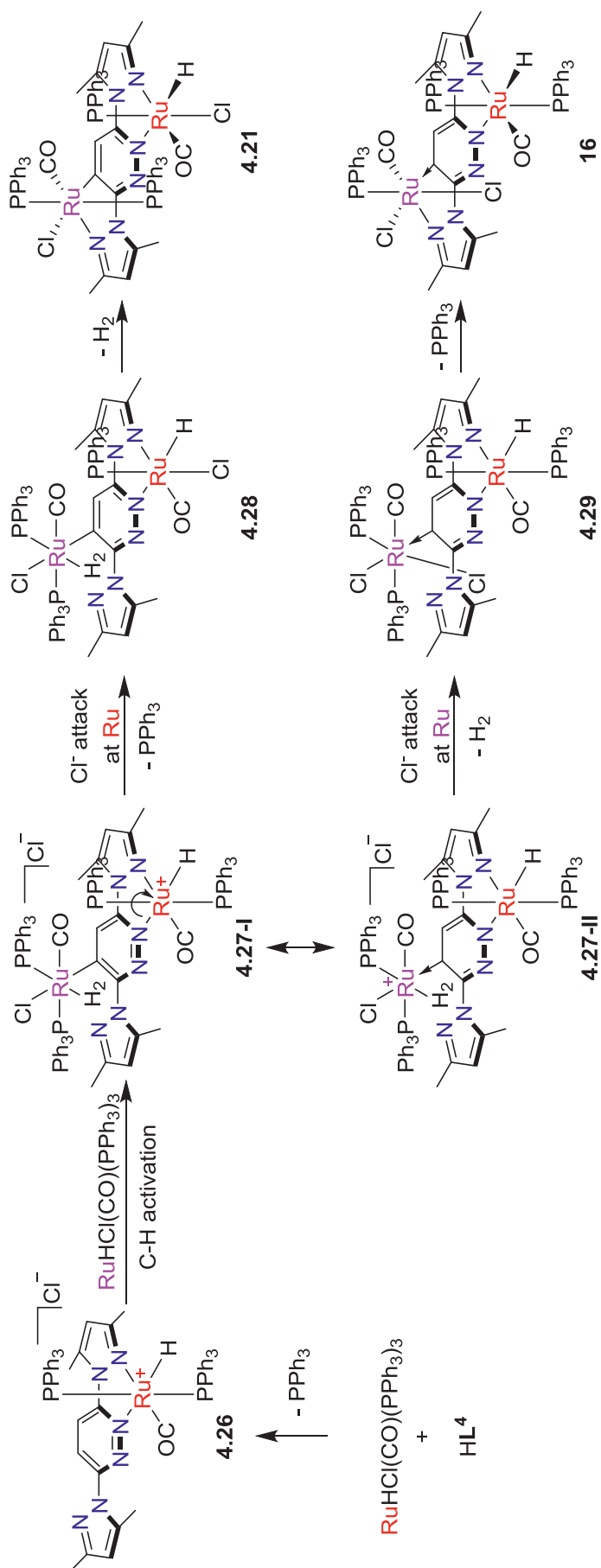
If the attack happens at the ruthenium ion (labeled in red) in the *N,N*-pocket, one of the former ancillary ligands, *i. e.*, PPh₃, CO, H[−] or the bidentate HL⁴ ligand, has to be removed in prior to the formation of a Ru–Cl bond. Apparently, PPh₃ is the easiest one to be removed. The replacement of PPh₃ with Cl[−] leads to the formation of intermediate **4.28**, which loses the labile ligand H₂ to give complex **4.21**.

If the attack happens at the ruthenium ion (labeled in magenta) in the *C,N*-pocket, the labile H₂ ligand is simultaneously replaced by Cl[−], forming intermediate **4.29**. The neutral complex **4.29** prefers to lose one PPh₃ ligand instead of other ancillary ligands to form **16** for two reasons. First, PPh₃ is a bulky ligand and the presence of four PPh₃ in the crowded metal complex **4.29** is not energetically favored. Second, from the perspective of the bonding energies, PPh₃ is most likely to dissociate compared to the anionic Cl[−] and strong donor ligands (carbene and CO).

From thermodynamic stability point of view, **4.21** is more stable than **16**, however, the kinetic pathways prefer the formation of complex **16**. For the formation of **4.21** (first pathway), because the removal of PPh₃ ligand from the stable [(HL⁴)RuH(PPh₃)₂(CO)]⁺ fragment is difficult, the reaction step from **4.27-I** to **4.28** should have a very high energy barrier.

For the formation of **16** (second pathway), in the reaction step from **4.27-II** to **4.29**, the dissociation of H₂ ligand is smooth and the coordination of Cl[−] to the metal ion has a reasonably low energy barrier. Therefore, the kinetically controlled product **16**, which is the first well-defined *N*-metallated *N*-heterocyclic carbene complex, is obtained from the reaction of HL⁴ and RuHCl(CO)(PPh₃)₃.

However, the proposed mechanism needs to be verified by DFT calculations.



Scheme 4.14. Proposed mechanism of the formation of complex **16** and the imaginative isomer **4.21**.

4.3 Conclusion

In conclusion, the first examples of pyridazin-4-ylene ruthenium complexes **16** and **18** are successfully synthesized. In either complex, one nitrogen atom of the pyridazine ring is bound to metal fragment and the carbon atom at its *para* position is bound to another metal fragment. The metallated carbon atom behaves as a two-electron donor, and the complex is thus regarded as metal carbene species. Primary DFT calculations indicate that the formation of complex **16** is kinetically controlled and a plausible mechanism of the formation is proposed. Although the formation of metal–carbene bonds in both complexes is well-substantiated, a thorough comprehension of the bonding types and properties of this novel type of NHC metal complexes are still demanded.



CHAPTER 5. Synthesis of Novel Indene Derived Carbene Ligands

5.1 Introduction and Motivation

5.1.1 Cyclopentadiene derived carbenes

Cyclopentadienyl derivatives are an important class of ligands for metal complexes by various binding modes (namely, η^1 , η^3 or η^5). Among them, η^5 -cyclopentadienyl was most widely used to form complexes with different metals¹⁰⁵ due to its strong stabilization effect. In addition, cyclopentadiene could also be functionalized to serve as carbene ligands (**Chart 5.1**). The carbene of **Type I** is simply formed by the removal of two hydrogen atoms from the saturated carbon atom in cyclopentadiene. In **Type II**, the two carbon atoms adjacent to the carbenic carbon form double bonds with other substituents. In this work, the synthesis of the **Type III** carbene species based on cyclopentadiene is attempted.

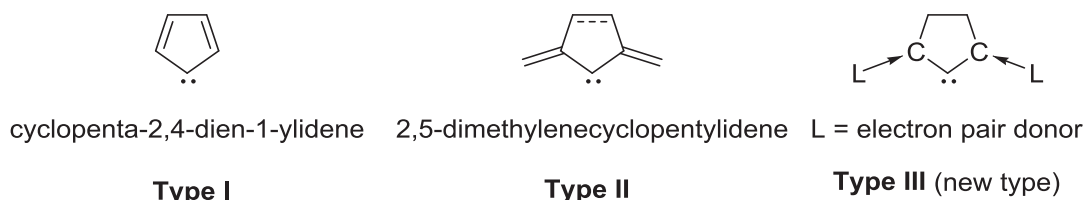
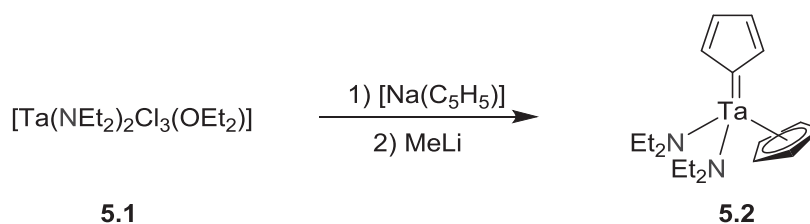


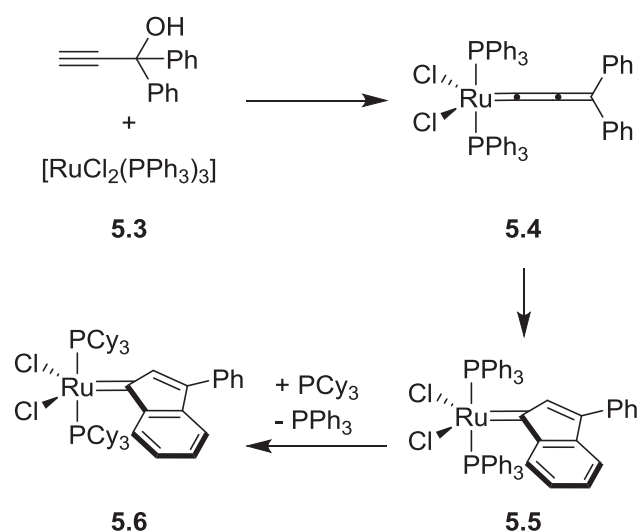
Chart 5.1. Different types of carbenes derived from cyclopentadiene.

The first complex based on **Type I** was the tantalum cyclopentadienylidene complex **5.2** (**Scheme 5.1**).¹⁰⁶ After the treatment of tantalum species **5.1** with sodium cyclopentadienide and then with methyllithium, one of the cyclopentadienide was transformed to an η^5 -cyclopentadienyl ligand and the other one was transformed to an indenylidene carbene ligand in complex **5.2**.



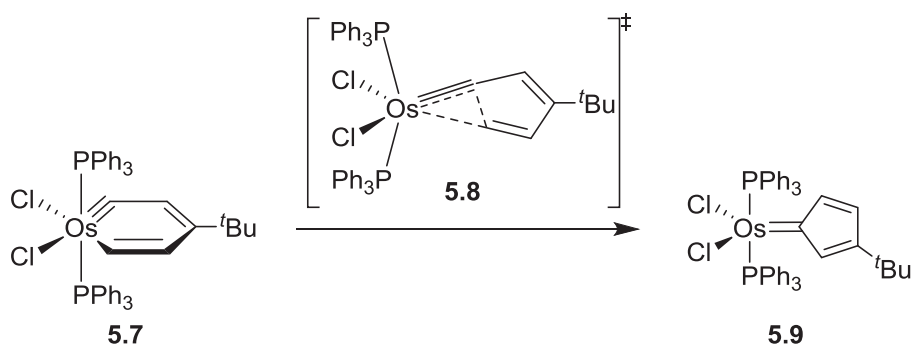
Scheme 5.1. Repors of synthesis of tantalum carbene complex **5.2** derived from cyclopentadiene.

Some of the Grubbs' catalysts were also **Type I** carbene complexes. For example, the synthesis of a Grubbs catalyst **5.6** was shown in **Scheme 5.2**. Treatment of ruthenium species **5.3** with 1,1-diphenylprop-2-yn-1-ol in mild condition gave the indenylidene ruthenium complex **5.5** *via* an allenylidene ruthenium intermediate **5.4**.¹⁰⁷ The replacement of PPh_3 in complex **5.5** to PCy_3 led to the formation of complex **5.6**. Note that, complex **5.6** was catalytically active for ring-closing metathesis while complex **5.5** showed almost no catalytic activity for the same reaction.



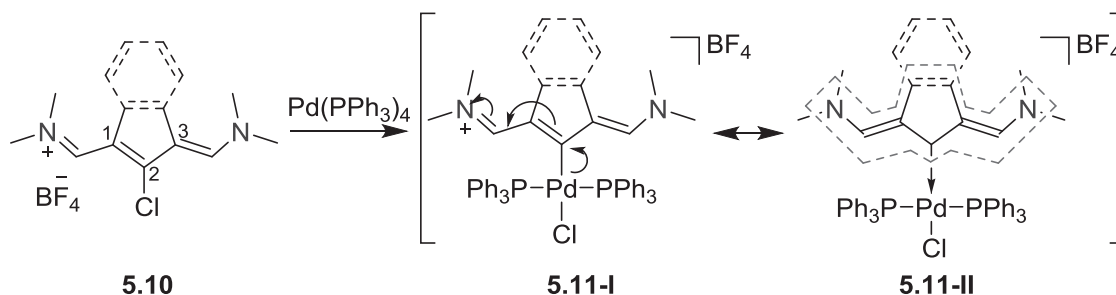
Scheme 5.2. Synthesis of the Grubbs-type catalyst **5.6**.

Meanwhile, carbene metal complex **5.9** was also isolated as the rearrangement product of metallabenzynes species **5.7** (**Scheme 5.3**), possibly *via* a 3-membered ring transition state structure **5.8**. Interestingly, the geometry of osmium carbene complex **5.9** was different from ruthenium complex **5.6**.¹⁰⁸ In complex **5.9**, the pentadienylidene ring was almost parallel to the P–Os bond while in complex **5.6**, the indenylidene ring was almost perpendicular to the P–Ru bond.



Scheme 5.3. Rearrangement of osmabenzynes to the corresponding carbene complex.

Besides the carbene metal complexes based on ligands of **Type I**, recently, a class of metal carbene complexes **5.11** based on ligands of **Type II** were also reported (**Scheme 5.4**).¹⁰⁹ The oxidative addition of the C–Cl bonds onto the Pd(0) species generated C–Pd–Cl fragments (**5.11-I**), which resonated to the carbene complexes **5.11-II**. By the formation of the large conjugated systems (highlighted in dashed line), the empty orbitals of the carbenic carbon atoms were well stabilized. As far as is concerned, complexes **5.11** were the only reported examples based on **Type II** ligands.



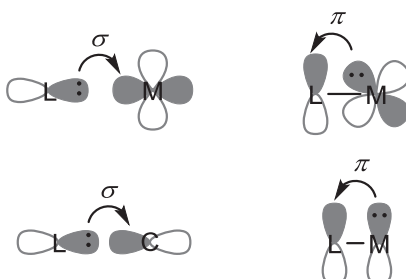
Scheme 5.4. Synthesis of palladium complexes **5.11** based on **Type II** ligands.

5.1.2 NHC substituted carbon compounds

As mentioned in **Scheme 1.22**⁷ in Chapter 1, in the bent allene **1.73**, the orbitals of the central carbon atom were sp^3 hybridized. Two of the orbitals were filled with the two carbenes of the NHC ligands, leaving the remaining two orbitals filled with four valence electrons of the carbon atom, *i. e.*, two electron pairs. Because of this, the bent allene **1.73** was also named ‘carbodicarbene compound’.

From the molecular orbital theory point of view, the carbon atom can form a captodative bonding mode with strong Lewis bases or strong two-electron donors, such as phosphine or NHC ligands. In compound **1.73**, the bonds between the central carbon atom and the NHC ligand include a σ bond from NHC to the carbon atom and a π back-donating bond

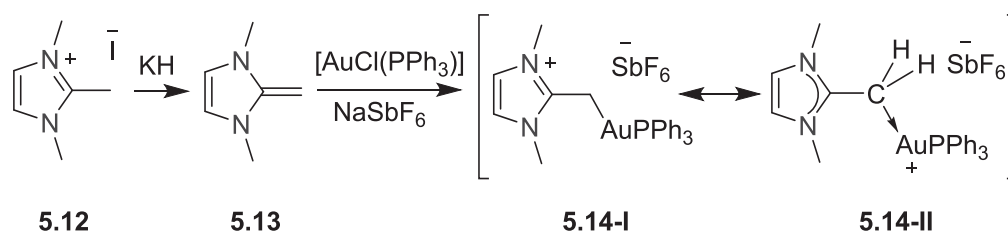
from the lone pair of the carbon atom to the ligand. In some sense, the central carbon behaves as a metal (**Scheme 5.5**).^{90, 110} Computational studies have confirmed the HOMO and HOMO-1 of the compound are π type and σ type lone pair orbitals, respectively.¹¹¹



Scheme 5.5. Interaction of a ligand and a metal fragment (top); and interaction of a ligand and a carbon atom (bottom), like the case in **1.73**.

At the same time of the synthesis of compound **1.73**, a mono-NHC-substituted organic compound **5.14** was also reported.¹¹² A simple 2-methylimidazolium salt **5.12** reacted with potassium hydride to give an olefin derivative **5.13**. Treatment of **5.13** with gold(I) species $[\text{AuCl}(\text{PPh}_3)]$ and non-coordinating anion $[\text{SbF}_6]^-$ led to the formation of **5.14-I**, in which the gold fragment and the imidazolium species were bridged by a methylene group (**Scheme 5.6**).

Although no computational studies have been done concerning this species, a similar isomeric structure **5.14-II** of **5.14-I** can be drawn as followed, based on previous studies on carbodicarbene compounds. In the same manner, the central carbon atom in **5.14-II** is also sp^3 hybridized. Two orbitals form two σ bonds with two hydrogen atoms and one orbital is occupied by NHC, leaving one electron pair on the remaining orbital, which is coordinated to the gold fragment.



Scheme 5.6. Synthesis of Carbomonocarbene compound **5.14**.

It was noticed that, the central carbon of **5.14** had pyramidal geometry¹¹² similar to that of a trialkylamine NR_3 , with the axial position occupied by lone pair and three equatorial

positions bound to NHC or R groups. Similarly, the carbodicarbene compound was like an ether derivative OR_2 (**Figure 5.1**).

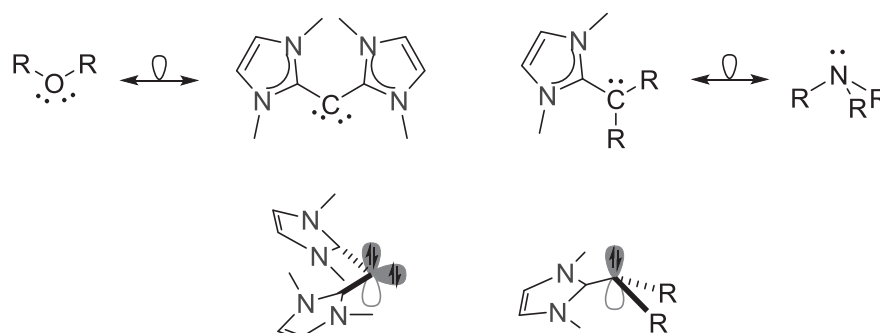


Figure 5.1. Similarity of carbodicarbene/carbomonocarbene to OR_2 and NR_3 .

The similarity of the electronic structure of $(NHC)CR_2$ to that of NR_3 leads to the thought of imidazolylidene, which contains two amino groups. In imidazolylidene **5.15** (**Figure 5.2**), the empty p orbital of carbenic carbon atom is stabilized by the lone pairs of the flanking amino groups (as showed in the red square). Replacement of the amino groups in **5.15** by monon-NHC-substituted carbon groups (carbomonocarbene) results in compound **5.16**. In the carbon atoms bound to NHC ligands in **5.16**, the p orbitals perpendicular to the cyclopentadiene ring are filled with electron pairs (like the right structure in **Figure 5.1**). As a result, two filled p orbitals, p orbitals of the $C=C$ double bond and the empty p orbital of the remaining carbon atom in the cyclopentadiene ring form a 5-center-6-electron system. In other words, the empty p orbital of the carbenic carbon atom is conjugated in the aromatic system and the carbene is therefore stabilized, as shown in the orbitals (**Figure 5.2**).

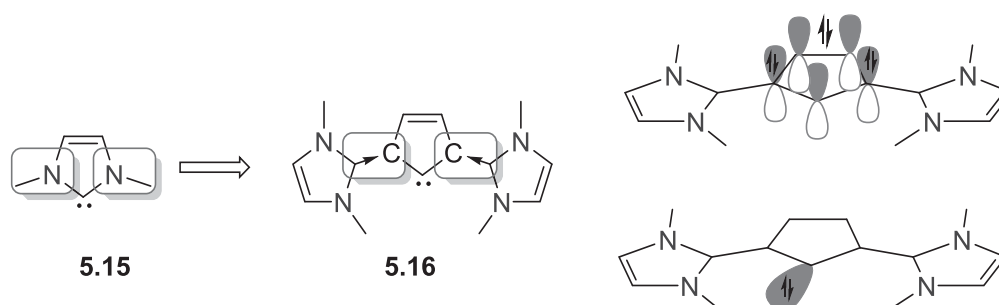
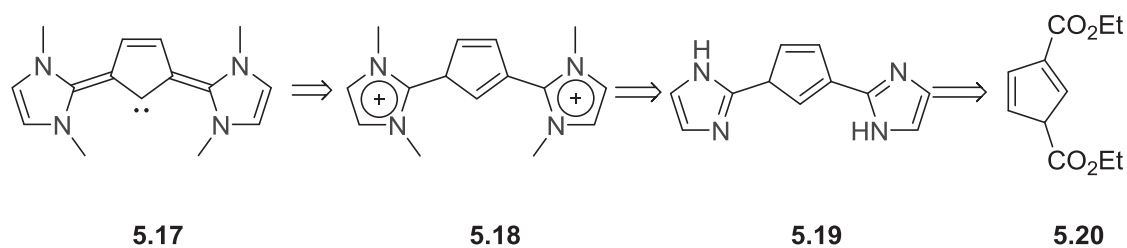


Figure 5.2. Proposal of the formation of a new cyclopentadienyliene, assisted by NHC ligands.

By *retro* synthetic analysis, the synthesis of the new type carbene could be deduced as below (**Scheme 5.7**). Cyclic carbenes **5.17** can be formed from their protonated salts **5.18**, which are synthesized after the full alkylation of cyclopentadiene bridged bis(1*H*-

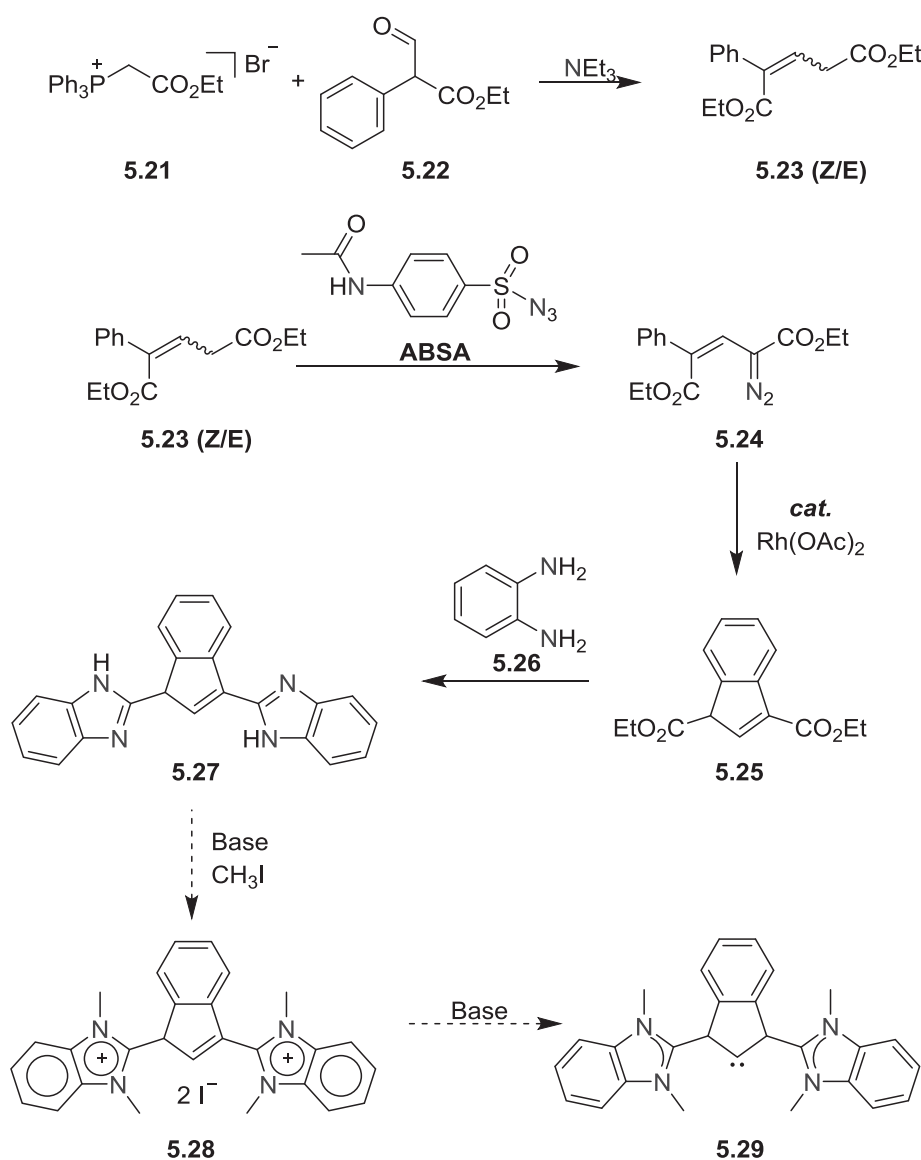
imidazole) **5.19**. Compound **5.19** can be generated by several methods, such as direct condensation of the corresponding diester **5.20** with diamine.



Scheme 5.7. *Retro* synthesis of the required carbene.

5.2 Ligand Synthesis

Diethyl cyclopenta-1,4-diene-1,3-dicarboxylate **5.20** has never been reported, but its analogue, diethyl 1*H*-indene-1,3-dicarboxylate **5.25** was already synthesized. (Scheme 5.8)¹¹³ The following synthetic route was designed based on the retro synthesis in Scheme 5.7. The synthesis of the intermediate **5.23** was not mentioned in literature, details of its preparation are described in the Experimental Section.

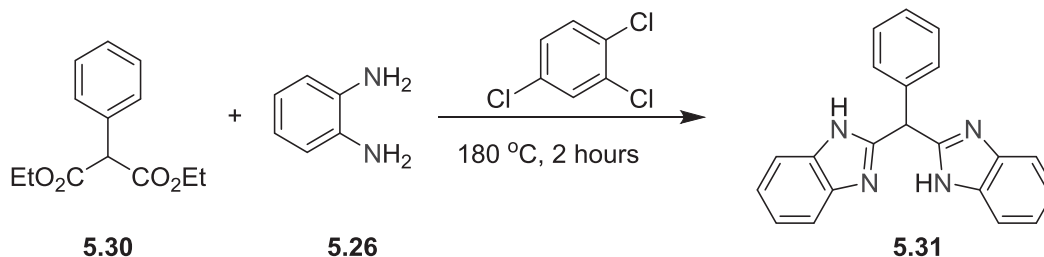


Scheme 5.8. Designed synthetic route for the new carbene.

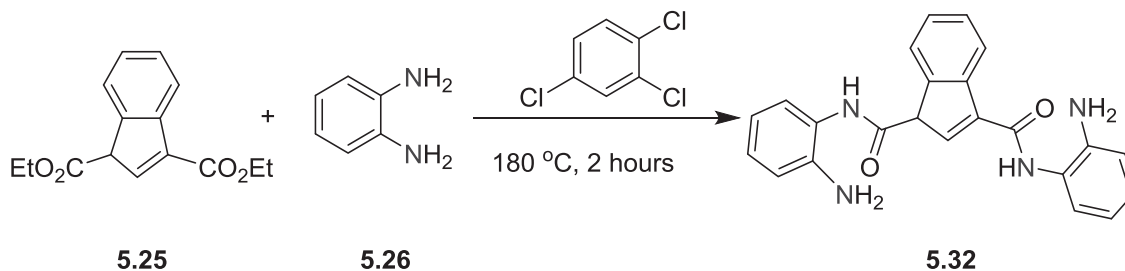
The synthesis of dibenzimidazole **5.31** from the reaction of a diester **5.30** and a diamine **5.26** in 1,2,4-trichlorobenzene in high temperatures was reported before (Scheme 5.9).¹¹⁴ By the same reaction condition in this work, an off-white powder pre-

precipitated from the reaction of diester **5.25** and diamine **5.26**. The powder was poorly soluble in all regular solvents, such as dichloromethane, acetone, acetonitrile, alcohols, DMSO or toluene. The ESI mass spectrum showed a major peak at $m/z = 385.2$ with similar isotope pattern to $[\text{C}_{23}\text{H}_{21}\text{N}_4\text{O}_2]^+$. It was assumed that, instead of the expected product **5.27**, a diamide **5.32** was formed (**Scheme 5.9**).

Literature



This work



Scheme 5.9. Unexpected formation of diamide compound **5.32** in this work.

When the reaction was carried out in 200 °C, a dark-brown solution without precipitate was obtained. After cooling to the ambient temperature, by the addition of copious pentane, a sticky black solid was precipitated and dried under vacuum. Then chromatography was used (silica gel as solid phase and a mixture of methanol and dichloromethane in the ratio of 1:8 as eluent) to get a yellow product in the yield of 15%~22%. The product was soluble in DMSO, slightly soluble in alcohols, acetone or dichloromethane and insoluble in toluene and hexane. Crystalline material could be obtained by dissolving the product in hot ethanol and letting the solution cool down gradually to room temperature. The X-ray diffraction showed that the molecular structure of the product **19** was protonated with hydrochloride (**Figure 5.3**).

The cation of **19** adopts C_{2v} symmetry. In the cation of **19**, all nitrogen atoms are bound to protons and there is only one proton left on the five membered ring of the indene moiety. The three rings are almost in the same plane, indicating strong conjugation among them. The torsion angles C3–C2–C6–N2 is 10.38°. The bond lengths C1–C2, C2–C3' and C3–C3' are 1.399(2) Å, 1.453(2) Å and 1.428(4) Å, respectively. C1–C2 and C3–C3'

are roughly aromatic C=C bonds and C2–C3 is more like a sp^2 - sp^2 single bond. The bond length C2–C6 is 1.357(2) Å, indicating a typical alkene double bond, which is normally around 1.34 Å. The N1–C6 and N2–C6 bond lengths are around 1.353(2)-1.357(2) Å, which are shorter than that of N1–C7 (1.395(2) Å) or N2–C12 (1.390(2) Å). The bridging C2–C6 bond length is 1.419(3) Å, slightly smaller than that of the reported imidazole-derived fulvene compound (1.430 Å),¹¹⁵ indicating a even stronger conjugation between the benzimidazole rings and the central ring.

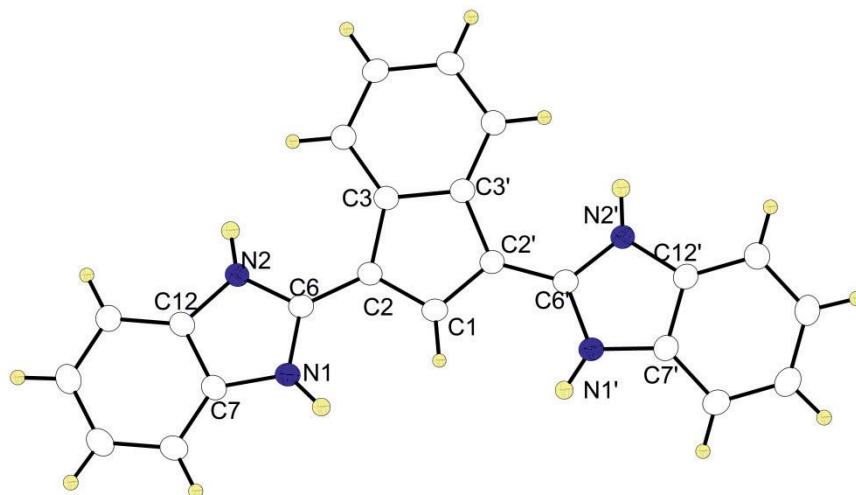
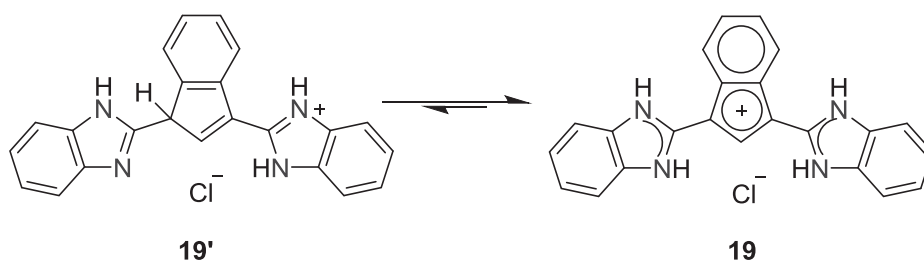


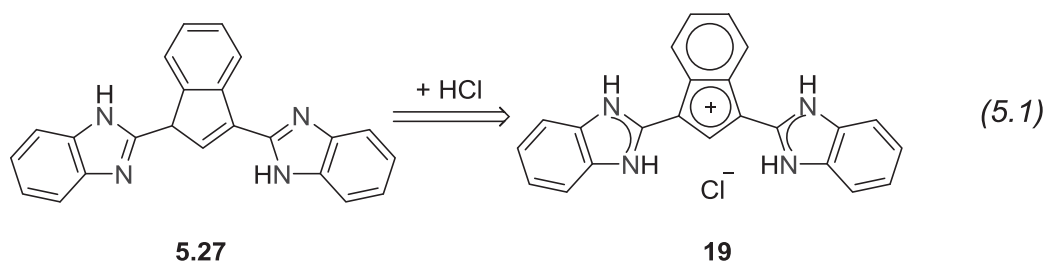
Figure 5.3. Molecular structure of the cation of **19**. Anisotropic displacement ellipsoids drawn at 30% probability level (except for H, which drawn at 5% probability for clarity). The anion and the solvent molecule are omitted for clarity. Selected bond lengths [Å] angles [°]: N2–C6 1.357(2), N2–C12 1.390(2), N1–C6 1.353(2), N1–C7 1.395(2), C1–C2 1.399(2), C2–C3 1.453(2), C3–C3' 1.428(4), C12–C7 1.388(3), C2–C6 1.419(3), C2–C1–C2' 110.1(2), C1–C2–C3 107.66, C2–C3–C3' 107.31(10), N1–C6–N2 107.48(16), N2–C6–C2–C3 10.381(319).

It is noteworthy that all nitrogen atoms are bound to proton atoms and there is only one proton left in the cyclopentadienyl ring in **19**. Theoretically, compound **19** has another tautomer **19'** as shown in **Scheme 5.10**. In tautomer **19'**, there are two protons left in the cyclopentadiene ring and one of the nitrogen atoms is not bound to proton. Compound **19** is more stable than **19'** because **19** is the only species isolated in solid state in the experiment. In **19'**, the bond between the left benzimidazole ring and the central ring is single bond, and only one benzimidazole ring and the central ring is conjugated; while in **19**, both benzimidazole rings are conjugated with the central ring. Probably the selective formation of **19** from the reaction can be ascribed to the special stabilization effect caused by the formation of the large conjugation system in compound **19**.

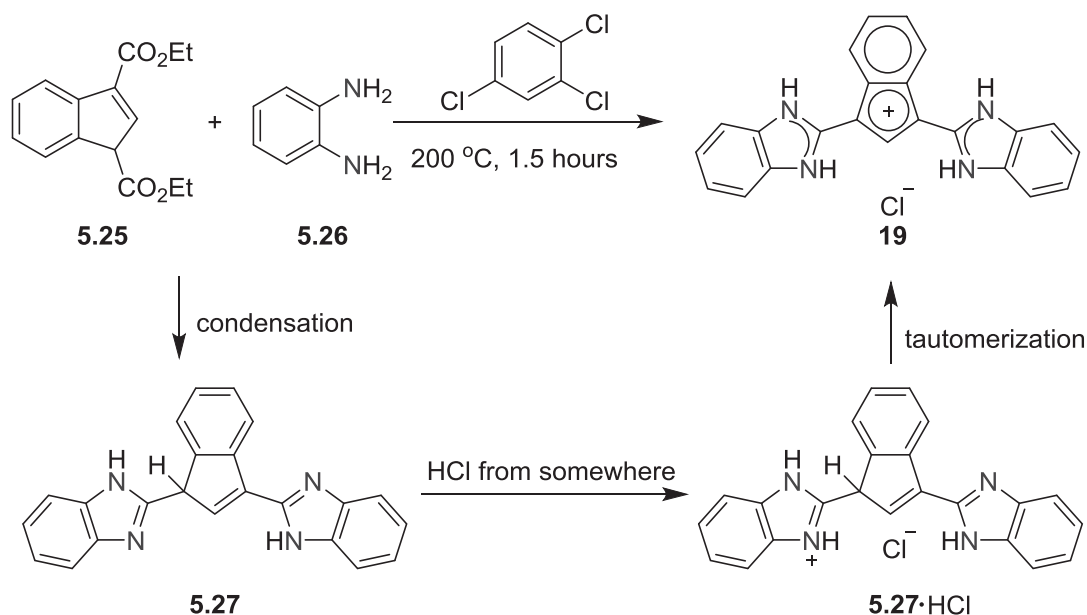


Scheme 5.10. Possible tautomerization between compound **19'** and **19**.

Theoretically, the direct condensation of **5.25** and **5.26** might give **5.27**, like the case in the formation of **5.31**. From the anticipated product **5.27** to the isolated compound **19**, one molecule of hydrochloride is added (Eq 5.1).

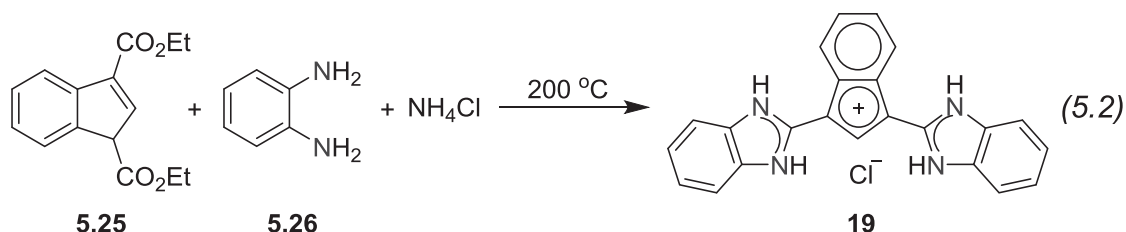


Intriguingly, during the synthesis or separation, no protic acids were used; hence, the only possible source of chloride should be the solvent 1,2,4-trichlorobenzene. It was proposed that, the anticipated product **5.27** was formed temporarily; at the same time, under the drastic reaction conditions, *o*-phenylenediamine reacted with the solvent, generating hydrogen chloride or aminium chloride derivatives, which then reacted with **5.27** to give the acidified species **5.27**·HCl. After tautomerization, **5.27**·HCl transformed to **19** (**Scheme 5.11**). Considering the basic reaction conditions because excessive *o*-phenylenediamine was used, it was assumed that the neutral bis(benzimidazole) substituted indene species **5.27** was a stronger base than *o*-phenylenediamine **5.27**.



Scheme 5.11. Reaction pathways of the synthesis of **5.1** in 1,2,4-trichlorobenzene.

It was noticed that the melting point of **5.26** was 102-104 °C and the boiling point was 205 °C, which suggested that in the reaction condition above (**Scheme 5.11**), the diamine **5.26** became liquid. Meanwhile, probably because of the side reactions involving the solvent 1,2,4-trichlorobenzene and the reagent **5.26**, the yield of the **5.27** or its derivatives was decreased. Therefore, the synthetic procedure was modified as followed. In the new method, no extra solvent was used; instead, an excessive amount of the diamine **5.26** in liquid state served as solvent under the given reaction condition (Eq 5.2). The new method without additional solvent was clean, efficient and atom-economic. The subsequent work-up was also much easier.

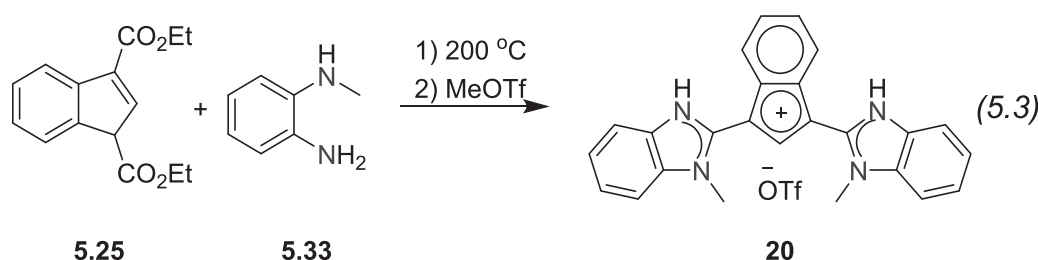


However, the subsequent trials to alkylate compound **19** failed. For example, treatment of compound **19** with strong alkylation reagent such as $[\text{Et}_3\text{O}]\text{BF}_4$ or MeOTf in acetonitrile gave dark red solutions. The solutions were treated with diethyl ether and red solids precipitated. In the ESI mass spectrum of the red solid in acetonitrile, the major peak indicated the presence of fragment $[\text{C}_{23}\text{H}_{17}\text{N}_6]^+$, consistent with the isotopic distribution pattern of the cation of **19**, suggesting that no alkylation occurred. Since chemicals $[\text{Et}_3\text{O}]\text{BF}_4$ and MeOTf were strong alkylation reagents, the failed alkylation may be as-

cribed to the fact that all nitrogen atoms in **19** were already bound to protons, therefore, the proton had to be removed from the nitrogen atoms in prior to possible alkylations.

Meanwhile, the reactions of compound **19**, alkyl halides and exterior bases were also attempted. For example, a suspension of **19**, excessive iodomethane and carbonates was refluxed for one day. However, according to the thin-layer chromatography, the product contained a number of different species, which were very difficult to separate.

Very recently, compound **20** was synthesized from the condensation reaction of **5.25** and **5.33** (Eq 5.3).



A mixture of **5.25** and **5.33** (4.0 equiv. to 6.0 equiv.) was heated at 200 °C in a Dean-Stark apparatus. After the complete removal of all the volatile components, the dark residue was washed with acetonitrile and diethyl ether to give a dark green solid. The solid suspended in acetonitrile was then treated with excessive MeOTf to give a dark red solution. A big amount of diethyl ether was added to the solution to precipitate a dark red solid. Orange crystals were obtained by slow diffusion of diethyl ether into the solution of the red solid in acetonitrile. The structure of the orange material was confirmed to be compound **20** by X-ray diffraction (**Figure 5.4**).

The cation of **20** adopts approximately C_2 symmetry. The torsion angles C3–C2–C10–N1 and C8–C9–C18–N3 are -25.0° and 13.2° , respectively. The bond N3–C18 is longer than N1–C10 by 0.015 Å and the bond N4–C18 is only slightly longer than N2–C10 by 0.006 Å. Normally C–C bond lengths in an aromatic ring are 1.38–1.40 Å and the aromaticity of the cyclopentadienyl ring is obviously sabotaged. The bond lengths C2–C3 and C8–C9 are 1.45–1.46 Å and the bond lengths C1–C2 and C1–C9 are around 1.40 Å; while the bond length C3–C8 is 1.43 Å. Similar patterns have been observed for the cation of **19**. The bond C2–C10 is slightly longer than C9–C18 by 0.02 Å, indicating a slightly stronger conjugation between the ring of benzimidazoleN3–N4 and the central ring. It is noteworthy that the lengths of the bridging C2–C10 and C9–C18 bonds are close to those of the reported imidazole-derived fulvene.¹¹⁵

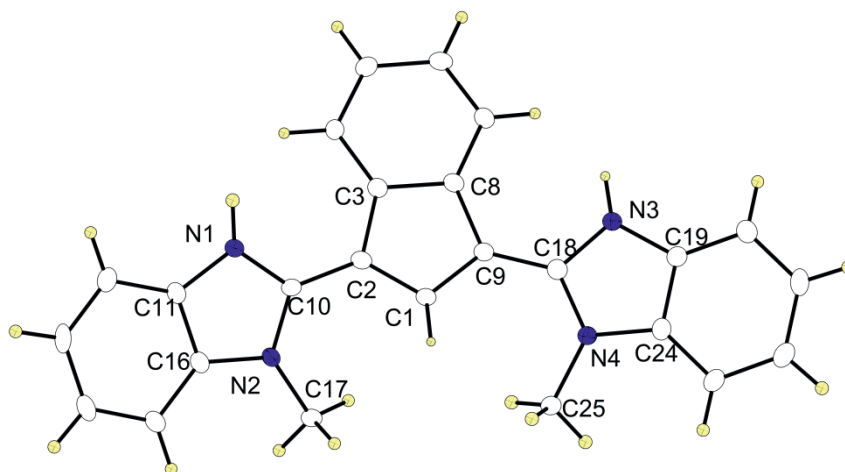


Figure 5.4. Molecular structure of the cation of **20**. Anisotropic displacement ellipsoids drawn at 30% probability level (except for H, which drawn at 5% probability for clarity). The solvent molecule and anion OTf⁻ have been omitted for clarity. Selected bond lengths [Å] angles [°]: C1–C2 1.399(4), C1–C9 1.405(4), C2–C3 1.450(4), C3–C8 1.431(4), C8–C9 1.456(4), N1–C10 1.346(4), N1–C11 1.391(4), N2–C10 1.355(3), N2–C16 1.396(4), N3–C18 1.361(4), N3–C19 1.385(4), N4–C18 1.361(3), N4–C24 1.399(4), C2–C10 1.435(4), C9–C18 1.415(4), N2–C17 1.458(4), N4–C25 1.472(3), C2–C1–C9 110.1(2), C1–C9–C8 107.1(2), C3–C8–C9 107.8(2), C2–C3–C8 106.9(2), C1–C2–C3 108.1(2), N1–C10–N2 108.2(2), N3–C18–N4 106.6(2).

In the structure of the cation of **20**, the two benzimidazole rings and the cyclopentadienyl ring were almost parallel to each other, indicating the strong conjugation among them, similar to the case in the cation of **19**. In addition, all nitrogen atoms were bound to either protons or methyl groups. Efforts to fully characterize both compounds **19** and **20** are on-going.

Two possible reasons that prevent the alkylation of the remaining two nitrogen atoms (as shown in Eq 5.2) are: a) from electronic point of view, because of the highly conjugated system, the bond between the proton and the nitrogen atom is so strong that MeOTf is not able to break it, or b) from the steric point of view, because of the fused benzene ring to the central cyclopentadienyl ring, there is no large space left between the N–H bond and the adjacent C–H bond of the fused ring, thus the alkylation of this nitrogen atom will severely distort the geometry of the compound in order to avoid the steric congestion, making the compound less stable.

5.3 Conclusion

In this work, precursors to the expected ligand **5.29**, compounds **19** and **20**, are synthesized. The bis(NHC) substituted indenenes tend to form cations after a spontaneous acidification in given reaction conditions, in which all nitrogen atoms are bound to either protons or methyl groups. In either **19** or **20**, the two imidazole rings and the central cyclopentadienyl ring are almost parallel to each other, indicating the three rings are conjugated and the bridging C–C bonds have double bond character. The cations of compounds **19** and **20** are so rigid that even strong alkylation reagent MeOTf failed to alkylate them. Possible reasons why the alkylation failed are also briefly discussed. More efforts are needed for the full characterization of both compounds.



CHAPTER 6. Experimental Section

6.1 General Remarks

All manipulations of syntheses were carried out under an anaerobic and anhydrous atmosphere of dry nitrogen/argon by standard Schlenk techniques or in a glovebox, unless otherwise stated. Chemical reagents and solvents were purchased from Sigma-Aldrich, STREM, TCI or ABCR. All solvents were in reagent grade. THF was dried with potassium and sodium in the presence of benzophenone, Et₂O was dried with sodium in the presence of benzophenone, MeCN was dried with CaH₂; all other solvents were distilled or degassed prior to use. Deuterated solvents were used without purification.

¹H NMR, ¹³C NMR, ³¹P NMR, HSQC and HMBC (¹³C-¹H correlation) spectra were recorded on a Bruker 500 MHz, 300 MHz or 200 MHz spectrometer. Chemical shifts were reported in ppm relative to residual proton signals of *d*⁶-DMSO at 2.50 ppm, CDCl₃ at 7.26 ppm, C₆D₆ at 7.16 ppm and CD₃CN at 1.94 ppm. Chemical shifts were reported in ppm relative to residual carbon signals of *d*⁶-DMSO at 39.52 ppm, CDCl₃ at 77.16 ppm, C₆D₆ at 128.06 ppm and CD₃CN at 1.32 ppm and 118.26 ppm.¹¹⁶

EI mass spectra were recorded with a Finnigan MAT 8200. ESI mass spectra were recorded with an Applied Biosystems API 2000 and a BRUKER HCT ultra. Elemental analyses were performed by the analytical laboratory of the Institute of Inorganic Chemistry at Georg-August-University using an Elementar Vario EL III instrument.

Infrared spectra of organic compounds were recorded on a Digilab Excalibur FTS3000 spectrometer. Solid state infrared measurements were performed with a Cary 630FTIR spectrometer and analyzed by FTIR MicroLab software.

Precursor of [L³Cl]BF₄, 3-Chloro-6-(3,5-dimethylpyrazol-1-yl)pyridazine, was synthesized according to reported procedure.¹¹⁷ Ligand precursors [H₄L^R]Cl₃ and [H₃L^R](PF₆)₂ were synthesized by procedures reported previously.^{10, 85, 91}

Geometry optimization and calculation of the single point energies of the models have been carried out with the ORCA program package at the BF86/RI/TZVPP level of theory.¹¹⁸ The Ahlrichs (2df, 2pd) polarization functions were obtained from the TurboMole basis set library under ftp.chemie.uni-karlsruhe.de/pub/basen.¹¹⁹ For the calculation of ligands (Chapter 4), This level of theory is denoted BP86/TZ2P.²⁴

X-ray data were collected on a STOE IPDS II diffractometer with an area detector (graphite monochromated Mo-K α radiation, $\lambda = 0.71073$ Å) by use of scans at 133 K (Table S3). The structures were solved by direct methods and refined on F^2 using all reflections with SHELX-97.¹²⁰ Non-hydrogen atoms were refined anisotropically. Hydrogen atoms were placed in calculated positions and assigned to an isotropic displacement parameter of 1.2 / 1.5 $U_{eq}(\text{C})$.



6.2 Synthesis of Ligand Precursors

Synthesis and characterization of $[L^1Cl]BF_4$

A solution of 3,6-dichloropyridazine (1.00 g, 6.71 mmol) in dry DCM (20.0 mL) was treated with $[Et_3O]BF_4$ (1.40 g, 7.38 mmol, 1.1 equiv.). The colorless solution was stirred at room temperature for one hour. The product normally precipitated as white powder when the reaction was complete. Otherwise, Et_2O (10.0 mL) could be added to the solution to help precipitate the product. The white solid was collected after filtration, washed with Et_2O (20.0 mL, twice) and dried under reduced pressure to give 1.50 g of $[L^1Cl]BF_4$ (5.68 mmol, 84.6%). The product is soluble in acetonitrile or acetone, slightly soluble in dichloromethane and insoluble in diethyl ether, THF, toluene or hexane. The product is stable in aerobic and humid conditions.

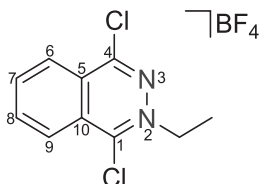
1H NMR (300 MHz, CD_3CN , 298 K): δ = 8.54 (d, J_{AB} = 9.1 Hz, 1H, C_4H), 8.46 (d, J_{AB} = 9.1 Hz, C_5H), 4.93 (q, J = 7.2 Hz, 2H, CH_2CH_3), 1.65 (t, J = 7.2 Hz, 3H, CH_3).

^{13}C NMR (75 MHz, CD_3CN , 298 K): δ = 156.7 (s, C_3), 154.3 (s, C_6), 139.6 (s, CH), 139.5 (s, CH), 60.3 (s, CH_2CH_3), 12.1 (s, CH_3).

HR MS (ESI^+) m/z calculated $[M - BF_4]^+$ 176.9981, observed 176.9980.

Elem. Anal. Calcd. for $C_6H_7BCl_2F_4N_2$: C 27.21, H 2.66, N 10.58; found: C 26.92, H 2.83, N 10.43.

Synthesis and characterization of $[L^2Cl]BF_4$



A solution of 1,4-dichlorophthalazine (100.0 mg, 0.502 mmol) in dry DCM (5.0 mL) was treated with $[Et_3O]BF_4$ (104.0 mg, 0.553 mmol, 1.1 equiv.). The colorless solution was stirred at room temperature for one hour. Et_2O (10.0 mL) was added to the solution to precipitate a white solid. This solid was collected by filtration, washed by Et_2O (10.0 mL, twice) and dried under reduced pressure to give 128 mg of $[L^2Cl]BF_4$.

(0.406 mmol, 81.0%). The product is soluble in acetonitrile or acetone, slightly soluble in dichloromethane and insoluble in diethyl ether, THF, toluene or hexane. The product is unstable at room temperature and better used as freshly prepared.

^1H NMR (300 MHz, CD_3CN , 298 K): δ = 8.85-8.78 (m, 1H, CH), 8.71-8.66 (m, 2H, CH), 8.54 (ddd, J_1 = 8.4 Hz, J_2 = 7.0 Hz, J_3 = 1.0 Hz, 1H, CH), 5.05 (q, J = 7.3 Hz, 2H, CH_2CH_3), 1.71 (t, J = 7.3 Hz, 3H, CH_3).

^{13}C NMR (75 MHz, CD_3CN , 298 K): δ = 156.4 (s, C_4Cl), 155.6 (s, C_1Cl), 140.8 (s, C_8H), 138.1 (s, C_7H), 129.2 (s, C_9H), 128.8 (s, C_5), 128.0 (s, C_{10}), 127.2 (s, C_6H), 59.7 (s, CH_2CH_3), 12.3 (s, CH_3).

HR MS m/z calculated $[\text{M} - \text{BF}_4]^+$ 227.0137, observed 227.0137.
(ESI⁺)

Elem. Anal. Calcd. for $\text{C}_{10}\text{H}_9\text{BCl}_2\text{F}_4\text{N}_2$: C 38.14, H 2.88, N 8.90; found: C 38.14, H 2.81, N 8.85.

Synthesis and characterization of $[\text{L}^3\text{Cl}]\text{BF}_4$

A solution of 3-chloro-6-(3,5-dimethylpyrazol-1-yl)pyridazine (100.0 mg, 0.479 mmol) in dry CH_3CN (8.0 mL) was treated with $[\text{Et}_3\text{O}]\text{BF}_4$ (109.0 mg, 0.575 mmol, 1.2 equiv.). The colorless solution was stirred at room temperature for 3 hours. Et_2O (15.0 mL) was added to the solution to precipitate a white solid. This solid was collected by filtration, washed by Et_2O (10.0 mL, twice) and dried under reduced pressure to give 105.0 mg of $[\text{L}^3\text{Cl}]\text{BF}_4$ (0.324 mmol, 67.6%). The product is soluble in acetonitrile or acetone, slightly soluble in dichloromethane and insoluble in diethyl ether, THF toluene or hexane. The product is stable at room temperature in solid state.

^1H NMR (300 MHz, CD_3CN , 298 K): δ = 8.85 (d, J = 9.5 Hz, 1H, CH^{Pyri}), 8.45 (d, J = 9.5 Hz, 1H, CH^{Pyri}), 6.33 (s, 1H, CH^{Pyra}), 4.91 (q, J = 7.2 Hz, 2H, CH_2CH_3), 2.68 (s, 3H, $\text{CH}_3^{\text{Pyra}}$), 2.31 (s, 3H, $\text{CH}_3^{\text{Pyra}}$), 1.67 (t, J = 7.2 Hz, 3H, CH_2CH_3).

^{13}C NMR (75 MHz, CD_3CN , 298 K): δ = 155.2 (s, C), 154.7 (s, C), 149.9 (s, C), 143.6 (s, C), 138.7 (s, CH^{Pyri}), 130.3 (s, CH^{Pyri}), 112.7 (s, CH^{Pyra}), 59.7 (s, CH_2CH_3), 13.9 (s, $\text{CH}_3^{\text{Pyra}}$), 12.5 (s, CH_2CH_3), 12.2 (s, $\text{CH}_3^{\text{Pyra}}$).



HR MS m/z calculated $[M - BF_4]^+$ 237.0902, observed 237.0901.
(ESI⁺)

Elem. Anal. Calcd. for C₁₁H₁₄BClF₄N₄: C 40.71, H 4.35, N 17.26; found: C 40.73, H 4.23, N 17.23.

Characterization of [H₃L^{Et}](PF₆)₂

¹H NMR (300 MHz, CD₃CN, 298 K): δ = 8.51 (t, 2H, J = 1.9 Hz, CH^{Imi2}), 7.42 (t, 2H, J = 1.9 Hz, CH^{Imi4/5}), 7.38 (t, 2H, J = 1.9 Hz, CH^{Imi4/5}), 6.50 (s, 1H, CH^{Pyr}), 5.34 (s, 4H, bridging CH₂), 4.17 (q, 4H, J = 7.3 Hz, CH₂CH₃), 1.46 (t, 6H, J = 7.3 Hz, CH₃).

¹³C NMR (75 MHz, CD₃CN, 298 K): δ = 136.2 (s, CH^{Imi2}), 123.5 (s, CH^{Imi4/5}), 123.4 (s, CH^{Imi4/5}), 107.1 (s, CH^{Pyr}), 46.1 (s, CH₂), 15.4 (s, CH₃).

Characterization of [H₃L^{nBu}](PF₆)₂.

¹H NMR (300 MHz, CD₃CN, 298 K): δ = 8.54 (dd, 2H, J_1 = 1.7 Hz, J_2 = 1.6 Hz, CH^{Imi2}), 7.40 (s, 2H, CH^{Imi4/5}), 7.39 (s, 2H, CH^{Imi4/5}), 6.48 (s, 1H, CH^{Pyr}), 5.35 (s, 4H, bridging CH₂), 4.12 (t, 4H, J = 7.3 Hz, CH₂CH₂CH₂CH₃), 1.87-1.74 (m, 4H, CH₂), 1.39-1.24 (m, 4H, CH₂), 0.93 (t, 6H, J = 7.3 Hz, CH₃).

¹³C NMR (75 MHz, CD₃CN, 298 K): δ = 136.5 (s, CH^{Imi2}), 123.7 (s, CH^{Imi4/5}), 123.5 (s, CH^{Imi4/5}), 106.9 (s, CH^{Pyr}), 50.6 (s, CH₂), 46.1 (s, bridging CH₂), 32.5 (s, CH₂), 20.0 (s, CH₂), 13.7 (s, CH₃).

Synthesis and characterization of HL⁴

A mixture of 3,5-dimethylpyrazole (677.5 mg, 7.05 mmol) and sodium hydride (95%, 7.38 mmol, 1.05 equiv.) in dry THF (30.0 mL) in inert gas was reflux for 1 hour. A solution of 3,6-dichloropyridazine (500.0 mg, 3.36 mol, 0.48 equiv.) in 20.0 mL of THF

was added slowly and reflux for another 4 hours. The reaction was cooled to room temperature and THF was removed under reduced pressure and 50.0 mL of DCM was added to dissolve the product. The solution was washed with water (twice, 30.0 mL each time) and dried through MgSO_4 . The solvent was removed under reduced pressure. The raw material was dissolved in 25.0 mL ethanol by heating and the solution was cooled to room temperature and then in fridge (0 °C) for overnight. The precipitated solid was collected by filtration to gave 536.0 mg white fluffy product (2.53 mmol, 52.7 %).

^1H NMR (300 MHz, CD_2Cl_2 , 298 K): δ = 8.18 (s, 2H, CH^{Pyr}), 6.06 (s, 2H, CH^{Pyr}), 2.70 (s, 6H, CH_3), 2.26 (s, 6H, CH_3).

^{13}C NMR (75 MHz, CD_2Cl_2 , 298 K): δ = 155.6 (s, NC^{Pyr}), 151.6 (s, CCH_3), 142.6 (s, CCH_3), 123.3 (s, CH^{Pyr}), 110.4 (s, CH^{Pyr}), 15.1 (s, CH_3), 13.9 (s, CH_3).

The ylide and ethyl 3-oxo-2-phenylpropanoate were commercially available or synthesized according to reported procedures.¹²¹ From 2-phenylpent-2-enedionate to diethyl 1*H*-indene-1,3-dicarboxylate was synthesized according to literature.¹¹³

Synthesis of diethyl 2-phenylpent-2-enedionate 5.23

Ylide (5.467 g, 12.73 mmol, 1.3 equiv.) was dissolved in 50.0 mL dichloromethane at 0 °C under inert gas atmosphere. Ethyl 3-oxo-2-phenylpropanoate (1.883 g, 9.797 mmol, 1.0 equiv.) was added one portion to the reaction system. NEt_3 (2.73 mL, 19.6 mmol, 2.0 equiv.) was added over 15 minutes. After the addition, the ice bath was removed and the yellow suspension was stirred at ambient temperature for 2 hours.

The solvent was removed under reduced pressure and the sticky residue was first washed with hexane (50.0 mL). The solution was collected after filtration and the white solid was washed with diethyl ether 3 times (30.0 mL each time). The combined organic layer was then dried under reduced pressure and purified by silica gel chromatography with the eluent of a mixture of ethyl acetate and hexanes in the ratio of 1:10. The product was a mixture of *Z*- and *E*- isomers, which could not be easily separated; however, the mixture could be used directly for the next step.

Diethyl (*Z*)-2-phenylpent-2-enedionate

^1H NMR (300 MHz, CDCl_3 , 298 K): 7.37-7.28 (m, 5H, Ph), 6.44 (t, J = 7.1 Hz, 1H, olefin-*H*), 4.29 (q, J = 7.1 Hz, 2H, CH_2CH_3), 4.19 (q, J = 7.1 Hz, 2H, CH_2CH_3), 3.58 (d, J = 7.1 Hz, $\text{CH}_2\text{CO}_2\text{Et}$), 1.31 (t, J = 7.1 Hz, CH_3), 1.29 (t, J = 7.1 Hz, 3H, CH_3).



^{13}C NMR (300 MHz, CDCl_3 , 298 K): 171.1 (s, $\text{C}=\text{C}-\text{CO}_2\text{Et}$), 167.5 (s, $\text{CH}_2\text{CO}_2\text{Et}$), 137.2 (s, $\text{C}=\text{CH}$), 136.8 (s, Ph), 132.2 (s, $\text{C}=\text{CH}$), 128.3 (s, Ph), 128.0 (s, Ph), 127.8 (s, Ph), 61.1 (s, CH_2CH_3), 61.0 (s, CH_2CH_3), 35.4 (s, $\text{CH}_2\text{CO}_2\text{Et}$), 31.0 (s, CH_3), 14.3 (s, CH_3).

Diethyl (E)-2-phenylpent-2-enedionate

^1H NMR (300 MHz, CDCl_3 , 298 K): 7.42-7.30 (m, 3H, Ph), 7.23-7.14 (m, 3H, Ph and olefin-*H*), 4.23 (q, $J = 7.1$ Hz, 2H, CH_2CH_3), 4.15 (q, $J = 7.1$ Hz, 2H, CH_2CH_3), 3.12 (d, $J = 7.4$ Hz, 2H, $\text{CH}_2\text{CO}_2\text{Et}$), 1.28 (t, $J = 7.1$ Hz, 3H, CH_3), 1.25 (t, $J = 7.1$ Hz, 3H, CH_3).

^{13}C NMR (300 MHz, CDCl_3 , 298 K): 170.5 (s, $\text{C}=\text{C}-\text{CO}_2\text{Et}$), 166.7 (s, $\text{CH}_2\text{CO}_2\text{Et}$), 136.9 (s, $\text{C}=\text{CH}$), 135.2 (s, $\text{C}=\text{CH}$), 134.6 (s, Ph), 129.7 (s, Ph), 128.3 (s, Ph), 128.0 (s, Ph), 61.3 (s, CH_2CH_3), 61.2 (s, CH_2CH_3), 35.3 (s, $\text{CH}_2\text{CO}_2\text{Et}$), 14.4 (s, CH_3), 14.3 (s, CH_3).

Synthesis of 19

A mixture of *o*-phenylenediamine (2.993 g, 27.68 mmol, 8.0 equiv.) and ammonium chloride (185.1 mg, 3.46 mmol, 1.0 equiv.) was placed in a two-necked Schlenk flask and the system was purged with argon. The mixture was stirred at 200 °C for 10 min and *o*-phenylenediamine was completely melted. Diethyl 1*H*-indene-1,3-dicarboxylate (900.0 mg, 3.46 mmol, 1.0 equiv.) was added dropwise to the mixture and the system was kept at 200 °C. During the reaction, lots of gas exuded and condensed as colorless liquid on the condenser. The reaction mixture turned to orange-yellow tablet and was no longer able to be stirred after 15 min. The system was cooled to room temperature and the residue was washed with acetonitrile for 3 times (30.0 mL each time). The obtained yellow solid was put in 50.0 mL of ethanol and the mixture was refluxed at 90 °C for 10 min and the solution was removed by filtration. The yellow powder was dried under vacuum to give the final product, in yield of 1.053 g (3.02 mmol, 87.4%).

HR MS (ESI⁺) m/z calculated $[\text{C}_{25}\text{H}_{21}\text{N}_4]^+$ 377.1761, observed 377.1761.

The product was slightly soluble in acetone, ethanol, methanol, dichloromethane or acetonitrile, insoluble in toluene or hexane. The crystalline material could be obtained by dissolving the product in hot ethanol in a slim tube and letting the system cooled down to room temperature very slowly.

6.3 Synthesis of Metal Complexes

Synthesis and characterization of 1

A mixture of the ligand precursor $[\text{L}^1\text{Cl}]\text{BF}_4$ (100.0 mg, 0.378 mmol) and $\text{Pd}(\text{PPh}_3)_4$ (436.0 mg, 0.378 mmol, 1.0 equiv.) in a Schlenk tube was degassed three times. Degassed acetone (12.0 mL) was added through a syringe. The suspension was stirred for 30 min until a clear yellow solution was formed. Degassed toluene (15.0 mL) was added and the mixture was stirred vigorously for 30 min; a white precipitates gradually appeared. The solid was collected by filtration, washed with toluene (8.0 mL) and diethyl ether (8.0 mL) and finally dried under reduced pressure to give 248.0 mg of an off-white powder (0.277 mmol, 73%). The product can be purified and obtained as colorless crystals by slow diffusion of diethyl ether into a solution of the crude material in dichloromethane or acetone. $[\text{LPd}(\text{PPh}_3)_2\text{Cl}]\text{BF}_4$ is soluble in dichloromethane, slightly soluble in acetone or acetonitrile and insoluble in THF, diethyl ether, toluene or hexane. The product is reasonably stable in solid state and slowly turns yellow as a solution in dichloromethane.

^1H NMR (300 MHz, CD_2Cl_2 , 298 K): δ = 7.72 (d, J = 8.8 Hz, 1H, CH^{Pyri}), 7.59-7.31 (m, 30H, CH^{Ph}), 6.70 (d, J = 8.8 Hz, 1H, CH^{Pyri}), 4.59 (q, J = 7.2 Hz, 2H, CH_2CH_3), 1.14 (t, J = 7.2 Hz, CH_3).

^{13}C NMR (75 MHz, CD_2Cl_2 , 298 K): δ = 192.6 (t, J = 6.9 Hz, PdC), 154.4 (s, ClC), 147.6 (t, J = 2.9 Hz, CH^{Pyri}), 134.5 (t, J = 6.3 Hz, CH^{Ph}), 132.2 (s, CH^{Ph}), 129.6 (s, CH^{Pyri}), 129.6 (t, J = 5.8 Hz, CH^{Ph}), 128.5 (t, J = 25.3 Hz, PC), 64.3 (s, CH_2CH_3), 13.9 (s, CH_3).

^{31}P NMR (121 MHz, CD_2Cl_2 , 298 K): δ = 20.9 (s).

MS (ESI^+) m/z (%) 808.8 (100, $[\text{M} - \text{BF}_4]^+$); **MS (ESI^- , CH_2Cl_2):** m/z (%) 87.0 (100, $[\text{BF}_4]^-$).

HR MS m/z calculated $[\text{M} - \text{BF}_4]^+$ 807.0849, observed 807.0835.
(ESI^+)

Elem. Anal. Calcd. for $\text{C}_{42}\text{H}_{37}\text{BCl}_2\text{F}_4\text{N}_2\text{P}_2\text{Pd}$: C 56.31, H 4.16, N 3.13; found: C 56.35, H 4.01, N 3.02.



Synthesis and characterization of complex 2

A mixture of the ligand precursor $[\mathbf{L}^2\text{Cl}]\text{BF}_4$ (50.0 mg, 0.159 mmol) and $\text{Pd}(\text{PPh}_3)_4$ (167.0 mg, 0.159 mmol, 1.0 equiv.) in a Schlenk tube was degassed three times. Degassed acetone (5.0 mL) was added through a syringe. The suspension was stirred for 30 min until a clear yellow solution was formed. Degassed diethyl ether (10.0 mL) was added to cause precipitation of a yellow solid. The solid was separated by filtration, washed with diethyl ether (8.0 mL) and dried under reduced pressure to give 91.0 mg of a yellow powder (0.096 mmol, 61%). $[\mathbf{L}^2\text{Pd}(\text{PPh}_3)_2\text{Cl}]\text{BF}_4$ can be purified and obtained as colorless crystals by slow diffusion of diethyl ether into a solution of the crude material in acetone or dichloromethane. The product is soluble in dichloromethane, slightly soluble in acetone or acetonitrile and insoluble in THF, diethyl ether, toluene or hexane. The product is reasonably stable in solid state and slowly turns yellow as a solution in dichloromethane.

^1H NMR (300 MHz, CD_2Cl_2 , 298 K): δ = 8.90 (d, J = 7.8 Hz, 1H, CH^{Phth}), 8.09-7.92 (m, 3H, CH^{Phth}), 7.55-7.28 (m, 30H, CH^{Ph}), 4.84 (q, J = 7.2 Hz, 4H, CH_2CH_3), 1.15 (t, J = 7.2 Hz, 3H, CH_3).

^{13}C NMR (75 MHz, CD_2Cl_2 , 298 K): δ = 199.4 (t, J = 6.3 Hz, PdC), 154.9 (s, C^{Phth}), 138.5 (s, CH^{Phth}), 136.5 (t, J = 1.8 Hz, C^{Phth}), 136.0 (s, CH^{Phth}), 135.2 (s, CH^{Phth}), 134.2 (t, J = 6.2 Hz, CH^{Ph}), 132.2 (s, C^{Ph}), 129.3 (t, J = 5.4 Hz, CH^{Ph}), 128.2 (t, J = 25.3 Hz, C^{Ph}), 127.0 (s, CH^{Phth}), 123.1 (s, C^{Phth}), 63.4 (s, CH_2CH_3), 13.4 (s, CH_3).

^{31}P NMR (121 MHz, D_6 -acetone, 298 K): δ = 21.1 (s).

MS (ESI⁺) m/z (%) 858.8 (83.0, $[\text{M} - \text{BF}_4]^+$).

MS (ESI⁻) m/z (%) 87.0 (100, $[\text{BF}_4]^-$).

Elem. Anal. Calcd. for $\text{C}_{46}\text{H}_{39}\text{N}_2\text{Cl}_2\text{P}_2\text{BF}_4\text{Pd} \cdot 1/3\text{CH}_2\text{Cl}_2$: C 57.12, H 4.10, N 2.88; Found: C 57.03, H 4.18, N 2.60.

Synthesis and characterization of complex 3

The ligand precursor $[\text{L}^1\text{Cl}]\text{BF}_4$ (100.0 mg, 0.378 mmol), NEt_4Cl (62.6 mg, 0.378 mmol, 1.0 equiv.) and $\text{Pd}_2(\text{dba})_3$ (119.0 mg, 0.208 mmol, 0.55 equiv.) were placed in a Schlenk tube that was then purged with N_2 . Degassed acetone (8.0 mL) was added through a syringe and the suspension was stirred under N_2 at room temperature for 30 min. During this time, the color of the solution turned gradually from dark purple to greenish yellow. PPh_3 (99.0 mg, 0.378 mmol, 1.0 equiv.) was added in the Schlenk tube as one portion, followed by degassed acetone (5.0 mL), and the mixture was stirred for further 15 min. The suspension was filtered and the gray solid was collected after filtration. The solid was dissolved in CH_2Cl_2 (8.0 mL) and the solution, containing a small amount of palladium black, was filtered through Celite 545 to give an almost colorless solution, which was dried under reduced pressure to give $\text{LPd}(\text{PPh}_3)\text{Cl}_2$ as an off-white solid (yield: 87.0 mg, 0.149 mmol, 40%). The product is soluble in dichloromethane, slightly soluble in acetone or acetonitrile and insoluble in THF, diethyl ether, toluene or hexane. Upon prolonged standing under aerobic conditions and under light solutions of the product in dichloromethane gradually give palladium black sediments. In solid state under light the product gradually turns green.

^1H NMR (300 MHz, CD_2Cl_2 , 298 K): δ = 7.95 (dd, J_1 = 8.8 Hz, J_2 = 1.1 Hz, 1H, CH^{Pyri}), 7.63-7.23 (m, 15H, CH^{Ph}), 6.89 (d, J = 8.8 Hz, 1H, CH^{Pyri}), 5.38 (dq, J_1 = 12.4 Hz, J_2 = 7.2 Hz, 1H, CH_2CH_3), 4.55 (m, 1H, CH_2CH_3), 1.53 (t, J = 7.2 Hz, 3H, CH_3).

^{13}C NMR (75 MHz, CD_2Cl_2 , 298 K): δ = 191.5 (s, PdC), 153.6 (s, ClC), 147.0 (d, J = 3.7 Hz, CH^{Pyri}), 134.6 (d, J = 11.1 Hz, CH^{Ph}), 131.8 (d, J = 2.7 Hz, CH^{Ph}), 129.9 (d, J = 53.6 Hz, C^{Ph}), 129.1 (d, J = 11.1 Hz, CH^{Ph}), 123.3 (s, CH^{Pyri}), 64.7 (s, CH_2CH_3), 14.6 (s, CH_3).

^{31}P NMR (121 MHz, CD_2Cl_2 , 298 K): δ = 26.1 (s).

HR MS m/z calculated $[\text{M} - \text{Cl}]^+$ 544.9929, observed 544.9923.
(ESI^+)

Elem. Anal. Calcd. for $\text{C}_{24}\text{H}_{22}\text{Cl}_3\text{N}_2\text{PPd}$: C 49.51, H 3.81, N 4.81; found: C 48.75, H 3.63, N 4.93.



Synthesis and characterization of complex 4

A mixture of the ligand precursor $[L^3Cl]BF_4$ (30.0 mg, 0.092 mmol) and $Pd(PPh_3)_4$ (106.8 mg, 0.092 mmol, 1.0 equiv.) in a Schlenk tube was degassed three times. Degassed acetone (4.0 mL) was added through a syringe. The suspension was stirred for 30 min until a clear yellow solution was formed. Degassed toluene (15.0 mL) was added to cause precipitation of an off-white solid. The solid was separated by filtration, washed with toluene (5.0 mL), diethyl ether (5.0 mL) and dried under reduced pressure to give 70.0 mg of a white powder (0.073 mmol, 80%). $[L^3Pd(PPh_3)_2Cl]BF_4$ can be purified and obtained as colorless crystals by slow diffusion of diethyl ether into a solution of the crude material in acetone or dichloromethane. The product is soluble in dichloromethane, slightly soluble in acetone or acetonitrile and insoluble in THF, diethyl ether, toluene or hexane. The product is reasonably stable in solid state.

1H NMR (300 MHz, CD_2Cl_2 , 298 K): δ = 7.62–7.28 (m, 32H, CH^{Ph} , CH^{Pyri}), 6.02 (s, 1H, CH^{Pyra}), 4.50 (q, J = 7.2 Hz, 2H, CH_2CH_3), 2.29 (s, 3H, CH_3^{Pyra}), 2.16 (s, 3H, CH_3^{Pyra}), 1.06 (t, J = 7.2 Hz, 3H, CH_2CH_3).

^{13}C NMR (75 MHz, CD_2Cl_2 , 298 K): δ = 187.5 (t, J = 6.9 Hz, PdC), 154.2 (s, Pyra- C^{Pyri}), 153.9 (s, CH_3C^{Pyra}), 145.6 (t, J = 3.0 Hz, CH^{Pyri}), 142.4 (s, CH_3C^{Pyra}), 134.5 (t, J = 6.2 Hz, CH^{Ph}), 132.2 (s, CH^{Ph}), 129.5 (t, J = 5.3 Hz, CH^{Ph}), 129.0 (t, J = 25.1 Hz, PC), 121.7 (s, CH^{Pyri}), 112.5 (s, CH^{Pyra}), 63.9 (s, CH_2CH_3), 15.0 (s, CH_3^{Pyra}), 13.8 (s, CH_2CH_3), 13.7 (s, CH_3^{Pyra}).

^{31}P NMR (121 MHz, CD_2Cl_2 , 298 K): δ = 21.5 (s).

HR MS m/z calculated $[M - BF_4]^+$ 867.1774, observed 867.1774.
(ESI⁺)

Elem. Anal. Calcd. for $C_{47}H_{44}BClF_4N_4P_2Pd \cdot 1/4 CH_2Cl_2$: C 58.10, H 4.59, N 5.74; found: C 58.25, H 4.46, N 5.72.

Synthesis and characterization of 5

Although treatment of $[\text{H}^4\text{L}^{\text{tBu}}]\text{Cl}_3$ with $\text{Pd}(\text{OAc})_2$ (2.0 equiv.) directly gave $^{\text{a}}\text{L}^{\text{tBu}}\text{Pd}_2\text{Cl}_3$ as the major product, the reaction mostly generated some dark-colored solid as well, which was assumed to be palladium black. Due to its poor solubility, $^{\text{a}}\text{L}^{\text{tBu}}\text{Pd}_2\text{Cl}_3$ obtained *via* this method was difficult to purify. Therefore, the alternative method of first synthesizing $[\text{L}^{\text{tBu}}_2\text{Pd}_2](\text{PF}_6)_2$ which then is converted to $^{\text{a}}\text{L}^{\text{tBu}}\text{Pd}_2\text{Cl}_3$ proved advantageous.

A suspension of $[\text{L}^{\text{tBu}}_2\text{Pd}_2](\text{PF}_6)_2$ (50.0 mg, 0.0846 mmol), NEt_4Cl (15.4 mg, 0.0931 mmol, 1.10 equiv.) and PdCl_2 (15.7 mg, 0.0889 mmol, 1.00 equiv.) in CH_3CN (20.0 mL) was heated to reflux for 5 h in air. The solution gradually turned to light-orange and some bright yellow solid was formed. The yellow solid was collected by filtration, washed with CH_3CN and Et_2O and dried under vacuum to give 50.9 mg of the product (0.0773 mmol, 91.3%).

^1H NMR (300 MHz, $\text{DMSO}-d_6$, 298 K): δ = 8.97 (d, J = 1.9 Hz, 2H, CH^{Imi}), 7.06 (d, J = 1.9 Hz, 2H, CH^{Imi}), 6.33 (s, 1H, CH^{Pyr}), 5.24 (s, 4H, bridging CH_2), 1.51 (s, 18H, CH_3).

Elem. Anal. Calcd. for $\text{C}_{19}\text{H}_{27}\text{N}_6\text{Cl}_3\text{Pd}_2$: C 34.65, H 4.13, N 12.76; found: C 34.84, H 4.28, N 12.90.

**General procedures of the synthesis of $[\text{L}^{\text{R}}_2\text{Pd}_2](\text{PF}_6)_2$ (6, 7 and 8)**

A solution of $[\text{H}_3\text{L}^{\text{R}}](\text{PF}_6)_2$ (1.0 equiv.), $\text{Pd}(\text{OAc})_2$ (1.0 equiv.) and NH_4OAc (2.0 equiv.) in 3.0 mL DMSO was stirred at room temperature for 30 min. The solution was heated to 105°C and stirred for another 8 hrs. The reaction was then cooled to room temperature and water (15.0 mL) was added. After stirring for 15 min, the solid was isolated by centrifuging. The residue was further washed by water for 3 times to remove the remaining DMSO. The yellowish solid was collected and dried under vacuum. The raw product was purified by silicon gel chromatography. In case the product still had some contamination, re-crystallization could be applied for further purification: diethyl ether was added gradually to a solution of the product in acetonitrile until the solution started to blur, then vigorous stirring for 10 min forced a complete precipitation of the product as white fine powder, which was collected and dried under vacuum.

General procedures of the synthesis of $[\text{L}^{\text{R}}_2\text{Pd}_2](\text{PF}_6)_2$ (9, 10, 11 and 12)

A solution of $[\text{H}_3\text{L}^{\text{R}}](\text{PF}_6)_2$ (1.0 equiv.) and $\text{Pd}(\text{OAc})_2$ (1.0 equiv.) in 3.0 mL DMSO was stirred at room temperature for 30 min. The solution was heated to 95°C and stirred for 1.5 hrs. A portion of NH_4OAc (1.0 equiv.) was added to the reaction system to work up and the solution was stirred at present temperature for another 30 min. The solution was cooled to room temperature and 15.0 mL water was added. After stirring for 15 min, the solid was isolated by centrifuging. The residue was further washed by water for 3 times to remove the remaining DMSO. The yellowish solid was collected and dried under vacuum. The raw product was purified by silicon gel chromatography. In case the product still had some contamination, re-crystallization could be applied for further purification: diethyl ether was added gradually to a solution of the product in acetonitrile until the solution started to blur, then vigorous stirring for 10 min forced a complete precipitation of the product as white fine powder, which was collected and dried under vacuum.

Synthesis and characterization of 6

[H₃L^{Et}](PF₆)₂ (400.0 mg, 0.694 mmol), Pd(OAc)₂ (155.9 mg, 0.694 mmol, 1.0 equiv.) and NH₄OAc (107.0 mg, 1.389 mmol, 2.0 equiv.) were used. DMSO was removed from the mixture after the reaction by distillation under reduced pressure until the remaining volume was about 1.0 mL. The eluent for chromatography was a mixture of acetonitrile and dichloromethane (1:3). Yield: 209.0 mg (0.363 mmol, 52.2%).

¹H NMR (300 MHz, CD₃CN, 298 K): δ = 7.36 (d, J = 2.0 Hz, 4H, CH^{Imi}), 7.24 (d, J = 2.0 Hz, 4H, CH^{Imi}), 6.56 (s, 2H, CH^{Pyr}), 5.47 (s, 8H, bridging CH₂), 3.75-3.50 (br, 8H, CH₂CH₃), 1.10 (t, J = 7.3 Hz, 12H, CH₃).

¹³C NMR (75 MHz, CD₃CN, 298 K): δ = 154.8 (s, PdC), 147.0 (s, CN^{Pyr}), 123.6 (s, CH^{Imi}), 123.0 (s, CH^{Imi}), 103.9 (s, CH^{Pyr}), 48.6 (s, bridging CH₂), 46.8 (s, CH₂CH₃), 15.8 (s, CH₃).

MS (ESI⁺) m/z 390.0 [M - (PF₆)₂]²⁺

HR MS m/z calculated [M - (PF₆)₂]²⁺ 390.0710, observed 390.0703.
(ESI⁺)

Elem. Anal. Calcd. for C₃₀H₃₈N₁₂F₁₂P₂Pd₂: C 33.69, H 3.58, N 15.72; found: C 33.29, H 3.79, N 15.12.

Synthesis and characteriaztion of 7

[H₃L^{nBu}](PF₆)₂ (300.0 mg, 0.475 mmol), Pd(OAc)₂ (106.5 mg, 0.475 mmol, 1.0 equiv.) and NH₄OAc (73.1 mg, 0.949 mmol, 2.0 equiv.) were used. The eluent for chromatography was a mixture of acetonitrile and dichloromethane (1:5). Yield: 135.0 mg (0.213 mmol, 44.9%).

¹H NMR (300 MHz, CD₃CN, 298 K): δ = 7.37 (d, J = 2.0 Hz, 4H, CH^{Imi}), 7.23 (d, J = 2.0 Hz, 4H, CH^{Imi}), 6.56 (s, 2H, CH^{Pyr}), 5.47 (s, 4H, bridging CH₂), 5.45 (s, 4H, bridging CH₂), 3.80-3.30 (br, 8H, CH₂CH₂CH₂H₃), 1.75-1.50 (br, 4H, CH₂CH₂CH₂CH₃), 1.40-1.10 (br, 12H, CH₂CH₂CH₂CH₃ and CH₂CH₂CH₂CH₃), 0.81 (t, J = 7.2 Hz, 12H, CH₃).



^{13}C NMR (75 MHz, CD_3CN , 298 K): δ = 155.0 (s, PdC), 147.0 (s, CN^{Pyr}), 123.7 (s, CH^{Imi}), 123.6 (s, CH^{Imi}), 104.0 (s, CH^{Pyr}), 51.6 (s, $\text{CH}_2\text{CH}_2\text{CH}_2\text{CH}_3$), 48.6 (s, bridging CH_2), 33.2 (s, $\text{CH}_2\text{CH}_2\text{CH}_2\text{CH}_3$), 20.4 (s, $\text{CH}_2\text{CH}_2\text{CH}_2\text{CH}_3$), 13.8 (s, CH_3).

MS (ESI⁺) m/z 445.7 $[\text{M} - (\text{PF}_6)_2]^{2+}$

HR MS m/z calculated $[\text{M} - (\text{PF}_6)_2]^{2+}$ 446.1336, observed 446.1331.
(ESI⁺)

Elem. Anal. Calcd. for $\text{C}_{38}\text{H}_{54}\text{N}_{12}\text{F}_{12}\text{P}_2\text{Pd}_2$: C 38.62, H 4.61, N 14.22; found: C 38.59, H 4.55, N 14.19.

Synthesis and characterization of 8

$[\text{H}_3\text{L}^{\text{Mes}}](\text{PF}_6)_2$ (400.0 mg, 0.694 mmol), $\text{Pd}(\text{OAc})_2$ (155.9 mg, 0.694 mmol, 1.0 equiv.) and NH_4OAc (107.0 mg, 1.389 mmol, 2.0 equiv.) were used. The eluent for chromatography was a mixture of acetonitrile and dichloromethane (1:5). Yield: 209.0 mg (0.363 mmol, 52.2%).

^1H NMR (300 MHz, CD_3CN , 298 K): δ = 7.33 (d, J = 2.0 Hz, 4H, CH^{Imi}), 7.15 (d, J = 2.0 Hz, 4H, CH^{Imi}), 7.12-7.08 (br, 4H, CH^{Mes}), 7.07-7.04 (br, 4H, CH^{Mes}), 6.18 (s, 2H, CH^{Pyr}), 4.95 (d, J = 16.1 Hz, 4H, bridging CH_2), 3.55 (d, J = 16.0 Hz, 4H, bridging CH_2), 2.42 (s, 12H, CH_3), 1.78 (s, 12H, CH_3), 1.50 (s, 12H, CH_3).

^{13}C NMR (75 MHz, CD_3CN , 298 K): δ = 161.8 (s, PdC), 146.5 (s, CN^{Pyr}), 141.3 (s, $\text{CCH}_3^{\text{Mes}}$), 138.8 (s, $\text{CCH}_3^{\text{Mes}}$), 135.5 (s, $\text{CCH}_3^{\text{Mes}}$), 130.6 (s, CH^{Mes}), 130.2 (s, CH^{Mes}), 125.0 (s, CH^{Imi}), 123.7 (s, CH^{Imi}), 102.4 (s, CH^{Pyr}), 47.9 (s, bridging CH_2), 21.0 (s, CH_3), 18.7 (s, CH_3), 18.3 (s, CH_3).

MS (ESI⁺) m/z 569.7 $[\text{M} - (\text{PF}_6)_2]^{2+}$

HR MS m/z calculated $[\text{M} - (\text{PF}_6)_2]^{2+}$ 570.1653, observed 570.1653.
(ESI⁺)

Elem. Anal. Calcd. for $\text{C}_{58}\text{H}_{62}\text{N}_{12}\text{F}_{12}\text{P}_2\text{Pd}_2$: C 48.72, H 4.37, N 11.75; found: C 48.07, H 4.22, N 11.69.

Synthesis and characterization of 9

[H₃L^{Et}](PF₆)₂ (200.0 mg, 0.347 mmol), Pd(OAc)₂ (77.9 mg, 0.347 mmol, 1.0 equiv.) and NH₄OAc (26.7 mg, 0.347 mmol, 1.0 equiv.) were used. DMSO was removed from the mixture after the reaction by distillation under reduced pressure until the remaining volume was about 1.0 mL. The eluent for chromatography was a mixture of acetonitrile and dichloromethane (1:3). Yield: 112.0 mg (0.194 mmol, 56.0%).

¹H NMR (300 MHz, CD₃CN, 298 K): δ = 8.29 (d, J = 1.3 Hz, 4H, NCHN^{Imi}), 7.07 (d, J = 1.5 Hz, 4H, CCHN^{Imi}), 6.31 (s, 2H, CH^{Pyr}), 5.19 (s, 8H, bridging CH₂), 4.07 (q, J = 7.3 Hz, 8H, CH₂CH₃), 1.42 (t, J = 7.3 Hz, 12H, CH₂CH₃).

¹³C NMR (75 MHz, CD₃CN, 298 K): δ = 143.7 (s, CN^{Pyr}), 139.0 (s, PdC), 134.3 (s, NCHN^{Imi}), 124.9 (s, CCHN^{Imi}), 102.5 (s, CH^{Pyr}), 47.9 (s, bridging CH₂), 44.6 (s, CH₂CH₃), 15.8 (s, CH₂CH₃).

MS (ESI⁺) m/z 390.0 [M - (PF₆)₂]²⁺

HR MS m/z calculated [M - (PF₆)₂]²⁺ 390.0710, observed 390.0702.
(ESI⁺)

Elem. Anal. Calcd. for C₃₀H₃₈N₁₂F₁₂P₂Pd₂: C 33.69, H 3.58, N 15.72; found: C 33.55, H 3.67, N 14.91.

Synthesis and characteriaztion of 10

[H₃L^{nBu}](PF₆)₂ (300.0 mg, 0.475 mmol), Pd(OAc)₂ (106.5 mg, 0.475 mmol, 1.0 equiv.) and NH₄OAc (36.6 mg, 0.475 mmol, 1.0 equiv.) were used. The eluent for chromatography was a mixture of acetonitrile and dichloromethane (1:5). Yield: 154.0 mg (0.244 mmol, 51.3%).

¹H NMR (300 MHz, CD₃CN, 298 K): δ = 8.30 (s, 4H, NCHN^{Imi}), 7.04 (d, J = 1.5 Hz, 4H, CCHN^{Imi}), 6.30 (s, 2H, CH^{Pyr}), 5.20 (s, 8H, bridging CH₂), 4.02 (t, J = 7.1 Hz, 8H, CH₂CH₂CH₂CH₃), 1.87-1.69 (m, 8H, CH₂CH₂CH₂CH₃), 1.37-1.17 (m, 8H, CH₂CH₂CH₂CH₃), 0.91 (t, J = 7.3 Hz, 12H, CH₃).

¹³C NMR (75 MHz, CD₃CN, 298 K): δ = 143.7 (s, CN^{Pyr}), 139.1 (s, PdC), 134.7 (s, NCHN^{Imi}), 125.2 (s, CCHN^{Imi}), 102.6 (s, CH^{Pyr}), 49.2



(s, bridging CH_2), 48.0 (s, $CH_2CH_2CH_2CH_3$), 32.8 (s, $CH_2CH_2CH_2CH_3$), 20.2 (s, $CH_2CH_2CH_2CH_3$), 13.7 (s, CH_3).

MS (ESI⁺) m/z 444.7 [M - (PF₆)₂]²⁺.

HR MS (ESI⁺) m/z calculated [M - (PF₆)₂]²⁺ 446.1336, observed 446.1333.

Elem. Anal. Calcd. for C₃₈H₅₄N₁₂F₁₂P₂Pd₂: C 38.62, H 4.61, N 14.22; found: C 38.02, H 4.55, N 13.80.

Synthesis and characterization of 11

[H₃L^{Mes}](PF₆)₂ (300.0 mg, 0.397 mmol), Pd(OAc)₂ (89.1 mg, 0.397 mmol, 1.0 equiv.) and NH₄OAc (30.6 mg, 0.397 mmol, 1.0 equiv.) were used. The eluent for chromatography was a mixture of acetonitrile and dichloromethane (1:5). Yield: 127.0 mg (0.168 mmol, 42.3%).

¹H NMR (300 MHz, CD₃CN, 298 K): δ = 8.46 (d, J = 1.5 Hz, 4H, CH^{Imi}), 7.08 (d, J = 1.5 Hz, 4H, CH^{Imi}), 7.04 (s, 8H, Ph), 6.43 (s, 2H, CH^{Pyr}), 5.40 (s, 8H, bridging CH_2), 2.30 (s, 12H, $p-CH_3^{Mes}$), 2.10-1.80 (merged with solvent peaks, 24H, $o-CH_3^{Mes}$).

¹³C NMR (75 MHz, CD₃CN, 298 K): δ = 143.6 (s, CN^{Pyr}), 141.3 (s, CH_3C^{Mes}), 139.3 (s, PdC), 135.8 (s, $NCHN^{Imi}$), 132.8 (s, CH_3C^{Mes}), 130.1 (s, CH^{Mes}), 126.5 (s, $CCHN^{Imi}$), 103.1 (s, CH^{Pyr}), 48.5 (s, bridging CH_2), 21.0 (s, $p-CH_3^{Mes}$), 17.5 (s, $o-CH_3^{Mes}$).

MS (ESI⁺) m/z 569.7 [M - (PF₆)₂]²⁺.

HR MS (ESI⁺) m/z calculated [M - (PF₆)₂]²⁺ 570.1653, observed 570.1652.

Elem. Anal. Calcd. for C₅₈H₆₂N₁₂F₁₂P₂Pd₂: C 48.72, H 4.37, N 11.75; found: C 48.50, H 4.53, N 11.56.

Synthesis and characterization of 12

$[\text{H}_3\text{L}^{\text{tBu}}](\text{PF}_6)_2$ (300.0 mg, 0.475 mmol), $\text{Pd}(\text{OAc})_2$ (106.5 mg, 0.475 mmol, 1.0 equiv.) and NH_4OAc (36.6 mg, 0.475 mmol, 1.0 equiv.) were used. The eluent for chromatography was a mixture of acetonitrile and dichloromethane (1:5). Yield: 187.0 mg (0.296 mmol, 62.3%).

^1H NMR (300 MHz, CD_3CN , 298 K): δ = 8.39 (d, J = 1.6 Hz, 4H, CH^{Imi}), 7.21 (d, J = 1.6 Hz, 4H, CH^{Imi}), 6.31 (s, 2H, CH^{Pyr}), 5.21 (s, 8H, bridging CH_2), 1.57 (s, 36H, CH_3).

^{13}C NMR (75 MHz, CD_3CN , 298 K): δ = 143.7 (s, CN^{Pyr}), 139.4 (s, PdC), 133.1 (s, NCHN^{Imi}), 122.3 (s, CCHN^{Imi}), 102.4 (s, CH^{Pyr}), 59.0 (s, CMe_3), 48.1 (s, bridging CH_2), 29.7 (s, CH_3).

HR MS m/z calculated $[\text{M} - (\text{PF}_6)_2]^{2+}$ 446.1336, observed 446.1332.
(ESI⁺)

Elem. Anal. Calcd. for $\text{C}_{38}\text{H}_{54}\text{N}_{12}\text{F}_{12}\text{P}_2\text{Pd}_2$: C 38.62, H 4.61, N 14.22; found: C 38.55, H 4.55, N 14.24.

Synthesis and characterization of 13

A suspension of $[\text{L}^{\text{Et}}_2\text{Pd}_2](\text{PF}_6)_2$ (81.0 mg, 0.151 mmol), NEt_4Cl (27.6 mg, 0.167 mmol, 1.1 equiv.) and PdCl_2 (26.9 mg, 0.151 mmol, 1.0 equiv.) in CH_3CN (20.0 mL) was heated to reflux for 5 h in air. The solution gradually turned to light-orange and some bright yellow solid formed. The yellow solid was collected by filtration, washed with CH_3CN and Et_2O and dried under vacuum to give 73.8 mg of the product (0.122 mmol, 81.1%).

^1H NMR (300 MHz, $\text{DMSO}-d_6$, 298 K): δ = 8.88 (d, J = 1.7 Hz, 2H, NCHN^{Imi}), 7.02 (d, J = 1.7 Hz, 2H, CCHN^{Imi}), 6.31 (s, 1H, CH^{Pyr}), 5.26 (s, 4H, bridging CH_2), 4.09 (q, J = 7.3 Hz, 4H, CH_2CH_3), 1.34 (t, J = 7.2 Hz, 6H, CH_2CH_3).

^{13}C NMR (75 MHz, $\text{DMSO}-d_6$, 298 K): δ = 141.7 (s, CN^{Pyr}), 132.8 (s, PdC), 124.7 (s, NCHN^{Imi}), 122.9 (s, CCHN^{Imi}), 101.5 (s, CH^{Pyr}), 46.4 (s, bridging CH_2), 43.3 (s, CH_2CH_3), 15.5 (s, CH_3).

Elem. Anal. Calcd. for $\text{C}_{15}\text{H}_{19}\text{N}_6\text{Cl}_3\text{Pd}_2$: C 29.90, H 3.18, N 13.95; found: C 29.80, H 3.12, N 14.08.



Synthesis and characteriaztion of 14

A suspension of [^aL^{Mes}₂Pd₂](PF₆)₂ (40.0 mg, 0.0559 mmol), NEt₄Cl (10.2 mg, 0.0615 mmol, 1.1 equiv.) and PdCl₂ (9.9 mg, 0.0559 mmol, 1.0 equiv.) in CH₃CN (10.0 mL) was heated to reflux for 5 h in air. The solution gradually turned to light-orange and some bright yellow solid formed. The yellow solid was collected by filtration, washed with CH₃CN and Et₂O and dried under vacuum to give 24.5 mg of the product (0.0313 mmol, 55.9%).

¹H NMR (300 MHz, DMSO-d₆, 298 K): δ = 9.08 (d, *J* = 1.7 Hz, 2H, NCHN^{Imi}), 7.09 (s, 4H, CH^{Mes}), 6.88 (d, *J* = 1.5 Hz, 2H, CCHN^{Imi}), 6.44 (s, 1H, CH^{Pyr}), 5.42 (s, 4H, bridging CH₂), 2.31 (s, 6H, CH₃), 1.98 (s, 12H, CH₃).

¹³C NMR (75 MHz, DMSO-d₆, 298 K): δ = 141.6 (s, CN^{Pyr}), 139.6 (s, CH₃C^{Mes}), 134.4 (s, PdC), 134.2 (s, NCHN^{Imi}), 131.8 (s, CH₃C^{Mes}), 129.1 (s, CH^{Mes}), 123.8 (s, CCHN^{Imi}), 102.0 (s, CH^{Pyr}), 46.9 (s, bridging CH₂), 20.6 (s, *p*-CH₃^{Mes}), 16.9 (s, *o*-CH₃^{Mes}).

Elem. Anal. Calcd. for C₂₉H₃₁N₆Cl₃Pd₂: C 44.50, H 3.99, N 10.74; found: C 43.82, H 3.98, N 10.80.

Synthesis and characteriaztion of 15

A mixture of [ⁿL^{Et}₂Pd₂](PF₆)₂ (181.0 mg, 0.169 mmol, 1.0 equiv.), PdCl₂ (59.7 mg, 0.337 mmol, 2.0 equiv.) and NEt₄Cl (61.4 mg, 0.370 mmol, 2.2 equiv.) in CH₃CN (15.0 mL) was heated to reflux for overnight in air. After cooled to ambient temperature, the solvent of the suspension was removed under reduced pressure to give a yellow solid, which was suspended in DMSO (1.0 mL). The suspension was treated with CH₃CN (15.0 mL) and the mixture was stirred under room temperature for half an hour and pale-yellow solid was collected after filtration and washed with CH₃CN (5.0 mL, three times) and diethyl ether (10.0 mL) and dried under vacuum to give 113.0 mg of the product (0.186 mmol, 55.4%).

¹H NMR (300 MHz, DMSO-d₆, 298 K): δ = 7.73 (d, *J* = 1.9 Hz, 2H, CH^{Imi}), 7.62 (d, *J* = 1.9 Hz, 2H, CH^{Imi}), 6.64 (s, 1H, CH^{Pyr}), 5.70 (d, *J* = 16.5 Hz, 2H, bridging CH₂), 5.54 (d, *J* = 16.4 Hz, 2H, bridging CH₂), 3.90-3.70 (m, 2H, CH₂CH₃), 3.70-3.50 (m, 2H, CH₂CH₃), 1.10 (t, *J* = 7.2 Hz, 6H, CH₃).

^{13}C NMR (75 MHz, DMSO- d^6 , 298 K): δ = 153.1 (s, PdC), 145.8 (s, CN^{Pyr}), 122.8 (s, CH^{Imi}), 122.4 (s, CH^{Imi}), 102.9 (s, CH^{Pyr}), 47.0 (s, bridging CH_2), 45.4 (s, CH_2CH_3), 15.3 (s, CH_3).

Elem. Anal. Calcd. for $\text{C}_{15}\text{H}_{19}\text{N}_6\text{Cl}_3\text{Pd}_2$: C 29.90, H 3.18, N 13.95; found: C 30.00, H 3.30, N 13.90.



Synthesis and characterization of 16

A mixture of ligand precursor **HL**⁴ (42.0 mg, 0.157 mmol, 1.00 equiv.) and RuHCl(CO)(PPh₃)₃ (300.0 mg, 0.313 mmol, 2.00 equiv.) in degassed chlorobenzene (3.0 mL) was heated at 120 °C for 8 hours. A portion of 3.0 mL of degassed toluene was added and the mixture was kept at the same temperature for another 2 hours. The following part could be carried out in aerobic atmosphere. The yellow precipitate was collected from the dark-brown solution by filtration, washed with toluene and dried under reduced pressure. The raw material was dissolved in 5.0 mL of dichloromethane and toluene was added gradually until the sediment of a yellow solid. The mixture was stirred vigorously until the precipitation was complete. The solid was collected through filtration, washed with toluene and hexane, and dried under vacuum to give 120.0 mg product (0.0867 mmol, 55.3 %). Bright yellow crystalline material can be obtained by slow diffusion of diethyl ether to a solution of the raw material in dichloromethane. The product is soluble in dichloromethane, acetone and DMSO, slightly soluble in acetonitrile and insoluble in non-polar solvent, such as toluene and hexane. The product is stable in aerobic and humid conditions.

¹H NMR (300 MHz, CD₂Cl₂, 298 K): δ = 7.80-6.80 (m, 46H, Ph and CH^{Pyri}), 5.99 (s, 1H, CH^{Pyra}), 5.53 (s, 1H, CH^{Pyra}), 2.91 (s, 3H, CH₃), 2.29 (s, 3H, CH₃), 2.15 (s, 3H, CH₃), 1.15 (s, 3H, CH₃), -11.42 (dd, J_1 = 13.2 Hz, J_2 = 11.7 Hz, 1H, RuH).

¹³C NMR (75 MHz, CD₂Cl₂, 298 K): δ = 206.4 (d, J = 18.5 Hz, CO), 204.4 (t, J = 15.4 Hz, CO), 187.0 (d, J = 10.2 Hz, RuC), 163.1 (s, NC^{Pyri}), 156.6 (s, CCH₃), 153.4 (s, CCH₃), 146.5 (s, NC^{Pyri}), 143.1 (s, CCH₃), 141.9 (s, CCH₃), 136.0-127.0 (m, Ph and CH^{Pyri}), 113.1 (s, CH^{Pyra}), 113.0 (s, CH^{Pyra}), 15.8 (s, CH₃), 15.7 (s, CH₃), 15.0 (s, CH₃), 14.4 (s, CH₃).

³¹P NMR (121 MHz, CD₂Cl₂, 298 K): δ = 51.8 (s), 46.1 (d, J = 273.1 Hz), 41.4 (d, J = 272.9 Hz)

HR MS m/z calculated [M - Cl]⁺ 1349.1865, observed 1349.1852.
(ESI⁺)

Elem. Anal. Calcd. for: C 60.74, H 4.44, N 6.07; found: C 61.23, H 4.51, N 5.52.

IR (KBr, cm⁻¹): 1943 (ν_{CO}), 1938 (ν_{CO})

Synthesis and characterization of 17

A solution of the ligand precursor (81.2 mg, 0.303 mmol, 1.1 equiv.) and $\text{RuCpCl(PPh}_3)_2$ (200.0 mg, 0.275 mmol, 1.0 equiv.) in degassed DMSO (8.0 mL) was heated at 120 °C for 2 hours. The reaction temperature was reduced to 95 °C and the solution was stirred at this temperature for another 18 hours. After cooled to ambient temperature, the red solution was mixed with 50.0 mL of DCM. The combined organic layer was washed with saturated brine (40 mL) for 3 times and dried over MgSO_4 . The solution was reduced to 3~5 mL at reduced pressure and treated with 15.0 mL of toluene. The mixture was vigorously stirred until a complete precipitation of red solid, which was filtered, washed with toluene (10.0 mL) and hexane (10.0 mL), dried under vacuum to give the final product as a bright-red powder in the yield of 127.0 mg (0.172 mmol, 56.8 %). Dark red crystalline materials were easily obtained by slow diffusion of diethyl ether into a solution of the crude product in dichloromethane. The product is soluble in dichloromethane, acetone, acetonitrile and DMSO and insoluble in non-polar solvent, such as toluene or hexane. The product is stable in aerobic and humid conditions.

$^1\text{H NMR}$ (300 MHz, CD_2Cl_2 , 298 K): δ = 8.18 (dd, J_1 = 9.8 Hz, J_2 = 0.9 Hz, 1H, CH^{Pyri}), 8.03 (d, J = 9.8 Hz, 1H, CH^{Pyri}), 7.45-7.05 (m, 15H, CH^{Ph}), 6.29 (s, 1H, CH^{Pyra}), 6.20 (s, 1H, CH^{Pyra}), 4.77 (s, 5H, CH^{Cp}), 2.87 (d, J = 0.7 Hz, 3H, CH_3), 2.69 (s, 3H, CH_3), 2.33 (d, J = 0.9 Hz, 3H, CH_3), 2.29 (s, 3H, CH_3).

$^{13}\text{C NMR}$ (75 MHz, CD_2Cl_2 , 298 K): δ = 156.5 (s, $\text{CH}_3\text{C}^{\text{Pyra}}$), 154.5 (s, C^{Pyri}), 152.9 (s, $\text{CH}_3\text{C}^{\text{Pyra}}$), 150.1 (s, C^{Pyri}), 144.3 (s, $\text{CH}_3\text{C}^{\text{Pyra}}$), 142.0 (s, $\text{CH}_3\text{C}^{\text{Pyra}}$), 133.5 (d, J = 42.0 Hz, C^{Ph}), 133.4 (d, J = 11.3 Hz, CH^{Ph}), 131.0 (d, J = 2.2 Hz, CH^{Ph}), 128.8 (d, J = 9.6 Hz, CH^{Ph}), 122.0 (s, CH^{Pyri}), 120.3 (s, CH^{Pyri}), 113.5 (s, CH^{Pyra}), 111.8 (s, CH^{Pyra}), 78.7 (d, J = 2.0 Hz, CH^{Cp}), 16.5 (s, CH_3), 15.6 (s, CH_3), 15.5 (s, CH_3), 14.0 (s, CH_3).

$^{31}\text{P NMR}$ (121 MHz, CD_2Cl_2 , 298 K): δ = 46.6

HR MS m/z calculated $[\text{M} - \text{Cl}]^+$ 697.1791, observed 697.1788.
(ESI^+)



Synthesis and characterization of 18

A mixture of complex **17** (50.0 mg, 0.067 mmol, 1.0 equiv.) and $\text{RuHCl(CO)(PPh}_3)_3$ (71.0 mg, 0.075 mmol, 1.10 equiv.) in degassed PhCl (2.0 mL) was stirred at 120 °C for 8 hours. 5.0 mL of degassed toluene was added to the suspension and the mixture was refluxed for one hour. The precipitate was filtered, washed with toluene (3.0 mL) and hexane (5.0 mL) and dried under reduced pressure to give a bright yellow powder in the yield of 22.0 mg (0.019 mmol, 28.4 %). Bright yellow tiny crystalline materials were obtained by slow diffusion of diethyl ether into a solution of the crude product in acetonitrile. The product is soluble in dichloromethane and DMSO, slightly soluble in acetone and acetonitrile and insoluble in non-polar solvent. The product is stable in aerobic and humid conditions.

^1H NMR (300 MHz, CD_2Cl_2 , 298 K): δ = 7.50-7.05 (m, 30H, CH^{Ph}), 7.02 (s, 1H, CH^{Pyri}), 6.00 (s, 2H, CH^{Pyra}), 4.70 (s, 5H, CH^{Cp}), 2.86 (s, 3H, CH_3), 2.50 (s, 3H, CH_3), 2.29 (s, 3H, CH_3), 2.21 (s, 3H, CH_3).

^{13}C NMR (75 MHz, CD_2Cl_2 , 298 K): δ = 206.2 (d, J = 17.8 Hz, CO), 185.6 (d, J = 10.8 Hz, RuC), 161.5 (s, NC^{Pyri}), 156.4 (s, CCH_3), 154.3 (d, J = 2.6 Hz, CCH_3), 145.6 (s, NC^{Pyri}), 142.3 (d, J = 1.6 Hz, CCH_3), 141.8 (s, CCH_3), 134.5-127.7 (m, *Ph*), 127.3 (s, CH^{Pyri}), 112.6 (s, CH^{Pyra}), 112.1 (s, CH^{Pyra}), 77.1 (d, J = 2.3 Hz, CH^{Cp}), 16.4 (s, CH_3), 15.3 (s, CH_3), 15.2 (s, CH_3), 14.5 (s, CH_3).

^{31}P NMR (121 MHz, CD_2Cl_2 , 298 K): δ = 48.6 (s), 48.5 (s).

HR MS m/z calculated $[\text{M} - \text{Cl}]^+$ 1123.1301, observed 1123.1312.
(ESI^+)

Elem. Anal. Calcd. for: C 58.08, H 4.35, N 7.26; found: C 58.12, H 4.21, N 7.19.

IR (KBr, cm^{-1}): 1937 (ν_{CO}).





References

- [1] Schuster, O.; Yang, L.; Raubenheimer, H. G.; Albrecht, M., *Chem. Rev.* **2009**, *109*, 3445-3478.
- [2] (a) Díez-González, S.; Marion, N.; Nolan, S. P., *Chem. Rev.* **2009**, *109*, 3612-3676; (b) Herrmann, W. A., *Angew. Chem. Int. Ed.* **2002**, *41*, 1290-1309.
- [3] Enders, D.; Niemeier, O.; Henseler, A., *Chem. Rev.* **2007**, *107*, 5606-5655.
- [4] Wanzlick, H.-W.; Schönherr, H.-J., *Angew. Chem. Int. Ed. Engl.* **1968**, *7*, 141-142.
- [5] Anthony J. Arduengo, I.; Harlow, R. L.; Kline, M., *J. Am. Chem. Soc.* **1991**, *113*, 361-363.
- [6] Herrmann, W. A.; Elison, M.; Fischer, J.; Köcher, C.; Artus, G. R. J., *Angew. Chem. Int. Ed. Engl.* **1995**, *34*, 2371-2374.
- [7] Dyker, C. A.; Lavallo, V.; Donnadieu, B.; Bertrand, G., *Angew. Chem. Int. Ed.* **2008**, *47*, 3206-3209.
- [8] Gründemann, S.; Kovacevic, A.; Albrecht, M.; Faller, J. W.; Crabtree, R. H., *Chem. Commun.* **2001**, 2274-2275.
- [9] Aldeco-Perez, E.; Rosenthal, A. J.; Donnadieu, B.; Parameswaran, P.; Frenking, G.; Bertrand, G., *Science* **2009**, *326*, 556-559.
- [10] Day, B. M.; Pugh, T.; Hendriks, D. I.; Guerra, C. I. F.; Evans, D. J.; Bickelhaupt, F. M.; Layfield, R. A., *J. Am. Chem. Soc.* **2013**, *135*, 13338-13341.
- [11] Garrison, J. C.; Youngs, W. J., *Chem. Rev.* **2005**, *105*, 3978-4008.
- [12] Kantchev, E. A. B.; O'Brien, C. J.; Organ, M. G., *Angew. Chem. Int. Ed.* **2007**, *46*, 2768.
- [13] Samojłowicz, C.; Bieniek, M.; Grela, K., *Chem. Rev.* **2009**, *109*, 3708-3742.
- [14] (a) Nolan, S. P., *Acc. Chem. Res.* **2011**, *44*, 91-100; (b) Gaillard, S.; Cazin, C. S. J.; Nolan, S. P., *Acc. Chem. Res.* **2012**, *45*, 778-787.
- [15] (a) Herrmann, W. A.; Kocher, C., *Angew. Chem. Int. Ed. Engl.* **1997**, *36*, 2162-2187; (b) Hahn, F. E.; Jahnke, M. C., *Angew. Chem. Int. Ed.* **2008**, *47*, 3122-3172; (c) Marion, N.; Nolan, S. P., *Acc. Chem. Res.* **2008**, *41*, 1440-1449; (d) Würtz, S.; Glorius, F., *Acc. Chem. Res.* **2008**, *41*, 1523-1533.
- [16] Niehues, M.; Erker, G.; Kehr, G.; Schwab, P.; Fröhlich, R., *Organometallics* **2002**, *21*, 2905-2911.
- [17] Jacobsen, H.; Correa, A.; Costabile, C.; Cavallo, L., *J. Organomet. Chem.* **2006**, *691*, 4350-4358.
- [18] Kelly, R. A.; Clavier, H.; Giudice, S.; Scott, N. M.; Stevens, E. D.; Bordner, J.; Samardjiev, I.; Hoff, C. D.; Cavallo, L.; Nolan, S. P., *Organometallics* **2008**, *27*, 202-210.
- [19] Benhamou, L.; Chardon, E.; Lavigne, G.; Bellemin-Laponnaz, S.; Cesar, V., *Chem. Rev.* **2011**, *111*, 2705-2733.
- [20] Díez-González, S.; Marion, N.; Nolan, S. P., *Chem. Rev.* **2009**, *109*, 3612-3676.
- [21] Appelhans, L. N.; Zuccaccia, D.; Kovacevic, A.; Chianese, A. R.; Miecznikowski, J. R.; Macchioni, A.; Clot, E.; Eisenstein, O.; Crabtree, R. H., *J. Am. Chem. Soc.* **2005**, *127*, 16299-16311.
- [22] (a) Eguillor, B.; Esteruelas, M. A.; Oliván, M.; Puerta, M., *Organometallics* **2008**, *27*, 445-450; (b) Kong, Y.; Wen, L.; Song, H.; Xu, S.; Yang, M.; Liu, B.; Wang, B., *Organometallics* **2011**, *30*, 153-159.
- [23] Chianese, A. R.; Kovacevic, A.; Zeglis, B. M.; Faller, J. W.; Crabtree, R. H., *Organometallics* **2004**, *23*, 2461-2468.
- [24] Tonner, R.; Heydenrych, G.; Frenking, G., *Chem. Asian J.* **2007**, *2*, 1555-1567.
- [25] Tan, K. V.; Dutton, J. L.; Skelton, B. W.; Wilson, D. J. D.; Barnard, P. J., *Organometallics* **2013**, *32*, 1913-1923.



- [26] (a) Heckenroth, M.; Neels, A.; Garnier, M. G.; Aebi, P.; Ehlers, A. W.; Albrecht, M., *Chem. Eur. J.* **2009**, *15*, 9375-9386; (b) Sau, S. C.; Roy, S. R.; Sen, T. K.; Mullangi, D.; Mandala, S. K., *Adv. Synth. Catal.* **2013**, *355*, 2982-2991.
- [27] Bacciu, D.; Cavell, K. J.; Fallis, I. A.; Ooi, L.-I., *Angew. Chem. Int. Ed.* **2005**, *44*, 5282-5284.
- [28] (a) Krüger, A.; Kluser, E.; Müller-Bunz, H.; Neels, A.; Albrecht, M., *Eur. J. Inorg. Chem.* **2012**, 1394-1402; (b) Kluser, E.; Neels, A.; Albrecht, M., *Chem. Commun.* **2006**, 4495-4497.
- [29] Arnold, P. L.; Liddle, S. T., *Organometallics* **2006**, *25*, 1485-1491.
- [30] Enders, P. D. D.; Breuer, D.-C. K.; Raabe, D. G.; Runsink, D. J.; Teles, D. J. H.; Melder, D. J.-P.; Ebel, D. K.; Brode, D. S., *Angew. Chem. Int. Ed. Engl.* **1995**, *34*, 1021-1023.
- [31] Herrmann, W. A.; Gerstberger, G.; Spiegler, M., *Organometallics* **1997**, *16*, 2209-2212.
- [32] Chaumonnot, A.; Donnadiou, B.; Sabo-Etienne, S.; Chaudret, B.; Buron, C.; Bertrand, G.; Metivier, P., *Organometallics* **2001**, *20*, 5614-5618.
- [33] Zanardi, A.; Mata, J. A.; Peris, E., *J. Am. Chem. Soc.* **2009**, *131*, 14531-14537.
- [34] Guerret, O.; Sole, S.; Gornitzka, H.; Teichert, M.; Trinquier, G.; Bertrand, G., *J. Am. Chem. Soc.* **1997**, *119*, 6668-6669.
- [35] Mas-Marz, E.; Peris, J. A. M. E., *Angew. Chem. Int. Ed.* **2007**, *46*, 3729-3731.
- [36] Viciano, M.; Sanau, M.; Peris, E., *Organometallics* **2007**, *26*, 6050-6054.
- [37] Zanardi, A.; Corberan, R.; Mata, J. A.; Peris, E., *Organometallics* **2008**, *27*, 3570-3576.
- [38] Zanardi, A.; Mata, J. A.; Peris, E., *Chem. Eur. J.* **2010**, *16*, 10502-10506.
- [39] Zanardi, A.; Mata, J. A.; Peris, E., *Organometallics* **2009**, *28*, 4335-4339.
- [40] Zanardi, A.; Mata, J. A.; Peris, E., *Organometallics* **2009**, *28*, 1480-1483.
- [41] Guo, S.; Huynh, H. V., *Organometallics* **2012**, *31*, 4565-4573.
- [42] Zanardi, A.; Mata, J. A.; Peris, E., *Chem. Eur. J.* **2010**, *16*, 13109-13115.
- [43] Sabater, S.; Mata, J. A.; Peris, E., *Chem. Eur. J.* **2012**, *18*, 6380-6385.
- [44] Rostovtsev, V. V.; Green, L. G.; Fokin, V. V.; Sharpless, K. B., *Angew. Chem. Int. Ed.* **2002**, *41*, 2596-2599.
- [45] Mathew, P.; Neels, A.; Albrecht, M., *J. Am. Chem. Soc.* **2008**, *130*, 13534-13535.
- [46] (a) Poulain, A.; Canseco-Gonzalez, D.; Hynes-Roche, R.; Mueller-Bunz, H.; Schuster, O.; Stoeckli-Evans, H.; Neels, A.; Albrecht, M., *Organometallics* **2011**, *30*, 1021-1029; (b) Saravanakumar, R.; Ramkumar, V.; Sankararaman, S., *Organometallics* **2011**, *30*, 1689-1694; (c) Huang, J.; Hong, J.-T.; Hong, S. H., *Eur. J. Org. Chem.* **2012**, 6630-6635.
- [47] (a) Keitz, B. K.; Bouffard, J.; Bertrand, G.; Grubbs, R. H., *J. Am. Chem. Soc.* **2011**, *133*, 8498-8501; (b) Prades, A.; Peris, E.; Albrecht, M., *Organometallics* **2011**, *30*, 1162-1167; (c) Bouffard, J.; Keitz, B. K.; Tonner, R.; Guisado-Barrios, G.; Frenking, G.; Grubbs, R. H.; Bertrand, G., *Organometallics* **2011**, *30*, 2617-2627; (d) Cai, J.; Yang, X.; Arumugam, K.; Bielawski, C. W.; Sessler, J. L., *Organometallics* **2011**, *30*, 5033-5037; (e) Ogata, K.; Inomata, S.; Fukuzawa, S.-i., *Dalton Trans.* **2013**, *42*, 2362-2365; (f) Hohloch, S.; Suntrup, L.; Sarkar, B., *Organometallics* **2013**, *32*, 7376-7385; (g) Kilpin, K. J.; Crot, S.; Riedel, T.; Kitchenb, J. A.; Dyson, P. J., *Dalton Trans.* **2014**, *43*, 1443-1448.
- [48] Inomata, H.; Ogata, K.; Fukuzawa, S.-i.; Hou, Z., *Org. Lett.* **2012**, *14*, 3986-3989.
- [49] Kilpin, K. J.; Paul, U. S. D.; Lee, A.-L.; Crowley, J. D., *Chem. Commun.* **2011**, *47*, 328-330.
- [50] (a) Lalrempuia, R.; McDaniel, N. D.; Müller-Bunz, H.; Bernhard, S.; Albrecht, M., *Angew. Chem. Int. Ed.* **2010**, *49*, 9765-9768; (b) Schuster, E. M.; Botoshansky, M.; Gandelman, M., *Dalton Trans.* **2011**, *40*, 8764-8767; (c) Guisado-Barrios, G.; Bouffard, J.; Donnadiou, B.; Bertrand, G., *Organometallics* **2011**, *30*, 6017-6021; (d) Alvarez, C. M.; García-Escudero, L. A.; García-Rodríguez, R.; Miguel, D., *Chem. Commun.* **2012**, *48*, 7209-7211.

- [51] Guisado-Barrios, G.; Bouffard, J.; Donnadiou, B.; Bertrand, G., *Angew. Chem. Int. Ed.* **2010**, *49*, 4759-4762.
- [52] Schaper, L.-A.; Öfele, K.; Kadyrov, R.; Bechlars, B.; Drees, M.; Cokoja, M.; Herrmann, W. A.; Kühn, F. E., *Chem. Commun.* **2012**, *48*, 3857-3859.
- [53] Prades, A.; Viciano, M.; Sanaú, M.; Peris, E., *Organometallics* **2008**, *27*, 4254-4259.
- [54] (a) Sivaram, H.; Jothibasu, R.; Huynh, H. V., *Organometallics* **2012**, *31*, 1195-1203; (b) Zhou, Y.; Liu, Q.; Lv, W.; Pang, Q.; Ben, R.; Qian, Y.; Zhao, J., *Organometallics* **2013**, *32*, 3753-3759.
- [55] Tukov, A. A.; Normand, A. T.; Nechaev, M. S., *Dalton Trans.* **2009**, 7015-7028.
- [56] Han, Y.; Huynh, H. V., *Chem. Commun.* **2007**, 1089-1091.
- [57] Han, Y.; Huynh, H. V.; Tan, G. K., *Organometallics* **2007**, *26*, 6581-6585.
- [58] Han, Y.; Lee, L. J.; Huynh, H. V., *Chem. Eur. J.* **2010**, *16*, 771-773.
- [59] (a) Crociani, B.; Bianca, F. D.; Giovenco, A., *J. Organomet. Chem.* **1983**, *251*, 393-411; (b) Meyer, W. H.; Deetlefs, M.; Pohlmann, M.; Scholz, R.; Esterhuysen, M. W.; Julius, G. R.; Raubenheimer, H. G., *Dalton Trans.* **2004**, 413-420; (c) Albrecht, M.; Stoeckli-Evans, H., *Chem. Commun.* **2005**, 4705-4707; (d) Strong, E. T. J.; Price, J. T.; Jones, N. D., *Dalton Trans.* **2009**, 9123-9125; (e) Yoshidomi, T.; Segawa, Y.; Itami, K., *Chem. Commun.* **2013**, *49*, 5648-5650.
- [60] Owen, J. S.; Labinger, J. A.; Bercaw, J. E., *J. Am. Chem. Soc.* **2004**, *126*, 8247-8255.
- [61] (a) Cabeza, J. A.; Río, I. d.; Pérez-Carreño, E.; Sánchez-Vega, M. G.; Vázquez-García, D., *Angew. Chem. Int. Ed.* **2009**, *48*, 555-558; (b) Cabeza, J. A.; Río, I. d.; Pérez-Carreño, E.; Sánchez-Vega, M. G.; Vázquez-García, D., *Organometallics* **2010**, *29*, 4464-4471; (c) Cabeza, J. A.; Río, I. d.; Pérez-Carreño, E.; Pruneda, V., *Organometallics* **2011**, *30*, 1148-1156; (d) Esteruelas, M. A.; Fernández-Alvarez, F. J.; Oñate, E., *J. Am. Chem. Soc.* **2006**, *128*, 13044-13045.
- [62] Buil, M. L.; Esteruelas, M. A.; Garcés, K.; Oliván, M.; Oñate, E., *J. Am. Chem. Soc.* **2007**, *129*, 10998-10999.
- [63] (a) Alvarez, E.; Conejero, S.; Paneque, M.; Petronilho, A.; Poveda, M. L.; Serrano, O.; Carmona, E., *J. Am. Chem. Soc.* **2008**, *128*, 13060-13061; (b) Álvarez, E.; Conejero, S.; Lara, P.; López, J. A.; Paneque, M.; Petronilho, A.; Poveda, M. L.; Río, D. d.; Serrano, O.; Carmona, E., *J. Am. Chem. Soc.* **2007**, *129*, 14130-14131; (c) Conejero, S.; Lara, P.; Paneque, M.; Petronilho, A.; Poveda, M. L.; Serrano, O.; Vattier, F.; Alvarez, E.; Maya, C.; Salazar, V. n.; Carmona, E., *Angew. Chem. Int. Ed.* **2008**, *47*, 4380-4383.
- [64] (a) Raubenheimer, H. G.; Cronje, S., *Dalton Trans.* **2008**, 1265-1272; (b) Cabeza, J. A.; García-Álvarez, P., *Chem. Soc. Rev.* **2011**, *40*, 5389-5405.
- [65] Roselló-Merino, M.; Díezb, J.; Conejero, S., *Chem. Commun.* **2010**, *46*, 9247-9249.
- [66] (a) Cabeza, J. A.; García-Álvarez, P.; Pérez-Carreño, E.; Pruneda, V., *Chem. Eur. J.* **2013**, *19*, 3426-3436; (b) Hildebrandt, B.; Reiß, G.; Ganter, C., *J. Organomet. Chem.* **2010**, *695*, 474-477; (c) Magriz, A.; Gómez-Bujedo, S.; Álvarez, E.; Fernández, R.; Lassaletta, J. M., *Organometallics* **2010**, *29*, 5941-5945.
- [67] Huynh, H. V.; Frison, G., *J. Org. Chem.* **2013**, *78*, 328-338.
- [68] Raubenheimer, H. G.; Lindeque, L.; Cronje, S., *J. Organomet. Chem.* **1996**, *511*, 177-184.
- [69] Miranda-Soto, V.; Grotjahn, D. B.; Cooksy, A. L.; Golen, J. A.; Moore, C. E.; Rheingold, A. L., *Angew. Chem. Int. Ed.* **2011**, *50*, 631-635.
- [70] Brill, M.; Diaz, J.; Huertos, M. A.; Lopez, R.; Perez, J.; Riera, L., *Chem. Eur. J.* **2011**, *17*, 8584-8595.
- [71] Kösterke, T.; Kösters, J.; Würthwein, E.-U.; Mück-Lichtenfeld, C.; Brinke, C. S. t.; Lahoz, F.; Hahn, F. E., *Chem. Eur. J.* **2012**, *18*, 14594-14598.
- [72] Huertos, M. A.; Perez, J.; Riera, L.; Diaz, J.; Lopez, R., *Chem. Eur. J.* **2010**, *16*, 8495-8507.



- [73] Bonati, F.; Burini, A.; Pietroni, B. R., *J. Organomet. Chem.* **1989**, 375, 147-160.
- [74] Bonati, F.; Oro, L. A.; Pinillos, M. T.; Tejel, C., *J. Organomet. Chem.* **1994**, 465, 267-274.
- [75] Xiang, L.; Xiao, J.; Deng, L., *Organometallics* **2011**, 30, 2018-2025.
- [76] Ye, J.; Zhang, X.; Chen, W.; Shimada, S., *Organometallics* **2008**, 27, 4166-4172.
- [77] (a) Ruiz, J.; Perandones, B. F., *J. Am. Chem. Soc.* **2007**, 129, 9298-9299; (b) Ruiz, J.; Berros, Á.; Perandones, B. F.; Vivanco, M., *Dalton Trans.* **2009**, 6999-7007.
- [78] Johnson, R. P., *Chem. Rev.* **1989**, 89, 1111-1124.
- [79] Tonner, R.; Frenking, G., *Angew. Chem. Int. Ed.* **2007**, 46, 8695-8698.
- [80] Lavallo, V.; Dyker, C. A.; Donnadiou, B.; Bertrand, G., *Angew. Chem. Int. Ed.* **2008**, 47, 5411-5414.
- [81] Gavrilova, A. L.; Bosnich, B., *Chem. Rev.* **2004**, 104, 349-384.
- [82] Schneider, B.; Demeshko, S.; Dechert, S.; Meyer, F., *Angew. Chem. Int. Ed.* **2010**, 49, 9274-9277.
- [83] Neudeck, S.; Maji, S.; López, I.; Meyer, S.; Meyer, F.; Llobet, A., *J. Am. Chem. Soc.* **2014**, 136, 24-27.
- [84] Frensch, L. K.; Pröpper, K.; John, M.; Demeshko, S.; Brückner, C.; Meyer, F., *Angew. Chem. Int. Ed.* **2011**, 50, 1420-1424.
- [85] Zhou, Y.; Chen, W., *Organometallics* **2007**, 26, 2742-2746.
- [86] Georgiou, M.; Wöckel, S.; Konstanzer, V.; Dechert, S.; John, M.; Meyer, F., *Z. Naturforsch.* **2009**, 64b, 1542-1552.
- [87] Scheele, U. J.; John, M.; Dechert, S.; Meyer, F., *Eur. J. Inorg. Chem.* **2008**, 373-377.
- [88] Jeon, S.-J.; Waymouth, R. M., *Dalton Trans.* **2008**, 437-439.
- [89] Reindl, S. A.; Pöthig, A.; Drees, M.; Bechlars, B.; Herdtweck, E.; Herrmann, W. A.; Kühn, F. E., *Organometallics* **2013**, 32, 4082-4091.
- [90] Dyker, C. A.; Bertrand, G., *Nature Chem.* **2009**, 1, 265-266.
- [91] Scheele, U. J.; John, M.; Dechert, S.; Meyer, F., *Eur. J. Inorg. Chem.* **2008**, 373-377.
- [92] Guo, T.; Dechert, S.; Meyer, S.; Meyer, F., *Organometallics* **2012**, 31, 8537-8543.
- [93] Carlsson, A.-C. C.; Gräfenstein, J.; Budnjo, A.; Laurila, J. L.; Bergquist, J.; Karim, A.; Kleinmaier, R.; Brath, U.; Erdélyi, M., *J. Am. Chem. Soc.* **2012**, 134, 5706-5715.
- [94] Stander-Grobler, E.; Schuster, O.; Heydenrych, G.; Cronje, S.; Tosh, E.; Albrecht, M.; Frenking, G.; Raubenheimer, H. G., *Organometallics* **2010**, 29, 5821-5833.
- [95] Coe, B. J.; Glenwright, S. J., *Coord. Chem. Rev.* **2000**, 203, 5-80.
- [96] Sachse, A.; John, M.; Meyer, F., *Angew. Chem.* **2010**, 122, 2030-2033.
- [97] Houghton, J.; Dyson, G.; Douthwaite, R. E.; Whitwood, A. C.; Kariukib, B. M., *Dalton Trans.* **2007**, 3065-3073.
- [98] Tapu, D.; Dixon, D. A.; Roe, C., *Chem. Rev.* **2009**, 109, 3385-3407.
- [99] Lebel, H.; Janes, M. K.; Charette, A. B.; Nolan, S. P., *J. Am. Chem. Soc.* **2004**, 126, 5046-5047.
- [100] Miranda-Soto, V.; Grotjahn, D. B.; DiPasquale, A. G.; Rheingold, A. L., *J. Am. Chem. Soc.* **2008**, 130, 13200-13201.
- [101] (a) Xu, Y.; Åkermark, T.; Gyollai, V.; Zou, D.; Eriksson, L.; Duan, L.; Zhang, R.; Åkermark, B.; Sun, L., *Inorg. Chem.* **2009**, 48, 2717-2719; (b) Xu, Y.; Duan, L.; Tong, L.; Åkermark, B.; Sun, L., *Chem. Commun.* **2010**, 46, 6506-6508.
- [102] Ghumaan, S.; Sarkar, B.; Patra, S.; Parimal, K.; Slagereen, J. v.; Fiedler, J.; Kaim, W.; Lahiri, G. K., *Dalton Trans.* **2005**, 706-712.
- [103] (a) Buil, M. a. L.; Esteruelas, M. A.; Goni, E.; Oliva'n, M.; On~ate, E., *Organometallics* **2006**, 25, 3076-3083; (b) Clark, A. M.; Rickard, C. E. F.; Roper, W. R.; Wright, L. J., *Organometallics* **1999**, 18, 2813-2820.
- [104] Esteruelas, M. A.; Fernández-Alvarez, F. J.; Oñate, E., *Organometallics* **2007**, 26, 5239-5245.



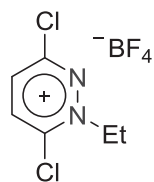
- [105] (a) Poli, R., *Chem. Rev.* **1991**, *91*, 509-551; (b) Halterman, R. L., *Chem. Rev.* **1992**, *92*, 965-994; (c) Wilkinson, G., *J. Organomet. Chem.* **1975**, *100*, 273-278; (d) Jutzi, P., *Chem. Rev.* **1999**, *99*, 969-990.
- [106] Briggs, P. M.; Victor G. Young, J.; Wigley, D. E., *Chem. Commun.* **1997**, 791-792.
- [107] Fürstner, A.; Guth, O.; Döffels, A.; Seidel, G.; Liebl, M.; Gabor, B.; Mynott, R., *Chem. Eur. J.* **2001**, *7*, 4811-4820.
- [108] Chen, J.; Shi, C.; Sung, H. H. Y.; Williams, I. D.; Lin, Z.; Jia, G., *Angew. Chem. Int. Ed.* **2011**, *50*, 7295-7299.
- [109] Alcarazo, M.; Radkowski, K.; Goddard, R.; Fürstner, A., *Chem. Commun.* **2011**, *47*, 776-778.
- [110] Alcarazo, M.; Lehmann, C. W.; Anoop, A.; Thiel, W.; Fürstner, A., *Nature Chem.* **2009**, *1*, 295-301.
- [111] Tonner, R.; Frenking, G., *Angew. Chem. Int. Ed.* **2007**, *46*, 8695-8698.
- [112] Fürstner, A.; Alcarazo, M.; Goddard, R.; Lehmann, C. W., *Angew. Chem. Int. Ed.* **2008**, *47*, 3210-3214.
- [113] Novikov, A. V.; Kennedy, A. R.; Rainier, J. D., *J. Org. Chem.* **2003**, *68*, 993-996.
- [114] Albers, A.; Demeshko, S.; Dechert, S.; Bill, E.; Bothe, E.; Meyer, F., *Angew. Chem. Int. Ed.* **2011**, *50*, 9191-9194.
- [115] Kunz, D.; Johnsen, E. Ø.; Monsler, B.; Rominger, F., *Chem. Eur. J.* **2008**, *14*, 10909-10914.
- [116] Gottlieb, H. E.; Kotlyar, V.; Nudelman, A., *J. Org. Chem.* **1997**, *62*, 7512-7515.
- [117] Blake, A. J.; Hubberstey, P.; Li, W.-S.; Russell, C. E.; Smith, B. J.; Wraith, L. D., *J. Chem. Soc., Dalton Trans.* **1998**, 647-656.
- [118] Neese, F., 2004.
- [119] Schäfer, A.; Horn, H.; Ahlrichs, R., *J. Chem. Phys.* **1992**, *97*, 2571-2577.
- [120] Sheldrick, G. M., *Acta Crystallogr.* **2008**, *A64*, 112-122.
- [121] (a) Pevet, I.; Brulé, C.; Tizot, A.; Gohier, A.; Cruzalegui, F.; Boutin, J. A.; Goldstein, S., *Bioorg. Med. Chem.* **2011**, *19* 2517-2528; (b) Mao, Y.; Mathey, F., *Org. Lett.* **2012**, *14*, 1162-1163.



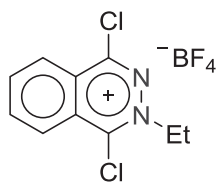
Appendix

Ligands Precursors and Compounds 19/20

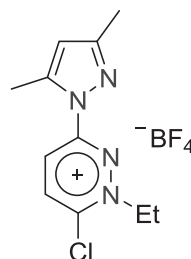
Chapter 2



[L¹Cl]BF₄

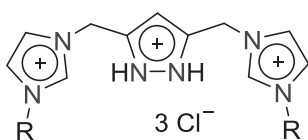


[L²Cl]BF₄

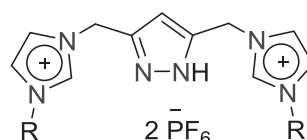


[L³Cl]BF₄

Chapter 3



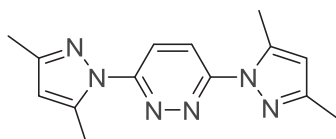
[H₄L^R]Cl₃



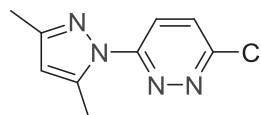
[H₃L^R](PF₆)₂

R = Et, ⁿBu, Mes or ^tBu

Chapter 4

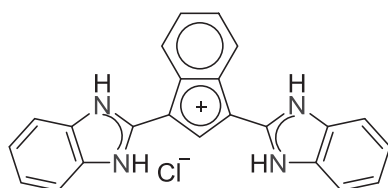


HL⁴

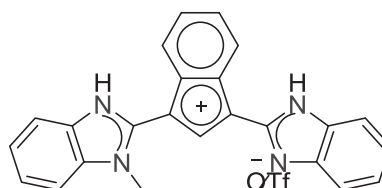


HL⁵

Chapter 5

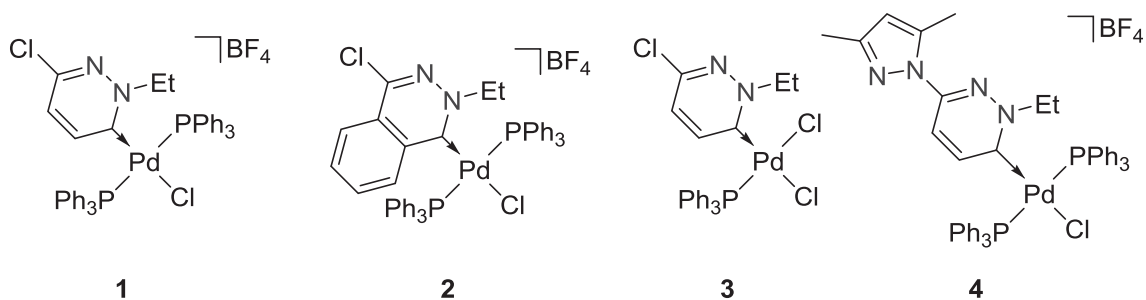


19

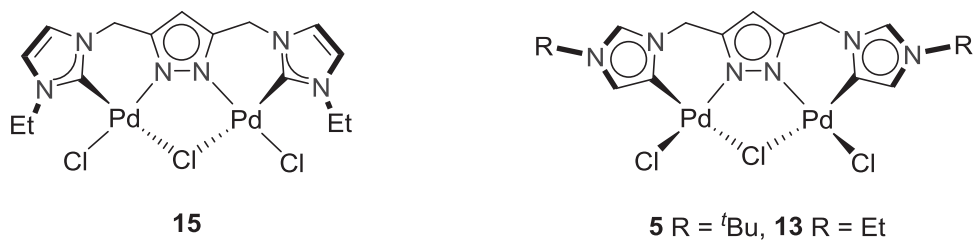
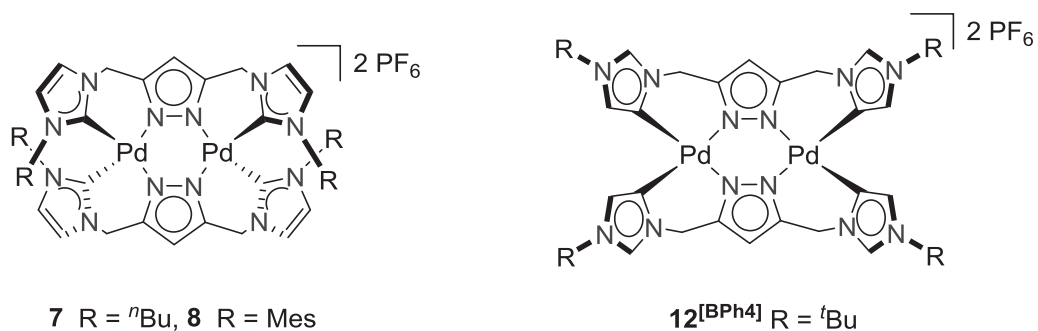


20

Structures of Complexes 1-4



Structures of Complexes 5, 7, 8, 12^[BPh4], 13 and 15.



Structures of Complexes 16-18

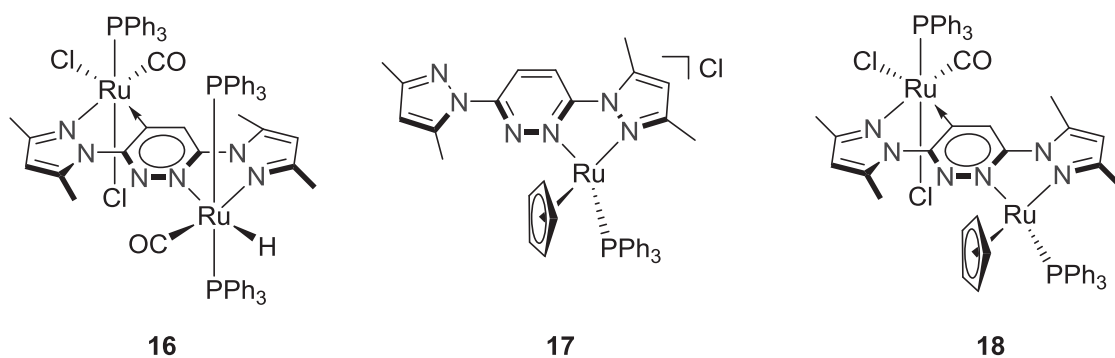


Table A1. Crystal data and refinement details of complex **1** to **4**.

	1	2	3	4
empirical formula	C ₄₂ H ₃₇ BCl ₂ F ₄ N ₂ P ₂ Pd	C ₄₇ H ₄₁ BCl ₄ F ₄ N ₂ P ₂ Pd	C ₂₄ H ₂₂ Cl ₃ N ₂ PPd	C ₄₈ H ₄₆ BCl ₃ F ₄ N ₄ P ₂ Pd
formula weight	895.79	1030.77	582.16	1040.39
crystal size [mm ³]	0.38 x 0.08 x 0.07	0.2 x 0.18 x 0.16	0.4 x 0.25 x 0.19	0.5 x 0.13 x 0.05
crystal system	monoclinic	orthorhombic	triklin	monoclinic
space group	<i>P</i> 2 ₁ / <i>c</i>	<i>Pnma</i>	<i>P</i> -1	<i>P</i> 2 ₁ / <i>c</i>
<i>a</i> [Å]	14.2981(4)	20.2183(4)	9.6593(9)	14.2960(5)
<i>b</i> [Å]	10.7660(2)	14.8686(4)	10.9025(10)	10.4914(2)
<i>c</i> [Å]	25.5110(7)	15.0359(3)	13.1195(12)	32.2000(12)
α [°]	90.00	90.00	114.633(6)	90.00
β [°]	92.774(2)	90.00	106.394(17)	97.243(3)
γ [°]	90.00	90.00	89.521(7)	90.00
<i>V</i> [Å ³]	3922.39(17)	4520.06(18)	1195.33(19)	4791.0(3)
<i>Z</i>	4	4	2	4
ρ [g/cm ³]	1.517	1.515	1.617	1.442
<i>F</i> (000)	1816	2088	584	2120
μ [mm ⁻¹]	0.744	0.771	1.193	0.675
<i>T</i> _{min} / <i>T</i> _{max}	0.6353 / 0.8886	0.7482 / 0.9079	0.6456 / 0.7913	0.8053 / 0.9608
θ range [°]	1.43 - 25.64	1.69 - 26.77	1.79 - 27.15	1.27 - 25.69
<i>hkl</i> range	-17 ≤ <i>h</i> ≤ 17	-25 ≤ <i>h</i> ≤ 25	-12 ≤ <i>h</i> ≤ 10	-17 ≤ <i>h</i> ≤ 17
	-13 ≤ <i>k</i> ≤ 12	-18 ≤ <i>k</i> ≤ 18	-13 ≤ <i>k</i> ≤ 13	-10 ≤ <i>k</i> ≤ 12
	-30 ≤ <i>l</i> ≤ 30	-19 ≤ <i>l</i> ≤ 18	-16 ≤ <i>l</i> ≤ 16	-39 ≤ <i>l</i> ≤ 39
measured refl.	46183	51589	11278	45238
unique refl. [<i>R</i> _{int}]	7391 [0.0685]	4987 [0.0662]	5116 [0.0277]	9032 [0.0929]
observed refl. (<i>I</i> > 2σ(<i>I</i>))	6544	4277	4681	7334
data / restr. / param.	7391 / 58 / 504	4987 / 0 / 308	5116 / 0 / 281	9032 / 70 / 598
goodness-of-fit (<i>F</i> ²)	1.017	1.072	1.031	1.047
<i>R</i> 1, <i>wR</i> 2 (<i>I</i> > 2σ(<i>I</i>))	0.0282, 0.0660	0.0508, 0.1181	0.0217, 0.0535	0.0528, 0.1352
<i>R</i> 1, <i>wR</i> 2 (all data)	0.0347, 0.0682	0.0637, 0.1246	0.0259, 0.0548	0.0669, 0.1437
resid. el. dens. [e/Å ³]	0.664 / -0.447	1.340 / -1.182	-0.372 / 0.526	1.173 / -1.519

Table A2. Crystal data and refinement details of complex **7**, **8** and **12**.

	7	8	12
empirical formula	C ₄₂ H ₆₀ F ₁₂ N ₁₄ P ₂ Pd ₂	C ₇₀ H ₈₆ F ₁₂ N ₁₂ O ₄ P ₂ Pd ₂	C ₉₆ H ₁₀₉ B ₂ N ₁₇ Pd ₂
formula weight	1263.78	1662.25	1735.42
crystal size [mm ³]	0.50 × 0.11 × 0.08	0.46 × 0.29 × 0.16	0.21 × 0.16 × 0.15
crystal system	monoclinic	monoclinic	monoclinic
space group	<i>P</i> 2 ₁ / <i>c</i>	<i>P</i> 2 ₁ / <i>n</i>	<i>P</i> 2 ₁ / <i>c</i>
<i>a</i> [Å]	22.8605(12)	12.9060(6)	21.1808(4)
<i>b</i> [Å]	7.9596(2)	20.2987(8)	17.0295(3)
<i>c</i> [Å]	28.0165(13)	14.3684(7)	26.5164(6)
α [°]	90.00	90.00	90.00
β [°]	92.004(4)	102.751(4)	111.240(2)
γ [°]	90.00	90.00	90.00
<i>V</i> [Å ³]	5094.8(4)	3671.3(3)	8914.7(3)
<i>Z</i>	4	2	4
ρ [g/cm ³]	1.648	1.504	1.293
<i>F</i> (000)	2560	1704	3624
μ [mm ⁻¹]	0.860	0.620	0.459
<i>T</i> _{min} / <i>T</i> _{max}	0.6559 / 0.9467	0.7152 / 0.9160	0.7013 / 0.9529
θ range [°]	1.45 - 25.62	1.77 - 25.72	1.45 - 25.67
<i>hkl</i> range	-27 ≤ <i>h</i> ≤ 27 -8 ≤ <i>k</i> ≤ 9 -34 ≤ <i>l</i> ≤ 34	-15 ≤ <i>h</i> ≤ 15 -24 ≤ <i>k</i> ≤ 24 -17 ≤ <i>l</i> ≤ 17	-25 ≤ <i>h</i> ≤ 25 -20 ≤ <i>k</i> ≤ 20 -32 ≤ <i>l</i> ≤ 32
measured refl.	51132	40210	106831
unique refl. [<i>R</i> _{int}]	9607 [0.0547]	6931 [0.0660]	16806 [0.1091]
observed refl. (<i>I</i> > 2σ(<i>I</i>))	8258	6112	12194
data / restr. / param.	9607 / 0 / 655	6931 / 6 / 481	16806 / 36 / 1035
goodness-of-fit (<i>F</i> ²)	1.018	1.028	1.038
<i>R</i> 1, <i>wR</i> 2 (<i>I</i> > 2σ(<i>I</i>))	0.0254, 0.0583	0.0314, 0.0753	0.0497, 0.0966
<i>R</i> 1, <i>wR</i> 2 (all data)	0.0336, 0.0605	0.0389, 0.0784	0.0806, 0.1048
resid. el. dens. [e/Å ³]	-0.747 / 0.423	-0.624 / 0.713	-0.971 / 0.826

**Table A3.** Crystal data and refinement details of complex **15**, **13** and **5**.

	5	13	15
empirical formula	C ₂₁ H ₃₃ Cl ₃ N ₆ OPd ₂ S	C ₁₅ H ₁₉ Cl ₃ N ₆ Pd ₂	C ₁₆ H _{20.50} Cl ₃ N _{6.50} Pd ₂
formula weight	736.74	602.51	623.04
crystal size [mm ³]	0.29 × 0.03 × 0.02	0.26 × 0.23 × 0.04	0.50 × 0.12 × 0.03
crystal system	triclinic	triclinic	triclinic
space group	<i>P</i> −1	<i>P</i> −1	<i>P</i> −1
<i>a</i> [Å]	8.4978(5)	8.5497(3)	8.4677(7)
<i>b</i> [Å]	10.0419(7)	12.7222(4)	11.5408(10)
<i>c</i> [Å]	16.2133(11)	18.0747(6)	11.9833(10)
α [°]	98.191(5)	92.151(3)	82.860(7)
β [°]	96.413(5)	96.359(3)	69.725(6)
γ [°]	90.112(5)	99.425(3)	71.791(6)
<i>V</i> [Å ³]	1360.64(15)	1924.42(11)	1043.32(15)
<i>Z</i>	2	4	2
ρ [g/cm ³]	1.798	2.080	1.983
<i>F</i> (000)	736	1176	610
μ [mm ^{−1}]	1.720	2.298	2.124
<i>T</i> _{min} / <i>T</i> _{max}	0.7750 / 0.8959	0.4790 / 0.7151	0.3879 / 0.7533
θ range [°]	2.05 - 26.79	1.63 - 26.72	1.81 - 25.10
<i>hkl</i> range	−10 ≤ <i>h</i> ≤ 9	−10 ≤ <i>h</i> ≤ 10	−10 ≤ <i>h</i> ≤ 10
	−12 ≤ <i>k</i> ≤ 12	−16 ≤ <i>k</i> ≤ 16	−13 ≤ <i>k</i> ≤ 13
	−20 ≤ <i>l</i> ≤ 20	−22 ≤ <i>l</i> ≤ 22	−14 ≤ <i>l</i> ≤ 14
measured refl.	16233	24434	20273
unique refl. [<i>R</i> _{int}]	5771 [0.0604]	8142 [0.0547]	20273 [0.0000]
observed refl. (<i>I</i> > 2σ(<i>I</i>))	4430	7186	13636
data / restr. / param.	5771 / 0 / 315	8142 / 0 / 484	20273 / 0 / 250
goodness-of-fit (<i>F</i> ²)	1.058	1.001	1.039
<i>R</i> 1, <i>wR</i> 2 (<i>I</i> > 2σ(<i>I</i>))	0.0422, 0.0743	0.0305, 0.0747	0.0995, 0.2685
<i>R</i> 1, <i>wR</i> 2 (all data)	0.0668, 0.0803	0.0368, 0.0774	0.1267, 0.2852
resid. el. dens. [e/Å ³]	−1.226 / 0.662	−1.459 / 0.948	−1.521 / 2.536

**Table A4.** Crystal data and refinement details of complexes **16**, **17** and **18**

	16	17	18
empirical formula	$C_{70}H_{61}Cl_2N_6O_2P_3Ru_2 \cdot \frac{3}{2}CH_2Cl_2$	$C_{37}H_{36}ClN_6PRu \cdot \frac{3}{2}CH_2Cl_2$	$C_{58}H_{53}Cl_2N_7OP_2Ru_2$
formula weight	1511.59	859.60	1199.05
crystal size [mm ³]	0.50 x 0.21 x 0.14	0.50 x 0.36 x 0.12	0.18 x 0.17 x 0.06
crystal system	monoclinic	monoclinic	monoclinic
space group	P n	P 2/c	$P2_1/c$
<i>a</i> [Å]	16.4860(3)	19.1582(4)	18.3723(4)
<i>b</i> [Å]	18.9441(5)	10.2239(3)	13.2364(2)
<i>c</i> [Å]	24.0177(5)	20.3380(5)	22.6923(6)
α [°]	90.00	90.00	90.00
β [°]	105.675(2)	106.771(2)	107.184(2)
γ [°]	90.00	90.00	90.00
<i>V</i> [Å ³]	7222.1(3)	3814.19(17)	5272.0(2)
<i>Z</i>	4	4	4
ρ [g/cm ³]	1.390	1.497	1.511
<i>F</i> (000)	3076	1756	2440
μ [mm ⁻¹]	0.717	0.770	0.783
<i>T</i> _{min} / <i>T</i> _{max}	<i>n./a.</i> / <i>n./a.</i>	0.5973 / 0.8349	0.8740 / 0.9549
θ range [°]	1.35 - 25.64	1.99 - 25.61	1.80 - 25.66
<i>hkl</i> range	-20 ≤ <i>h</i> ≤ 20	-23 ≤ <i>h</i> ≤ 23	-22 ≤ <i>h</i> ≤ 22
	-23 ≤ <i>k</i> ≤ 23	-12 ≤ <i>k</i> ≤ 12	-16 ≤ <i>k</i> ≤ 16
	-24 ≤ <i>l</i> ≤ 29	-24 ≤ <i>l</i> ≤ 21	-24 ≤ <i>l</i> ≤ 27
measured refl.	74956	39897	51170
unique refl. [<i>R</i> _{int}]	24544 [0.0579]	7186 [0.0626]	9921 [0.0663]
observed refl. (<i>I</i> > 2σ(<i>I</i>))	21550	6273	7572
data / restr. / param.	24544 / 340 / 1652	7186 / 0 / 474	9921 / 1 / 622
goodness-of-fit (<i>F</i> ²)	1.011	1.013	1.015
<i>R</i> 1, <i>wR</i> 2 (<i>I</i> > 2σ(<i>I</i>))	0.0389, 0.0943	0.0274, 0.0680	0.0408, 0.0615
<i>R</i> 1, <i>wR</i> 2 (all data)	0.0454, 0.0964	0.0338, 0.0700	0.0673, 0.0666
resid. el. dens. [e/Å ³]	0.781, -0.573	0.590 / -0.454	0.410 / -0.617

**Table A5.** Crystal data and refinement details of **19** and **20**.

	19	20
empirical formula	C ₂₇ H ₂₉ ClN ₄ O ₂	C ₂₆ H ₂₁ F ₃ N ₄ O ₃ S
formula weight	476.99	526.53
crystal size [mm ³]	0.500 x 0.440 x 0.040	0.500 x 0.040 x 0.030
crystal system	monoclinic	monoclinic
space group	C 2/ <i>c</i>	C 2/ <i>c</i>
<i>a</i> [Å]	10.0111(5)	33.233(2)
<i>b</i> [Å]	18.9078(12)	7.0725(2)
<i>c</i> [Å]	13.3992(7)	20.5120(12)
α [°]	90.00	90.00
β [°]	107.559(4)	103.414(5)
γ [°]	90.00	90.00
<i>V</i> [Å ³]	7222.1(3)	4689.6(4)
<i>Z</i>	4	8
ρ [g/cm ³]	1.310	1.491
<i>F</i> (000)	1008	2176
μ [mm ⁻¹]	0.190	0.200
<i>T</i> _{min} / <i>T</i> _{max}	0.9148 / 0.9920	0.9485 / 0.9947
θ range [°]	2.154 – 26.745	2.041 – 26.733
<i>hkl</i> range	-12 ≤ <i>h</i> ≤ 12	-42 ≤ <i>h</i> ≤ 40
	-23 ≤ <i>k</i> ≤ 23	-8 ≤ <i>k</i> ≤ 7
	-16 ≤ <i>l</i> ≤ 16	-25 ≤ <i>l</i> ≤ 25
measured refl.	15242	20082
unique refl. [<i>R</i> _{int}]	2572 [0.0979]	4959 [0.1232]
observed refl. (<i>I</i> > 2σ(<i>I</i>))	2026	2970
data / restr. / param.	2572 / 0 / 193	4959 / 0 / 348
goodness-of-fit (<i>F</i> ²)	1.109	0.976
<i>R</i> 1, <i>wR</i> 2 (<i>I</i> > 2σ(<i>I</i>))	0.0503, 0.1013	0.0607, 0.1015
<i>R</i> 1, <i>wR</i> 2 (all data)	0.0708, 0.1088	0.1181, 0.1168
resid. el. dens. [e/Å ³]	0.176, -0.190	0.322 / -0.272

Table A6. Selected bond lengths [\AA] and angles [$^\circ$] for the structure of **1**.

Pd1–C1	1.996(2)	Pd1–P1	2.3331(5)	Pd1–P2	2.3343(5)
Pd1–Cl1	2.3422(5)	Cl2–C4	1.718(2)	N1–C5	1.487(3)
N1–N2	1.357(3)	N1–C1	1.337(3)	C1–C2	1.419(3)
C2–C3	1.361(3)	C3–C4	1.405(4)	N2–C4	1.301(3)
C5–C6	1.503(4)				
C1–Pd1–P1	91.50(6)	C1–Pd1–P2	89.72(6)	P1–Pd1–P2	168.99(2)
C1–Pd1–Cl1	178.51(7)	P1–Pd1–Cl1	88.962(19)	P2–Pd1–Cl1	90.10(2)
C1–N1–N2	126.13(19)	C1–N1–C5	123.10(18)	N2–N1–C5	110.74(18)
C4–N2–N1	116.0(2)	N1–C1–C2	115.8(2)	N1–C1–Pd1	123.03(16)
C2–C1–Pd1	121.20(16)	C3–C2–C1	120.7(2)	C2–C3–C4	116.7(2)
N2–C4–C3	124.6(2)	N2–C4–Cl2	115.75(19)	C3–C4–Cl2	119.65(19)
N1–C5–C6	112.18(19)				

Table A7. Selected bond lengths [\AA] and angles [$^\circ$] for the structure of **2**.

Pd1–C1	1.989(5)	Pd1–P1	2.3439(8)	Pd1–P1'	2.3439(3)
Pd1–Cl2	2.3513(12)	Cl1–C8	1.832(6)	N1–C9	1.473(7)
N1–N2	1.377(6)	N1–C1	1.340(6)	C1–C2	1.423(7)
C2–C7	1.404(8)	C7–C8	1.434(9)	N2–C8	1.278(8)
C9–C10	1.415(9)				
C1–Pd1–P1'	88.89(2)	C1–Pd1–P1	88.89(2)	P1'–Pd1–P1	177.46(5)
C1–Pd1–Cl2	176.94(15)	P1'–P1–Cl2	91.08(2)	P1–Pd1–Cl2	91.08(2)
C1–N1–N2	125.4(5)	C1–N1–C9	121.0(4)	N2–N1–C9	113.6(4)
N1–N2–C8	116.3(5)	N1–C1–C2	117.6(5)	N1–C1–Pd1	121.0(4)
C2–C1–Pd1	121.4(4)	C7–C2–C1	119.1(5)	C3–C2–C1	120.9(5)
C2–C7–C8	125.8(5)	N2–C8–C7	125.8(5)	N2–C8–Cl1	113.6(5)
C7–C8–Cl1	120.6(5)				



Table A8. Selected bond lengths [Å] and angles [°] for the structure of **3**.

Pd1–C1	1.9772(18)	Pd1–Cl2	2.3540(5)	Pd1–P1	2.2618(5)
Pd1–Cl1	2.3693(5)	N1–C1	1.333(2)	N1–N2	1.355(2)
N1–C5	1.498(2)	N2–C4	1.318(3)		
C1–Pd1–P1	90.86(5)	C1–Pd1–Cl2	177.65(5)	P1–Pd1–Cl2	88.342(17)
C1–Pd1–Cl1	89.15(5)	P1–Pd1–Cl1	178.626(16)	Cl2–Pd1–Cl1	91.700(18)
C1–N1–C5	122.64(16)	N2–N1–C5	111.87(15)	C1–N1–N2	125.49(16)
C4–N2–N1	116.28(17)	N1–C1–C2	115.61(16)	N1–C1–Pd1	122.93(13)
C2–C1–Pd1	121.39(13)	N2–C4–C3	125.05(18)	N1–C5–C6	111.59(16)
N2–C4–Cl3	115.77(16)				

Table A9. Selected bond lengths [Å] and angles [°] for the structure of **4**.

Pd1–C1	1.982(4)	Pd1–P1	2.3208(9)	Pd1–P2	2.3431(10)
Pd1–Cl1	2.3463(10)	N1–C10	1.491(5)	N3–C4	1.405(5)
N1–N2	1.350(4)	N1–C1	1.336(5)	C1–C2	1.433(6)
C2–C3	1.346(6)	C3–C4	1.405(6)	N2–C4	1.305(5)
N3–N4	1.374(5)	C10–C11	1.475(7)		
C1–Pd1–P1	89.40(10)	C1–Pd1–P2	89.39(10)	P1–Pd1–P2	176.54(4)
C1–Pd1–Cl1	178.38(10)	P1–Pd1–Cl1	88.99(3)	P2–Pd1–Cl1	92.24(4)
C1–N1–N2	126.0(3)	C1–N1–C10	122.8(3)	N2–N1–C10	111.1(3)
C4–N2–N1	116.5(3)	N1–C1–C2	115.6(4)	N1–C1–Pd1	123.7(3)
C2–C1–Pd1	120.7(3)	C3–C2–C1	120.3(4)	C2–C3–C4	117.5(4)
N2–C4–C3	123.9(4)	N2–C4–N3	115.7(4)	C3–C4–N3	120.3(4)
N1–C10–C11	112.0(4)				

Table A10. Selected bond lengths [\AA] and angles [$^\circ$] for the structure of **5**.

Pd1–C6	1.965(5)	Pd1–N1	2.007(4)	Pd1–Cl1	2.3219(13)
Pd1–Cl2	2.4096(12)	Pd2–C14	1.954(5)	Pd2–N2	1.998(4)
Pd2–Cl3	2.3131(12)	Pd2–Cl2	2.3929(13)		
N1–C2	1.349(6)	N1–N2	1.368(5)	N2–C3	1.338(6)
C1–C2	1.385(7)	C1–C3	1.394(6)		
N3–C5	1.335(6)	N3–C6	1.410(6)	N3–C4	1.467(6)
N4–C5	1.328(6)	N4–C7	1.396(6)	N4–C8	1.502(6)
N5–C13	1.334(7)	N5–C14	1.404(6)	N5–C12	1.470(6)
N6–C13	1.338(6)	N6–C15	1.400(7)	N6–C16	1.487(7)
C6–C7	1.371(7)	C14–C15	1.371(7)		
C6–Pd1–N1	88.00(18)	C6–Pd1–Cl1	91.24(14)	N1–Pd1–Cl1	179.16(11)
C6–Pd1–Cl2	176.92(15)	N1–Pd1–Cl2	89.83(11)	Cl1–Pd1–Cl2	90.93(4)
C14–Pd2–N2	88.29(18)	C14–Pd2–Cl3	89.81(14)	N2–Pd2–Cl3	177.31(14)
C14–Pd2–Cl2	177.52(14)	N2–Pd2–Cl2	89.39(12)	Cl3–Pd2–Cl2	92.48(5)
Pd2–Cl2–Pd1	95.41(5)	C2–N1–N2	107.6(4)	C3–N2–N1	108.1(4)
C2–C1–C3	104.3(4)	C15–C14–N5	103.8(4)	C7–C6–N3	104.4(4)
C2–N1–Pd1	129.5(3)	N2–N1–Pd1	122.9(3)	N3–C6–Pd1	123.8(3)
C7–C6–Pd1	131.5(4)				
N1–N2–Pd2	123.1(3)	C3–N2–Pd2	128.6(3)	C15–C14–Pd2	132.4(4)
N5–C14–Pd2	123.6(3)				

**Table A11.** Selected bond lengths [Å] and angles [°] for the structure of the cation of **7**.

Pd1–C5	1.973(2)	Pd1–C25	1.979(2)	Pd1–N1	2.0767(17)
Pd1–N11	2.0873(17)	Pd2–C13	1.974(2)	Pd2–C33	1.980(2)
Pd2–N12	2.0815(17)	Pd2–N2	2.0873(17)		
N1–N2	1.371(2)	N11–N12	1.380(2)		
N1–C2	1.354(3)	N2–C3	1.352(3)	N3–C5	1.348(3)
N4–C5	1.353(3)	N5–C13	1.344(3)	N6–C13	1.350(3)
N11–C22	1.345(3)	N12–C23	1.350(3)	N13–C25	1.346(3)
N14–C25	1.355(3)	N16–C33	1.348(3)	N17–C33	1.355(3)
C1–C2	1.377(3)	C1–C3	1.382(3)		
C21–C22	1.375(3)	C21–C23	1.379(3)		
C5–Pd1–C25	91.57(9)	C5–Pd1–N1	87.13(8)	C25–Pd1–N1	158.59(8)
C5–Pd1–N11	162.28(8)	C25–Pd1–N11	87.18(8)	N1–Pd1–N11	100.34(6)
C13–Pd2–C33	90.26(8)	C13–Pd2–N12	158.65(8)	C33–Pd2–N11	88.43(7)
C13–Pd2–N2	86.47(8)	C33–Pd2–N2	162.54(7)	N12–Pd2–N2	100.75(7)
C2–N1–N2	107.27(16)	C3–N2–N1	107.79(16)		
C22–N11–N12	107.71(16)	C23–N12–N11	106.88(16)		
N3–C5–N4	105.17(18)	N5–C13–N6	105.50(19)		
N13–C25–N14	105.17(19)	N16–C33–N17	105.43(17)		
N3–C5–Pd1	125.09(15)	C2–N1–Pd1	120.36(14)		
N13–C25–Pd1	125.89(16)	C22–N11–Pd1	120.82(14)		
N5–C13–Pd2	126.13(16)	C3–N2–Pd2	120.38(13)		
C23–N12–Pd2	121.06(14)	N16–C33–Pd2	125.15(15)		

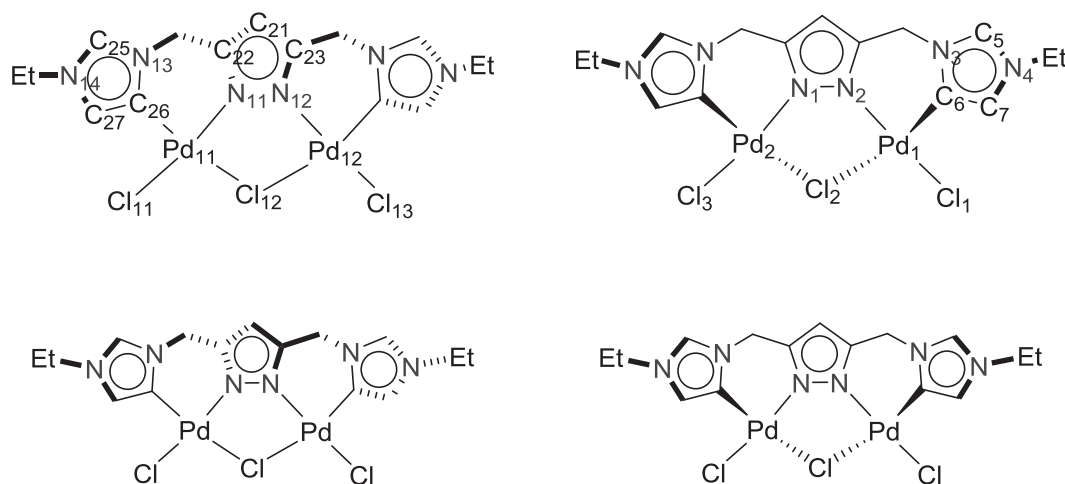
**Table A12.** Selected bond lengths [\AA] and angles [$^\circ$] for the structure of the cation of **8**.

Pd1–C5	1.965(2)	Pd1–C18'	1.967(2)	Pd1–N2'	2.0721(18)
Pd1–N1	2.0738(18)	Pd1'–N2	2.0722(18)	Pd1'–C18	1.967(2)
N1–C2	1.351(3)	N1–N2	1.369(3)	N2–C3	1.355(3)
C1–C2	1.386(3)	C1–C3	1.374(3)	C6–C7	1.348(4)
N3–C5	1.339(3)	N3–C6	1.388(3)		
N4–C5	1.358(3)	N4–C7	1.388(3)		
N5–C18	1.333(3)	N5–C19	1.383(3)		
N6–C18	1.353(3)	N6–C20	1.390(3)		
C19–C20	1.338(4)				
C5–Pd1–C18'	93.36(9)	C5–Pd1–N2'	160.03(9)		
C18'–Pd1–N2'	85.18(8)	C5–Pd1–N1	85.55(8)		
N1–Pd1–C18'	159.59(9)	N1–Pd1–N2'	102.62(7)		
C2–N1–N2	107.84(17)	C2–N1–Pd1	119.50(15)		
N2–N1–Pd1	128.46(14)	C3–N2–N1	107.47(18)		
C3–N2–Pd1'	119.52(15)	N1–N2–Pd1'	128.92(14)		
N3–C5–Pd1	126.02(17)	N4–C5–Pd1	126.44(17)		
N5–C18–Pd1'	126.23(17)	N6–C18–Pd1'	126.12(17)		
N3–C5–N4	105.65(19)	N5–C18–N6	106.2(2)		

**Table A13.** Selected bond lengths [Å] and angles [°] for the structure of **12**^[BPh₄].cation

Pd1–C6	1.980(4)	Pd1–C44	1.990(4)	Pd1–N1	2.061(3)
Pd1–N12	2.063(3)	Pd2–C36	1.983(4)	Pd2–C14	1.991(4)
Pd2–N11	2.050(3)	Pd2–N2	2.065(3)	C6–C7	1.380(5)
N1–C2	1.333(5)	N2–C3	1.343(5)	C14–C15	1.371(5)
C1–C2	1.382(6)	C1–C3	1.377(5)		
N3–C5	1.335(5)	N3–C6	1.408(5)		
N4–C7	1.385(6)	N4–C5	1.324(6)		
N5–C13	1.334(5)	N5–C14	1.403(4)		
N6–C13	1.327(5)	N6–C15	1.389(4)		
N1–N2	1.369(4)	N11–N12	1.363(4)		
C31–C32	1.382(5)	C31–C33	1.392(5)		
C36–C37	1.361(5)	C44–C45	1.367(5)		
C6–Pd1–C44	92.61(16)	C6–Pd1–N1	87.54(14)	C44–Pd1–N1	178.33(14)
C6–Pd1–N12	174.49(14)	C44–Pd1–N12	86.07(14)	N1–Pd1–N12	93.93(12)
C36–Pd2–C14	91.43(15)	C36–Pd2–N11	87.87(13)	C14–Pd2–N11	179.29(15)
C36–Pd2–N2	173.93(13)	C14–Pd2–N2	87.23(13)	N11–Pd2–N2	93.48(12)
N3–C6–C7	103.0(3)	C6–C7–N4	109.3(4)	C7–N4–C5	108.5(3)
N4–C5–N3	108.2(4)	C5–N3–C6	111.0(4)	N5–C14–C15	102.8(3)
N13–C36–C37	102.8(3)	N15–C44–C45	103.1(3)		
C2–N1–Pd1	127.6(3)	N3–C6–Pd1	121.8(3)		
C33–N12–Pd1	124.3(3)	N15–C44–Pd1	120.2(3)		
N5–C14–Pd2	119.9(3)	C3–N2–Pd2	124.1(2)		
N13–C36–Pd2	121.4(3)	C32–N11–Pd2	126.3(2)		

Table A14. Selected bond lengths [Å] and angles [°] for the structures of the two conformers of **13**



conformer **E**

conformer **F**

conformer F		conformer E		conformer F		conformer E	
Pd1–C6	1.963(3)	Pd11–C26	1.986(3)	C2–N1–N2	107.6(3)	C22–N11–N12	107.6(3)
Pd1–N1	2.002(3)	Pd11–N11	2.021(3)	N1–N2–C3	108.3(3)	N11–N12–C23	125.2(2)
Pd1–Cl1	2.3050(8)	Pd11–Cl11	2.2948(8)	N3–C5–N4	108.6(3)	N13–C25–N14	107.7(3)
Pd1–Cl2	2.4075(9)	Pd11–Cl12	2.3815(8)	C5–N3–C6	110.3(3)	C25–N13–C26	111.1(3)
Pd2–C12	1.969(3)	Pd12–C32	1.971(3)	C5–N4–C7	108.3(3)	C25–N14–C27	108.8(3)
Pd2–N2	2.011(3)	Pd12–N12	2.025(3)	N4–C7–C6	108.5(3)	N14–C27–C26	108.8(3)
Pd2–Cl3	2.3084(8)	Pd12–Cl13	2.3033(8)	N3–C6–C7	104.2(3)	N13–C26–C27	103.6(3)
Pd2–Cl2	2.4097(8)	Pd12–Cl12	2.3845(8)	C6–Pd1–N1	88.81(12)	C26–Pd11–N11	91.17(12)
N1–C2	1.343(4)	N11–C22	1.348(4)	C6–Pd1–Cl1	88.87(10)	C26–Pd11–Cl11	88.57(9)
N1–N2	1.362(4)	N11–N12	1.370(4)	N1–Pd1–Cl1	174.11(7)	N11–Pd11–Cl11	178.08(8)
N2–C3	1.336(4)	N12–C23	1.343(4)	C6–Pd1–Cl2	176.65(9)	C26–Pd11–Cl12	174.98(9)
C1–C3	1.387(5)	C21–C23	1.393(4)	N1–Pd1–Cl2	89.40(8)	N11–Pd11–Cl12	90.81(8)
C1–C2	1.389(4)	C21–C22	1.377(5)	Cl1–Pd1–Cl2	93.17(3)	Cl11–Pd11–Cl12	89.30(3)
N3–C5	1.320(4)	N13–C25	1.339(4)	C12–Pd2–N2	87.63(12)	Cl12–Pd12–N12	89.31(8)
N3–C6	1.400(4)	N13–C26	1.399(4)	C12–Pd2–Cl3	90.84(10)	C32–Pd12–Cl13	88.56(10)
C6–C7	1.367(5)	C26–C27	1.372(5)	N2–Pd2–Cl3	176.73(8)	N12–Pd12–Cl13	178.12(8)
N4–C5	1.327(4)	N14–C25	1.321(4)	C12–Pd2–Cl2	173.31(9)	C32–Pd12–Cl12	173.49(9)
N4–C7	1.381(5)	N14–C27	1.389(4)	N2–Pd2–Cl2	90.37(8)	N12–Pd12–Cl12	89.31(8)
				Cl3–Pd2–Cl2	91.47(3)	Cl13–Pd12–Cl12	92.35(3)
				Pd1–Cl2–Pd2	92.83(3)	Pd11–Cl12–Pd12	103.86(3)

**Table A15.** Selected bond lengths [Å] and angles [°] for the structure of **15**.

Pd1–N1	1.966(6)	Pd1–C5	1.971(8)	Pd1–Cl1	2.3052(18)
Pd1–Cl2	2.3729(17)	Pd2–C11	1.987(7)	Pd2–N2	1.991(6)
Pd2–Cl3	2.3089(19)	Pd2–Cl2	2.3834(18)		
N1–C2	1.368(9)	N1–N2	1.370(9)	N2–C3	1.342(9)
C1–C2	1.364(10)	C1–C3	1.404(11)		
N3–C5	1.349(10)	N3–C6	1.365(10)		
N4–C5	1.353(10)	N4–C7	1.380(10)		
N5–C11	1.353(10)	N5–C12	1.400(10)		
N6–C11	1.330(10)	N6–C13	1.374(11)		
N1–Pd1–C5	86.2(3)	N1–Pd1–Cl1	171.67(18)	C5–Pd1–Cl1	93.7(2)
N1–Pd1–Cl2	88.16(17)	C5–Pd1–Cl2	171.5(2)	Cl1–Pd1–Cl2	92.79(6)
C11–Pd2–N2	86.0(3)	C11–Pd2–Cl3	94.6(2)	N2–Pd2–Cl3	173.00(19)
C11–Pd2–Cl2	172.5(2)	N2–Pd2–Cl2	88.68(18)	Cl3–Pd2–Cl2	91.36(6)
N3–C5–N4	105.0(7)	N6–C11–N5	105.9(6)	Pd1–Cl2–Pd2	100.30(6)
C3–N2–N1	109.3(6)	C2–N1–N2	107.0(6)		
C2–N1–Pd1	126.4(5)	N2–N1–Pd1	126.3(5)		
N3–C5–Pd1	122.8(6)	N4–C5–Pd1	131.4(6)		
C3–N2–Pd2	125.3(5)	N1–N2–Pd2	124.0(4)		
N6–C11–Pd2	131.9(6)	N5–C11–Pd2	121.5(6)		

Table A16. Selected bond lengths [\AA] and angles [$^\circ$] for the structure of **16**.

Ru1–C15	1.823(5)	Ru1–N4	2.163(4)	Ru1–C2	2.020(5)
Ru1–P1	2.2856(13)	Ru1–Cl2	2.4430(16)	Ru1–Cl1	2.5005(12)
Ru2–C16	1.847(6)	Ru2–N6	2.114(4)	Ru2–N2	2.141(4)
Ru2–P2	2.3437(15)	Ru2–P3	2.3416(15)		
N1–C1	1.315(6)	N1–N2	1.351(5)	N2–C4	1.345(6)
C1–C2	1.395(7)	C2–C3	1.396(7)	C3–C4	1.398(6)
N3–N4	1.384(5)	N5–N6	1.395(5)		
C15–Ru1–C2	93.3(2)	C15–Ru1–N4	169.93(17)	C2–Ru1–N4	78.21(18)
C15–Ru1–P1	91.09(16)	C2–Ru1–P1	91.57(15)	N4–Ru1–P1	94.49(12)
C15–Ru1–Cl2	89.67(16)	C2–Ru1–Cl2	89.11(15)	N4–Ru1–Cl2	84.87(12)
P1–Ru1–Cl2	178.96(6)	C15–Ru1–Cl1	93.46(14)	C2–Ru1–Cl1	171.99(15)
N4–Ru1–Cl1	94.65(10)	P1–Ru1–Cl1	92.62(5)	Cl2–Ru1–Cl1	86.62(5)
C16–Ru2–N6	174.11(19)	C16–Ru2–N2	99.80(19)	N6–Ru2–N2	74.42(14)
C16–Ru2–P3	88.51(18)	N6–Ru2–P3	92.99(13)	N2–Ru2–P3	94.04(12)
C16–Ru2–P2	85.90(19)	N6–Ru2–P2	93.98(13)	N2–Ru2–P2	100.54(12)
P3–Ru2–P2	165.08(4)				
C1–N1–N2	118.4(4)	C4–N2–N1	119.2(4)	N2–C4–C3	122.0(5)
C2–C3–C4	119.9(5)	C1–C2–C3	112.7(4)	N1–C1–C2	127.5(5)

**Table A17.** Selected bond lengths [Å] and angles [°] for the structure of the cation of **17**.

Ru1–N1	2.0591(15)	Ru1–N3	2.0830(16)	Ru1–C19	2.167(2)
Ru1–C18	2.168(2)	Ru1–C15	2.207(2)	Ru1–C17	2.2118(19)
Ru1–C16	2.223(2)	Ru1–P1	2.3238(5)		
N1–C1	1.342(2)	N1–N2	1.353(2)	N2–C4	1.324(2)
C3–C4	1.402(3)	C2–C3	1.365(3)	C1–C2	1.399(3)
N3–N4	1.381(2)	N5–N6	1.388(2)		
N1–Ru1–N3	75.74(6)	N1–Ru1–C19	104.19(7)	N3–Ru1–C19	159.61(8)
N1–Ru1–C18	139.98(7)	N3–Ru1–C18	145.26(7)	C19–Ru1–C18	38.34(8)
N1–Ru1–C15	98.01(7)	N3–Ru1–C15	121.80(8)	C19–Ru1–C15	37.82(10)
C18–Ru1–C15	63.09(9)	N1–Ru1–C17	160.36(7)	N3–Ru1–C17	109.93(7)
C19–Ru1–C17	63.72(8)	C18–Ru1–C17	37.86(8)	C15–Ru1–C17	62.77(7)
N1–Ru1–C16	123.97(7)	N3–Ru1–C16	99.91(8)	C19–Ru1–C16	62.77(9)
C18–Ru1–C16	62.71(8)	C15–Ru1–C16	36.87(9)	C17–Ru1–C16	37.56(7)
N1–Ru1–P1	88.68(4)	N3–Ru1–P1	92.27(4)	C19–Ru1–P1	108.12(7)
C18–Ru1–P1	90.19(6)	C15–Ru1–P1	145.91(7)	C17–Ru1–P1	109.44(5)
C16–Ru1–P1	147.00(5)				
C1–N1–N2	120.52(15)	C4–N2–N1	118.38(16)	N2–C4–C3	123.79(17)
C2–C3–C4	117.55(17)	C3–C2–C1	117.69(18)	N1–C1–C2	122.04(17)

Table A18. Selected bond lengths [Å] and angles [°] for the structure of **18**.

Ru1–N3	2.072(3)	Ru1–N1	2.076(3)	Ru1–C18	2.183(4)
Ru1–C17	2.186(3)	Ru1–C19	2.188(3)	Ru1–C15	2.201(3)
Ru1–C16	2.207(3)	Ru1–P1	2.3252(9)		
Ru2–C38	1.823(4)	Ru2–C3	2.003(3)	Ru2–N5	2.181(3)
Ru2–P2	2.3076(9)	Ru2–Cl1	2.4492(8)	Ru2–Cl2	2.5050(9)
N1–C1	1.337(4)	N1–N2	1.354(4)	C1–C2	1.387(5)
C2–C3	1.382(5)	C3–C4	1.416(5)	N2–C4	1.309(4)
N3–N4	1.375(4)	N5–N6	1.384(4)		
N3–Ru1–N1	75.19(10)	N3–Ru1–C18	142.32(13)	N3–Ru1–P1	89.80(8)
N1–Ru1–P1	88.73(8)	C18–Ru1–P1	95.10(10)	C17–Ru1–P1	113.84(11)
C19–Ru1–P1	111.44(11)	C15–Ru1–P1	148.74(12)	C16–Ru1–P1	151.65(11)
C38–Ru2–C3	90.60(14)	C38–Ru2–N5	168.92(13)	C3–Ru2–N5	78.31(11)
C38–Ru2–P2	87.65(11)	C3–Ru2–P2	90.44(10)	N5–Ru2–P2	92.65(7)
C38–Ru2–Cl1	93.57(11)	C3–Ru2–Cl1	88.29(9)	N5–Ru2–Cl1	85.91(7)
P2–Ru2–Cl1	85.91(7)	C38–Ru2–Cl2	94.57(11)	C3–Ru2–Cl2	173.29(10)
N5–Ru2–Cl2	94.46(7)	P2–Ru2–Cl2	94.03(3)	Cl1–Ru2–Cl2	87.12(3)
C1–N1–N2	119.1(3)	C4–N2–N1	117.2(3)	N2–C4–C3	128.5(3)
C2–C3–C4	111.8(3)	C3–C2–C1	120.0(3)	N1–C1–C2	123.2(3)

**Table A19.** Selected bond lengths [\AA] and angles [$^\circ$] for the structure of the cation of **19**.

C1–C2	1.399(2)	C2–C3	1.453(2)
C2–C6	1.419(3)	C3–C3'	1.428(4)
C6–N1	1.353(2)	C7–N1	1.395(2)
C6–N2	1.357(2)	C12–N2	1.390(2)
C7–C12	1.388(3)		
C2–C1–C2'	110.1(2)	C1–C2–C3	107.66(16)
C2–C3–C3'	107.31(10)	C1–C2–C6	124.69(16)
C3–C2–C6	127.62(16)	C2–C6–N1	125.49(17)
C2–C6–N2	127.02(16)	N1–C6–N2	107.48(16)
C6–N2–C12	109.74(15)	N2–C12–C7	106.54(16)
C12–C7–N1	106.69(16)	C7–N1–C6	109.55(16)

Table A20. Selected bond lengths [\AA] and angles [$^\circ$] for the structure of the cation of **20**.

C1–C2	1.399(4)	C2–C3	1.450(4)
C3–C8	1.431(4)	C8–C9	1.456(4)
C1–C9	1.405(4)	C2–C10	1.435(4)
C9–C18	1.415(4)	C10–N1	1.346(4)
C10–N2	1.355(3)	N1–C11	1.391(4)
N2–C16	1.396(4)	C11–C16	1.392(4)
N3–C18	1.361(4)	N4–C18	1.361(3)
N3–C19	1.385(4)	N4–C24	1.399(4)
C19–C24	1.387(4)		
C2–C1–C9	110.1(2)	C1–C2–C3	108.1(2)
C1–C9–C8	107.1(2)	C2–C3–C8	106.9(2)
C9–C8–C3	107.8(2)	N1–C10–N2	108.2(2)
C16–C11–N1	106.3(2)	C10–N1–C11	109.8(2)
C10–N2–C16	108.8(2)	N2–C16–C11	106.9(2)
N3–C18–N4	106.6(2)	C24–N4–C18	109.8(2)
C19–N3–C18	110.4(2)	N3–C19–C24	106.8(2)
N4–C24–C19	106.4(2)		

Table A21. Comparison of bond lengths [\AA] and angles [$^\circ$] of complex **1** to **4** in Chapter 2. $\text{C}^{\text{carbene}}$, N^{Et} and N^{non} stand for the carbenic carbon atom, the ethylated nitrogen atom and the non-alkylated nitrogen atom, respectively.

	1	2	3	4
$\text{C}^{\text{carbene}}\text{-Pd}$	1.996(2)	1.989(5)	1.977(2)	1.982(4)
$\text{C}^{\text{carbene}}\text{-C}$	1.419(3)	1.423(7)	1.432(9)	1.433(6)
$\text{C}^{\text{carbene}}\text{-N}^{\text{Et}}$	1.337(3)	1.340(6)	1.333(2)	1.336(5)
$\text{C}(\text{-C}^{\text{carbene}})\text{-C}$	1.361(3)	1.404(8)	1.357(1)	1.346(6)
$\text{N}^{\text{Et}}\text{-N}^{\text{non}}$	1.357(3)	1.377(6)	1.355(2)	1.350(4)
$\text{N}^{\text{non}}\text{-C}$	1.301(3)	1.278(8)	1.318(3)	1.305(5)
$\text{C}(\text{-N}^{\text{non}})\text{-C}$	1.405(4)	1.434(9)	1.388(6)	1.405(6)
Pd-P	2.3331(5)	2.3439(8)	2.2618(5)	2.3208(9)
	2.3343(5)	2.3438(8)		2.3431(1)
Pd-Cl	2.3422(5)	2.3513(1)	2.3540(5)	2.3463(1)
			2.3693(5)	
$\text{C}^{\text{carbene}}\text{-Pd-P}$	91.50(6)	88.89(2)	90.65(5)	89.40(10)
	89.72(6)	88.89(2)		89.39(10)
$\text{C}^{\text{carbene}}\text{-Pd-Cl}$	178.51(7)	176.94(15)	89.15(5)	178.38(10)
			177.65(5)	
P-Pd-Cl	88.962(19)	91.08(2)	88.342(17)	88.99(3)
	90.10(2)	91.08(2)		92.24(4)
P-Pd-P	168.99(2)	177.46(5)	<i>n./a.</i>	176.54(4)
Cl-Pd-Cl	<i>n./a.</i>	91.700(18)	<i>n./a.</i>	
$\text{N}^{\text{non}}\text{-N}^{\text{Et}}\text{-C}^{\text{carbene}}$	126.13(19)	125.4(5)	125.49(16)	126.0(3)
$\text{N}^{\text{Et}}\text{-C}^{\text{carbene}}\text{-C}$	115.8(2)	117.6(5)	115.61(16)	115.6(4)
$\text{N}^{\text{Et}}\text{-N}^{\text{non}}\text{-C}$	116.0(2)	116.3(5)	116.28(17)	116.5(3)
$\text{C}^{\text{carbene}}\text{-C-C}$	120.7(2)	119.1(5)	121.413(190)	120.3(4)
$\text{N}^{\text{non}}\text{-C-C}$	124.6(2)	125.8(5)	125.05(18)	123.9(4)
$\text{C}(\text{-C}^{\text{carbene}})\text{-C-C}(\text{-N}^{\text{non}})$	116.7(2)	115.8(5)	116.061(201)	117.5(4)

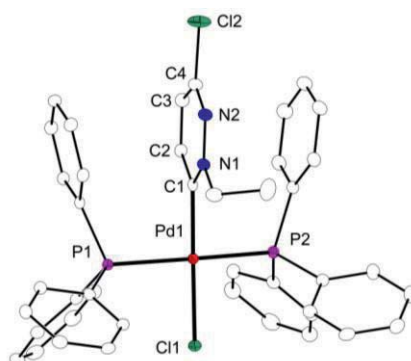
**Table A22.** Comparison of selected bond lengths [\AA] and angles [$^\circ$] of the structure of the dinuclear palladium complexes in Chapter 3.

bond lengths / angles	7	8	12 ^[BPh4]	15	13	5
Pd-C	1.973(2) - 1.980(2)	1.965(2) / 1.967(2)	1.980(4) - 1.991(4)	1.971(8) / 1.987(8)	1.963(3) - 1.986(3)	1.953(5) / 1.965(5)
Pd-N	2.077(2) - 2.087(2)	2.072(2) / 2.074(2)	2.050(3) - 2.065(3)	1.966(6) / 1.991(6)	2.002(3) - 2.025(3)	1.997(4) / 2.007(4)
Pd-Cl		<i>n./a.</i>		2.305(2) - 2.383(2)	2.295(1) - 2.410(1)	2.313(1) - 2.410(1)
Pd \cdots Pd	4.0376(2)	3.9606(3)	3.8157(5)	3.6517(9)	3.4893(3) / 3.7522(4)	3.5525(5)
N-C(-Pd)	1.344(3) - 1.355(3)	1.333(3) - 1.358(3)	1.400(5) - 1.407(4)	1.330(11) - 1.353(10)	1.387(4) - 1.400(4)	1.409(6) - 1.404(6)
N-C	1.375(3) - 1.387(3)	1.383(3) - 1.390(3)	1.324(6) - 1.390(5)	1.365(10) - 1.400(10)	1.319(5) - 1.389(4)	1.329(6) - 1.400(6)
(N-C)-C(-N)	1.342(3) - 1.349(3)	1.338(4) / 1.348(4)	1.361(5) - 1.380(5)	1.340(13) / 1.349(13)	1.367(5) - 1.373(5)	1.370(6) / 1.370(7)
N-C(-Pd)-N	105.2(2) - 105.5(2)	105.7(2) / 106.2(2)	<i>n./a.</i>	105.0(7) / 105.9(6)	<i>n./a.</i>	<i>n./a.</i>
C-C-N	106.4(2) - 106.7(2)	106.4(2) / 106.8(2)		105.6(7) / 107.0(7)		
C-C(-Pd)-N		<i>n./a.</i>	102.8(3) - 103.1(3)	<i>n./a.</i>	103.6(3) - 104.9(3)	103.7(4) / 104.4(4)
N-C-N			108.2(4) - 108.6(3)		107.7(3) - 108.6(3)	108.7(4) / 108.3(4)
Pd \cdots N/N/C/C	0.037 / 0.040	0.005	0.030 / 0.050		<i>n./a.</i>	
Pd \cdots N/C/Cl/Cl		<i>n./a.</i>		0.051 / 0.062	0.023 - 0.055	0.012 / 0.029

Table A23. Comparison of selected bond lengths [\AA] and angles [$^\circ$] of complex **16**, **17** and **18**. $\text{Ru}^{\text{C,N}}$ and $\text{Ru}^{\text{N,N}}$ represent Ru atoms in the C,N-pocket and the N,N-pocket, respectively. N^{pyri} and C^{pyri} refer to N and C atoms in the pyridazine ring bound to the metal atoms. N^{pyra} represents N atom in the pyrazole bound to Ru atom.

		16	17	18
Bond length/Å	Ru ^{N,N} –N ^{pyri}	2.141(4)	2.0591(15)	2.076(3)
	Ru ^{N,N} –N ^{pyra}	2.114(4)	2.0830(16)	2.072(3)
	Ru ^{N,N} –P	2.3416(15)	2.3238(5)	2.3252(9)
		2.3437(15)		
	N ^{pyri} –N	1.351(5)	1.353(2)	1.354(4)
	N ^{pyri} –C	1.345(6)	1.342(2)	1.337(4)
	C(–N ^{pyri})–C(–C ^{pyri})	1.398(6)	1.399(3)	1.387(5)
	C ^{pyri} –C(–C)	1.396(7)	1.365(3)	1.382(5)
	C ^{pyri} –C(–N)	1.395(5)	1.402(3)	1.416(5)
	N(–N ^{pyri})–C(–C ^{pyri})	1.315(6)	1.324(2)	1.309(4)
	Ru ^{C,N} –C ^{pyri}	2.020(5)	<i>n./a.</i>	2.003(3)
	Ru ^{C,N} –N ^{pyra}	2.163(4)		2.181(3)
	Ru ^{C,N} –Cl	2.5005(12)		2.5050(9)
		2.4430(16)		2.4492(8)
Angle/°	N–Ru ^{N,N} –N	74.42(14)	75.74(6)	75.19(10)
	N–Ru ^{N,N} –P	100.54(12)	88.68(4)	88.73(8)
		94.04(12)		
	C ^{pyri} –Ru ^{C,N} –P	91.57(15)	<i>n./a.</i>	90.44(10)
	Cl–Ru ^{C,N} –Cl	86.62(5)		87.12(3)
	P–Ru ^{C,N} –C(O)	90.09(16)		87.65(11)
	N ^{pyra} –Ru ^{C,N} –C(O)	169.93(17)		168.92(13)

Table A24: Selected bond lengths [Å] and angles [°] of **1** and of the calculated structures **A1-A4** and **B1-B4**. The following figure is the molecular structure of complex **1** determined by X-ray diffraction.



	1*	A1	A1'[§]	B1	A2	B2	A3	B3	A4	B4
Pd1–C1	1.996	2.038	2.048	2.029	2.032	2.028	2.035	2.027	2.029	2.027
Pd1–Cl1	2.342	2.376	2.382	2.388	2.376	2.388	2.378	2.389	2.378	2.388
Pd1–P	2.333	2.431	2.333	2.418	2.428	2.416	2.397	2.385	2.397	2.384
	2.334	2.435	2.334	2.420	2.431	2.421	2.397	2.387	2.397	2.387
C1–C2	1.419	1.423	1.423	1.427	1.421	1.428	1.426	1.430	1.423	1.430
C2–C3	1.361	1.374	1.374	1.376	1.375	1.375	1.375	1.376	1.376	1.377
C3–C4	1.405	1.413	1.412	1.403	1.412	1.405	1.415	1.405	1.414	1.404
C4–N2	1.301	1.313	1.313	1.342	1.315	1.343	1.315	1.343	1.317	1.343
N2–N1	1.357	1.350	1.350	1.359	1.351	1.362	1.350	1.362	1.352	1.363
N1–C1	1.337	1.355	1.354	1.335	1.356	1.333	1.358	1.340	1.359	1.341
N1–C(R)	1.487	1.490	1.491	<i>n./a.</i>	1.475	<i>n./a.</i>	1.490	<i>n./a.</i>	1.475	<i>n./a.</i>
N2–C(R)		<i>n./a.</i>		1.487	<i>n./a.</i>	1.473	<i>n./a.</i>	1.489	<i>n./a.</i>	1.474
C4–Cl2	1.718	1.731	1.731	1.724	1.730	1.724	1.726	1.721	1.725	1.718
C–C(Et)	1.503	1.523	1.523	1.526	<i>n./a.</i>	<i>n./a.</i>	1.524	1.526	<i>n./a.</i>	
Cl1–Pd–C1	178.5	177.6	177.0	178.1	178.3	178.6	179.2	178.6	178.3	178.4
P1–Pd–P2	167.0	171.4	172.6	174.6	173.1	175.1	169.5	170.8	169.7	170.8
Pd...C1/Cl1/P1/P2 [§]	0.20	0.05	0.03	0.02	0.04	0.03	0.05	0.01	0.05	0.01

^{*}) values obtained from the solid state molecular structure at 133K,

[§]) Pd–P distance constraint [§]) distance of Pd from the least-squares plane

Table A25. Comparison of selected bond lengths [Å] and angles [°] of the calculated structures of **C** and **D** models for $[\text{}^{\text{n}}\text{L}^{\text{R}}_2\text{Pd}_2]^{2+}$ and $[\text{}^{\text{a}}\text{L}^{\text{R}}_2\text{Pd}_2]^{2+}$.

	$[\text{}^{\text{n}}\text{L}^{\text{R}}_2\text{Pd}_2]^{2+}$		$[\text{}^{\text{a}}\text{L}^{\text{R}}_2\text{Pd}_2]^{2+}$	
	C	D	C	D
Pd–C	2.024-2.025	2.041-2.085	2.016	2.036-2.038
Pd–N	2.138	2.042-2.102	2.153-2.155	2.103-2.106
Pd···Pd	4.122	3.902	4.138	3.892
N–C(–Pd)–N	104.9	103.7-104.9	<i>n./a.</i>	
C–C(–Pd)–N	<i>n./a.</i>		104.0	103.5
C–C–N	106.3	106.5-106.6	<i>n./a.</i>	
N–C–N	<i>n./a.</i>		107.8	108.0
Pd···N/N/C/C*	0.000	0.101/0.111	0.000/0.001	0.051/0.053

*) distance of Pd atom from the least-squares plane

Table A26. Comparison of selected bond lengths [Å] and angles [°] for the calculated structures of **E** and **F** models for $\text{}^{\text{a}}\text{L}^{\text{R}}\text{Pd}_2\text{Cl}_3$ and $\text{}^{\text{a}}\text{L}^{\text{R}}\text{Pd}_2\text{Cl}_3$.

	$\text{}^{\text{n}}\text{L}^{\text{R}}\text{Pd}_2\text{Cl}_3$		$\text{}^{\text{a}}\text{L}^{\text{R}}\text{Pd}_2\text{Cl}_3$	
	E	F	E	F
Pd–C	2.018	2.006/2.010	1.998/2.000	1.991/1.992
Pd–N	2.073/2.074	2.048/2.049	2.080/2.081	2.063/2.064
Pd–Cl	2.339-2.414	2.336-2.430	2.316-2.415	2.334-2.434
Pd···Pd	3.827	2.693	3.795	3.678
N–C(–Pd)–N	104.3	104.6/104.7	<i>n./a.</i>	
C–C(–Pd)–N	<i>n./a.</i>		103.9	104.1
C–C–N	106.3	106.4	<i>n./a.</i>	
N–C–N	<i>n./a.</i>		107.5	107.6
Pd···N/C/Cl/Cl*	0.035/0.041	0.034/0.036	0.064/0.075	0.027/0.023

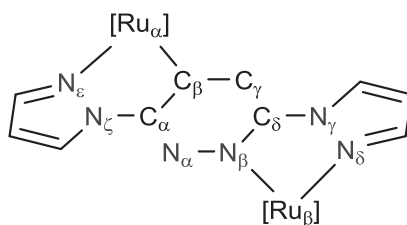
*) distance of Pd atom from the least-squares plane



Table A27. Comparison of selected bond lengths [Å] angles [°] of complex **16** and models **G** and **H**. Ru^{C,N}, Ru^{N,N}, C^{pyri}, N^{pyri}, N^{pyra} stand for the Ru atom in *C,N*- and *N,N*-pocket, C atom and N atom in the pyridazine ring bound to Ru atom, and N atom in the pyrazole ring bound to Ru atom, respectively.

	16	G	H		16	G	H
Ru ^{C,N} –C ^{pyri}	2.020(5)	1.987	2.028	Ru ^{C,N} –N ^{pyra}	2.163(4)	2.134	2.143
Ru ^{C,N} –Cl	2.4430(16)	2.456	2.479	Ru ^{C,N} –C(O)	1.823(5)	1.832	1.834
	2.5005(12)	2.472					
Ru ^{C,N} –P	2.2856(13)	2.298	2.376	Ru ^{N,N} –N ^{pyra}	2.114(4)	2.122	2.124
			2.377				
Ru ^{N,N} –N ^{pyri}	2.141(4)	2.174	2.166				
Ru ^{N,N} –C(O)	1.847(6)	1.841	1.835	Ru ^{N,N} –P	2.3437(15)	2.343	2.253
Ru ^{N,N} –Cl	<i>n./a.</i>		2.456		2.3416(15)	2.356	
N ^{pyri} –N	1.351(5)	1.340	1.329	N ^{pyri} –C	1.345(6)	1.341	1.342
C ^{pyri} –C	1.395(7)	1.435	1.393	N ^{pyra} –N	1.384(5)	1.357	1.355
	1.396(7)	1.397	1.422		1.395(5)	1.361	1.361
C(–C ^{pyri})–C	1.398(6)	1.387	1.392	N(–N ^{pyri})–C	1.315(6)	1.315	1.314
N–Ru ^{C,N} –C	78.21(18)	78.79	78.21	N–Ru ^{N,N} –N	74.42(14)	74.91	74.89

Table A28. Comparison of selected bond lengths [Å] of models **G** and **H**



Bond	G	H	Difference [H - G]	Bond	G	H	Difference [H - G]
Ru _α –C _β	1.987	2.028	0.041	Ru _β –N _β	2.174	2.166	-0.008
Ru _α –N _ε	2.134	2.143	0.009	Ru _β –N _δ	2.122	2.124	0.002
C _α –C _β	1.435	1.422	-0.013	C _β –C _γ	1.397	1.393	-0.004
C _γ –C _δ	1.387	1.392	0.005	N _β –C _δ	1.341	1.342	0.001
N _α –C _α	1.315	1.314	-0.001	N _γ –C _δ	1.415	1.405	-0.010
N _ζ –C _α	1.403	1.410	0.007	N _ε –N _ζ	1.357	1.355	-0.002
N _γ –N _δ	1.361	1.361	0.000				

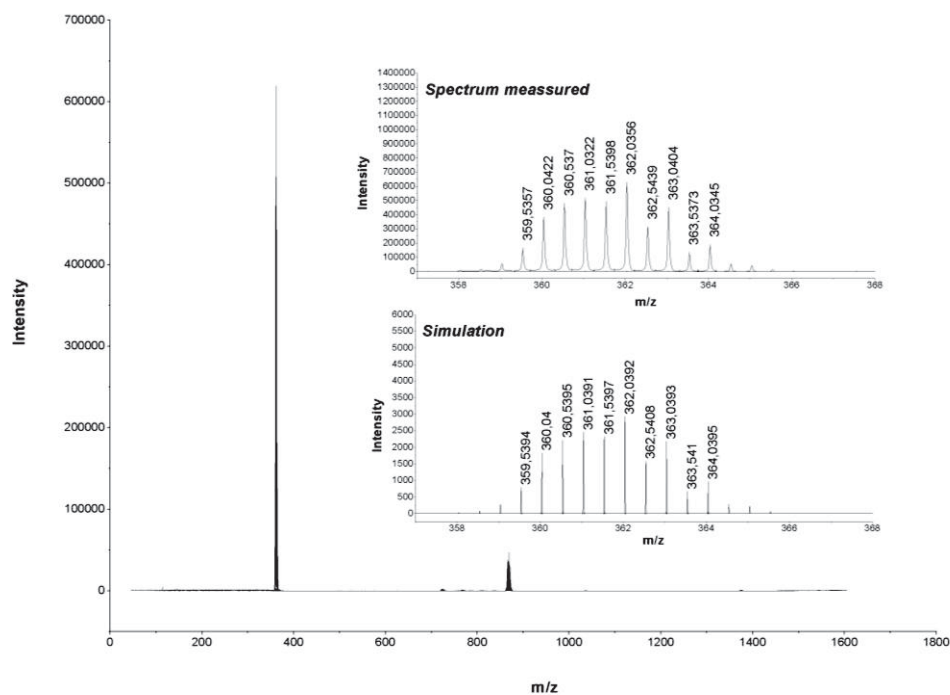


Figure A1. HR ESI-MS spectrum of $[\text{nL}^{\text{Et}}_2\text{Pd}_2](\text{PF}_6)_2$ (complex **6**) in acetonitrile, the inset shows the experimental and simulated isotopic distribution patterns for $[\text{nL}^{\text{Et}}_2\text{Pd}_2]^{2+}$.

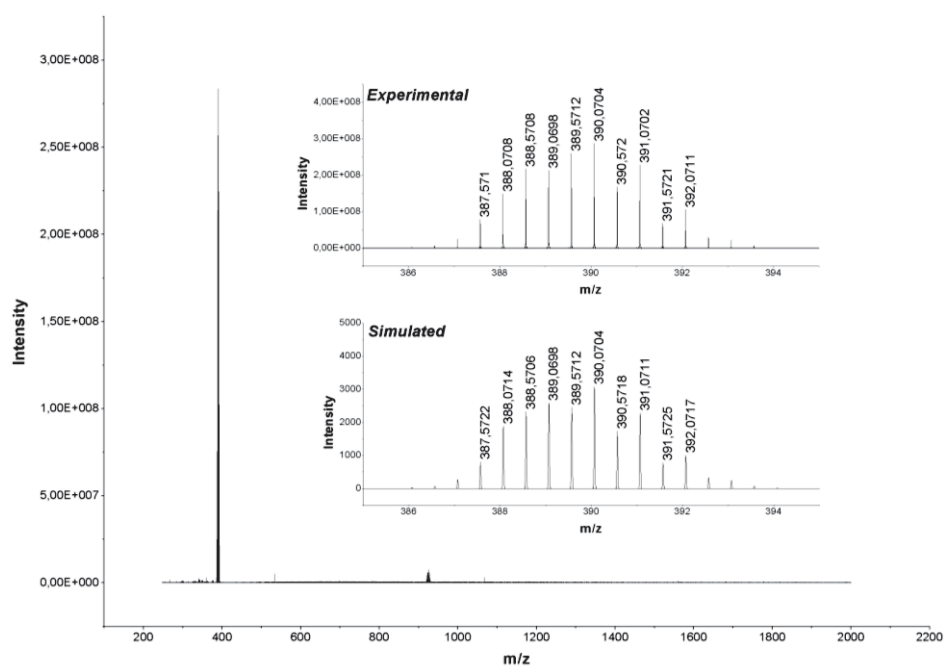


Figure A2. HR ESI-MS spectrum of $[\text{aL}^{\text{Et}}_2\text{Pd}_2](\text{PF}_6)_2$ (complex **9**) in acetonitrile, the inset shows the experimental and simulated isotopic distribution patterns for $[\text{aL}^{\text{Et}}_2\text{Pd}_2]^{2+}$.

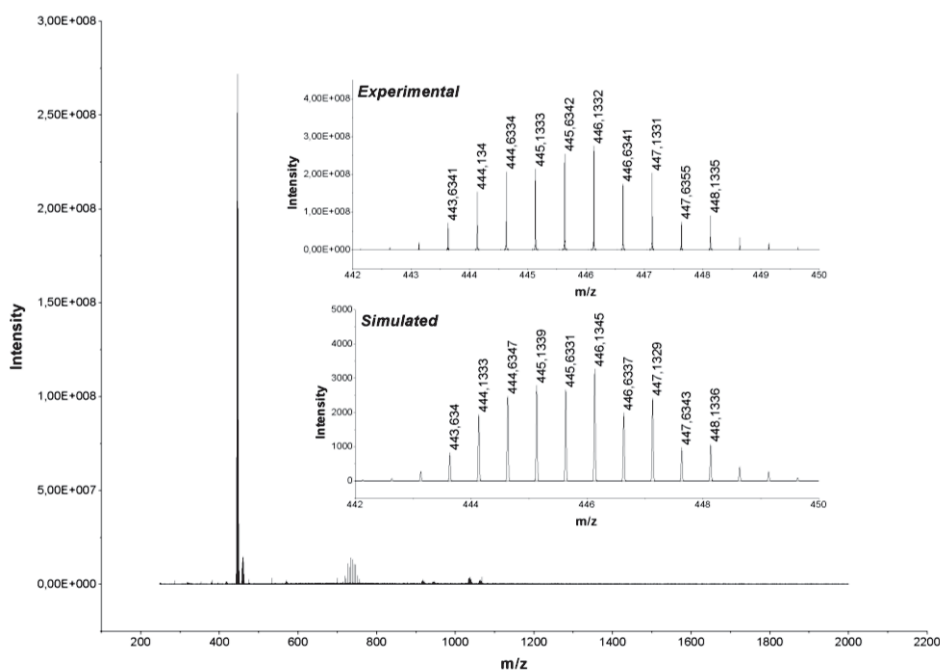


Figure A3. HR ESI-MS spectrum of $[\text{nL}^{\text{nBu}}_2\text{Pd}_2](\text{PF}_6)_2$ (complex **7**) in acetonitrile, the inset shows the experimental and simulated isotopic distribution patterns for $[\text{nL}^{\text{nBu}}_2\text{Pd}_2]^{2+}$.

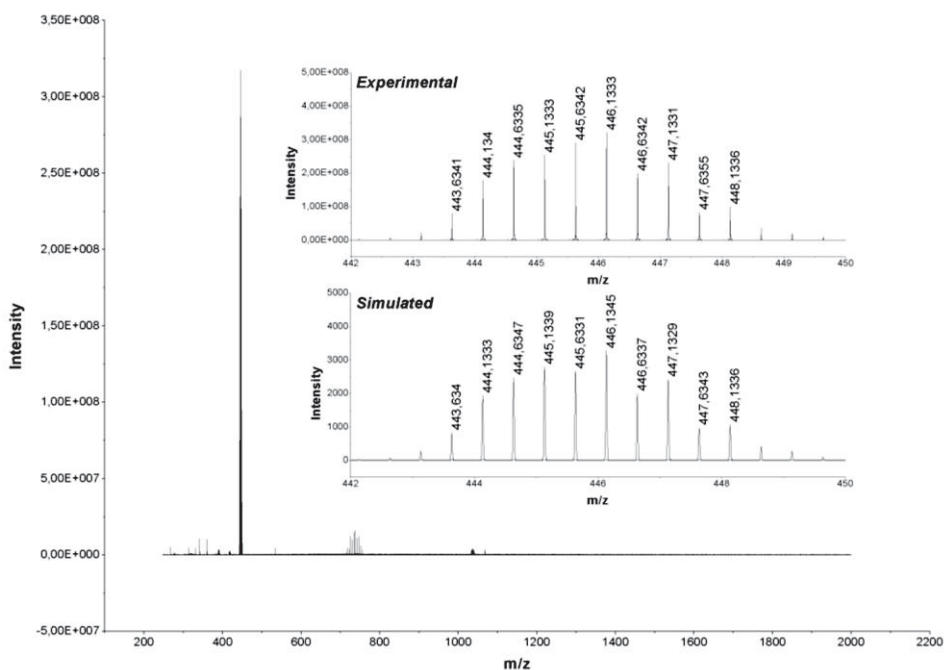


Figure A4. HR ESI-MS spectrum of $[\text{aL}^{\text{nBu}}_2\text{Pd}_2](\text{PF}_6)_2$ (complex **10**) in acetonitrile, the inset shows the experimental and simulated isotopic distribution patterns for $[\text{aL}^{\text{nBu}}_2\text{Pd}_2]^{2+}$.

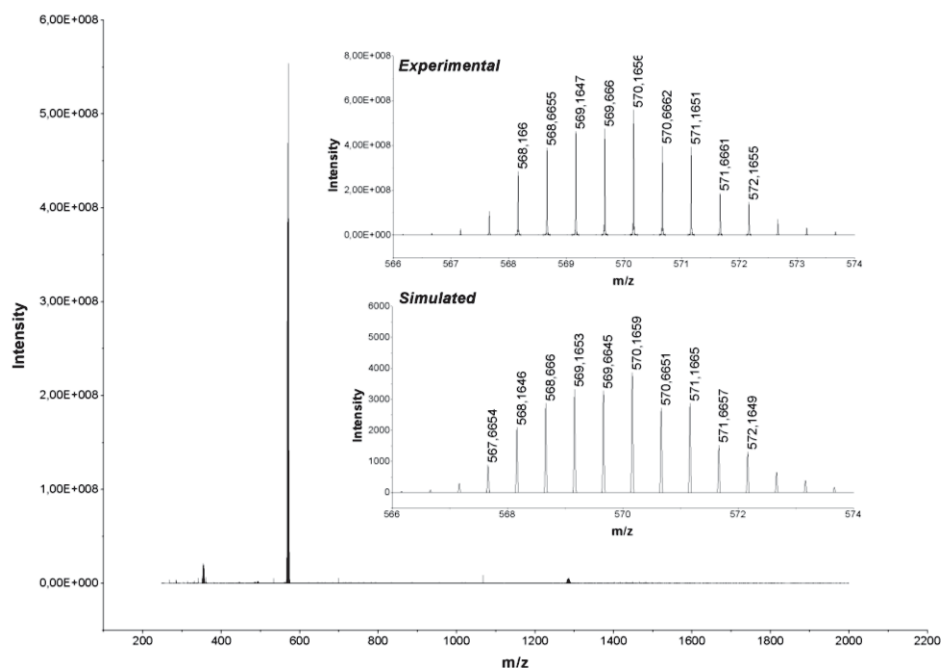


Figure A5. HR ESI-MS spectrum of $[\text{nL}^{\text{Mes}}_2\text{Pd}_2](\text{PF}_6)_2$ (complex **8**) in acetonitrile, the inset shows the experimental and simulated isotopic distribution patterns for $[\text{nL}^{\text{Mes}}_2\text{Pd}_2]^{2+}$.

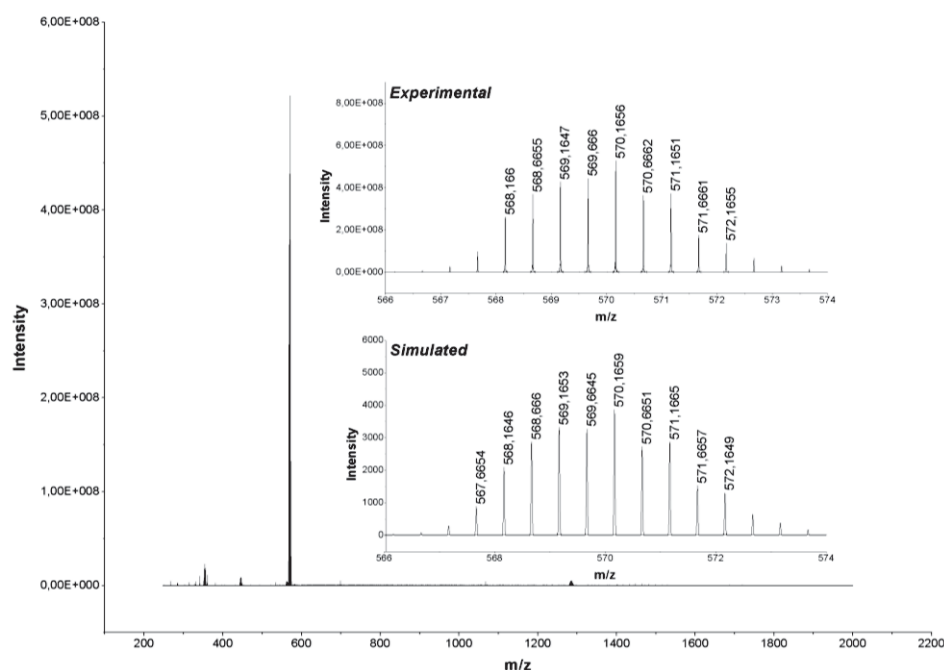


Figure A6. HR ESI-MS spectrum of $[\text{aL}^{\text{Mes}}_2\text{Pd}_2](\text{PF}_6)_2$ (complex **11**) in acetonitrile, the inset shows the experimental and simulated isotopic distribution patterns for $[\text{aL}^{\text{Mes}}_2\text{Pd}_2]^{2+}$.

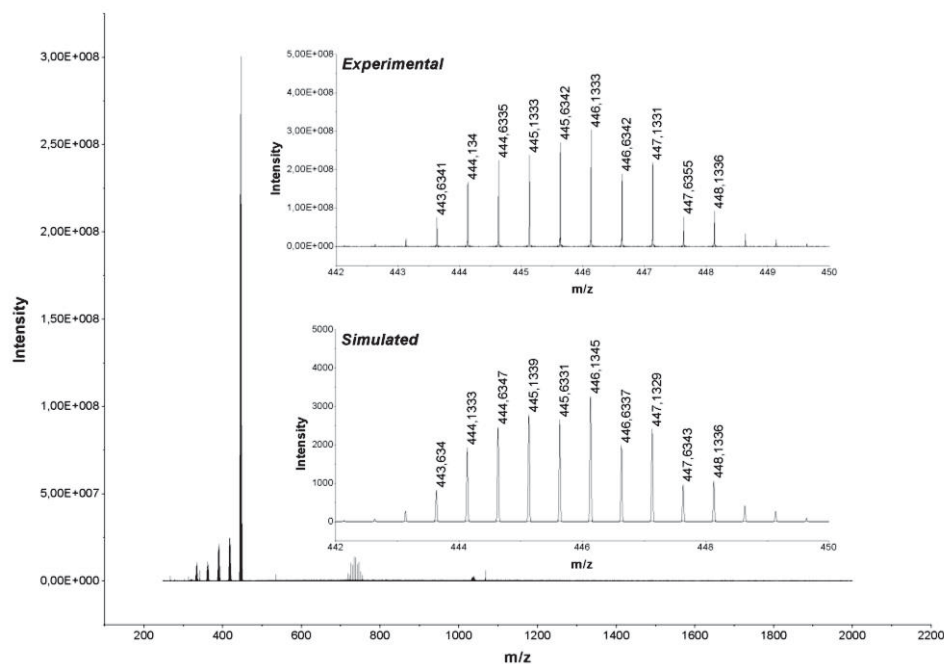


Figure A7. HR ESI-MS spectrum of $[\text{aL}^{\text{tBu}}_2\text{Pd}_2](\text{PF}_6)_2$ (complex **12**) in acetonitrile, the inset shows experimental and simulated isotopic distribution patterns for $[\text{aL}^{\text{tBu}}_2\text{Pd}_2]^{2+}$.

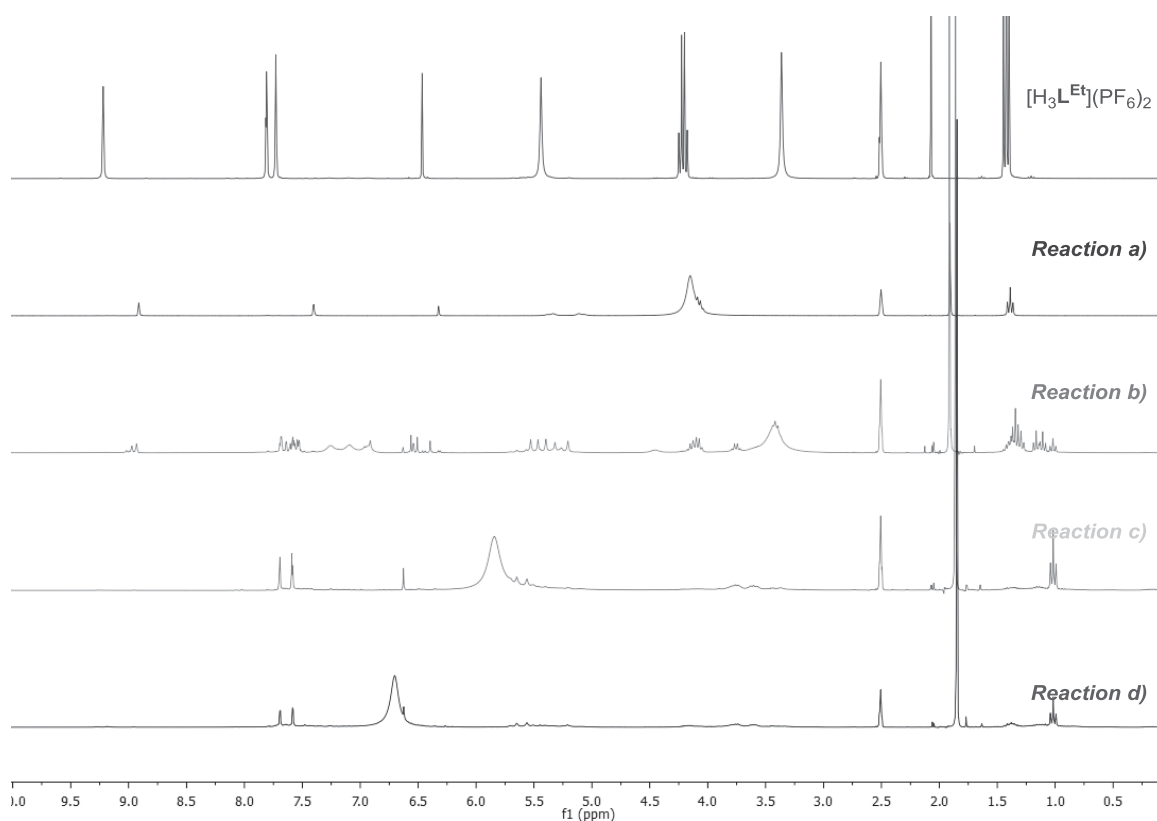


Figure A8. ^1H NMR spectra of $[\text{H}_3\text{L}^{\text{Et}}](\text{PF}_6)_2$ in CD_3CN and *in situ* reactions of $[\text{H}_3\text{L}^{\text{Et}}](\text{PF}_6)_2$ (1.0 equiv.), NH_4OAc (n equiv.) and $\text{Pd}(\text{OAc})_2$ (1.0 equiv.) in d^6 -DMSO. Reaction conditions: a) $n = 0$, at 95°C for 1.5 hours; b) $n = 1$, at 105°C for overnight; c) $n = 2$, at 105°C for overnight; d) $n = 3$, at 105°C for overnight.

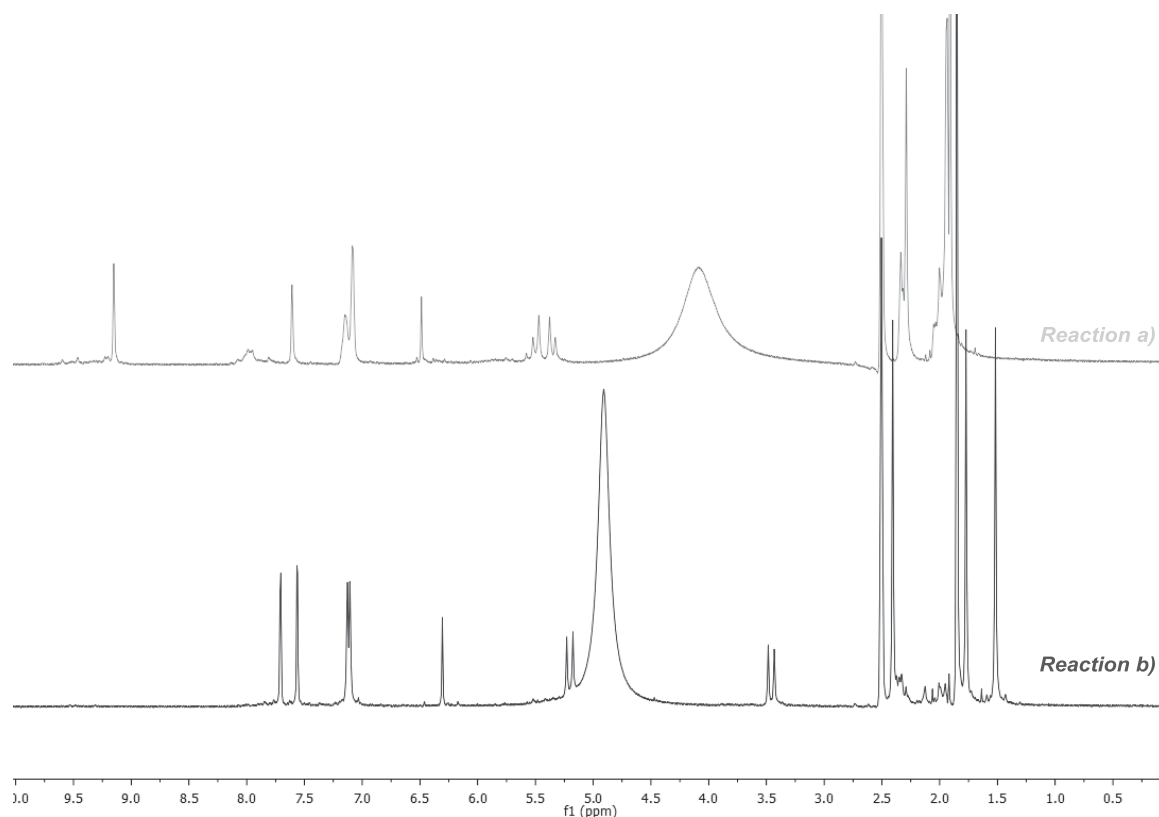


Figure A9. ^1H NMR spectra of *in situ* reactions of $[\text{H}_3\text{L}^{\text{Mes}}](\text{PF}_6)_2$ (1.0 equiv.), NH_4OAc (n equiv.) and $\text{Pd}(\text{OAc})_2$ (1.0 equiv.) in d^6 -DMSO. Conditions: a) $n = 0$, at 95°C for 1.5 hours; b) $n = 2$, 105°C for 3 hours.

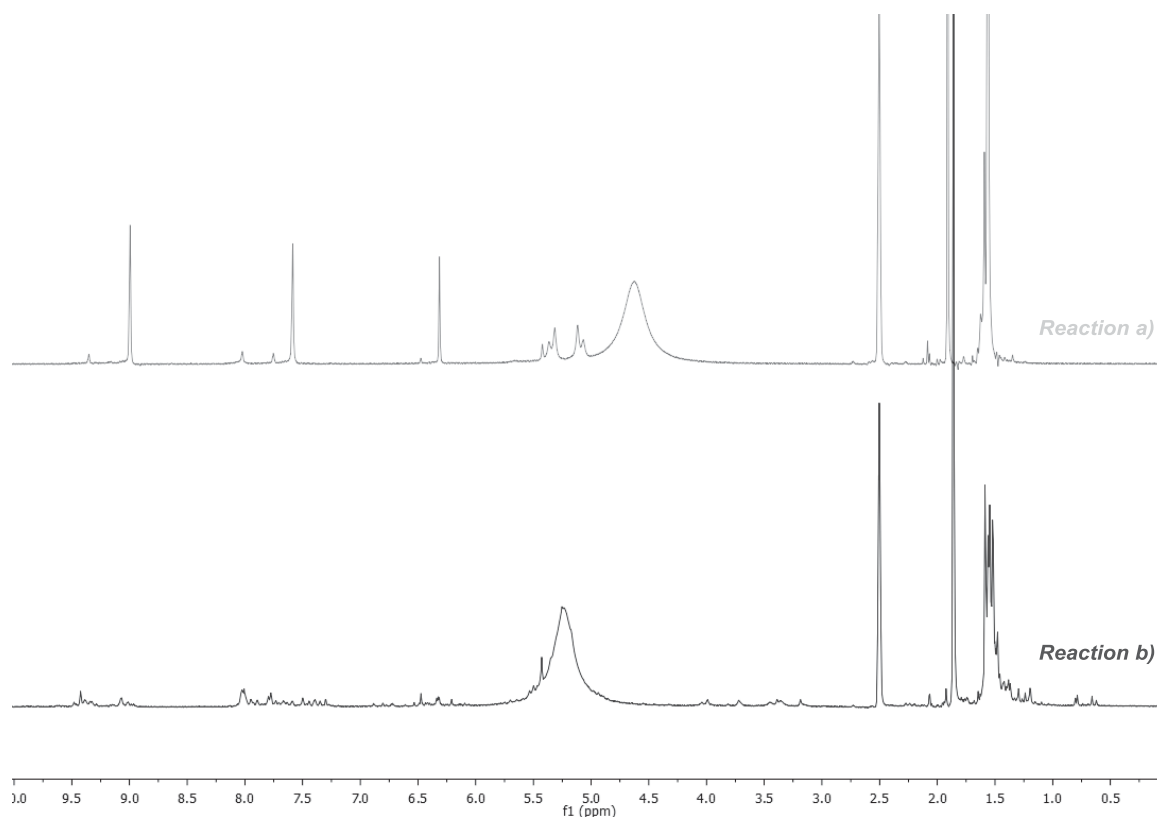


Figure A10. ^1H NMR spectra of *in situ* reactions of $[\text{H}_3\text{L}^{\text{tBu}}](\text{PF}_6)_2$ (1.0 equiv.), NH_4OAc (n equiv.) and $\text{Pd}(\text{OAc})_2$ (1.0 equiv.) in d^6 -DMSO. Conditions: a) $n = 0$, at $95\text{ }^\circ\text{C}$ for 1.5 hours; b) $n = 2$, $105\text{ }^\circ\text{C}$ for 3 hours.

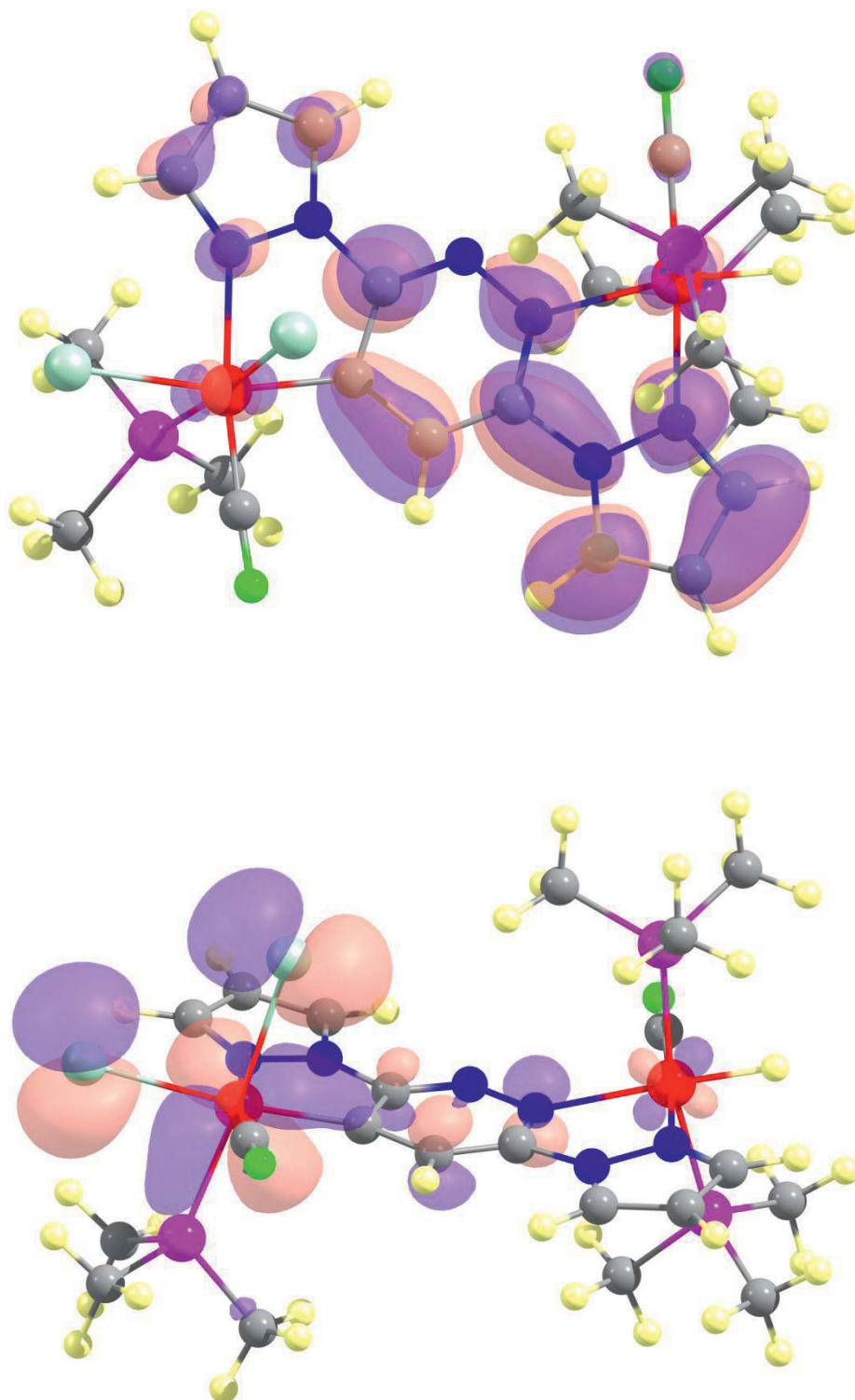


Figure A11. LUMO (top) and HOMO (bottom) of the calculated model **G**.

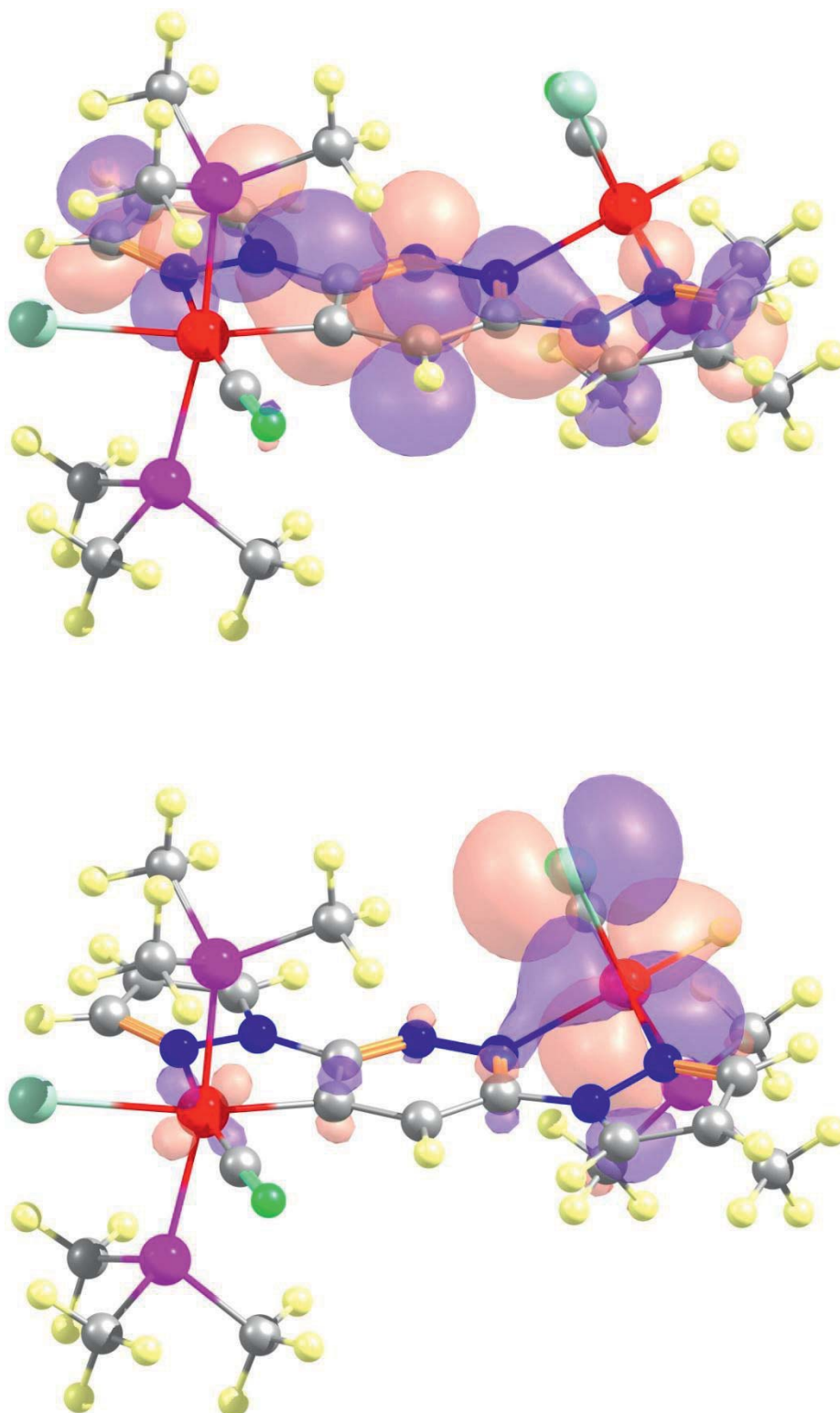


Figure A12. LUMO (top) and HOMO (bottom) of the calculated model **H**.



TONGXUN GUO

Am Weendespring 8a	+49 (0)176 8489 6056
D-37077, Göttingen, Germany	tongxun.guo@stud.uni-goettingen.de
Date/Place of Birth	20.12.1985/Hebei
Nationality	P. R. China

EDUCATION

Doctoral Candidate, Program ‘Catalysis for Sustainable Synthesis’	<i>July 2014</i>
Institute of Inorganic Chemistry, Georg-August-University Göttingen	<i>Göttingen,</i>
Thesis Title: Novel <i>N</i> -Heterocyclic Carbene Ligands and their Metal Complexes	
Master of Philosophy, Chemistry, GPA 11.0/12.0	<i>August 2010</i>
Chemistry Department, Hong Kong University of Science & Technology	<i>Hong Kong</i>
Thesis Title: Organometallic Reactions of Ru, Os and Re Complexes	
Bachelor, Applied Chemistry, GPA 3.80/4.00	<i>July 2008</i>
College of Science, China Agricultural University (<i>abbr.</i> CAU)	<i>Beijing</i>

RESEARCH EXPERIENCE

Doctorate Student, Inorganic Laboratory	<i>October 2010 - present</i>
Work Group Franc Meyer, Institute of Inorganic Chemistry, University Göttingen	
<ul style="list-style-type: none"> ➤ Pyrazole bridged <i>N</i>-heterocyclic carbene ligands and their dinuclear palladium complexes: selective formation of 2- or 4-imidazolylidene palladium complexes. ➤ Pyridazine derived <i>N</i>-heterocyclic carbene palladium complexes: synthesis of the first class of pyridazinylidene palladium complexes. ➤ <i>N</i>-metallated <i>N</i>-heterocyclic carbene complex: novel type of metal <i>N</i>-heterocyclic carbene complex. 	
Master Student, Organometallic Laboratory	<i>September 2008 - August 2010</i>
Work Group Jia, Chemistry Department, Hong Kong Univ. of Science & Technology	
<ul style="list-style-type: none"> ➤ Insertion reactions of ruthenium/osmium hydride complexes with allene derivatives: from both experimental and computational perspectives. ➤ Ruthenium catalyzed intramolecular amination reactions of aryl-/vinyl azides: study on kinetic isotope effect by comparing reactivity of non-deuterated and deuterated substrates. 	



- Study on the stabilization effect of ligand and substituent on cyclopentadienyl ring: by DFT calculation of the rearrangement reactions of metallabenzenes to cyclopentadienyl complexes.
- DFT calculations of the effect of PPh_3 on the formation of ruthenium cyclopentadienyl complexes.

Bachelor Student, Catalysis Laboratory

July 2007 - May 2008

Work Group Min Wang, College of Science, China Agricultural University

- Chiral BINAP-gold(I) catalyzed asymmetric annulation of 1-hydroxy-4,5-hexadiene derivatives: synthesis, complexation, catalysis and characterization.

SKILLS

Laboratory Schlenk Technology, Glove Box, Centrifuge, Column Chromatography, Gas Chromatography, HPLC, Nuclear Magnetic Resonance, Mass Spectrometry, Infrared Spectroscopy

Software Diamond, Mercury, EndNote, GaussView, Gaussian03, ChemDraw, MNova
et al

Languages Mandarin (mother tongue), English (fluent), German (medium), Cantonese (fundamental)

PUBLICATIONS

- Novel *N*-Metallated *N*-Heterocyclic Carbene Ruthenium Complexes. T. Guo, S. Dechert, F. Meyer, *in preparation*.
- Dinuclear Palladium Complexes of Pyrazole-Bridged Bis(NHC) Ligands: a Delicate Balance Between Normal and Abnormal Carbene Coordination. T. Guo, S. Dechert, F. Meyer, *Organometallics*, *under submission*.
- Convenient Synthetic Route to Palladium Complexes of Unconventional *N*-Heterocyclic Carbenes Derived from Pyridazine and Phthalazine. T. Guo, S. Dechert, S. Meyer, F. Meyer, *Organometallics*, **2012**, *31*, 8537-8543
- Theoretical Study on the rearrangement of metallabenzenes to cyclopentadienyl complexes. C. Shi, T. Guo, K. C. Poon, Z. Lin, G. Jia. *Dalton Trans.*, **2011**, *40*, 11315-11320
- Synthesis and Characterization of Rhenabenzenes. K. C. Poon, L. Liu, T. Guo, J. Li, H. H.-Y. Sung, I. D. Williams, Z. Lin, G. Jia, *Angew. Chem. Int. Ed.*, **2010**, *49*, 2759-2762

- Ruthenium-Catalyzed Intramolecular Amination Reactions of Aryl- and Vinylazides. W. G. Shou, J. Li, T. Guo, Z. Lin, G. Jia, *Organometallics*, **2009**, 28, 6847-6854.
- Synthesis of Monosubstituted Cyclopentadienyl Ruthenium Complexes from the Reactions of 6-Substituted Fulvenes with RuHCl(PPh₃)₃. S. K. S. Tse, T. Guo, H. H.-Y. Sung, I. D. Williams, Z. Lin, G. Jia, *Organo- metallics*, **2009**, 28, 5529-5535.

POSTERS & PRESENTATIONS

Selected Posters

- “Novel *N*-Heterocyclic Carbenes: *N*-Metallated Pyridazinylidene Metal Complexes.” 20th EuCheMS Conference on Organometallic Chemistry, St. Andrews, UK, June 30 - July 4, 2013.
- “A Convenient Synthetic Route to Palladium Complexes of Unconventional *N*-Heterocyclic Carbenes Derived from Pyridazine and Phthalazine.” 16. Vortragstagung der Wöhler-Vereinigung, Göttingen, DE, September 26-28, 2012; Niedersächsisches Katalyse Symposium 2012, Göttingen, DE, October 18-19, 2012; 9. Koordinationschemie-Treffen, Bayreuth, DE, February 24-26, 2013.
- “Ruthenium-Catalyzed Intramolecular Amination Reaction.” The Seventeenth Symposium on Chemistry Postgraduate Research in Hong Kong, Hong Kong SAR, CN, April 24, 2010.

Oral Presentation

- “Pyrazole-Bridged Bis-(*N*-Heterocyclic Carbene) Ligands and the Corresponding Bimetallic Palladium Complexes.” Joint Workshop of Ph.D. Programme “Catalysis for Sustainable Synthesis” and Landesforschungs- schwerpunkt “Nanostrukturierte Katalysatoren für eine effizientere Nutzung von Rohstoffen”, Braunschweig, DE, June 27-29, 2012.

SELECTED TEACHING EXPERIENCE

Teaching Assistance, Catalytic Practice Laboratory

Summer Semester 2011-2013

Master Synthetic Laboratory, Institute of Inorganic Chemistry, University Göttingen

Teaching Assistance, Inorganic Synthesis

Winter Semester 2010-2013

Bachelor Synthetic Laboratory, Institute of Inorganic Chemistry, University Göttingen

- Chemicals order and distribution, troubleshooting of equipment and apparatus, improvement of scripts, protocols correction.

Teaching Assistance, Synthetic Laboratory*Several semesters 2010, 2009*

Synthetic Lab, Department of Chemistry, Hong Kong Univ. of Science & Technology

- Pre-lab quiz invigilation and correction, safety inspection, equipment instruction, theoretical explanation, toxicity control, performance evaluation and final exams invigilation.

Teaching Assistance, Organic Chemistry II*Spring Semester 2010*

Undergraduate Course, Department of Chemistry, Hong Kong Univ. of Science & Technology

Teaching Assistance, Fundamental Chemistry*Spring Semester 2010*

Bachelor Course, Department of Chemistry, Hong Kong Univ. of Science & Technology

- Opening hours to help students understanding lectures and solving homework problems; review lectures on the difficulties before the final examination; final examination invigilation, correction and afterward paper-checking; collaboration with the professor and other TA's on course materials and grading policies

METHOD COURSES, EXCURSIONS & WORKSHOPS**Method Courses**

- “Spectroscopic Methods in Catalysis Research (X-Ray technique related)” by Jun.-Prof. Dr. M. Bauer (University Kaiserslautern), Göttingen, DE, April 24-25, 2012.
- “Kinetics Methods on Radical Polymerization”, by Prof. Dr. Buback and Prof. Dr. Vana (University Göttingen), Göttingen, DE, February 15&22, 2012.
- “Spectroscopic Methods in Catalysis Research (Gas Chromatography technique related)” by Prof. O. Trapp, Göttingen, DE, October 20-21, 2010.

Excursions

- BASF Ludwigshafen, January 18, 2012.
- Kali + Salz Heringen, February 16-18, 2011.
- Merck Darmstadt, May 20, 2011.

Workshops

- Joint Workshop of Ph.D. Programme “Catalysis for Sustainable Synthesis” and Landesforschungs-schwerpunkt “Nanostrukturierte Katalysatoren für eine effizientere Nutzung von Rohstoffen”, Braunfels, DE, June 27-29, 2012.

- Ph.D. Program “Catalysis for Sustainable Synthesis” Workshop, Goslar, DE, June 24-25, 2011. SciencePlus Workshop “Career Planning for Ph.D. Students“, Göttingen, DE, June 7, 2011.

SELECTED AWARDS & HONORS

Beijing Merit Student , Beijing City	<i>December 2006</i>
University President Scholarship , China Agricultural University	<i>November 2006</i>
Outstanding Volunteer , 100 th anniversary of the foundation of CAU	<i>September 2005</i>

SOCIAL ACTIVITIES & SERVICE

Representative of 10 th Beijing Student Federation	<i>December 2006</i>
President of student union, College of Science, CAU	<i>2006 - 2007</i>
Volunteer for centennial anniversary of the foundation of CAU	<i>May 2005</i>

REFERENCES

Prof. Dr. Franc Meyer	Dr. Guochen Jia, Professor
Institute of Inorganic Chemistry,	Department of Chemistry,
Tammanstrasse 4, D-37077,	Hong Kong Univ. of Sci. & Tech.,
Göttingen, Germany	Hong Kong SAR, P. R. China
+49-(0)551-39-33012	+852-2358-7373,
franc.meyer@chemie.uni-goettingen.de	chjiag@ust.hk
Relationship: Ph.D. Supervisor	Relationship: M.Phil. Supervisor





